Activation of Environmental Carcinogens in Human Tissue Organoid Cultures

Caipa Garcia, Angela

Awarding institution:
King's College London

ACTIVATION OF ENVIRONMENTAL CARCINOGENS IN HUMAN TISSUE ORGANOID CULTURES

Submitted by Angela Lorena Caipa García
to King's College London for the
Degree of Doctor of Philosophy

February 2022

Analytical, Environmental & Forensic Sciences Division
School of Cancer & Pharmaceutical Sciences
King's College London
United Kingdom

Declaration

I hereby declare that, as the author of this thesis, all the work reported here was carried out by myself. Assistance provided by other people has been acknowledged and all previous work has been identified and acknowledged. The work is original and has not been submitted for any other degree.

Angela Lorena Caipa García

Abstract

Human exposure to environmental carcinogens is often unavoidable. Many of these compounds initiate carcinogenesis by inducing mutagenic DNA damage. Some of these environmental carcinogens require metabolic activation to be able to damage DNA resulting in the formation of bulky DNA adducts. However, organ specificity of oncogenesis, in many cases, cannot be explained solely by DNA adduct formation in target tissue(s), as other cellular processes, including gene expression changes, also contribute to tumour development. Therefore, it is important to study the metabolic activation and/or detoxication of environmental carcinogens and the cellular changes they induce to understand which host factors contribute to their tissue specific carcinogenesis. Many studies of these mechanisms have been carried out in experimental animals, immortalised cell lines and primary cells; however, there can be inconsistencies between the translation of *in vivo* and *in vitro* findings. Human organoids are 3D cultures that to some extent reproduce the structure, composition and function of the organ they derive from; therefore, they offer the opportunity to investigate environmental carcinogens in an *in vitro* setting with more *in vivo*-like characteristics. Here, human organoids from normal gastric, pancreas, liver, colon and kidney tissues were used to study their ability to metabolise four well-characterised environmental carcinogens that have different target tissues: benzo[*a*]pyrene (BaP), aflatoxin B_1 (AFB_1), aristolochic acid I (AAI) and 2-amino-1-methyl-6-phenylimidazo[4,5-*b*]pyridine (PhIP). The aims of this study were to assess the potential of these tissue organoids to metabolically activate environmental carcinogens, and then to investigate carcinogen organotropism using this model system. For this purpose, organoids were treated with the selected carcinogens at a range of concentrations and different endpoints were measured. Cytotoxicity measurements were first used to select suitable concentrations of the agents for further experiments. Then metabolic activation was investigated by analysing the induction of xenobiotic-metabolising enzymes (XMEs) involved in the activation of the individual carcinogens. Bioactivation of the carcinogens was confirmed

by investigating activation of the DNA damage response (DDR) pathway, and the formation of carcinogen-DNA adducts. In order to study tissue-specific responses, organoids from target and non-target tissues were selected for each compound. BaP, AFB_1 and AAI treatment led to the induction of XMEs at various levels in the different tissue organoids. All carcinogens were activated by the organoids to some extent, as evidenced by DNA adduct formation and DDR protein induction. As PhIP induced the lowest levels of adducts, its reactive metabolite *N*-OH-PhIP was also tested on the organoids showing an increased level of adducts and therefore suggesting that the required XMEs may not be present at sufficient levels to activate PhIP. Additionally, in order to explore differences in gene expression between organoid types after BaP treatment, high-throughput RT-qPCR was used to study a panel of genes involved in cell cycle, DNA damage and repair, apoptosis, metabolism and stress responses. In general, the results of the organotropism study were inconclusive as the differences found between organoid types did not fully differentiate target from non-target organs. However, the results showed that tissue organoids are useful models in the study of environmental carcinogens and genetic toxicology.

Acknowledgements

Firstly, I would like to express my sincere gratitude to my supervisors Prof. David Phillips and Dr Volker Arlt for allowing me to join their group to pursue my PhD and for their constant support and guidance. I would also like to thank Dr Jill Kucab for acting as a third supervisor throughout my project, answering all my questions and helping me to develop as a scientist. I feel very fortunate to have had the opportunity to work with them and to have learned so much from them. I also want to thank Dr Ellie Wilde, as she introduced me to the organoid field and gave me guidance when choosing my PhD project.

I would also like to thank all other present and past members of the Environmental Carcinogenesis group, especially Halh Al-Serori and Rebekah Beck, as they gave me the encouragement I needed this final year, as well as their support in the lab and during thesis writing. I also want to thank the members of the Sturzenbaum group, especially Norah Almutairi and Yuzhi Chen, for all the fun and encouraging chats.

I want to thank all my collaborators and all the students who contributed to this project. Drs Madjda Bellamri, Lihua Yaol, Robert Turesky, John Groopman and Silvia Balbo, and Andrew Floeder in the USA for their help with the adduct analysis. Prof. Andrea Hartwig, Dr Matthias Hufnagel and Franziska Fischer in Germany for the HT RT-qPCR analysis.

I am very grateful because this PhD not only allowed me to learn many things about science but also allowed me to make very good friends, who have now become part of my family. Thanks to Halh and Lisa for always being there for me and for helping me through stressful times. Thanks to them and Jill (and her kids) for all the fun chats and enjoyable moments in and out of the lab. I also want to thank Hersi for all his help, support and understanding from the beginning, and for all his efforts in trying to keep me calm even when I thought it was not possible.

Finally, I want to give the biggest thanks to all my family for their constant support, not only during my PhD but throughout my life, without them this would have not been

possible. Thank you to my mum for the daily walks and for always being there for me, for accompanying me when I had to work during the weekends or when I had to go back to the lab at midnight! Thanks to my dad and my brother for all their calls and messages, for believing in me and giving me all their support. Thanks to Fredy and Nancy for their support. I also want to thank my grandmas and Maita for their daily calls and prayers. Lastly, I want to thank Maisie for her company and unconditional love during the first three years of my PhD.

Table of contents

Declaration 2
Abstract 3
Acknowledgements 5
Table of contents 7
List of figures 11
List of tables 14
Abbreviations 15
Chapter 1 Introduction 20
1.1 Cancer 20
1.2 Environmental carcinogenesis 23
1.2.1 Metabolic activation of carcinogens 26
1.2.2 DNA damage induced by carcinogens 28
1.2.3 DNA damage response 30
1.3 Genes and cancer 34
1.4 Test carcinogens 36
1.4.1 Benzo[*a*]pyrene 36
1.4.2 Aflatoxin B_1 39
1.4.3 Aristolochic acid I 41
1.4.4 2-Amino-1-methyl-6-phenylimidazo[4,5-*b*]pyridine 44
1.5 Tissue-specific oncogenesis 47
1.6 Organoids 48
1.6.1 Types of organoids and their features 52
1.6.2 Organoid use in drug screening and toxicology 58
1.6.3 Advantages and limitations over other 3D models 65
1.7 Aims of the project 67
Chapter 2 Materials and methods 70
2.1 Environmental carcinogens 70

2.2 Organoid culture 70
2.2.1 Culture conditions 70
2.2.2 Organoid splitting and seeding 75
2.2.3 Organoid cryopreservation and thawing 76
2.2.4 Liver organoid differentiation 76
2.2.5 Treatment with carcinogens 78
2.3 Measurement of cell viability 78
2.4 Protein expression analysis 79
2.4.1 Preparation of organoid lysates 79
2.4.2 Protein quantitation 79
2.4.3 Sodium dodecyl sulphate polyacrylamide gel electrophoresis (SDS-PAGE) 80
2.4.4 Western blot analysis 80
2.5 DNA adduct analysis 82
2.5.1 Preparation of organoid samples 82
2.5.2 DNA extraction by phenol-chloroform 82
2.5.3 DNA adduct analysis by LC-ESI-MS/MS after treatment with BaP 83
2.5.4 DNA adduct analysis by UPLC-ESI/MS^3 after treatment with AAI, PhIP or *N*-OH-PhIP 87
2.5.5 DNA adduct analysis by LC-MS/MS after treatment with AFB_1 90
2.6 Gene expression analysis 92
2.6.1 Preparation of organoid samples 92
2.6.2 RNA extraction 92
2.6.3 cDNA synthesis 93
2.6.4 Real time quantitative polymerase chain reaction (RT-qPCR) 93
2.6.5 Quantification of relative gene expression using the ΔΔCt method 95
2.7 High-throughput (HT) RT-qPCR 95

2.7.1 Sample preparation and cDNA synthesis 95
2.7.2 Specific target amplification (STA) and exonuclease digestion 96
2.7.3 HT RT-qPCR 98
2.7.4 Analysis of HT RT-qPCR 100
2.8 Metabolite analysis by high performance liquid chromatography (HPLC) 100
2.9 Statistical analysis 101
Chapter 3 Metabolic activation and cellular responses to benzo[*a*]pyrene 102
3.1 Introduction 102
3.2 Materials and methods 103
3.3 Results 104
3.3.1 Liver organoid differentiation and characterisation 104
3.3.2 Cell viability assessment of organoids after BaP treatment 106
3.3.3 Xenobiotic-metabolising enzyme expression after treatment with BaP 107
3.3.4 Induction of DDR proteins after BaP treatment 112
3.3.5 Analysis of BaP metabolites after BaP treatment 114
3.3.6 Formation of DNA adducts after treatment with BaP 116
3.3.7 Gene expression analysis by high throughput RT-qPCR 117
3.4 Discussion 124
Chapter 4 Metabolic activation and cellular responses to aflatoxin B_1 131
4.1 Introduction 131
4.2 Materials and methods 132
4.3 Results 133
4.3.1 Cell viability assessment of organoids treated with AFB_1 133
4.3.1 Xenobiotic-metabolising enzyme expression after AFB_1 treatment 134
4.3.2 Induction of DDR proteins after AFB_1 treatment 137
4.3.3 DNA adduct formation after AFB_1 exposure 139

4.4 Discussion 141

Chapter 5 Metabolic activation and cellular responses to aristolochic acid 146

5.1 Introduction 146

5.2 Materials and methods 147

5.3 Results 148

5.3.1 Cell viability assessment of organoids after AAI treatment 148

5.3.2 Xenobiotic-metabolising enzyme expression after treatment with AAI 149

5.3.3 Induction of DDR proteins after AAI treatment 151

5.3.4 DNA adduct formation after AAI treatment 152

5.4 Discussion 153

Chapter 6 Metabolic activation and cellular responses to *N*-hydroxy-2-amino-1-methyl-6-phenylimidazo[4,5-*b*]pyridine 158

6.1 Introduction 158

6.2 Materials and methods 159

6.3 Results 159

6.3.1 Cell viability assessment of organoids after PhIP treatment 159

6.3.2 Induction of DDR proteins after PhIP treatment 160

6.3.3 Cell viability assessment of organoids after *N*-OH-PhIP treatment 161

6.3.4 Induction of DDR proteins after *N*-OH-PhIP treatment 162

6.3.5 DNA adduct formation after PhIP and *N*-OH-PhIP treatment 163

6.4 Discussion 165

Chapter 7 General discussion 170

Appendix 183

References 188

Publications and presentations 241

List of figures

Figure 1.1. Hallmarks and enabling characteristics of cancer. 21
Figure 1.2. Estimated world age-standardised incidence and mortality rates in 2020 in low and very high HDI countries for the most common cancers. 21
Figure 1.3. Environmental risk factors by cancer incidence suggesting number of preventable cases in the UK for both sexes in 2015. 22
Figure 1.4. Contribution of individual CYP enzymes to the bioactivation of carcinogens (A) and drug metabolism (B). 28
Figure 1.5. Cellular responses to DNA damage. 31
Figure 1.6. Repair pathways triggered according to the type of DNA damage. 32
Figure 1.7. Overview of the nucleotide excision repair pathway. 34
Figure 1.8. Metabolic activation and DNA adduct formation by BaP. 38
Figure 1.9. Metabolic activation and DNA adduct formation by AFB_1. 41
Figure 1.10. Metabolic activation, detoxification and DNA adduct formation by AAI. 44
Figure 1.11. Metabolic activation and adduct formation by PhIP. 47
Figure 1.12. Scheme showing the origin and application of organoid systems. 51
Figure 1.13. Scheme of liver organoid culture formation from pluripotent stem cells or adult stem cells. 56
Figure 1.14. Scheme with the original study design of this PhD project. 68
Figure 2.1. Liver organoid differentiation timeline from seeding to treatment or analysis. 77
Figure 2.2. CellTiter-Glo Assay reaction. 78
Figure 2.3. Diagram of the analysis of BaP-DNA adducts by LC−ESI-MS/MS. 86
Figure 2.4. Diagram of the analysis of AAI and PhIP-DNA adducts by UPLC-ESI/MS^3. 89
Figure 2.5. Diagram of the analysis of AFB_1-DNA adducts by LC-MS/MS. 91
Figure 2.6. Diagram of the 96.96 Dynamic Array IFC chip. 99
Figure 3.1. Morphology of the liver organoids during differentiation and their characterisation. 105
Figure 3.2. Cell viability in human tissue organoids after treatment with BaP. 107
Figure 3.3. Relative gene expression of *CYP1A1* in human tissue organoids after treatment with BaP. 109

Figure 3.4 Relative gene expression of *NQO1* in human tissue organoids after treatment with BaP.....111
Figure 3.5. Expression of DDR proteins in normal human tissue organoids after treatment with BaP.....113
Figure 3.6. BaP metabolite levels in human tissue organoids after BaP exposure. 115
Figure 3.7. DNA adduct formation in human tissue organoids after treatment with BaP.....117
Figure 3.8. Heatmap of the relative gene expression in human organoids after BaP treatment. 119
Figure 3.9. Effects of BaP in the gene expression of XMEs measured by HT RT-qPCR. 120
Figure 3.10. Effects of BaP in the expression of genes involved in DDR measured by HT RT-qPCR. 122
Figure 3.11. Effects of BaP in the expression of genes in the PCC, TF, OS and AP groups measured by HT RT-qPCR.....123
Figure 4.1. Cell viability in human tissue organoids after AFB_1 treatment. 134
Figure 4.2. Relative gene expression of *CYP3A4* in normal human tissue organoids after AFB_1 treatment.....135
Figure 4.3. Relative gene expression of *CYP1A2* in normal human organoids after AFB_1 treatment.....136
Figure 4.4. Relative gene expression of *CYP3A4* and *CYP1A2* in normal human organoids. .137
Figure 4.5. Expression of DDR proteins in human organoids after treatment with AFB_1.....139
Figure 4.6. DNA adduct formation in human tissue organoids after treatment with AFB_1. 141
Figure 5.1. Cell viability in human tissue organoids after treatment with AAI.....148
Figure 5.2. Relative gene expression of *CYP1A1, CYP1A2* and *NQO1* in normal human tissue organoids after AAI treatment.....150
Figure 5.3. Expression of DDR proteins in normal human organoids after AAI treatment.....151
Figure 5.4. Representative chromatograms and product ion spectra from the UPLC-ESI/MS^3 analysis.....152
Figure 5.5. DNA adduct formation in human tissue organoids after treatment with AAI.....153
Figure 6.1. Cell viability in human tissue organoids after treatment with PhIP.....160
Figure 6.2. Expression of DDR proteins in normal human organoids after PhIP treatment.....161
Figure 6.3. Cell viability in human tissue organoids after treatment with *N*-OH-PhIP.....162

Figure 6.4. Expression of DDR proteins in normal human organoids after *N*-OH-PhIP treatment. 163
Figure 6.5. Representative chromatograms and product ion spectra from the UPLC-ESI/MS^3 analysis.....164
Figure 6.6. DNA adduct formation in human organoids after treatment with PhIP.....164
Figure 6.7. DNA adduct formation in human organoids after treatment with *N*-OH-PhIP.....165
Figure 7.1. dG-N^2-BPDE adduct levels and relative mRNA expression of *CYP1A1* and *NQO1* in human tissue organoids. 171
Figure 7.2. AFB_1-FapyGua adduct levels and relative mRNA expression of *CYP3A4* and *CYP1A2* in human tissue organoids.....172
Figure 7.3. dA-AL-I adduct levels and relative mRNA expression of *CYP1A1*, *CYP1A2* and *NQO1* in human tissue organoids.....173
Figure 7.4. dG-C8-PhIP adduct levels in human tissue organoids. 174
Figure 7.5. Relative mRNA levels of XMEs in normal human tissue organoids. 176
Figure 7.6. DDR protein expression relative to GAPDH in normal human tissue organoids. ...178

List of tables

Table 1.1. Classification of carcinogens according to the IARC Monographs.....24

Table 1.2. Examples of Group 1 environmental agents according to carcinogen type and associated cancer site with sufficient evidence in humans. 24

Table 1.3. Key characteristics of carcinogens. 26

Table 1.4. Examples of genes driving carcinogenesis. 36

Table 1.5. Studies using organoids in environmental toxicology. 62

Table 2.1. Growth media recipes for organoids derived from different human tissues.....73

Table 2.2. Organoid donors from different human tissues 74

Table 2.3. Liver starting and differentiation media recipes.....77

Table 2.4. High-Capacity RNA-to-cDNA Kit reaction components 93

Table 2.5. High-Capacity cDNA Reverse Transcription Kit reaction components.....94

Table 2.6. Cycling parameters for cDNA synthesis 94

Table 2.7. List of primers and probes used for gene expression analysis 94

Table 2.8. RT-qPCR reaction components.....95

Table 2.9. Cycling parameters for iScript cDNA synthesis. 96

Table 2.10. List of target genes classified by pathway.....97

Table 2.11. STA pre-mix components.....98

Table 2.12. STA temperature programme.....98

Table 2.13. Thermal cycling protocol for the 96.96 chip 99

Abbreviations

(i)PSC	(induced) Pluripotent stem cells
2D	Two-dimensional
3D	Three-dimensional
AAI	Aristolochic acid I
AAIa	Aristolochic acid Ia
AAN	Aristolochic acid nephropathy
AFB_1	Aflatoxin B_1
AFB_1-FapyGua	8,9-dihydro-8-(2,6-diamino-4-oxo-3,4-dihy-dropyrimid-5-yl-formamido)-9-hydroxyaflatoxin B_1
AFB_1-N^7-Gua	8,9-dihydro-8-(N^7- guanyl)-9-hydroxy AFB_1
AFBO	AFB_1-8,9-epoxide
AFM/P/Q_1	Aflatoxin M/P/Q_1
AhR	Aryl hydrocarbon receptor
ALB	Albumin
AP	Apoptosis
ASC	Adult stem cells
ATM	Ataxia telangiectasia mutated
ATP	Adenosine triphosphate
ATR	Ataxia telangiectasia mutated and Rad3 related
BaP	Benzo[*a*]pyrene
BCA	Bicinchoninic acid
BEN	Balkan endemic nephropathy
BER	Base excision repair
BME2	Basement membrane matrix extract, type 2
BMP7	Bone Morphogenetic Protein 7
BPDE	Benzo[*a*]pyrene-7,8-diol-9,10-epoxide
BSA	Bovine serum albumin

cDNA	Complementary DNA
CHK2	Checkpoint kinase
CM	Conditioned medium
CS	Cockayne syndrome
CSA/B	Cockayne syndrome related proteins A/B
CYP	Cytochrome P450
dA-AL-I	7-(deoxyadenosin-N^6-yl) aristolactam I
dA-N^6-BPDE	10-(deoxyadenosin-N^6-yl)-7,8,9-trihydroxy-7,8,9,10-tetrahydro-BaP
DAPT	N-[N-(3,5-Difluorophenacetyl-L-alanyl)]-S- phenylglycine t-Butyl Ester
DDB	Damaged DNA-binding protein
DDR	DNA damage response
dG-AL-I	7-(deoxyguanosin-N^2-yl) aristolactam I
dG-C8-PhIP	*N*-(deoxyguanosin-8-yl)-PhIP
dG-N^2-BPDE	10-(deoxyguanosin-N^2-yl)-7,8,9-trihydroxy-7,8,9,10-tetrahydro-BaP
Diol	BaP-t-7,8-dihydrodiol; BaP-t-7,8-dihydrodiol; (±)-trans-7,8-dihydroxy-7,8-dihydrobenzo[*a*]pyrene
DMBA	7,12-dimethylbenz[*a*]anthracene
DMEM/F12	Dulbecco's Modified Eagle Medium/Ham's F-12
DMSO	Dimethyl sulfoxide
DSB	Double-strand breaks
ECL	Enhanced chemiluminescence
EDTA	Ethylenediaminetetraacetic acid
EGF	Epidermal growth factor
EMT	Epithelial-mesenchymal transition
ER	Oestrogen receptor

ERCC1	Excision repair cross complementing 1
FGF	Fibroblast growth factor
GAPDH	Glyceraldehyde 3-phosphate dehydrogenase
gDNA	Genomic DNA
GG-NER	Global genome NER
GSK-3β	Glycogen synthase kinase 3 βeta
GSTs	Glutathione *S*-transferases
HAA	Heterocyclic aromatic amine
HBV	Hepatitis B virus
HCC	Hepatocellular carcinoma
HGF	Hepatocyte growth factor
hHR23B	Human homologue of RAD23B
HNF4	Hepatocyte nuclear factor 4
HPLC	High performance liquid chromatography
HR	Homologous recombination
HRP	Horseradish peroxidase
HT RT-qPCR	High throughput RT-qPCR
IARC	International Agency for Research of Cancer
IFC	Integrated fluidic circuit
KCs	Key characteristics
LC−ESI-MS/MS	Liquid chromatography−electrospray ionization tandem mass spectrometry
LC-MS/MS	Liquid chromatography-tandem mass spectrometry
Lgr5	Leucine-rich repeat containing G-protein-coupled receptor 5
MMR	Mismatch repair
MNU	*N*-methyl-*N*-nitrosourea
MOC	Mini organ cultures
MPS	Microphysiological systems

mRNA	Messenger RNA
NATs	*N*-acetyltransferases
NER	Nucleotide excision repair
NHEJ	Non-homologous end joining
N-OH-PhIP	*N*-hydroxy-2-amino-1-methyl-6-phenylimidazo[4,5-*b*]pyridine
NQO1	NAD(P)H:quinone oxidoreductase 1
OS	Oxidative stress
p21	Cyclin-dependent kinase inhibitor $p21^{CIP1}$
p53	Tumour protein 53
PAH	Polycyclic aromatic hydrocarbon
PBS	Phosphate-buffered saline
PCC	Proliferation and cell cycle control
PCNA	Proliferating cell nuclear antigen
PCR	Polymerase chain reaction
PGE2	Prostaglandin E_2
PhIP	2-Amino-1-methyl-6-phenylimidazo[4,5-*b*]pyridine
POR	NADPH:cytochrome P450 oxidoreductase
PPAR	Peroxisome proliferator-activated receptor
RFC	Replication factor C
ROS	Reactive oxidative species
RPA	Replication protein A
RT	Reverse transcription
RT-qPCR	Real time quantitative polymerase chain reaction
SD	Standard deviation
SDS-PAGE	Sodium dodecyl sulphate polyacrylamide gel electrophoresis
SEM	Standard error of the mean
SRM	Selected reaction monitoring
SSB	Single-strand breaks

STA	Specific target amplification
SULTs	Sulphotransferases
TBS(T)	Tris-buffered saline (0.1% Tween-20)
TC-NER	Transcription-coupled NER
Tetrol	BaP-tetrol-I-1; (±)-*r*-7,*t*-8,*t*-9,*c*-10-tetrahydroxy-7,8,9,10-tetrahydrobenzo[*a*]pyrene
TF	Transcription factors
TFIIH	Transcription factor II H
TGF	Transforming growth factor
tMS^2	Positive ion targeted MS^2
UGTs	Uridine diphosphate glucuronosyltransferases
UPL	Universal probe library
$UPLC\text{-}ESI/MS^3$	Ultra-performance liquid chromatography coupled with electrospray ionisation tandem mass spectrometry
USA	United States of America
UV	Ultraviolet
XAB2	XPA binding protein 2
XM	Xenobiotic metabolism
XMEs	Xenobiotic metabolising enzymes
XP	Xeroderma pigmentosum
XPA-G	Xeroderma pigmentosum proteins A-G

Chapter 1 Introduction

1.1 Cancer

The global burden of cancer is steadily increasing. Cancer is the first or second leading cause of death before the age of 70 in over 100 countries, accounting for 29.8% of deaths from noncommunicable diseases (Wild et al., 2020). In 2020 there were approximately 19.3 million new cancer cases and 9.9 million cancer deaths worldwide, and incidence is expected to rise by 47% in 2040 (Sung et al., 2021). More than half of these cases and deaths occurred in Asia, where almost 60% of the global population lives. This was followed by Europe with 22.8% of total cancer cases and 19.6% of deaths (although it has less than 10% of the global population), and the Americas with 20.9% and 14.2% cases and deaths, respectively (Sung et al., 2021). Cancer affects every region of the world; therefore, it is extremely important to continue to investigate its underlying causes to develop more initiatives for prevention and control of the disease (Sung et al., 2021).

Carcinogenesis is a complex multistep process that involves cells undergoing a series of alterations that lead to their uncontrolled growth. To achieve this, malignant cells accumulate multiple mutations in key genes, *i.e.,* oncogenes or tumour suppressor genes (Bertram, 2001). Hanahan and Weinberg (2000) suggested that there are six essential physiological alterations required for tumour growth and dissemination. The hallmarks of cancer are acquired capabilities that allow cancer cells to 1) proliferate independently of external growth signals, 2) evade growth suppressors, 3) resist cell death, 4) acquire limitless replicative potential, 5) induce angiogenesis and 6) invade and metastasise (Hanahan and Weinberg, 2000). These hallmarks were then updated, and two emerging hallmarks were added to the list: reprogramming of cellular energy metabolism and evasion of the immune system. Additionally, two enabling characteristics were described: the development of genomic instability and tumour-promoting inflammation (Hanahan and Weinberg, 2011). A diagram summarising the hallmarks and enabling characteristics of cancer is shown in Figure 1.1.

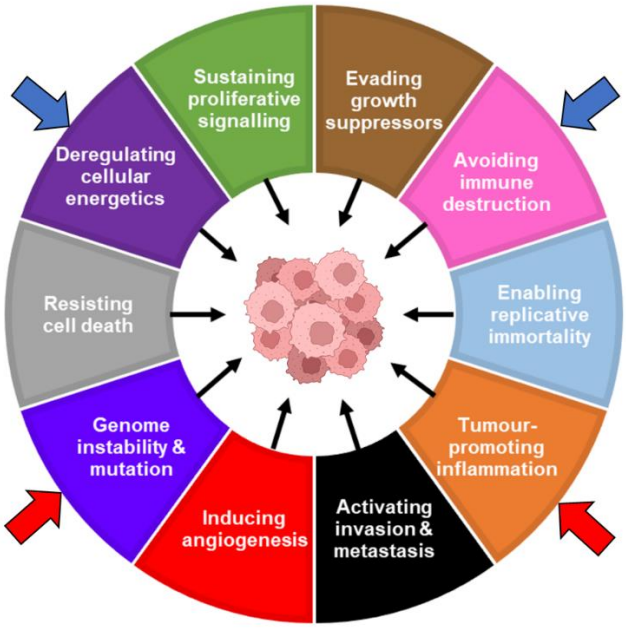

Figure 1.1. Hallmarks and enabling characteristics of cancer. The six original hallmarks described by Hanahan and Weinberg in 2000, along with the two emerging hallmarks (blue arrows) and enabling characteristics (red arrows) added in 2011. Adapted from Hanahan and Weinberg (2011). Created with BioRender.com.

Epidemiological data show that cancer incidence varies dramatically across populations, for example between countries with low and high human development indexes (HDI; Figure 1.2).

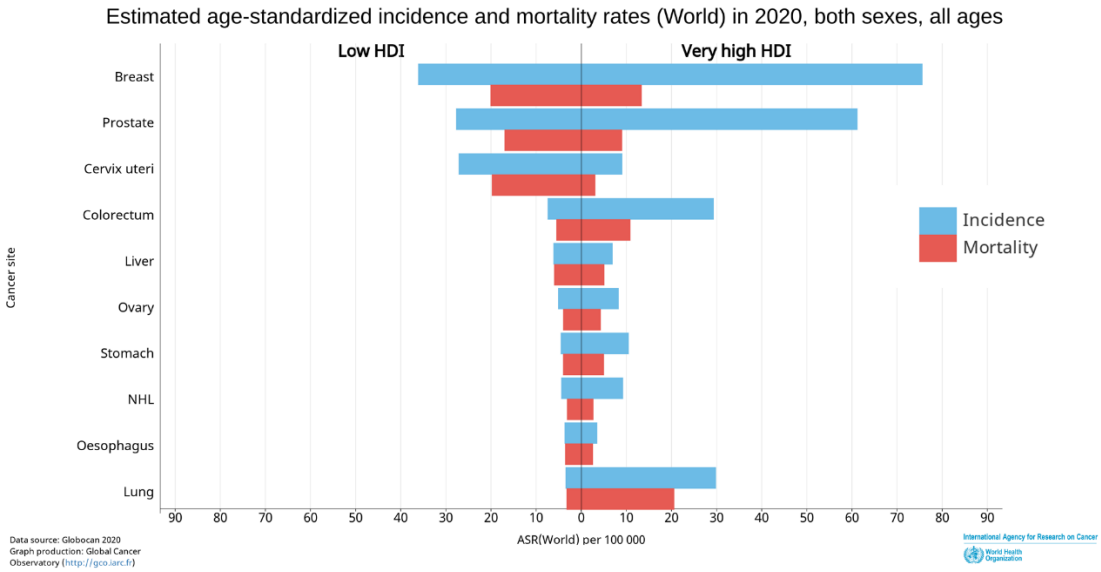

Figure 1.2. Estimated world age-standardised incidence and mortality rates in 2020 in low and very high HDI countries for the most common cancers. Data source: GLOBOCAN 2020; Graph production: Global Cancer Observatory (http://gco.iarc.fr/) 2021.

Except for certain familial cancers, the contribution of hereditary factors to cancer is a small proportion, whereas environmental factors are a main cause in sporadic cancers, as was highlighted by studies on twin cohorts from Denmark, Sweden, and Finland (Lichtenstein et al., 2000). A recent update on the twin studies, which also included cohorts from Norway, indicated a higher familial risk for more cancers, however, unique and common environmental factors could influence the onset and the risk of cancer development at certain sites, respectively (Harris et al., 2019). Moreover, this has been supported by studies on cancer incidence in migrant populations showing that they acquire the pattern of local cancer risk (Jaehn et al., 2019; McDonald et al., 2017; Peto, 2001; van der Wal et al., 2019). Due to the strong influence of environmental factors such as life-style choices including smoking, alcohol consumption and an unhealthy diet (including obesity), occupational exposures, and infections, it is thought that more than 40% of sporadic cancers could be prevented (Danaei et al., 2005). In 2015 a vast number of cancer cases attributable to known risk factors could have been reduced by avoiding the use of tobacco and more than 20000 cases in the UK could have been avoided by maintaining a healthy body weight. Overall, if exposure to the risk factors presented in Figure 1.3 was reduced, more than 135000 cases of cancer could be prevented every year in the UK (Brown et al., 2018).

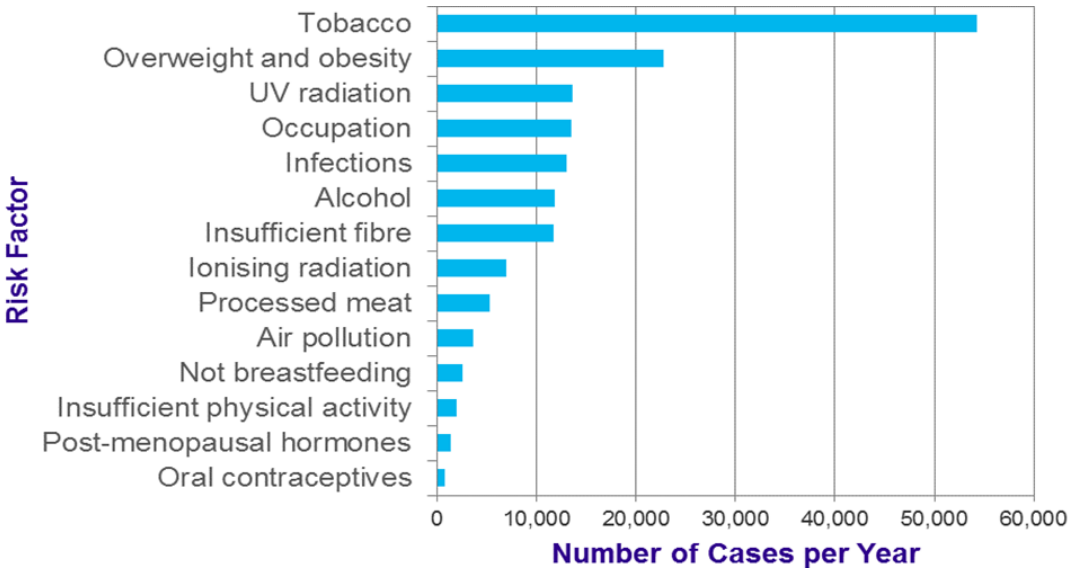

Figure 1.3. Environmental risk factors by cancer incidence suggesting number of preventable cases in the UK for both sexes in 2015. Data Source: Brown et al., (2018). Graph source: cruk.org/cancerstats.

1.2 Environmental carcinogenesis

The link between environmental pollutants and disease has been considered for centuries, with some of the first carcinogenic compounds being identified due to occupational exposures (Luch, 2005). In 1761, John Hill described the relationship between long-term use of snuff and the occurrence of cancer in the nasal mucosa (Hill, 1761). A few years later, Percival Pott associated high incidence of scrotal cancer in chimney sweepers with their prolonged exposure to soot (Pott, 1775). After this the study of the links of cancer with chemical exposure continued, and by 1907 it was officially recognised in Great Britain that exposure to pitch or tar could lead to cancer in any cutaneous site (Henry, 1946). But it was not until 1915 that chemically induced cancer could be reproduced in an experimental model (Luch, 2005). Yamagiwa and Ichikawa (1918), performed a series of experiments in which they painted the ears of rabbits with coal-tar, leading to the formation of carcinomas, particularly on the inner surface of the ear. Later, the attempts of Kennaway, Cook and colleagues to characterise the carcinogens present in coal tar led to the identification and isolation of the polycyclic aromatic hydrocarbon (PAH) benzo[*a*]pyrene (BaP) (Cook et al., 1933).

The first studies on the mechanisms of action of carcinogens showed that compounds could bind to cellular macromolecules, by showing the covalent binding of carcinogens to proteins in rat liver and then in mouse skin (Miller, 1951; Miller and Miller, 1947). Around the same time, it was demonstrated that some carcinogens ('procarcinogens') require enzymatic activation into their carcinogenic forms by using rat liver microsomes (Mueller and Miller, 1948). Soon after, it was also shown that certain carcinogens are capable of inducing microsomal proteins (Conney et al., 1956). After the discovery of the structure of DNA by Watson and Crick in 1953, studies by Brookes and Lawley showed that the extent of binding to DNA of a PAH correlated to its carcinogenic potential (Brookes and Lawley, 1964). This observation was supported by previous investigations where the carcinogen 'nitrogen mustard' was found to interact with DNA *in vivo* (Wheeler and Skipper, 1957). The subsequent development of the 'Ames Test' in 1973 showed

that many of these carcinogens were mutagens and therefore the bacterial test allowed the identification of potential carcinogenic chemicals (Ames et al., 1973; Zeiger, 2019).

Since the establishment of the International Agency for Research of Cancer (IARC) in 1965, hundreds of compounds have been classified as known or suspected human carcinogens, as shown in Table 1.1. The agents considered by IARC comprise chemicals, including complex mixtures, physical and biological agents (Cogliano et al., 2011), and their biological activity and carcinogenic risk to humans are compiled in a series of monographs. Examples of carcinogenic environmental agents are given in Table 1.2.

Table 1.1. Classification of carcinogens according to the IARC Monographs.

Group 1	Carcinogenic to humans	121 agents
Group 2A	Probably carcinogenic to humans	90 agents
Group 2B	Possibly carcinogenic to humans	323 agents
Group 3	Not classifiable as to its carcinogenicity to humans	498 agents

Adapted from https://monographs.iarc.who.int/

Table 1.2. Examples of Group 1 environmental agents according to carcinogen type and associated cancer site with sufficient evidence in humans.

Carcinogen	**Type**	**Cancer site**
Aflatoxins	Chemical	Liver
Alcoholic beverages	Chemical	Liver, oral cavity, pharynx, oesophagus, colorectal, larynx, breast
Aristolochic acid	Chemical	Renal pelvis and ureter
Benzo[*a*]pyrene	Chemical	Lung
Engine exhaust, diesel	Chemical (complex mixture)	Lung
Helicobacter pylori	Biological	Stomach, leukaemia and/or lymphoma
Hepatitis B virus	Biological	Liver
Human papillomavirus	Biological	Cervix, oral cavity, tonsil, pharynx, anus, vagina, vulva, penis
Solar radiation	Physical	Skin (melanoma, basal and squamous cell carcinoma)
Tobacco smoking	Chemical (complex mixture)	Lung, oral cavity, colorectal, stomach, oesophagus, nasopharynx, liver, pancreas, ovary, cervix, urinary tract, leukaemia and/or lymphoma

Taken from IARC https://monographs.iarc.who.int/ and Cogliano et al., (2011).

After the most recent review of all the Group 1 carcinogens a few challenges in the evaluation of the evidence for carcinogen hazard identification were identified (Smith et al., 2016). First, it was noted that there was no systematic method for identifying, organising and summarising relevant mechanistic data. It was also evident that human carcinogens share a number of characteristics related to the mechanisms by which these agents cause cancer, and each agent may present a different number of these characteristics. Lastly, for many of the carcinogens evaluated before monograph 100 few data were available on important mechanisms such as epigenetic alterations (Guyton et al., 2018b, 2018a; Smith et al., 2016). Therefore, to address these issues a group of experts identified 10 key characteristics (KCs) that represent the majority of established properties of human carcinogens; these are summarised in Table 1.3. It is important to point out that the KCs are distinct to the hallmarks of cancer (Section 1.1), as the former are the 'properties of human carcinogens' and the latter are the 'properties of cancer cells' (Smith et al., 2020).

The KCs have been used by IARC since 2015 to evaluate more than 30 different chemicals and it has been demonstrated that they facilitate the identification of gaps in evidence and prevent the introduction of bias in the assessment of carcinogenic hazards (Guyton et al., 2018b). Although this approach allows a more comprehensive analysis of data in cancer hazard identification, there are still areas for improvement. Recently, Smith et al., (2020) published a more detailed definition of the KCs and highlighting some of the biomarkers and assays that can be used to measure them in different experimental settings. For example, the electrophilic activity of carcinogens can be assessed *in vivo* and *in vitro* by measuring DNA and protein adducts; genotoxicity can be studied by next generation high-throughput sequencing or by the micronucleus, transgenic rodent mutation assays (*e.g.*, mutations in Big Blue rat) and comet assays; alterations in DNA repair or genomic instability can be tested by karyotyping or next-generation sequencing; and epigenetic alterations can be investigated by histone mapping and by bisulfite and/or RNA sequencing. However, development and optimisation of more assays are required

to fill in research gaps in certain KCs, including *in vivo* alternatives such as organoids (described in Section 1.6) (Smith et al., 2020).

Table 1.3. Key characteristics of carcinogens.

Characteristic	Example of relevant evidence
Is electrophilic or metabolically activated	Parent compound or metabolite with an electrophilic structure (*e.g.*, epoxide, quinone, etc.), formation of DNA and protein adducts
Is genotoxic	DNA damage (DNA strand breaks, DNA-protein cross-links, unscheduled DNA synthesis), intercalation, gene mutations, cytogenetic changes (*e.g.*, chromosome aberrations, micronuclei, aneuploidy)
Alters DNA repair or causes genomic instability	Alterations of DNA replication or repair (*e.g.*, topoisomerase II, base-excision or double-strand break repair, cell cycle regulation)
Induces epigenetic alterations	DNA methylation, histone modification, microRNA expression
Induces oxidative stress	Oxygen radicals, oxidative stress, oxidative damage to macromolecules (*e.g.*, DNA, lipids, proteins)
Induces chronic inflammation	Elevated white blood cells, myeloperoxidase activity, altered cytokine and/or chemokine production
Is immunosuppressive	Decreased immunosurveillance, immune system dysfunction
Modulates receptor-mediated effects	Receptor in/activation (*e.g.*, ER, PPAR, AhR) or modulation of endogenous ligands (including hormones)
Causes immortalisation	Inhibition of senescence, cell transformation
Alters cell proliferation, cell death or nutrient supply	Increased proliferation, decreased apoptosis, changes in growth factors, energetics and signalling pathways related to cellular replication or cell-cycle control, angiogenesis

Taken from Smith et al., (2016).

1.2.1 Metabolic activation of carcinogens

Chemical carcinogens can function either by genotoxic (induce damage to DNA) or non-genotoxic mechanisms. Some genotoxic carcinogens can directly react with DNA to cause mutagenesis (*e.g.,* alkylating agents), but most need enzymatic bioactivation to exert their mutagenic carcinogenic effects (Gonzalez and Kimura, 2001; Kondo et al., 2010). Procarcinogens such as PAHs, heterocyclic aromatic amines (HAAs) and mycotoxins are metabolised into electrophilic compounds by xenobiotic-metabolising enzymes (XMEs). XME gene expression is tissue-specific, time-specific, organ-specific

and cell-type-specific. Additionally, there are human polymorphisms in these enzymes that may be key in determining cancer susceptibility (Landi et al., 2005; Nebert, 1997; Nebert and Dalton, 2006; Stanley, 2017).

The metabolism of xenobiotics, such as drugs and environmental chemicals, can be divided into three phases: phase I (oxidation, functionalisation), phase II (conjugation) and phase III (xenobiotic transport) (Nebert and Dalton, 2006; Omiecinski et al., 2011; Stanley, 2017). Most of the reactions in phase I are catalysed by cytochrome P450 (CYP) enzymes, which are capable of bioactivating and detoxifying several environmental carcinogens. CYPs were discovered by Klingenberg in 1958, who described a new carbon monoxide binding pigment in rat liver microsomes with an absorption at 450 nm (Klingenberg, 1958). This pigment was later characterised by Omura and Sato (1962) and shown to be a haemoprotein. Since then, 57 human CYP genes have been identified, classified in 18 families (Nebert et al., 2013). CYPs contribute to around 66% of the bioactivation of carcinogens, of which 77% is due to six enzymes: CYP 1A1 (20%), 1A2 (17%), 1B1 (11%), 2A6 (8%), 2E1 (11%), and 3A4 (10%) (Figure 1.4 A), which differs from the contribution of these enzymes to drug metabolism where CYP 3A4 is the major contributor (Figure 1.4 B) (Rendic and Guengerich, 2012, 2015). These enzymes hydroxylate procarcinogens into poorly reactive stable compounds or unstable reactive oxygenated intermediates that can covalently bind to nucleic acids and proteins (Nebert and Dalton, 2006). Another important phase I enzyme is the flavoprotein NAD(P)H:quinone oxidoreductase 1 (also called NAD(P)H quinone dehydrogenase 1; NQO1), which is a two-electron reductase that catalyses the conversion of quinones to hydroquinones with the aid of NAD(P)H as a reducing cofactor (Ross and Siegel, 2004; Ross et al., 2000). Other phase I enzymes include hydroxylases, reductases, cyclooxygenases and oxidases.

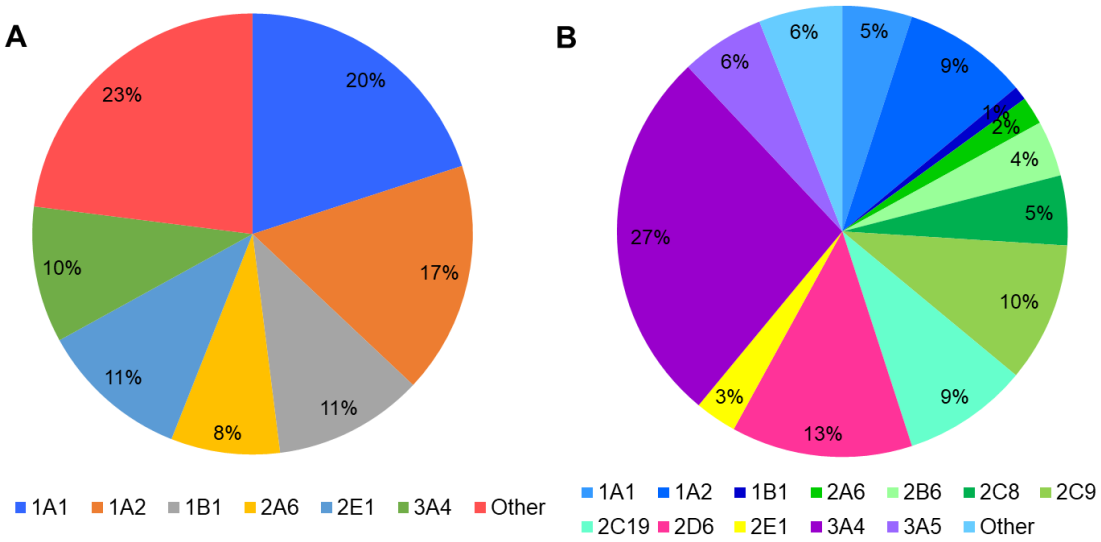

Figure 1.4. Contribution of individual CYP enzymes to the bioactivation of carcinogens (A) and drug metabolism (B). Data from Rendic and Guengerich (2012, 2015).

Phase II reactions are catalysed by XMEs such as uridine diphosphate glucuronosyltransferases (UGTs), glutathione *S*-transferases (GSTs), sulphotransferases (SULTs), epoxide hydrolases or *N*-acetyltransferases (NATs) (Stanley, 2017). This phase consists of conjugation reactions where sulphate, glucuronic acid, mercapturic acid, methyl, and acetylated moieties are added to xenobiotics or their metabolites to make them more polar and to facilitate their excretion (Nebert and Dalton, 2006; Omiecinski et al., 2011). However, conjugation can sometimes lead to further activation of the compounds by forming highly electrophilic compounds that, as previously mentioned, can interact with macromolecules like DNA (Luch, 2005; Stanley, 2017). Lastly, phase III involves the export of the compounds from the cells by energy-dependent transporters such as the ATP-binding cassette superfamily (Stanley, 2017). The metabolic activation of the compounds tested in this study is described in Section 1.4.

1.2.2 DNA damage induced by carcinogens

As previously mentioned, carcinogens can induce damage either by directly interacting with DNA or by non-genotoxic mechanisms such as endocrine modifications, altered inflammatory responses and immune suppression (Hernández et al., 2009). Here, the

focus will be on genotoxic carcinogens, their reactive metabolites, and their modes of action.

Genotoxic carcinogens can induce chromosomal and DNA alterations. One of the main modifications carcinogens or their reactive metabolites can induce in DNA is the formation of covalent adducts. These are generally caused by the binding of compounds to the purine and pyrimidine bases, particularly to guanines (Phillips and Arlt, 2009; Poirier et al., 2000). The presence of DNA adducts in certain positions of the bases (*e.g.,* position N7 of guanine) can destabilise the base-sugar bond and trigger the loss of the affected base causing the formation of apurinic/apyrimidinic sites. In addition, some carcinogens can cause inter- or intra-strand crosslinks in DNA, which are covalent links between two bases in opposite DNA strands or within the same strand, respectively (Phillips and Arlt, 2009). Carcinogens can also cause DNA damage by promoting oxidative stress. Xenobiotics can generate reactive oxidative species (ROS) or free radicals either through their bioactivation reactions or by activating endogenous sources of ROS. Oxidative damage to DNA leads to breaks in the sugar-phosphate backbone of one (single-strand breaks; SSB) or both DNA strands (double-strand breaks; DSB), crosslinking or base modifications. The major ROS induced adduct is 8-hydroxy-2′-deoxyguanosine, which is formed by the oxidation of a guanine at the C8 position and is used as a biomarker for oxidative damage to DNA (Barnes et al., 2018; Chao et al., 2021; Klaunig et al., 2011; Valko et al., 2006).

The formation of DNA adducts can result in mutations that activate proto-oncogenes such as *RAS* or alter the function of tumour suppressor genes like *TP53*. Mutations at different sites of these genes have been found in different human tumours and are useful when linking the exposure to certain carcinogens and certain cancer types (Phillips and Arlt, 2009).

Several methods of DNA adduct detection have been developed, including ^{32}P-postlabelling, immunoassays, immunohistochemistry, gas chromatography/mass spectrometry and liquid chromatography/mass spectrometry (Krais et al., 2019). These

techniques have been used to detect adducts in a variety of tissues and cell types, and in the urine of experimental animals and humans (Yun et al., 2020). Associations between adduct formation, mutation and tumour incidence have been found, experimental studies have showed that at low doses there is a linear relationship between adduct levels, dose, and tumour outcome, however, the linearity is lost at high doses (Phillips and Arlt, 2009; Poirier et al., 2000). It has also been demonstrated that genotoxic carcinogens do not always form tumours in the presence of adducts, but there is no tumour formation without adducts, therefore, other events, including some that are tissue-specific, may be necessary for tumour formation (Poirier, 2016; Poirier et al., 2000). Tissue-specificity, or organotropism, is covered in more detail in Section 1.5.

1.2.3 DNA damage response

DNA damage caused by both endogenous and exogenous sources, including DNA adduct formation, can lead to the incorporation of mutations if not repaired correctly. To reduce the frequency of this happening, cells have DNA damage response (DDR) pathways that can sense the damage and trigger responses according to the damage (Figure 1.5). DDR pathways are controlled by cell cycle checkpoints that when activated can lead to cell cycle arrest and repair of the damaged DNA or, if repair is not possible, the cells may become senescent or undergo apoptosis (Roos et al., 2016). When these mechanisms fail replication of the damaged DNA template during cell division can lead to the misreading of the sequence and incorporation of the wrong base and, if critical genes are mutated, the carcinogenesis process may be initiated (Branzei and Foiani, 2008; Hakem, 2008).

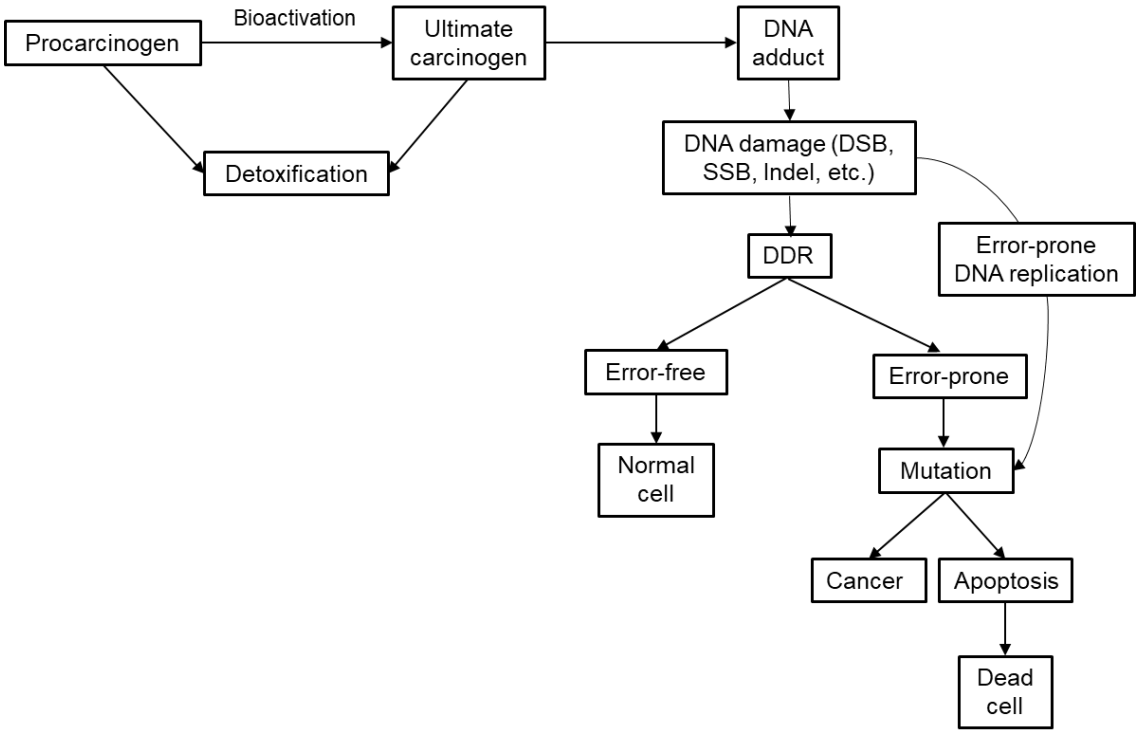

Figure 1.5. Cellular responses to DNA damage. Procarcinogens can be bioactivated into ultimate carcinogens or detoxified. Ultimate carcinogens lead to the formation of DNA adducts which damage DNA. This damage can be repaired by DDR via error-free or error-prone pathways. Error-prone DNA replication can also lead to mutations. Adapted from King and Robins (2006).

The DDR consists of a series of events that start with the detection of the damage by sensor proteins such as γ-H2AX, ataxia telangiectasia mutated (ATM) and ataxia telangiectasia mutated and Rad3 related (ATR). This is followed by the activation of transducers, which transmit the signal (*e.g.*, CHK1 and CHK2), and the induction of effectors that mediate the outcomes (*i.e.*, apoptosis, cell cycle arrest, repair, senescence) like p53 and p21 (Blanpain et al., 2011; Srinivas et al., 2019). The repair pathways triggered depend on the type of damage, for example: DSB, SSB and crosslinks are repaired by non-homologous end joining (NHEJ) or homologous recombination (HR) depending on cell cycle stage; SSB and small adducts can be repaired by base excision repair (BER); base mismatches, deletions and insertions are repaired by mismatch repair (MMR); and bulky DNA adducts are repaired by nucleotide excision repair (NER), which will be the focus here (Figure 1.6) (Blanpain et al., 2011; Roos et al., 2016).

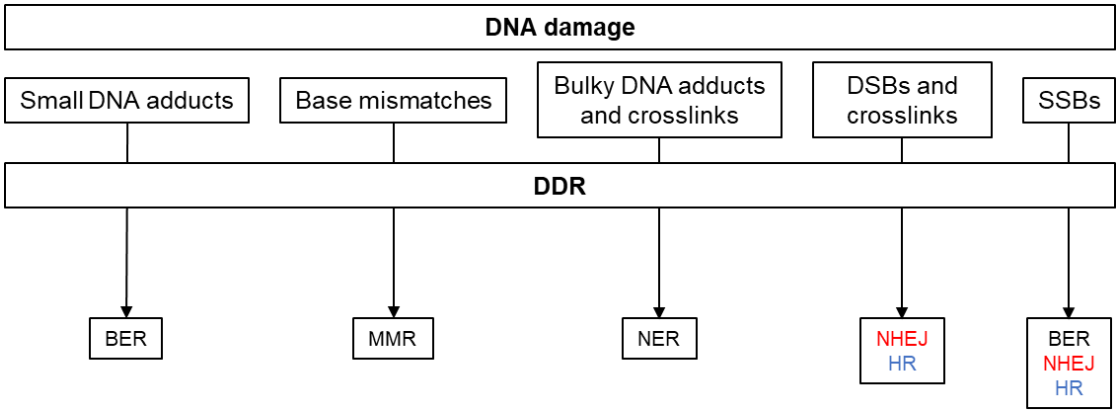

Figure 1.6. Repair pathways triggered according to the type of DNA damage. Pathways in blue and red are known for being error-free and error-prone, respectively. See text for more details. Adapted from Roos et al., (2016).

There are two NER sub-pathways, global genome (GG-) NER, which can occur throughout the genome, and transcription-coupled (TC-) NER, which repairs lesions in the transcribed strand of active genes (Schärer, 2013). Although they are initiated by different factors, they both require core NER factors to complete the process (Figure 1.7). While GG-NER is initiated by the xeroderma pigmentosum group C (XPC) and human homologue of RAD23B (hHR23B) complex together with damaged DNA-binding proteins (DDB), TC-NER is initiated when RNA polymerase is blocked at the sites of damage with the help of Cockayne syndrome related proteins, CSA and CSB, and XAB2 (XPA binding protein 2) (Melis et al., 2011; Schärer, 2013). After the recognition step, the transcription factor II H (TFIIH), comprised of 10 subunits, is recruited and the DNA around the damage is unwound by the helicases, XPB and XPD. This is followed by the formation of the preincision complex around the damaged site to confirm the lesion and allow the assembly of the repair machinery, this consists of XPA, replication protein A (RPA) and XPG. Once this complex is correctly positioned, endonucleases XPG and excision repair cross complementing 1 (ERCC1)-XPF carry out 3' and 5' incisions, respectively, that result in the excision of a single strand fragment of 24-32 nucleotides. This excision is then repaired by DNA synthesis, using the opposite, undamaged, DNA strand as template, and ligation into its original undamaged state. This final step is carried out by DNA polymerase Ɛ or δ, replication factor C (RFC), proliferating cell

nuclear antigen (PCNA), RPA and ligase I or III (Melis et al., 2011; Petruseva et al., 2014; Schärer, 2013).

Mutations in genes encoding for proteins involved in the DDR pathways lead to increased cancer risk demonstrating the importance of these pathways. A clear example is Xeroderma pigmentosum (XP), a disease in which the NER pathway is impaired. As NER is responsible for the repair of ultraviolet (UV)-induced DNA damage, people suffering from XP are prone to develop skin cancer from an early age. They have more than a 1000-fold increased risk of skin cancer and 10-20-fold increase in developing internal cancers (Melis et al., 2011). In another example, mutations in *BRCA1* and *BRCA2*, two genes encoding for proteins involved in the HR DNA repair pathway, are linked to increased risk in breast and ovarian cancer (Narod and Foulkes, 2004). Moreover, mutations in MMR pathway components lead to an 80% lifetime risk of developing hereditary nonpolyposis human colorectal cancer or Lynch syndrome (Blanpain et al., 2011; Hakem, 2008). These are only a few examples of increased cancer predisposition related to defects in the DDR pathways, several other disorders, including other cancer types and developmental disorders, result from faults in these mechanisms (Hakem, 2008).

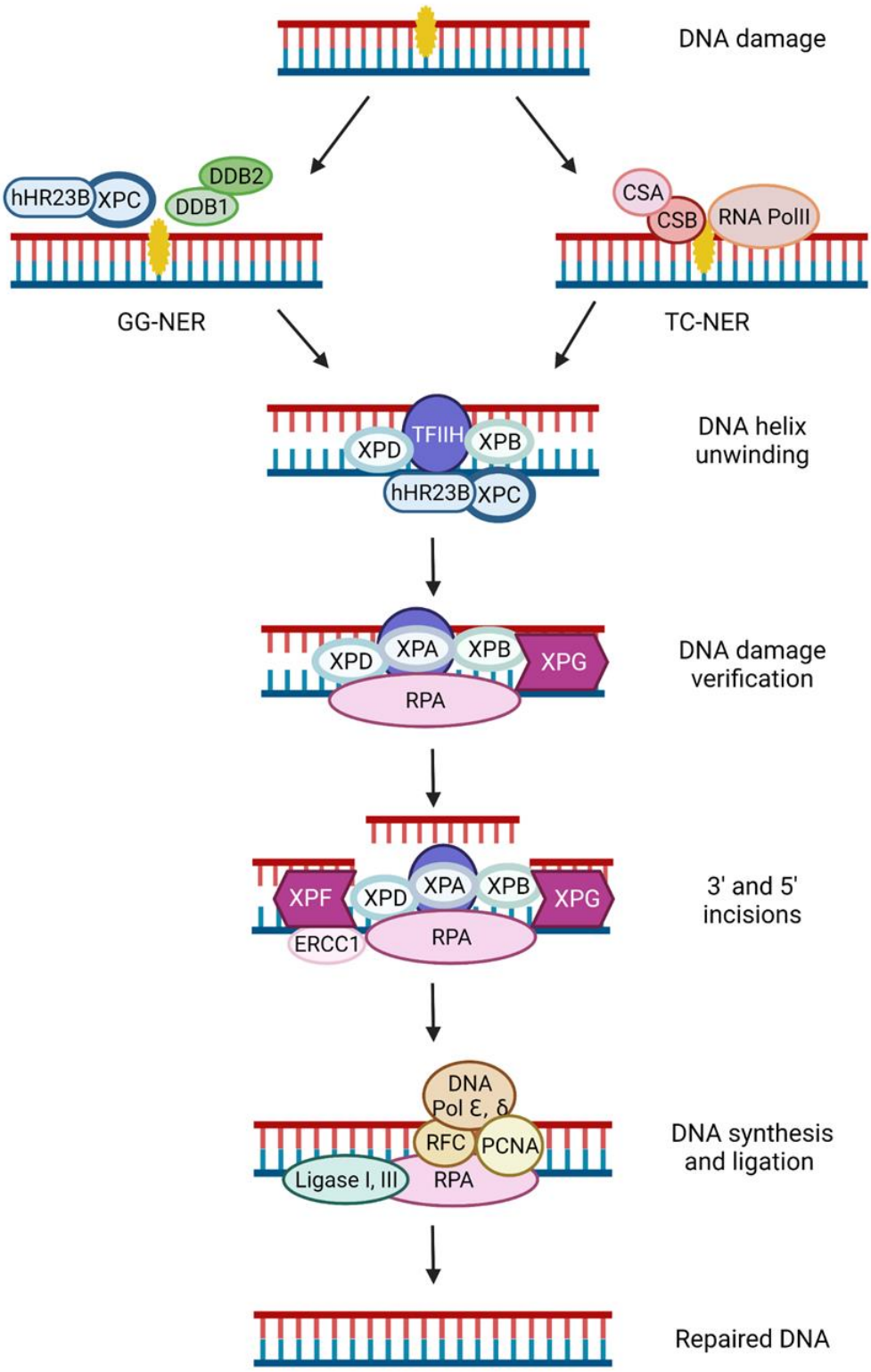

Figure 1.7. Overview of the nucleotide excision repair pathway. See text for details. Adapted from Melis et al., (2011). Created with BioRender.com.

1.3 Genes and cancer

As previously discussed, carcinogenesis is a multistep process and it has traditionally been divided in three steps: initiation, promotion, and progression. The initiation step

involves irreversible alterations of DNA, like gene mutations, which can be spontaneous or induced by exposure to carcinogens. Promotion consists of the expansion of the initiated cells, driven by the continued exposure to the promoting agent or genomic changes associated with regulation of cell proliferation. This step is reversible as it could be altered by chemopreventive agents. Lastly, the progression step results from the accumulation of major genetic alterations, including chromosomal aberrations, and can lead to fast tumour growth, invasion, and metastasis (Pitot, 1993; Siddiqui et al., 2015).

Cancer cells accumulate mutations over time, and they are classified depending on their role in cancer development as driver and passenger mutations. Driver mutations have been selected during the carcinogenesis process as they benefit cancer cells by giving them growth advantages and it is likely that cancers require more than one driver mutation to develop. Passenger mutations are all the other mutations present in the tumour but that don't have an effect in the tumour formation process (Stratton et al., 2009). Driver mutations occur in oncogenes, tumour suppressor and stability genes, *e.g.*, DNA repair, cell cycle control, etc. Mutations in oncogenes are dominant and only one allele needs to be mutated to contribute to the carcinogenesis process. Oncogenes control cell growth and differentiation, and mutations usually result in increased proliferative activity. Tumour suppressors inhibit proliferation and when they are mutated, the result is a loss of protein function. These mutations are recessive, therefore both alleles need to be mutated or one allele needs to be mutated and the other one lost (loss of heterozygosity) (Stratton et al., 2009; Venitt, 1994; Vogelstein and Kinzler, 2004). Stability genes are responsible for preventing or correcting DNA alterations and are involved in processes like DNA repair, mitotic recombination, and chromosome segregation. Generally, stability genes require both alleles to be mutated for a physiological effect to be seen and their inactivation leads to an increased mutation rate in both passenger and cancer driver genes (Vogelstein and Kinzler, 2004). Table 1.4 shows examples of genes that are commonly mutated in cancer.

Table 1.4. Examples of genes driving carcinogenesis.

Gene	Function	Associated cancer
Oncogene		
BCL2	Inhibits apoptosis	Lymphoma
MYC	Transcription factor	Lymphomas, neuroblastomas, small cell lung cancers
MDM2	Inactivates p53	Sarcomas
Tumour suppressors		
TP53	Regulates cell cycle, apoptosis, DNA repair	Most adult cancers
AXIN2	Regulates WNT pathway	Colon
RB1	Regulates cell cycle	Eye
Stability genes		
BRCA1	DNA repair	Breast, ovary
BRCA2	Transcription factor, DNA repair	Breast, ovary, colon
ATM	DNA damage sensor	Leukaemia, lymphoma, brain

Adapted from Vogelstein and Kinzler (2004)*, Vogelstein et al.,* (2013) *and Kopnin* (2000)*.*

1.4 Test carcinogens

The following test carcinogens have been selected for the treatment of human tissue organoids as they are dietary genotoxic carcinogens with well-characterised modes of action. Their sources of exposure, effects on human health and metabolic pathways are presented here in more detail.

1.4.1 Benzo[*a*]pyrene

PAHs are formed by the incomplete combustion of organic matter and humans are exposed to them daily through air pollution, tobacco smoke, diet, and occupational exposure (IARC, 2012a; Phillips, 1999). The diet is the major source of PAH exposure as they have been found in uncooked foods, possibly due to soil, water, and air contamination, as well as food preservation processes like curing, and the cooking of foods at high temperatures like grilling, frying, and smoking (Phillips, 1999; Sampaio et al., 2021). Many PAHs are carcinogenic and mutagenic and are thought to make a considerable contribution towards the overall cancer burden in humans. Exposure to

these compounds has been linked to the development of a number of human cancers including skin, lung and bladder (Baird et al., 2005; Phillips, 1983, 1999).

BaP is the most studied PAH, and it is used as an indicator of environmental exposure and as a model of PAH carcinogenicity (Boström et al., 2002; Boysen and Hecht, 2003). Due to the confirmed carcinogenicity of BaP in animals, the evidence of tumours in humans exposed to BaP-containing PAH mixtures, and taking into account its known mechanistic data, it has been classified as a human carcinogen (Group 1) by IARC (IARC, 2012a). As for other PAHs, BaP is a chemically inert compound that requires metabolic activation to exert its biological effects. In general, PAHs are metabolised into diol epoxides that can covalently bind to macromolecules such as DNA (Phillips, 1983). BaP metabolism involves the action of phase I and II enzymes, and its activation is mainly catalysed by CYP1A1 and CYP1B1 (Arlt et al., 2008). During the first reaction an epoxide group is added to form BaP-7,8-epoxide. This intermediate is then converted to BaP-7,8-dihydrodiol by epoxide hydrolase. This metabolite can be further metabolised by CYPs to produce the ultimate carcinogen benzo[*a*]pyrene-7,8-diol-9,10-epoxide (BPDE). BPDE reacts with DNA to form bulky DNA adducts preferentially at the N^2 position of guanine residues, resulting in 10-(deoxyguanosin-N^2-yl)-7,8,9-trihydroxy-7,8,9,10-tetrahydro-BaP (dG-N^2-BPDE) adducts. Misreplication of dG-N^2-BPDE adducts leads principally to GC to TA mutations (Alexandrov et al., 2016; Arlt et al., 2008; Baird et al., 2005; Boysen and Hecht, 2003; IARC, 2012a). BPDE has also been found to form small amounts of adducts at the N^6 position of adenines, 10-(deoxyadenosin-N^6-yl)-7,8,9-trihydroxy-7,8,9,10-tetrahydro-BaP (dA-N^6-BPDE), however these appear to be less promutagenic (Chakravarti et al., 2008; Chen et al., 1996). Acid hydrolysis of DNA containing dG-N^2-BPDE adducts releases BaP-tetrols, which are sometimes used to measure the levels of BPDE-adducts (Boysen and Hecht, 2003). A scheme of the metabolic activation of BaP can be found in Figure 1.8.

In addition to the diol epoxide pathway described above, BaP can also be metabolised through the radical cation mechanism to form unstable depurinating adducts, and the

ortho quinone pathway leading to the formation of unstable depurinating and stable adducts, and ROS (IARC, 2012a; Krais et al., 2019; Shimada, 2006). Moreover, BaP is an aryl hydrocarbon receptor (AhR) ligand, therefore it can induce the expression of enzymes such as *CYP1A1* and *CYP1B1* to enhance its own bioactivation. Lastly, the detoxification of BaP is catalysed by several enzymes including GSTs, SULTs, UGTs and epoxide hydrolases. Additionally, NQO1 has been found to reduce quinone-mediated DNA damage (Baird et al., 2005; Luch and Baird, 2005; Shimada, 2006). Genetic polymorphisms in phase I and II enzymes can alter their catalytic activity and therefore influence the levels of activation and/or detoxification of BaP and its metabolites and thus genotoxicity. For example, some polymorphisms in *SULT1A1* have been reported to have lower activity and to increase risk of lung cancer (Shimada, 2006).

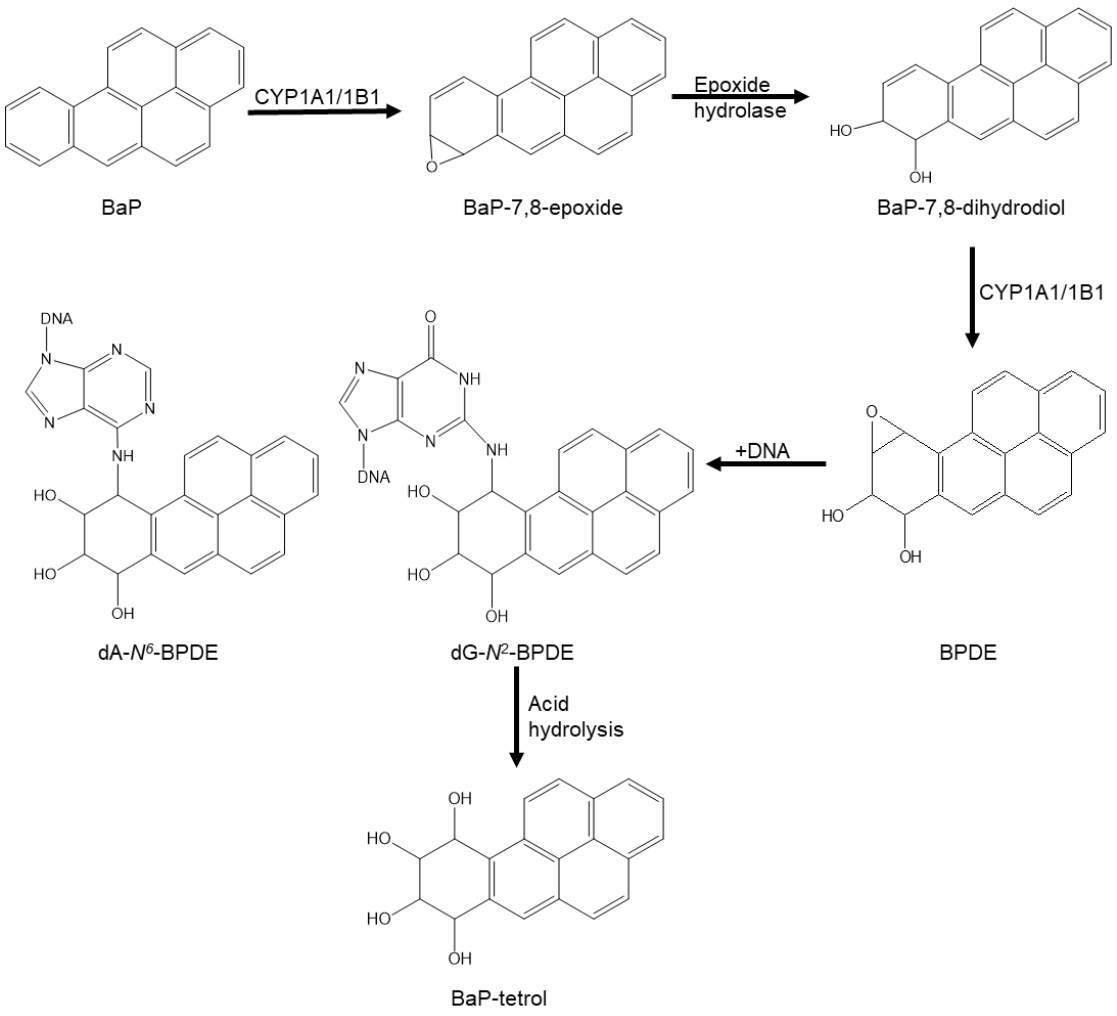

Figure 1.8. Metabolic activation and DNA adduct formation by BaP. See details in text. Adapted from Moserovä et al., (2009) and Boysen and Hecht (2003).

1.4.2 Aflatoxin B_1

Aflatoxins are mycotoxins mainly produced by the *Aspergillus flavus* and *Aspergillus parasiticus* fungi. These contaminate food commodities, including maize and nuts, in the fields and when not properly stored (Liu and Wu, 2010). Aflatoxin B_1 (AFB_1) is the most potent naturally produced liver carcinogen and has been classified as an IARC Group 1 human carcinogen (IARC, 2002, 2012a). AFB_1 contamination is prevalent worldwide, but it is higher in areas with high temperatures and humidity, such as Southeast Asia and Sub-Saharan Africa. However, it is expected that due to climate change additional regions start to see higher levels of AFB_1 contamination in their crops (Battilani et al., 2016; Haerani et al., 2020). In 2010 it was calculated that AFB_1 exposure was responsible for 4.6-28.2% of all global hepatocellular carcinoma (HCC) cases, with the majority of these cases being in Africa (40%) and Southeast Asia (27%). The HCC risk attributable to AFB_1 exposure is increased by 30-fold when combined with Hepatitis B virus (HBV) infections, which are also prevalent in these areas (Liu and Wu, 2010).

AFB_1 is activated primarily by liver CYPs, mainly CYP3A4 and CYP1A2, to produce the ultimate carcinogen AFB_1-8,9-epoxide (AFBO), which has two isomers: *exo*- and *endo-epoxide*, of which only the *exo* isomer is genotoxic due to its higher affinity to guanine residues in DNA (Guengerich et al., 1998). At high concentrations of AFB_1 CYP3A4 is the main enzyme producing AFBO, while at low concentrations CYP1A2 has this role (Deng et al., 2018; Rushing and Selim, 2019). This metabolite is highly electrophilic and can bind covalently to DNA to form adducts at guanine residues, 8,9-dihydro-8-(N^7-guanyl)-9-hydroxy-AFB_1 (AFB_1-N^7-Gua). These adducts are unstable and can either undergo depurination or convert into open ring structures. The first leads to the creation of apurinic sites on the DNA backbone and the release of free AFB_1-N^7-guanine in urine, which can then be used as a biomarker for AFB_1 exposure. The second leads to the formation of stable 8,9-dihydro-8-(2,6-diamino-4-oxo-3,4-dihydropyrimid-5-yl-form-amido)-9-hydroxyaflatoxin B_1 (AFB_1-FapyGua) adducts (Rushing and Selim, 2019). A scheme of this process can be found in Figure 1.9. Both lesions are precursors of DNA

mutations that, depending on their location in the genome, can be the start of the carcinogenesis process. One of the most common mutations associated with AFB_1 exposure is the G to T transversion in *TP53*, which is almost exclusively at codon 249 in human liver tumours (Benkerroum, 2020; Rushing and Selim, 2019).

As AFBO is unstable, it can hydrolyse to form AFB_1 dihydrodiol which is in equilibrium with AFB_1 dialdehyde. This metabolite can bind to the N-termini and lysine side chains of proteins forming protein adducts, which can also serve as biomarkers of exposure (Rushing and Selim, 2019). Additionally, AFB_1 can be hydroxylated into other more polar and less toxic metabolites. The main one is aflatoxin M_1 (AFM_1), which is commonly detected in milk of humans and cattle and is produced by the action of CYP1A2. It has been shown that AFM_1 induces tumours in rats and rainbow trout, and it is classified as an IARC Group 2B carcinogen (possibly carcinogenic to humans) (Marchese et al., 2018; Rushing and Selim, 2019). AFQ_1 and AFP_1 are some of the main AFB_1 detoxication products which are also produced by CYP enzymes. Lastly, the conjugation reaction of AFBO by GSTs is also involved in the detoxication of AFB_1 (Deng et al., 2018; Rushing and Selim, 2019).

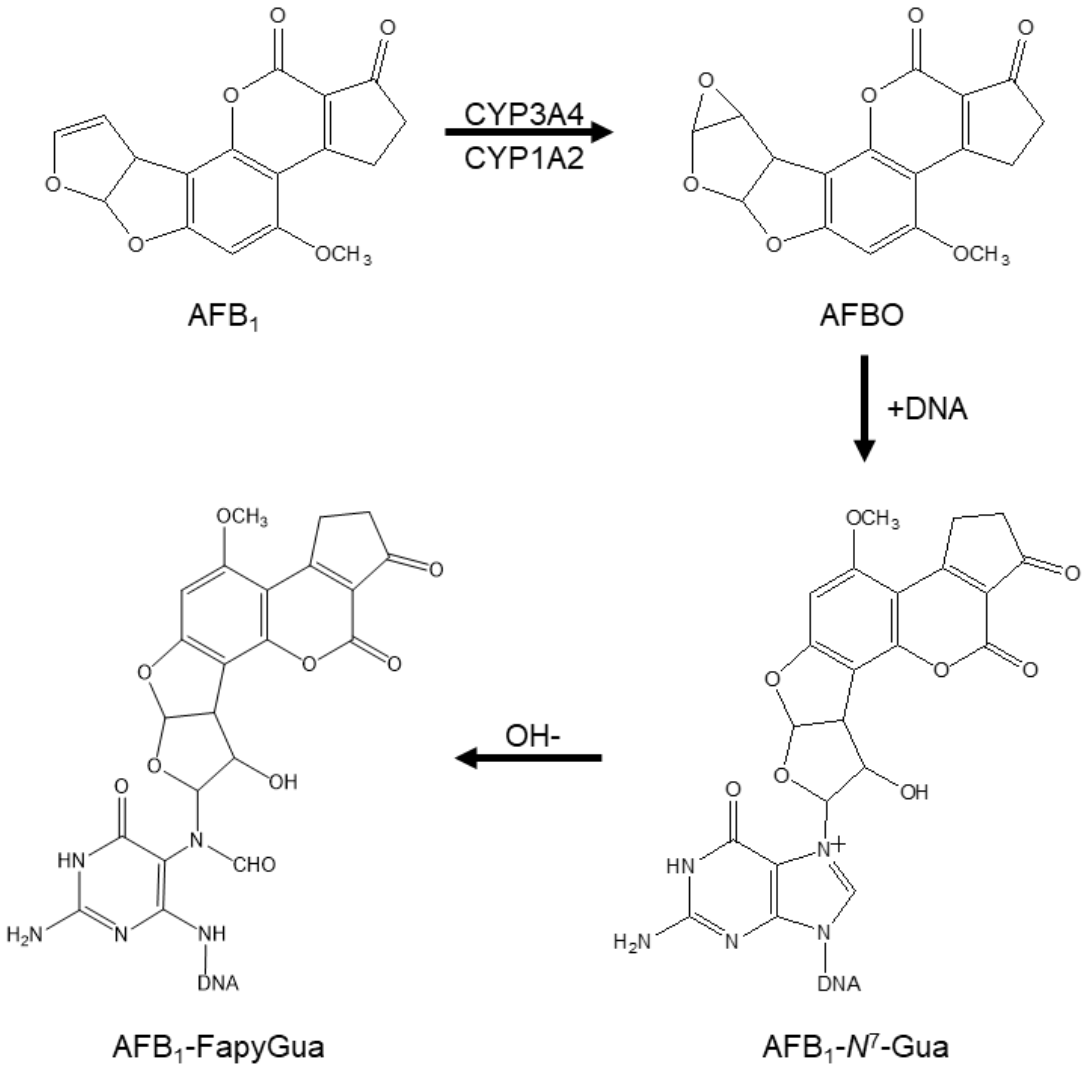

Figure 1.9. Metabolic activation and DNA adduct formation by AFB_1. See details in text. Adapted from Smela et al., (2002) and Rushing and Selim (2019).

1.4.3 Aristolochic acid I

The plant extract aristolochic acid (AA) derived from *Aristolochia* species contains the main components aristolochic acid I (AAI; 8-methoxy-6-nitrophenanthro[3,4-*d*]-1,3-dioxole-5-carboxylic) and aristolochic acid II (AAII; 6-nitrophenanthro[3,4-*d*]-1,3-dioxole-5-carboxylic acid). *Aristolochia* species are often used in traditional herbal medicine for different purposes, including as an anti-inflammatory, a diuretic, an antiseptic and to treat oedemas (Arlt et al., 2002; Gökmen et al., 2013; IARC, 2012b). Although they are most used in Chinese medicine, their use has also been reported worldwide including in other Asian countries, Europe, Africa, and America (Han et al., 2019; Heinrich et al., 2009). The toxicity and carcinogenicity of AAs, particularly AAI, has been shown in animals and

humans, therefore, products containing these compounds have been banned in most countries and AA has been classified as an IARC Group 1 carcinogen (Arlt et al., 2002; Han et al., 2019; IARC, 2012b).

In the 1990s, the prolonged consumption of slimming pills that mistakenly contained *Aristolochia fangchi* instead of *Stephania tetrandra* was first associated with rapidly progressive renal fibrosis in young Belgian women (Vanherweghem et al., 1993). Other nephropathies related to AA exposure were later reported and called aristolochic acid nephropathy (AAN) (Debelle et al., 2008; Gökmen et al., 2013). After a few years, many of these women developed end-stage nephropathies and an approximately 50% risk of developing upper tract urothelial cancer (Nortier et al., 2000).

Another renal disease associated with AA exposure is Balkan endemic nephropathy (BEN), which is very similar to AAN and increases the risk of cancers in the upper urinary tract. BEN is endemic to villages in the Danube Valley and is caused by the chronic exposure to *Aristolochia clematitis*, a common plant known to grow in wheat fields in the region (Han et al., 2019; Jelaković et al., 2019). It estimated that around 100000 people are at risk and 25000 have the disease in Bosnia-Herzegovina, Croatia, Macedonia, Serbia, Bulgaria, and Romania (Stiborová et al., 2016). AA-DNA adducts have been detected in renal tissues of AAN and BEN patients, demonstrating the link between dietary/oral exposure to AA and the development of these diseases and their role as biomarkers for exposure (Arlt et al., 2004, 2007; Schmeiser et al., 2014).

The major bioactivation pathway of AAI is nitroreduction to *N*-hydroxyaristolactam I by the action of both cytosolic and microsomal enzymes: mainly NQO1 in the cytosol and CYP1A2 in liver microsomes, although CYP1A1, NADPH:cytochrome P450 oxidoreductase and prostaglandin H synthase also play a role in AAI activation (Stiborová et al., 2003, 2008a, 2012). Subsequently, *N*-hydroxyaristolactam I is converted to the reactive cyclic aristolactam I nitrenium ion which has delocalised positive charges and binds to the exocyclic amino groups of adenine and guanine bases to form DNA adducts (Figure 1.10) (Han et al., 2019; Stiborová et al., 2017). Both dA-AL-I

(7-(deoxyadenosin-N^6-yl) aristolactam I) and dG-AL-I (7-(deoxyguanosin-N^2-yl) aristolactam I) are formed; however, dA-AL-I adducts are more persistent and more mutagenic than dG-AL-I; similar results were reported for AAII adducts (Attaluri et al., 2009; Han et al., 2019; Mei et al., 2006). AAI-DNA adduct formation can lead to A to T transversions in the genome, including in critical cancer genes such as *TP53* and H-*ras* (Arlt et al., 2007; Kucab et al., 2019; Nik-Zainal et al., 2015; Poon et al., 2013; Rosenquist and Grollman, 2016). Characteristic A to T transversion mutations in *TP53* have been found in urothelial tumours of AAN and BEN patients, as well as in human *TP53* knock-in mouse fibroblasts treated with AAI (Chen et al., 2012; Grollman et al., 2007; Liu et al., 2004; Lord et al., 2004).

The contribution of phase II XMEs to AAI activation has also been reported. The role of SULT enzymes in this process is conflicting. Some studies have shown increased mutagenicity in cells expressing human SULT1A1 or SULT1B1, by converting *N*-hydroxyaristolactam I to *N*-sulfate esters, which are highly reactive and can lead to DNA adduct formation (Meinl et al., 2006; Sidorenko et al., 2014). In contrast, other reports found that SULTs had no impact on AAI bioactivation and thus adduct formation in *in vitro* systems and mice carrying human *SULT1A1/2* (Arlt et al., 2017; Stiborova et al., 2011). On the other hand, the detoxication of AAI can occur by the oxidation of AAI to aristolochic acid Ia (8-hydroxyaristolochic acid I; AAIa); this reaction is catalysed by CYPs, mainly CYP1A2, CYP1A1, CYP2C9 and CYP3A4. Additionally, AAI can be detoxified as a result of the further reduction of *N*-hydroxyaristolactam I to aristolactam I, which occurs by the action of CYP1A1 and CYP1A2 (Figure 1.10) (Stiborová et al., 2008b, 2017). These metabolites and their conjugates (*e.g*., sulfates and glucuronides) are readily excreted in urine and faeces (Stiborová et al., 2017).

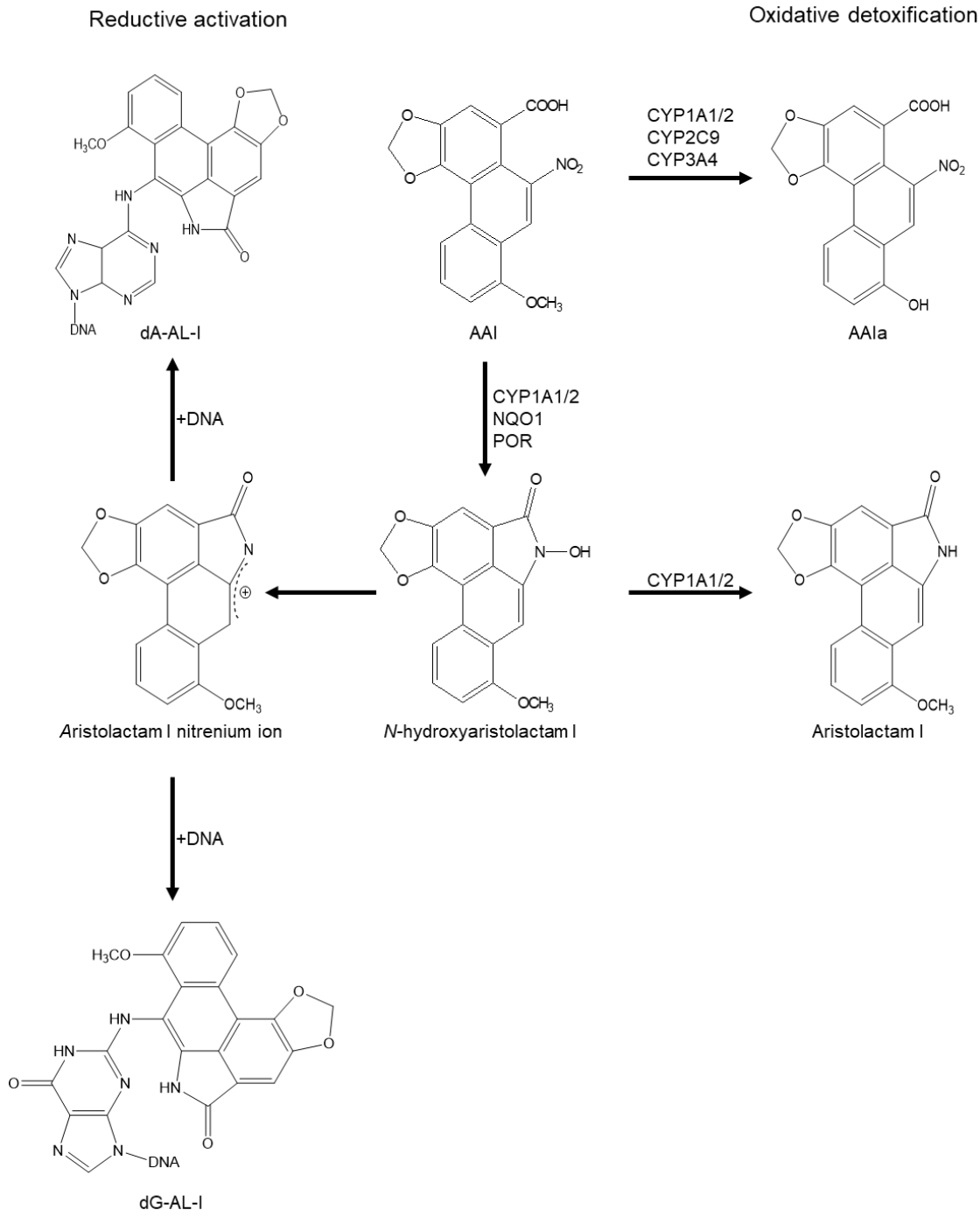

Figure 1.10. Metabolic activation, detoxification and DNA adduct formation by AAI. See details in text. Adapted from Stiborová et al., (2017).

1.4.4 2-Amino-1-methyl-6-phenylimidazo[4,5-*b*]pyridine

The HAA 2-amino-1-methyl-6-phenylimidazo[4,5-*b*]pyridine (PhIP) is part of the family of genotoxic compounds referred to as aminoimidazoazaarenes. It was first isolated by acid extraction from fried beef cooked at more than 200°C. PhIP was found to be the most abundant HAA by mass but also the one with the lowest mutagenic potential (Felton et al., 1986). The formation of PhIP and other HAA occurs through the Maillard reaction,

which is a heat catalysed reaction of free amino acids, sugars and creatine, a substance present in muscle cells (Robbana-Barnat et al., 1996; Turesky, 2007). As well as being the most abundant HAA in grilled beef, it is also the most abundant in grilled pork, fish and poultry, and additionally it is found in tobacco smoke (Manabe et al., 1991; Turesky, 2007). Human intake of PhIP is very variable as it depends on an individual's diet and on the cooking time and temperature of consumed food. A study of a German cohort estimated that the mean exposure to PhIP is of ~48 ng per day, while similar studies in the United States (USA) usually estimate higher intakes that can be more than 200 ng per day (Cantwell et al., 2004; Keating and Bogen, 2004; Rohrmann et al., 2007). PhIP has been shown to be mutagenic and carcinogenic in colon, prostate, and breast tissues of rodents (Andreassen et al., 2001; Ito et al., 1991; Nagao and Sugimura, 1993; Shirai et al., 1997; Wang et al., 2016); however, evidence of its human carcinogenicity in humans is insufficient, leading to its classification as possibly carcinogenic to humans (Group 2B) by IARC (IARC, 1993).

PhIP requires the action of XMEs to exert its genotoxicity; a scheme of the metabolic activation and adduct formation of PhIP is shown in Figure 1.11. The first step is the oxidation of the exocyclic amine group to produce *N*-hydroxy-2-amino-1-methyl-6-phenylimidazo[4,5-*b*]pyridine (*N*-OH-PhIP), a reaction that is mainly catalysed by CYP1A2 in the liver, but CYP1A1 and CYP1B1 may contribute in other tissues (Turesky, 2002, 2007; Turesky and le Marchand, 2011). *N*-OH-PhIP itself can react with DNA; however, DNA adduct formation is enhanced by phase II metabolism. Further activation by NATs and SULTs, of which NAT2 and SULT1A1 are the most active, leads to esterification (*i.e.*, formation of N^2-acetoxy-PhIP and N^2-sulfonyloxy-PhIP). The esters produced are highly unstable and may undergo heterolytic cleavage generating reactive nitrenium ions, which in turn lead to the formation of DNA adducts (Schut and Snyderwine, 1999; Turesky, 2007; Turesky and le Marchand, 2011). PhIP-DNA adducts are mainly formed at the C8 position of guanines, *N*-(deoxyguanosine-8-yl)-PhIP

(dG-C8-PhIP) and have been shown to induce G to T transversions in DNA (Schut and Snyderwine, 1999; Turesky, 2002).

The major detoxication product of PhIP in rodents, 2-amino-4'-hydroxy-1-methyl-6-phenylimdazo[4,5-*b*]pyridine (4'-OH-PhIP), is formed by the oxidation of the heterocyclic ring by the action of CYP1A2 in rats. In humans, *N*-OH-PhIP can be detoxicated by UGTs, mainly UGT1A1, to form stable glucuronide conjugates such as N^2-(β-1-glucosiduronyl-2-(hydroxyamino)-1-methyl-6-phenylimidazo[4,5-*b*]pyridine, which is the main metabolite excreted in human urine. GSTs may be involved in the detoxication of N^2-acetoxy-PhIP by catalysing its reduction back to the parent compound through the formation of a glutathione conjugate (Girard et al., 2005; Turesky, 2007; Turesky and le Marchand, 2011). Additionally, NADH-dependent reduction of *N*-OH-PhIP to PhIP has also been seen in human and rat systems (King et al., 1999; Kurian et al., 2006).

Additionally, PhIP has oestrogenic activity which is mediated through the oestrogen receptor α (ER-α). Oestrogen targets influence a wide range of physiological effects, including the development of the mammary glands, male sex accessory growth (Lauber and Gooderham, 2007). Prolonged exposure to oestrogens has been linked with increased risk of breast cancer, and it has been shown that ER-α is important for breast cancer progression and, possibly, initiation. Oestrogen stimulation has also been considered to be involved in the development of colorectal and prostate cancer. Therefore, due to the ability of PhIP to stimulate ER-α induced activation of oestrogen related responses, including proliferation, it may influence the development of oestrogen-dependent cancers (Gooderham et al., 2007; Lauber et al., 2004).

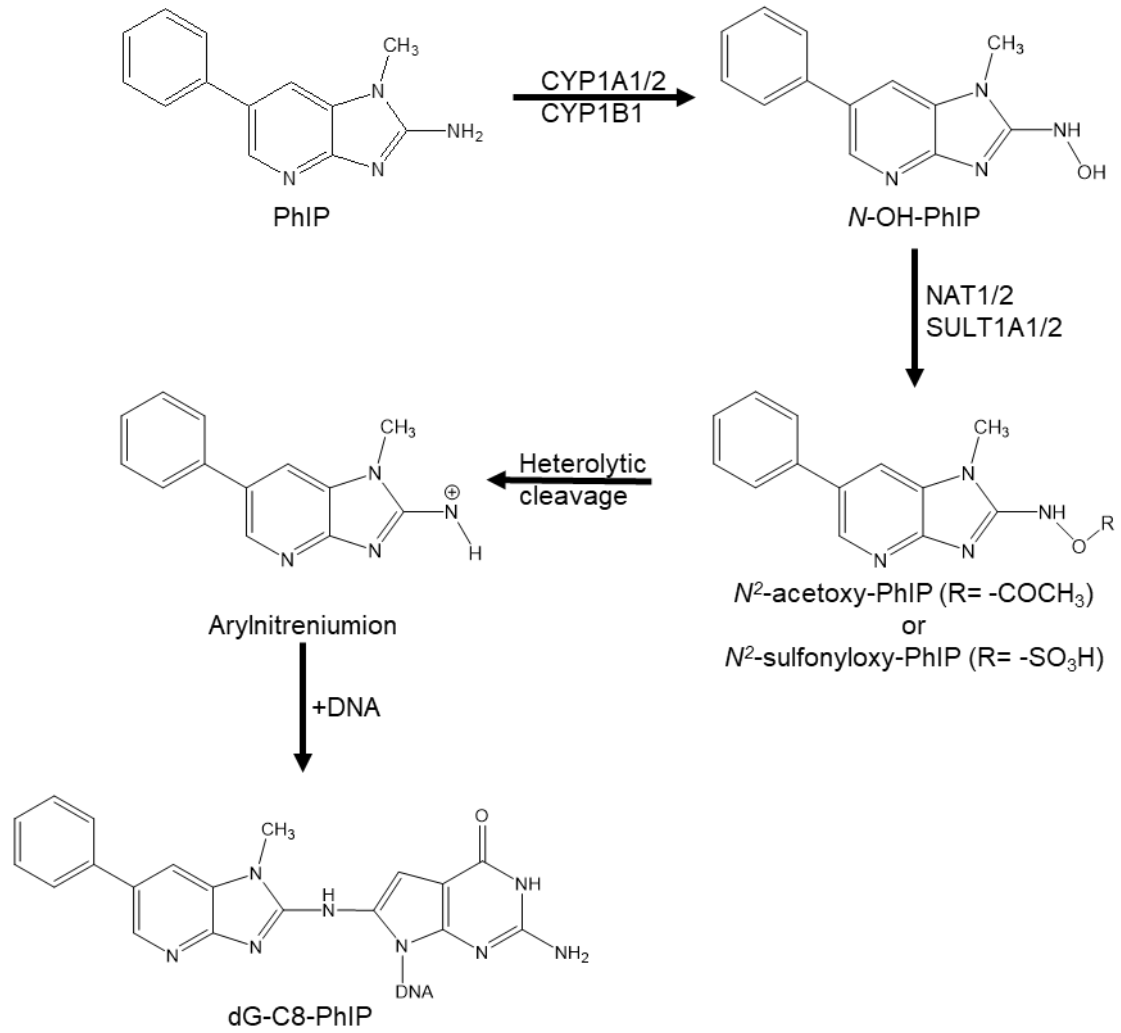

Figure 1.11. Metabolic activation and adduct formation by PhIP. See details in text. Adapted from Schut and Snyderwine (1999).

1.5 Tissue-specific oncogenesis

Many environmental carcinogens or their reactive metabolites induce genotoxicity through the formation of DNA adducts. DNA adducts are often used as biomarkers of human carcinogen exposure, and their detection and characterisation can help understand the causes of several cancers, assess carcinogenic risk, and investigate preventative strategies (Phillips, 2005; Phillips and Arlt, 2009). DNA adduct formation is considered to be one of the first steps in carcinogenesis, and linear relationships between dose, adduct levels and tumour incidence have been shown in target tissues (Otteneder and Lutz, 1999). However, several studies have shown that DNA adduct formation occurs in both target and non-target tissues, and it is not sufficient for carcinogenesis; therefore, the events after DNA damage and mutation are key in

tumourigenesis and the identification of target tissues, and these are likely to be tissue-specific (Mei et al., 2006; Poirier and Beland, 1994; Zuo et al., 2014).

Investigations of gene expression changes in mice, rats and human cell lines after carcinogen exposure have revealed tissue-specific gene expression changes, as well as differences between target and non-target tissues. These studies have highlighted alterations in genes involved in processes such as apoptosis, cell cycle, stress response, immune response and metabolism. These include oncogenes and tumour suppressors like *TP53*, *MYC*, *MDM2* and *RB1*, and XMEs like CYP1A1, which may be key in the study of carcinogen organotropism (Arbillaga et al., 2008; Arlt et al., 2011a; Chen et al., 2006; Simões et al., 2008, 2018; Zuo et al., 2014). It is worth mentioning that the levels of XMEs in different tissues and polymorphisms in these genes may influence the metabolism of the compounds, thus contributing to tissue-specific responses (Arlt et al., 2017; Girard et al., 2005; Hu and Wells, 2004; Meinl et al., 2006; Nebert and Dalton, 2006).

Other host factors that contribute towards organ-specific responses in carcinogenesis include epigenetic changes, such as persistent hyper- and hypo-methylation of genes (Meng et al., 2021; Rieswijk et al., 2016; Tryndyak et al., 2018), and hormone-dependence of certain tissues, which could be important in the study of the organotropism of carcinogens like PhIP. It has been observed that PhIP can act as a substrate for proteins that bind oestrogen, particularly the ER, and can trigger oestrogen responses that have been implicated in the development of malignancies in tissues like breast and prostate (Lauber and Gooderham, 2007; Lauber et al., 2004).

1.6 Organoids

Advances of three-dimensional (3D) cell culture technology in recent years have increased its use in several fields including organ development, disease modelling and drug screening. Several 3D models have been established, from simple unicellular spheroid cultures to more complex systems, like organoids and microphysiological systems (MPS) (Knight and Przyborski, 2015; Lin and Chang, 2008; Truskey, 2018).

Organoids are multicellular 3D cultures derived from stem cells that self-assemble into structures that contain organ-specific cell types and that recreate some of the *in vivo* cell organisation and functions of the organ of origin (Lancaster and Knoblich, 2014). As shown in Figure 1.12, organoids can originate from pluripotent stem cells (PSCs), both embryonic and induced pluripotent stem cells (iPSCs), or adult stem cells (ASCs), which can proliferate indefinitely in culture and have shown the ability to differentiate and re-organise to mimic their source organs (Clevers, 2016).

The derivation process of PSC organoids exploits both the ability of these stems cells to differentiate into several cell types and the organ development process, including spatial patterning and morphogenesis (Clevers, 2016; Eiraku et al., 2011; Spence et al., 2011). The ability to generate organoids from ASCs started with the identification of the stem cell marker leucine-rich repeat containing G-protein-coupled receptor 5 (*Lgr5*) in intestinal epithelium, which allowed the characterisation of multipotent and self-renewing adult stem cell populations in several other tissues, including colon (Barker et al., 2007), stomach (Barker et al., 2010), pancreas (Huch et al., 2013a) and liver (Huch et al., 2013b). These *Lgr5*$^{+}$ ASCs, isolated cells or from dissected tissue fragments, can be used to establish organoids by providing an adequate environment to mimic tissue homeostasis and regeneration (Barker et al., 2010; Clevers, 2016; Huch et al., 2013b; Sato et al., 2009).

The use of human organoids has become increasingly widespread over the past few years as alternatives to more routinely used model systems, such as animals and two-dimensional (2D) mammalian cell culture. The perceived need for more physiologically relevant *in vitro* models has been the main reason for this shift towards the use of 3D cultures in different research fields (Forsythe et al., 2018; Li et al., 2018; Morizane et al., 2015; Naruse et al., 2020; Sachs et al., 2019). Although experimental animals, mainly rodents, have provided substantial amounts of information about many biological processes and have been a key resource for chemical and drug safety studies, these animal models do not always accurately represent the human response due to

species-specific disease states and reactions (Olson et al., 2000; Ruggeri et al., 2014; Webb, 2014). Similarly, 2D mammalian cell cultures have been widely used in research for more than a hundred years and have led to the discovery of countless pathways and processes in biology. Despite this, the dependability of results from studies using 2D cultures for drug and chemical safety and efficacy can been questioned due to the highly artificial nature of their culture environment (Antoni et al., 2015; Kolenda et al., 2018). Therefore, the use of human organoids and other 3D cultures may allow the collection of data more relevant to human physiology while contributing to reductions in the use of animals in basic and applied research (Clark, 2018; Kim et al., 2020; Lou and Leung, 2018; Pampaloni et al., 2007; Silva-Almeida et al., 2020)

As mentioned above, the application of human organoid systems includes, but is not limited to, organ development, disease modelling and pharmacological studies (Figure 1.12). PSC-derived human organoids have proved to be very useful for studying organ development where their propensity to resemble embryonic stages of development has allowed the replication of key steps in organogenesis, such as spatial organisation of the heart, the brain, the gastrointestinal tract, and other organs (Finkbeiner et al., 2015; McCracken et al., 2014; Renner et al., 2017; Rossi et al., 2019). The use of human organoids in disease modelling has led to the establishment of assays and models that assist with diagnosis, drug screening and personalised treatment. This has been achieved for several conditions like cystic fibrosis, for which tubuloids from urine, intestinal and airway organoids from patients have been used to identify treatments that benefit patients with specific mutations (Dekkers et al., 2013; Sachs et al., 2019; Schutgens et al., 2019). Great progress has also been made in cancer research, using biobanks of human tumour and normal organoids derived from cancer patients to better understand tumour heterogeneity and responses to chemotherapeutic treatment, as well as aiding the improvement of personalised therapy (Calandrini et al., 2020; Li et al., 2019; Weeber et al., 2017; van de Wetering et al., 2015). Drug screening using human organoids is already being carried out to facilitate pre-clinical drug development, as well

as to predict an individual patient's response to treatment (Li et al., 2018; Sachs et al., 2019; van de Wetering et al., 2015). It is anticipated that this will not only maximise clinical benefits, but also enable increased adoption of novel therapeutics (Berkers et al., 2019). Engraftment of organoids in mice has demonstrated the use of organoids in regenerative medicine and transplantation is also very promising, as it appears to minimise the risks of transplant rejection and increase the availability of healthy tissue (Xu et al., 2018). Additionally, organoids show great potential in drug toxicology studies (Grabinger et al., 2014; Lu et al., 2017; Mun et al., 2019; Park et al., 2019; Pendergraft et al., 2017; Saito et al., 2019). However, their use in environmental and genetic toxicology is at a relatively early stage.

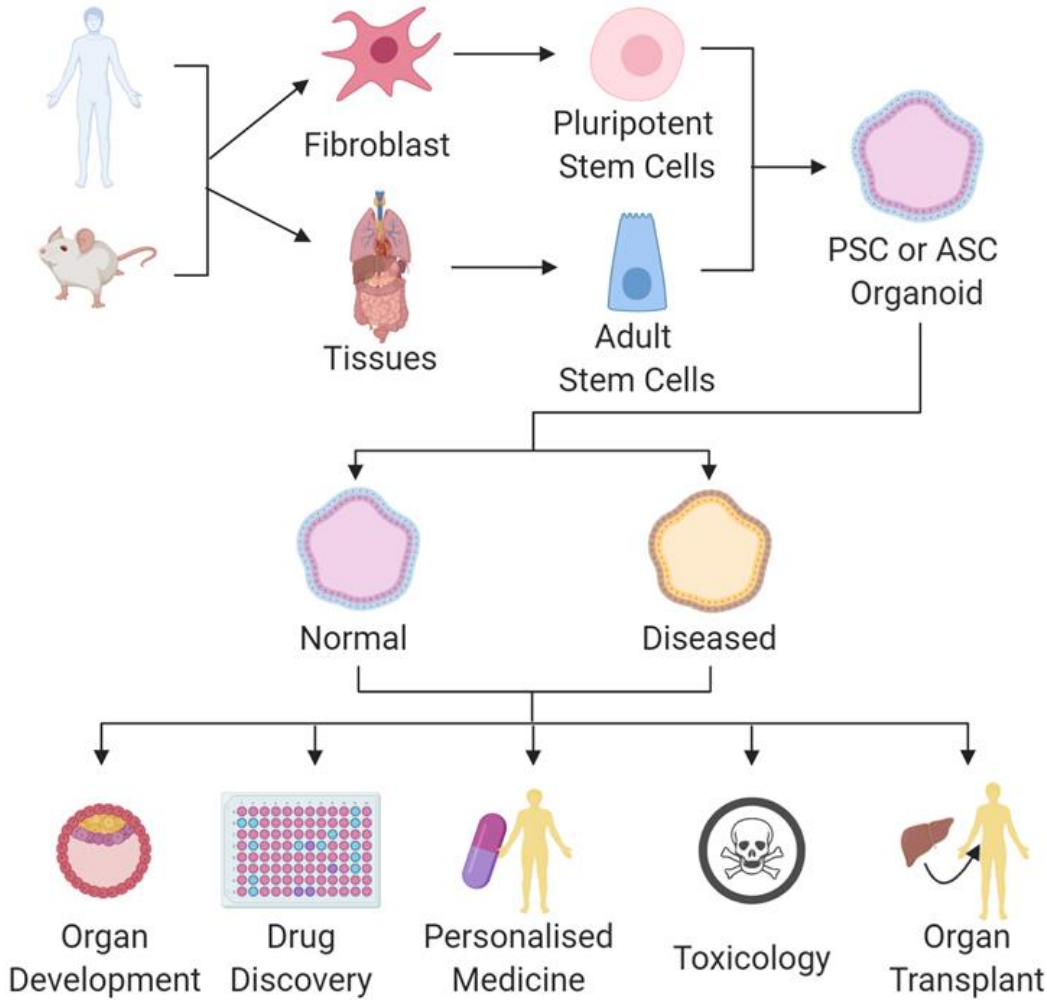

Figure 1.12. Scheme showing the origin and application of organoid systems. Organoids can be derived from human and animal (*e.g.*, mouse) pluripotent or adult stem cells. Normal and diseased organoids can be used for many applications such as disease modelling, organ development, drug screening, personalised medicine, toxicology and organ transplant and replacement. Taken from Caipa Garcia et al., (2022). Created with BioRender.com.

1.6.1 Types of organoids and their features

Organoid models are characterised by the self-organisation of cells in culture into *in vivo*-like structures; however, their derivation process depends on the starting material. Organoids from both embryonic and induced pluripotent stem cells have been established from several organs, including gut, kidney, liver, lung, intestine and brain (Rossi et al., 2018). Derivation of these PSC organoids utilises knowledge of the cell sorting and lineage commitment pathways, combined with growth in culture under conditions specific for the desired differentiation pathway (Lancaster and Knoblich, 2014). This process usually takes between three and four weeks to generate mature organoids (Spence et al., 2011). In the case of ASC-derived organoids, Wnt signalling pathway activation is key for their establishment (Clevers et al., 2014). These organoids, which originate from *Lgr5*$^{+}$ stem cells obtained from single cell sorting or dissected tissue fragments, are grown in organ-specific culture media that contains Wnt activators such as R-spondin 1 and, in some cases, Wnt3A (Clevers et al., 2014). Organoid types that have been derived from ASCs include gut, liver, pancreas, intestine, kidney as also from mammary and salivary glands (Rossi et al., 2018). These organoids can also be expanded and kept in culture for weeks to months. In contrast to PSC-derived organoids, the process to generate mature organoids from ASCs takes only a few days (between four and 10 days) (Huch et al., 2013a; Sato et al., 2009).

Although this study only included organoids derived from human tissues (*i.e.,* ASCs), the characteristics of PSC-derived organoids will also be described for comparison. Similarly, information about small intestine organoids is provided as these are a well-characterised organoid model that has been used in toxicology studies.

1.6.1.1 Small intestine organoids

Although both PSC and ASC-derived organoids can be grown in culture for several months, they have distinct differences, not only in the stages of development they represent, but also in the cell types they contain, and therefore in their complexity (Figure 1.13). A clear example of this can be seen with gastrointestinal tract organoids (Min et

al., 2020). Those derived from ASCs contain only organ-specific epithelial and stem cells, while organoids derived from PSCs contain epithelial cells as well as mesenchymal cells, including fibroblasts and smooth muscle, due to the ability of PSCs to differentiate into any cell type (Yin and Zhou, 2018). Small intestine organoids were first derived from ASCs by the Clevers lab at the Hubrecht Institute, the Netherlands (Sato et al., 2009). These organoids established from single *Lgr5*$^{+}$ cells form crypts containing Paneth cells as well as *Lgr5*$^{+}$ stem cells that surround a central lumen lined by a villus-like epithelium with polarised enterocytes, and goblet and enteroendocrine cells dispersed throughout the organoid (Sato et al., 2009, 2011). This has been replicated various times from murine and human tissues and adapted for the establishment of intestinal organoids from cystic fibrosis patients (Dekkers et al., 2013; Fujii et al., 2018; Schwank et al., 2013). Intestinal tissue organoids originating from human PSCs were first reported by Spence et al., (2011). In this study embryonic intestinal development was mimicked by using a series of culture conditions that included growth factors to induce intestinal growth, morphogenesis and cytodifferentiation. These organoids contained polarised, columnar epithelium resembling villus- and crypt-like structures with all intestinal endothelial cells present, as well as a layer of mesenchymal cells including subepithelial myofibroblasts, smooth muscle and fibroblasts (Spence et al., 2011). This model has been replicated and used for different purposes such as generating *in vivo* human organoid engraftment mouse models and viral infection models, amongst others (Finkbeiner et al., 2012; Watson et al., 2014).

1.6.1.2 Colon organoids

As with the small intestine, colon and gut organoids have also been derived both from PSCs and from ASCs. Colon *Lgr5*$^{+}$ ASCs were identified in the Clevers lab, where colon organoids were later established from human and murine tissues (Barker et al., 2007; Sato et al., 2011). Human tissue-derived colonic organoids appeared as cystic or budding structures with proliferative cells and the central region contained dead cells resembling the intestinal lumen. Organoids with budding structures could be kept in

culture for months and their continuous culture led to the formation of large mature organoids that contained both stem cell and differentiated cell compartments, which could be expanded. Subsequently when culture conditions were modified, goblet and enteroendocrine cells were also present (Mohammad et al., 2018; Sato et al., 2011). Human PSC-derived colon organoids were established by stimulating bone morphogenetic protein (BMP) signalling; these organoids were comprised of colon-specific goblet and enteroendocrine cells as well as mesenchyme (Múnera et al., 2017). At the same time, others also generated PSC-colonic organoids by using a differentiation method that involved the modulation of the Wnt pathway via the addition of glycogen synthase kinase (GSK)-3β inhibitors as well as BMP regulation (Crespo et al., 2017).

1.6.1.3 Gastric organoids

Gut or gastric organoids were first derived from mouse *Lgr5*$^{+}$ ASCs and they resembled the pyloric epithelium organised around a central lumen (Barker et al., 2010). Human ASC gastric organoids were later established from different regions of the stomach; these consisted of budding or cystic structures (Bartfeld et al., 2015; Schlaermann et al., 2016). Schlaermann et al., (2016) reported cystic organoids that consisted of a central lumen surrounded by a layer of cylindrical epithelial cells, these were positive for the gastric markers mucin 6 and pepsinogen C, which are expressed in gland mucous and chief cells, respectively, as well as proliferative cell markers. These can then be differentiated into budding structures consisting of mucin 5AC producing pit mucous cells instead of mucous gland cells and had a lower expression of the chief cell marker (Schlaermann et al., 2016). Bartfeld et al., (2015) used culture conditions in which organoids started as cysts and after expansion they developed buddings that comprised proliferative cells, mucous gland, chief and enteroendocrine cells surrounding a central lumen. These ‘complete’ human tissue gastric organoids that contained gland and pit domains can also be further differentiated by altering the culture conditions in order to direct differentiation into either gastric pit or gland cell lineages (Bartfeld et al., 2015). In a similar way, PSC-derived gut organoids formed simple gland and pit domains and

contained *Lgr5*$^{+}$ cells as well as mucous and endocrine cells; however, they represented early developmental stages and contained submucosal myofibroblasts and a small population of subepithelial myofibroblasts (McCracken et al., 2014).

1.6.1.4 Liver organoids

As mentioned above, organoids derived from both types of stem cell populations have also been established for the liver, pancreas, and kidney (see below for more details on pancreatic and kidney organoids). In adults, *Lgr5* expression in these organs is low under normal conditions, however, after injury, the Wnt pathway is activated leading to increased expression of *Lgr5*, and therefore, tissue regeneration (Huch et al., 2013b, 2013a). ASC-derived liver organoids were first reported by Huch and co-workers (Huch et al., 2013b); they consisted of large cysts that expressed *Lgr5* and progenitor markers for hepatocyte and bile duct cells, while mature hepatocyte markers were only weakly expressed. Although the initial organoids mainly consisted of bile duct cells, hepatocyte maturation was achieved by altering culture conditions; however, this led to a concurrent decrease in the expression of proliferative cells. These differentiated organoids secreted albumin and CYP function was induced (Broutier et al., 2016; Huch et al., 2013b, 2015; Schneeberger et al., 2020). Hepatocyte-derived organoids were later established from murine and human single mature hepatocytes. They resembled the main functions and gene expression patterns of hepatocytes *in vivo* and could proliferate in culture for at least 6 months (Hu et al., 2018; Peng et al., 2018). PSC-derived liver organoids were first generated as vascularised liver buds. These liver organoids originated by co-culturing human hepatic endoderm and stromal cells, expressed early liver-specific markers including alpha-fetoprotein and albumin, and were capable of drug metabolism (Takebe et al., 2013). More recently, hepatobiliary organoids obtained from human PSCs were established. These organoids displayed functions of both hepatocytes (*e.g.*, drug metabolism and albumin production) and bile duct cells (Wu et al., 2019) (Figure 1.13). Other investigators have established hepatocyte-like organoids that resemble adult liver tissue-derived organoids (Mun et al., 2019).

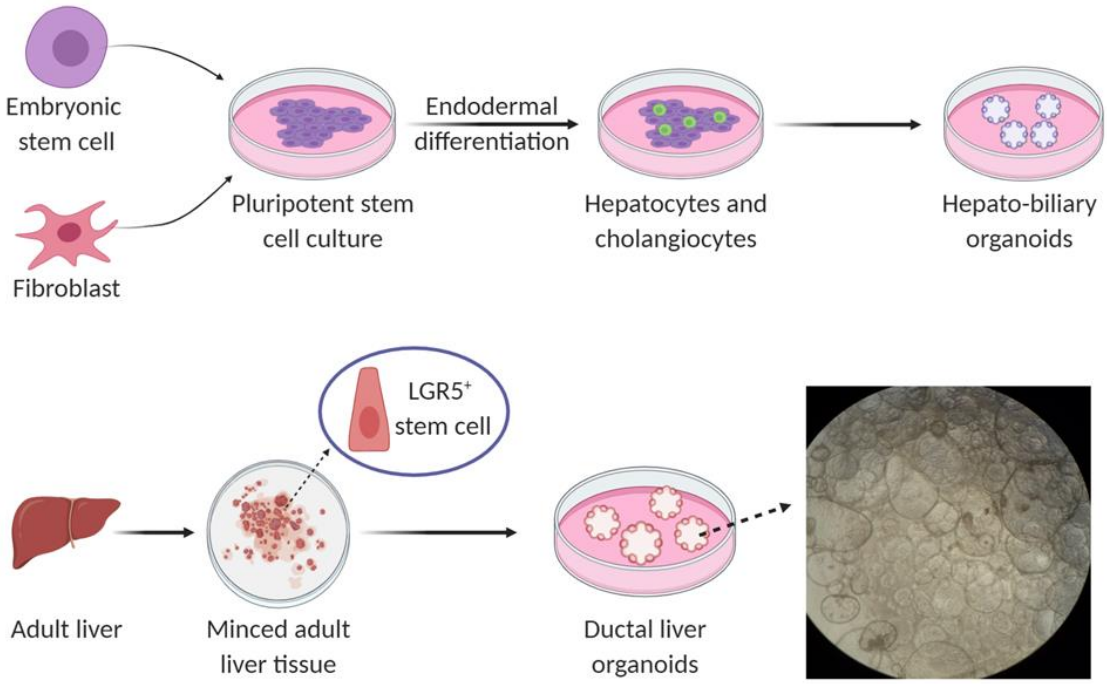

Figure 1.13. Scheme of liver organoid culture formation from pluripotent stem cells or adult stem cells. On the top panel, pluripotent stem cells, embryonic or induced, undergo differentiation towards the desired cell type. PSCs are differentiated into hepatocytes and cholangiocytes which then generate organoid cultures containing both hepatocytes and bile duct cells. The bottom panel shows how organoids can be derived from minced adult tissue which contains Lgr5^{+} stem cells that in this case can give rise to liver organoid cultures containing ductal cells. Organoid cultures are embedded in basement membrane extract and are grown in media complemented with essential growth factors. An example of normal human adult liver organoids is shown on the right in the bottom panel. Scheme adapted from Kretzschmar and Clevers (2016) and Wu et al., (2019). Figure taken from Caipa Garcia et al., (2022). Created with BioRender.com.

1.6.1.5 Pancreatic organoids

Pancreatic organoids were first made from ductal fragments of mouse pancreas. These formed cysts that contained duct cells *in vitro,* some of which differentiated into endocrine cells *in vivo* (Huch et al., 2013a). This protocol was then adapted for the growth of human tissue organoids that were also comprised of stem and ductal cells (Boj et al., 2015; Broutier et al., 2016; Georgakopoulos et al., 2020). Human tissue pancreatic organoids that have the potential to differentiate into endocrine lineage cells *in vitro* were later produced from digested islet-depleted pancreatic tissue. Initially these formed budding structures with almost all cells displaying a ductal phenotype with progenitor cells at the tip regions, some of which differentiated into endocrine cells and produced insulin after

transplantation (Loomans et al., 2018). Organoids that recapitulate pancreatic development were also derived from mouse foetal pancreatic progenitors. These were composed of epithelial cells that expressed progenitor markers such as *Pdx1*, *Sox9*, *Hnf1b* and *Nkx2.2*, which then differentiated into ductal and exocrine lineages (Greggio et al., 2013). Pancreatic organoids from PSCs formed hollow structures surrounded by a layer of polarised epithelium comprised of cells expressing exocrine and progenitor cell markers, as well as cells capable of secreting collagen IV and laminin-α5 (Huang et al., 2015).

1.6.1.6 Kidney organoids

Kidney organoids have been mainly derived from human PSCs and several protocols have been published for the generation of kidney organoids containing different kidney cell types. The formation of kidney organoids from human embryonic stem cells through stepwise differentiation into the key developmental lineages of the kidney has been reported (Takasato et al., 2014). These organoids contain ureteric buds and metanephric mesenchyme, including early nephrons, as well as cells expressing podocyte, proximal tubule and collecting duct genes. Others reported deriving organoids from mouse and human stem cells in which proximal and distal tubules were formed, as well as glomerulus-like structures, and cells with podocyte markers were also seen (Taguchi et al., 2014). Like these, many other nephron organoids expressing podocyte, proximal tubule, loops of Henle and distal tubule markers with different degrees of differentiation and complexity have been generated from human and murine embryonic and pluripotent stem cells (Li et al., 2016; Morizane et al., 2015; Takasato et al., 2015, 2016; Tanigawa et al., 2016). ASC-derived kidney organoids have been named ‘tubuloids’, as they mainly contain tubular epithelial cells, and similarly to organoids derived from adult tissues they recapitulate tissue regeneration rather than development (Ooms et al., 2020). Tubuloids from normal human adult tissue were reported consisting of cystic structures containing tubular epithelial cells that resembled proximal tubular cells and that expressed the renal tubule protein Tamm-Horsfall (Jun et al., 2018). Others established tubuloids from

human tissues that showed high expression of proximal tubule markers, as well as some collecting duct, loop of Henle and distal tubule markers (Schutgens et al., 2019). Tubuloids were also established from cells isolated from urine of cystic fibrosis patients and from kidney tumours (Schutgens et al., 2019).

1.6.2 Organoid use in drug screening and toxicology

Due to their structural and functional features, organoid models have great potential in toxicology studies. Different aspects have been investigated, from the effects and efficiency of drugs to the toxicity of environmental pollutants. The former has been covered more widely, possibly due to the opportunity that testing of large libraries of therapeutic compounds on patient-derived organoids offers to bridge the gap between monolayer cell culture and animal models, and the relevance of the results for human physiology in pre-clinical trials (Langhans, 2018; Park et al., 2019).

1.6.2.1 Metabolic potential of organoids

A few studies have focused on investigating the xenobiotic metabolic potential of organoids, primarily in liver and intestinal organoids. These studies have shown that the expression and function of enzymes responsible for the biotransformation of xenobiotic compounds, *e.g.,* CYPs, are maintained in the organoids (Huch et al., 2015; Lu et al., 2017; Park et al., 2019; Schneeberger et al., 2020; Wu et al., 2019). CYP3A4 is one of the main XMEs in liver and intestine (Zanger and Schwab, 2013). The expression of this enzyme in differentiated liver organoids, *i.e.,* hepatocyte-like organoids, has been shown to be at levels slightly lower than those in adult liver but significantly higher than those seen in foetal liver and stem cells (Huch et al., 2015; Wu et al., 2019). The activity of CYP3A4 has also been shown to be significantly higher in differentiated liver organoids than in commonly used cell lines such as human hepatoma HepG2 cells (Huch et al., 2015; Wu et al., 2019). Levels of expression of other CYP enzymes important in drug metabolism were compared in mouse small intestine and liver organoids with the respective tissues. These investigations showed that mouse *Cyp1a2* and *Cyp3a11* mRNA levels were higher in intestinal organoids than those in the tissue, whilst only

Cyp1a2 mRNA was greater in the liver organoids than in the tissue (Park et al., 2019). Another study compared the CYP levels between iPSC-derived intestinal organoids and the human colorectal adenocarcinoma cell line Caco-2, showing that organoids had significantly higher levels of various CYPs, including *CYP1B1*, however, *CYP1A1* expression was lower in the organoids. The expression of *CYP3A4* was limited, but it was enhanced by the addition of the small molecule DAPT (Janssen et al., 2020, 2021). The ability of organoids to metabolise drugs was also investigated in mouse crypt organoids, which express both phase I and phase II XMEs (Lu et al., 2017). In the latter study, organoid toxicity was also seen after treatment with camptothecin-11, demonstrating that crypt organoids can metabolise this compound. Furthermore, the induction of CYP enzymes such as *CYP1A1*, *CYP1B1* and *CYP3A4* after treatment with β-naphthoflavone, phenobarbital and rifampicin has been shown in human iPSC-derived intestinal organoids (Janssen et al., 2020, 2021). Collectively, these studies illustrate the utility of organoids for investigations of xenobiotic metabolism and toxicity.

1.6.2.2 Disease modelling and drug screening

The use of organoids for disease modelling could provide a very valuable tool in many areas including drug screening and personalised therapy (Lancaster and Huch, 2019). The availability of organoids derived from patient samples has allowed research on these areas by modelling different disease conditions, including cystic fibrosis, infectious diseases, and cancer. Cystic fibrosis was one of the first conditions to be modelled; organoids from cystic fibrosis patient ASCs (intestinal, lung and tubuloids), as well as human PSCs have been established (Dekkers et al., 2013; Mithal et al., 2020; Sachs et al., 2019; Schutgens et al., 2019; Schwank et al., 2013). These organoids have facilitated the assessment of the cystic fibrosis transmembrane conductance regulator function in individual patients *in vitro*, and in turn the effect of different drugs used to treat cystic fibrosis, including VX-809 (lumacaftor) and VX-770 (ivacaftor) (Dekkers et al., 2013).

There have also been several advances in the use of organoids for drug screening for cancer therapies. Cancer organoids or tumoroids have been derived from several

primary tumour types from which they retain the genetic and morphologic features (Huang et al., 2015; Saito et al., 2019; van de Wetering et al., 2015). Organoids derived from colorectal cancer patients were used in a proof-of-concept drug screening in which drug sensitivity and its correlation with the genetic background of the organoids were investigated (van de Wetering et al., 2015). This screening generated thousands of organoid-drug interactions and showed a wide range of sensitivities to the compound library, which included drugs in clinical use, those currently in clinical trials and those under pre-clinical investigation. They have been tested in organoids from different patients and in multiple organoids derived from the same patient (van de Wetering et al., 2015). Tumour heterogeneity has also been addressed with organoids from other cancer types, including pancreatic ductal adenocarcinoma and liver cancer; different combinations of drugs were used to treat organoids from different patients, resulting in the organoids displaying differential responses (Huang et al., 2015; Li et al., 2019). Liver tumoroids derived from different sections of the same primary tumour showed heterogeneity as some drugs, *e.g*., belinostat, dasatinib, gemcitabine and ceritinib, were effective only in a subset of the organoids (Li et al., 2019). Due to the varied responses seen between patient organoids, this model could aid the field of personalised medicine as patient-derived organoids can be used to test drug efficacy *in vitro*, and toxicity comparisons between disease and normal organoids could identify therapies with higher efficiency and fewer side effects (Saito et al., 2019).

1.6.2.3 Environmental toxicology

Thus far studies investigating the effects of environmental agents in organoids are scarce, although studies using both human and mouse organoids have been reported. Table 1.5 lists studies in which organoids derived from various human and animal tissues from both PSCs and ASCs have been used in environmental toxicology research. In one study, mouse intestinal crypt organoids were exposed to cisplatin, 5-fluorouracil, UV, and X-ray radiation to examine cell death and survival of intestinal epithelial cells, as well as investigate the role of certain genes in cell death regulation (Grabinger et al., 2014). The

results obtained were closer to those obtained in primary tissue cells and *in vivo* than those obtained from immortalised cell lines, thereby demonstrating the usefulness of this model (Grabinger et al., 2014). Mammary organoids derived from mice have been used to study the effect of bisphenols and phthalates on the proteome, showing that although the compounds had different effects, they altered the abundance of proteins involved in apoptosis, cell adhesion and proliferation (Williams et al., 2016). Human mammary organoids were recently utilised to test the effects of cadmium exposure on stem cell proliferation and differentiation by looking at organoid formation and morphology, showing a negative impact on these processes at concentrations relevant to human physiology (Rocco et al., 2018). The treatment of human liver and heart organoids with lead, mercury, thallium, and glyphosate led to damaging and toxic effects such as a decrease in the beating activity of cardiac organoids (Forsythe et al., 2018). Human colon organoids have been used to explore the effect of prolonged ethanol exposure in healthy colon cells by analysing the changes in gene expression and chromatin accessibility, identifying almost 2000 gene expression changes (Devall et al., 2020). Additionally, the effects of prenatal alcohol exposure were investigated in PSC-derived brain organoids, the results showed detrimental effects at cellular, subcellular, metabolic and gene expression levels. Alcohol exposure induced apoptosis, particularly in neurons, and led to mitochondrial dysfunction and metabolic stress (Arzua et al., 2020). Furthermore, other studies used cerebral organoids to test the neurotoxic effects of prenatal exposure to the dietary carcinogen acrylamide and the plant-derived pesticide rotenone showing their negative effects on neuronal development and differentiation (Bu et al., 2020; Pamies et al., 2018). Others recently established an organoid-based model in which the carcinogenicity of environmental chemicals could be studied by treating organoids *in vitro* and then injecting them into nude mice. This study showed that the morphological carcinogenic alterations seen in the treated organoids were then also found in the nude mouse model (Naruse et al., 2020). Moreover, Yen et al., (2020) investigated the cellular origin of carcinogenesis in intestinal organoids by treating them with 7,12-dimethylbenz[*a*]anthracene (DMBA), *N*-methyl-*N*-nitrosourea (MNU) and PhIP in

combination with protein phosphatase 2A depletion. This study showed that *Lgr5*$^{+}$ cells were transformed and had higher levels of epithelial-mesenchymal transition (EMT) and stem cell markers. Similar results were seen *in vivo* (Yen et al., 2020).

Collectively, these first advances in the use of organoids in the field of environmental and genetic toxicology indicate that organoids will allow the investigation of the relationship between the effects of environmental exposure and the increased risk of developing adverse human effects, including cancer (Devall et al., 2020). Organoid models will also allow the study of early molecular events in tumour formation and therefore aid the study of the modes of action and mechanisms of different carcinogens (Devall et al., 2020; Naruse et al., 2020).

Table 1.5. Studies using organoids in environmental toxicology.

Organoid type	Aim of the study	Key findings	Reference
Liver and cardiac – PSCs	Viability and cytotoxicity assessment of liver and cardiac organoids after exposure to the environmental pollutants lead, mercury, thallium, and glyphosate.	Liver and cardiac organoids showed toxicity after treatment with environmental pollutants (lead, mercury, thallium, and glyphosate) with thallium being the most toxic compound tested. All pollutants led to a decrease in cardiac organoid beating activity.	(Forsythe et al., 2018)
Brain – PSCs	Studying binge drinking related foetal alcohol spectrum disorders by assessing the downstream toxic effects of alcohol on neural pathology phenotypes and signalling pathways.	Alcohol exposure led to detrimental effects in the organoids by inducing apoptosis, structural changes, mitochondrial dysfunction, and metabolic stress. Gene expression changes in 199 genes were found.	(Arzua et al., 2020)
Brain – PSCs	Investigating the neurodevelopmental toxicity of acrylamide.	Exposure to acrylamide led to changes in the transcriptional profile, increased nuclear factor erythroid 2-related factor 2, apoptosis, repressed	(Bu et al., 2020)

Organoid type	Aim of the study	Key findings	Reference
		neuronal differentiation and tau hyperphosphorylation.	
Brain – PSCs	Assessment of neurotoxicity and developmental neurotoxicity after exposure to the pesticide rotenone.	Rotenone caused toxicity in different cell types. Induced ROS and mitochondrial dysfunction. Changes in pathways required for brain development were also found.	(Pamies et al., 2018)
Brain (organoid on chip) – PSCs	Assessment of the effects of nicotine in brain organoids on a chip that recapitulated features of the developing foetal human brain at early stages.	Organoids exposed to nicotine showed premature and abnormal neuronal differentiation. Brain regionalisation and development were also affected.	(Wang et al., 2018)
Colon – ASCs	Investigating the effect of ethanol exposure in normal colon organoids on gene expression and chromatin accessibility.	Identification of more than 1500 differentially expressed genes and 2000 differentially accessible chromatin regions in normal colon organoids after ethanol treatment.	(Devall et al., 2020)
Intestinal – ASCs	Investigating cellular origin in carcinogenesis by treating intestinal organoids with DMBA, MNU, or PhIP, in combination with protein phosphatase 2A deficiency.	Treatment induced tumourigenesis in *Lgr5*$^{+}$ cells but not in differentiated cells. Transformed cells showed an increase in stem cell signature and upregulated EMT markers.	(Yen et al., 2020)
Intestinal – ASCs	Studying toxicity and cell death induction in normal intestinal organoids after exposure to cisplatin, 5-fluorouracil, UV, or X-ray radiation. Comparison of results to those obtained in colon carcinoma cell lines.	Intestinal organoids were more sensitive to chemotherapeutic drugs than colon carcinoma cell lines, mimicking the *in vivo* situation. The organoids also responded much more sensitively to radiation exposure than the immortal cell lines.	(Grabinger et al., 2014)

Organoid type	Aim of the study	Key findings	Reference
Small intestine and liver – ASCs	Assessment of drug-metabolising enzymes and evaluation of CYP induction after treatment of organoids with the CYP inducers dexamethasone, β-naphthoflavone and 1,4-bis-2-(3,5-dichloro-pyridyloxy)-benzene in murine intestinal and liver organoids.	Expression of *CYP1A1, CYP1A2, CYP2A12, CYP2C37, CYP3A11*, and *CYP3A13* in both intestinal and liver organoids. These CYPs were differentially induced indicating high drug-metabolising capacity.	(Park et al., 2019)
Lung, liver and mammary – ASCs	Assessment of the *in vivo* tumorigenicity of organoids after *in vitro* treatment with ethyl methanesulfonate, acrylamide, diethylnitros-amine and DMBA.	Lung, liver and mammary organoids treated *in vitro* with ethyl methanesulfonate, acrylamide, diethylnitrosamine and DMBA were injected into mice leading to the formation of subcutaneous nodules *in vivo,* indicating the carcinogenic potential of the chemicals tested.	(Naruse et al., 2020)
Mammary – ASCs	Studying the effect on organoid formation and morphology in organoids derived from mammoplasty patients treated with physiologically relevant doses of cadmium.	Cadmium negatively affected mammary organoid formation and branching at the highest concentration tested, 2.5 µM. Gene expression analysis showed the up-regulation of metal response genes, like metallothioneins and zinc transporters, and inhibited hypoxia inducible factor-1α activity.	(Rocco et al., 2018)
Mammary – ASCs	Studying the effects of bisphenol A, mono-n-butyl phthalate and polychlorinated biphenyl 153 on the proteome in mammary organoids.	Treatment of mammary organoids with bisphenol A, mono-n-butyl phthalate and polychlorinated biphenyl 153 induced differential effects on the proteome. Treatment also	(Williams et al., 2016)

Organoid type	Aim of the study	Key findings	Reference
		altered the abundance of protein splice variants.	
Endometrial –ASCs	Characterisation of the impact of zinc stearate (plastic additive) on the development of organoids from endometrial cells from domestic cats.	Zinc stearate did not affect morphology, viability or cellular composition of endometrial organoids. The model developed could be used in future studies investigating the effects of plastic additives or drugs.	(Dundon et al., 2019)

Adapted from Caipa Garcia et al., (2022).

1.6.3 Advantages and limitations over other 3D models

Various other 3D cell culture models have been used recently in toxicology studies which, like organoids, aim to provide a more representative microenvironment and physiology than monolayer cultures (Augustyniak et al., 2019; Lynch et al., 2019; Mazzoleni et al., 2009). For example, genotoxicity assays using 3D skin models have been established and validated, while liver and lung tissue models are at earlier validation stages as more robust protocols are required (Pfuhler et al., 2020a).

Spheroids, which are cellular aggregates made from cell lines, have been used in toxicological studies for different endpoints, including drug toxicity, cytotoxicity, and genotoxicity (Amaral et al., 2017; David and Gooderham, 2016; Elje et al., 2019; Shah et al., 2018; Štampar et al., 2019; Zhang et al., 2020). For example, liver spheroids from both primary hepatocyte (HepaRG) and tumour (HepG2, JHH1 and Huh7) cell lines have been particularly useful in the modelling of human toxicity. Multiple studies have demonstrated different cellular responses between liver, lung, bladder and mammary cell line spheroids and their monolayer cell line counterparts, showing that 3D structures are more sensitive to damage and present higher expression levels of metabolic enzymes like CYPs (Conway et al., 2020; Shah et al., 2018; Štampar et al., 2019; Terashima et al., 2015; Zhang et al., 2020). Although, spheroids provide more relevant results due to their 3D microenvironment and are relatively easy to use, they are less

complex than organoids as they only contain a single cell type and are unable to replicate the relevant tissue structure (Augustyniak et al., 2019).

Mini organ cultures (MOCs) have also been employed in toxicological studies. These cultures consist of small tissue fragments that maintain the structure of the tissues of origin and, in the case of those derived from the respiratory tract, ciliary beat activity (Ginzkey et al., 2010; Hackenberg et al., 2011; Kleinsasser et al., 2004). Although MOCs provide the 3D structure of the tissue of origin, they need to be kept at certain size and cannot be grown for extended periods of time as their structure starts to change and viability decreases (Ginzkey et al., 2010; Hackenberg et al., 2011).

More complex models such as MPS have also been developed. These MPS models aim to recreate human physiological systems *in vitro* by interconnecting multiple organs in the form of organ-on-chips and/or organoids (Truskey, 2018). MPS for many organs including the liver, heart, kidney, skeletal muscle, and vasculature have been established, and these MPS organs can be connected in different combinations from two to thirteen organs in one system depending on the interactions to be replicated (Truskey, 2018). These systems have been used for the assessment of toxicity of drugs and other xenobiotics, including environmental compounds (Baudy et al., 2020; Chang et al., 2017; Rajan et al., 2020; Theobald et al., 2018; Wang et al., 2018). Although it has been demonstrated that MPS are useful in the study of organ-organ interactions and are able to replicate a range of functions such as absorption, metabolism and contractile forces, their complexity limits the development of high throughput assays as there can be too much variability (Truskey, 2018).

Lastly, the use of 3D *in vitro* skin models has been key in various industries to test the toxicity of compounds such as drugs and cosmetics (Abd et al., 2016). There are several skin models available, which provide different advantages depending on their origin. However, due to the increase in regulations on the use of animals and the limited availability of human skin for *ex vivo* assays, artificial models made from different polymers or skin substitutes such as reconstructed epidermis or full thickness skin have

become more widely used (Abd et al., 2016; Chau et al., 2013; Netzlaff et al., 2005). Reconstructed skin models have been developed for normal and diseased skin and consist of layers of human cells grown on a polymer matrix and can be of various complexities (Abd et al., 2016; Flaten et al., 2015). Many different reconstructed epidermis models are commercially available and are being used to test toxicity and irritation, as well as effects of formulations (Flaten et al., 2015). It has been shown that human reconstructed skin and full thickness models express XMEs although at levels that do not replicate those in native tissue (Jäckh et al., 2011). CYP enzyme levels are also very low in human skin and 3D skin models, but higher than in immortalised keratinocytes, so the reconstructed skin model is the better option for toxicology studies (Götz et al., 2012). Due to the ban in animal testing of cosmetics, reconstructed human skin models are validated and widely used, however, they are still being improved by adding additional layers of complexity like immune cells (Chau et al., 2013; Pfuhler et al., 2020b; Pupovac et al., 2018; Reisinger et al., 2018).

1.7 Aims of the project

The modes of action of many environmental carcinogens, describing changes as a result of carcinogen exposure, have been well-characterised, however, the mechanisms of action, describing changes at the molecular level, of most of these carcinogens are not yet fully understood. It is well known that target tissues for carcinogenesis cannot be identified by the levels of DNA damage alone, therefore investigation of other host factors contributing to this process is required. The study of organotropism is important to further understand the mechanism of environmental carcinogen-induced tumour formation and the causes of some cancer types thereby helping to identify ways of cancer prevention. Organotropism has been investigated in animal models and cell lines; however, as some responses may be species-specific or may be affected by the physiological conditions of *in vitro* experiments, they may not accurately predict human responses. Therefore, a model more relevant to human physiology, like human tissue derived organoids, may be useful in the fields of environmental carcinogenesis and toxicology.

The overall aim of this PhD project was to investigate the metabolic potential of human tissue organoids to activate environmental carcinogens from different chemical classes and to assess tissue-specific responses in organoids from target and non-target organs. Gastric organoids were selected as a non-target organ. The organoids from the target organs of the selected carcinogens were chosen as they are cancer targets in humans and/or animal models, or there is epidemiological data identifying them as possible targets. These were as follows:

- BaP: Pancreas and liver
- AFB_1: Liver
- AAI: Kidney
- PhIP: Colon.

The original study design of the project is shown in Figure 1.14.

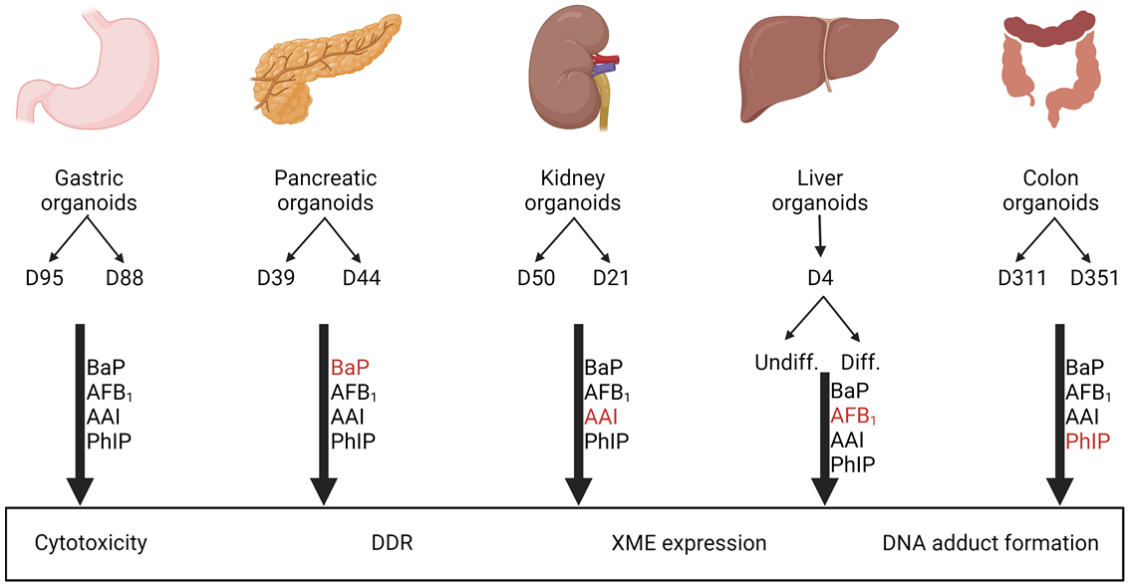

Figure 1.14. Scheme with the original study design of this PhD project. Normal human organoids derived from gastric, pancreas, kidney, liver and kidney tissues were treated with the selected environmental carcinogens (BaP, AFB_1, AAI and PhIP) to investigate different end-points (bottom panel). Gastric organoids were used as a non-target organ for all compounds, while each of the other organoid types was a target or possible target for carcinogenesis for one of the compounds (shown in red). Organoid cultures from two donors were used for each organoid type, except the liver, for which one donor culture was used. Liver organoids were used as undifferentiated organoids (ductal cells) and differentiated organoids (hepatocytes).

The first aim of the project was to assess if the organoids could metabolically activate the selected carcinogens. For this purpose, the organoids were first treated with the selected carcinogens to assess the effects on cell viability to then select concentrations for further investigations. The induction of the XMEs relevant to the bioactivation of each carcinogen were then evaluated and the metabolic activation of the compounds was investigated by analysing DNA damage response and DNA adduct formation. As the resources were available on-site, the formation of the main BaP metabolites (BaP-t-7,8-dihydrodiol and BaP-tetrol-I-1) was also assessed. Additionally, because the initial liver organoids were of ductal origin, these were differentiated into hepatocyte organoids as these are the liver cells that are most involved in metabolism, and both liver organoid types were used in the experiments.

The final aim of this study was to investigate carcinogen organotropism using human tissue organoid cultures to explore differences between target and non-target tissues after the treatment with the selected environmental carcinogens. For this, investigations were carried out in the target tissue organoid and in at least one non-target tissue organoid for each agent. In addition, organoids from two donors were used for all tissues, except liver, in order to assess donor-specific responses. Differences in XME expression, DDR and adduct formation were investigated. Moreover, alterations in gene expression of genes involved in apoptosis, oxidative stress, cell cycle, proliferation, transcription, metabolism, DDR and DNA damage repair were evaluated in organoids treated with BaP, as well as the presence of its main metabolites.

Although the original plan was to treat all organoids with the four test carcinogens (as shown in Figure 1.14), difficulties with the culture of some organoid types (particularly the pancreas and liver) and time constraints owing to the restrictions imposed by the COVID-19 pandemic did not allow the completion of all planned experiments. Thus, the study design was modified subsequently because of this.

Chapter 2 Materials and methods

2.1 Environmental carcinogens

BaP (purity ≥ 96%; Sigma, #B1760) stock solution was prepared at 25 mM in dimethyl sulfoxide (DMSO; Sigma, #D2650). AAI (purity ≥ 97%; Sigma, #A9451) was prepared at 20 mM by dissolving it in sterile water. AFB_1 (purity ≥ 98%; Sigma, #A6636; Enzo, #ALX-630-093) stock solution was prepared at 30 mM in DMSO. PhIP (purity ≥ 98%; synthesised at the Biochemical Institute for Environmental Carcinogens, Lurup, Germany) was prepared at 25 mM in DMSO. All compounds were aliquoted and stored at −20ºC until use. *N*-OH-PhIP (purity ≥ 95% synthesised at the Biochemical Institute for Environmental Carcinogens, Lurup, Germany) was prepared at 20 mM in DMSO; aliquots were purged with nitrogen gas, sealed with parafilm, and stored at −80ºC until use.

2.2 Organoid culture

2.2.1 Culture conditions

Organoid stocks were grown in 24-well plates, embedded in 50 µL BME2 gel (Cultrex, #3533-010-02), except for colon organoids which where embedded in 50 µL Matrigel (Corning, #356231), and overlaid with 500 µL organoid growth medium. The extracellular matrix was diluted at 65-75% with wash medium (Advanced Dulbecco's Modified Eagle Medium/Ham's F-12 [DMEM/F12; Life technologies, #12634-010], 10 mM HEPES [Life Technologies, #15630-056], 1X GlutaMAX [Life technologies, #35050-038]). The growth medium was changed every 2-3 days. Medium was prepared as described below and stored at 4ºC for up to 2 weeks for gastric and colon organoids, and up to 4 weeks for pancreas, kidney, and liver organoids. Growth media recipes for all organoid types can be found in Table 2.1 and the role of each of the supplements can be found in Supplementary Table 1. Two donors were used for each tissue, except for the liver organoids for which only one donor was used. More information about the donors found in Table 2.2. It is important to note that the age of the organoid donors ranges from

paediatric (three to 11 years old) to adults (over 60 years old). These were the available materials at the time the project was carried out.

2.2.1.1 Stomach

Gastric organoids were kindly provided by Drs Matthew Garnett and Hayley Francies at the Wellcome Trust Sanger Institute, Hinxton, UK (Li et al., 2018) and cultured in gastric expansion medium, using either the 'Schlaermann' or 'Bartfeld' recipe. Organoids grown in 'Schlaermann' media were expected to consist of gland mucous and chief cells, while organoids in 'Bartfeld' media also contained enteroendocrine cells (Bartfeld et al., 2015; Schlaermann et al., 2016).

The 'Schlaermann' medium consisted of Advanced DMEM/F12 supplemented with 10 mM HEPES, 1X GlutaMAX, 25% R-Spondin-1 conditioned medium (Cultrex, #3710-001-01), 50% WNT3A conditioned medium (ATCC CRL-2647 cell line), 1.25 mM *N*-acetyl-L-cysteine (Sigma, #A9165), 150 ng/mL Noggin (Peprotech, #120-10C), 20 ng/mL recombinant human EGF (Gibco, #PHG0313), 150 ng/mL FGF-10 (Peprotech, #100-26-25), 10 nM Gastrin I (Sigma, #G9020), 1X B27 (with vitamin A; Invitrogen, #17504001), 1 µM A83-01 (Tocris, #2939), 1X N2 supplement (Gibco, #17502001), 10 mM nicotinamide (Sigma, #N0636) and 2 µM SB202190 (Stem Cell Technologies, #72634) (Schlaermann et al., 2016).

The 'Bartfeld' medium consisted of Advanced DMEM/F12 supplemented with 10 mM HEPES, 1X GlutaMAX, 10% R-Spondin-1 conditioned medium, 50% WNT3A conditioned medium, 1.25 mM *N*-acetyl-L-cysteine, 150 ng/mL Noggin, 50 ng/mL recombinant human EGF, 100 ng/mL FGF-10, 1 nM Gastrin I, 1X B27 (with vitamin A), 2 µM A83-01 and 10 mM nicotinamide (Bartfeld et al., 2015).

2.2.1.2 Pancreas

Pancreatic organoids were kindly provided by Dr Meritxell Huch at the Max Planck Institute of Molecular Cell Biology and Genetics, Dresden, Germany (Broutier et al., 2016) and grown in pancreatic expansion medium consisting of Advanced DMEM/F12

supplemented with 10 mM HEPES, 1X GlutaMAX, 10% R-Spondin-1 conditioned medium, 1.25 mM *N*-acetyl-L-cysteine, 3 µM PGE2 (Tocris, #2296), 25 ng/mL Noggin, 50 ng/mL recombinant human EGF, 100 ng/mL FGF-10, 10 nM Gastrin I, 1X B27 (without vitamin A; Invitrogen, #12587001), 5 µM A83-01, 1X N2, 10 µM Forskolin (Tocris, #1099) and 10 mM nicotinamide.

2.2.1.3 Liver

Liver organoids were kindly provided by Dr Meritxell Huch at the Max Planck Institute of Molecular Cell Biology and Genetics, Dresden, Germany (Huch et al., 2015). Organoids were grown in liver expansion medium consisting of Advanced DMEM/F12 supplemented with 10 mM HEPES, 1X GlutaMAX, 10% R-Spondin-1 conditioned medium, 1.25 mM *N*-acetyl-L-cysteine, 1X B27 (without vitamin A), 1X N2, 10 mM nicotinamide, 10 nM Gastrin I, 50 ng/mL recombinant human EGF, 100 ng/mL FGF-10, 25 ng/mL HGF (Peprotech, #100-39), 10 µM Forskolin and 5 µM A83-01.

2.2.1.4 Kidney

Kidney organoids were kindly provided by Dr Jarno Drost, Princess Maxima Centre for Pediatric Oncology, Utrecht, the Netherlands (Schutgens et al., 2019). Kidney growth medium consisted of Advanced DMEM-F12 supplemented with 10 mM HEPES, 1X GlutaMAX, 10% R-Spondin-1, 1 mM *N*-acetyl-L-cysteine, 50 ng/mL recombinant human EGF, 100 ng/mL FGF-10, 1.5% B27 (with vitamin A), 5 µM A83-01.

2.2.1.5 Colon

Colon organoids were kindly provided by Dr Matthias Zilbauer, University of Cambridge, Cambridge, UK (Howell et al., 2018). Colon medium consisted of Advanced DMEM-F12 supplemented with 10 mM HEPES, 1X GlutaMAX, 20% R-Spondin-1, 50% WNT3A, 1X B27 (with vitamin A), 1.25 mM *N*-acetyl-L-cysteine, 100 ng/mL mouse Noggin (Peprotech, #250-38-250ug), 50 ng/mL recombinant mouse EGF (Gibco, #PMG8041), 10 nM Gastrin I, 0.5 µM A83-01, 10 mM nicotinamide and 10 µM SB202190.

Table 2.1. Growth media recipes for organoids derived from different human tissues

Medium component	**Final concentration**					
	Schlaermann	**Bartfeld**	**Pancreas**	**Liver**	**Kidney**	**Colon**
Advanced DMEM/F12	√	√	√	√	√	√
HEPES	10 mM	10 mM	10 mM	10 mM	10 mM	10 mM
Glutamax	1X	1X	1X	1X	1X	1X
WNT3A CM	50%	50%	-	-	-	50%
R-Spondin-1 CM	25%	10%	10%	10%	10%	20%
N-acetyl cysteine	1.25 mM	1.25 mM	1.25 mM	1.25 mM	1 mM	1.25 mM
Human Noggin	150 ng/mL	150 ng/mL	25 ng/mL	-	-	-
Mouse Noggin	-	-	-	-	-	100 ng/mL
Recombinant Human EGF	20 ng/mL	50 ng/mL	50 ng/mL	50 ng/mL	50 ng/mL	-
Recombinant Mouse EGF	-	-	-	-	-	50 ng/mL
FGF-10	150 ng/mL	100 ng/mL	100 ng/mL	100 ng/mL	100 ng/mL	-
HGF	-	-	-	25 ng/mL	-	-
Gastrin I human	10 nM	1 nM	10 nM	10 nM	-	10 nM
B27 Supplement (+ Vitamin A)	1X	1X	-	-	1.50%	1X
B27 Supplement (- Vitamin A)	-	-	1X	1X	-	-
A83-01	1 µM	2 µM	5 µM	5 µM	5 µM	0.5 µM
PGE2	-	-	3 µM	-	-	-
N2 Supplement	1X	-	1X	1X	-	-
Forskolin	-	-	10 µM	10 µM	-	-
Nicotinamide	10 mM	10 mM	10 mM	10 mM	-	10 mM
SB202190	2 µM	-	-	-	-	10 µM

Table 2.2. Organoid donors from different human tissues

Tissue	Donor ID	Age (years)	Gender	Specific biopsy information	Collaborating research team	Research Ethics Committee (REC)	REC #
Gastric	D88	76	Male	Normal gastric tissue from the upper stomach was removed from two patients (Donor 88 and Donor 95) that were undergoing biopsy for an oesophageal tumour.	Hayley Francies/ Mathew Garnett (Wellcome Trust Sanger Institute, Hinxton, UK)	London - Camden and Kings Cross Research Ethics Committee	16/L0/1110
	D95	69	Male				
Colon	SC311 (D311)	6	Male	Normal sigmoid colon tissue taken by endoscopy from healthy, control donors (note that this was part of an IBD study).	Matthias Zilbauer (Department of Paediatrics, University of Cambridge, Cambridge, UK)	East of England Cambridge South Research Ethics Committee	17/EE/0265
	SC351 (D351)	11	Female				
Kidney	JD021H (D21)	3	Female	Normal tissue was taken following nephrectomy or biopsy.	Jarno Drost (Princess Maxima Centre for Pediatric Oncology, Utrecht, The Netherlands)	Medical Ethical Committee of the Erasmus Medical Center (Rotterdam, The Netherlands).	MEC-2016-739
	JD050H (D50)	4	Female				
Pancreas	D39	unknown	Male	Biopsies of normal pancreatic or liver tissue were obtained from deceased patients during surgery for organ transplantation.	Meritxell Huch (Max Planck Institute of Molecular Cell Biology and Genetics, Dresden, Germany)/ Kourosh Saeb-Parsy (Department of Surgery, Addenbrooke's Hospital, Cambridge, UK)	NRES Committee East of England - Cambridge Central	12/EE/0253; 16/EE/0227
	D44	unknown	Male				
Liver	D4	unknown	Female				

2.2.2 Organoid splitting and seeding

Organoids were passaged every 7 to 10 days depending on density. The medium was removed, and 1 mL of ice-cold wash medium was added to dissociate the organoids from the gel. Organoids were then scraped off the plate and transferred into a 15-mL Falcon tube (maximum 3 wells per tube). Tubes were centrifuged at 350 x *g* for 1 to 5 min at 4ºC and the supernatant was removed. Organoids were broken up by vigorous pipetting in ~300 µL wash media, then a further 5 mL of cold wash media was added, and the tube was incubated on ice for 10 min. The suspension was centrifuged at 350 x *g* for 5 min and the supernatant was removed. The organoids were then seeded as described below or broken down further by adding 500 µL TrypLE (Gibco, #12605028) per well and incubating at 37ºC for 2-3 min, depending on the organoid type. To inactivate the TrypLE, 5 mL of cold wash medium was added, and the centrifugation step repeated. After removing the supernatant, the organoid pellet was incubated on ice. The required volume of BME2/Matrigel (diluted to 65-75% with wash medium) was added, and the pellet resuspended by carefully pipetting up and down. The BME2/Matrigel-organoid mix was seeded into the wells of pre-warmed plates, 50 µL in a 24-well plate and 10 µL in a 96-well plate. Plates were incubated at 37ºC for 20 min, and if seeded in a 24-well plate the plate was flipped during the incubation. The required medium (500 µL in a 24-well plate and 75 µL in a 96-well plate) was pre-warmed and supplemented with 10 µM Y-27632 (Stem Cell Technologies, #72308) before adding it to the wells.

Organoid stocks were split by alternating between vigorous pipetting and TrypLE. For cell viability experiments, gastric, colon and kidney organoids were split by adding TrypLE, and pancreatic and liver organoids by vigorous pipetting. For all other experiments all organoids were split by vigorous pipetting from TrypLE stocks.

Colon organoid stocks were grown in Matrigel. For experiments, colon organoids were grown in BME2 due to inactivity of the compounds in Matrigel (Supplementary Figure 1).

2.2.3 Organoid cryopreservation and thawing

Frozen stocks were prepared from one confluent well by dissociating the organoids from the BME2/Matrigel as explained in Section 2.2.2. For frozen stocks, organoids were broken down slightly by pipetting and pelleted at 350 x *g* for 5 min at 4ºC. The supernatant was removed, and the pellet resuspended in 500-750 µL Recovery Cell Culture Freezing Medium (Gibco, #12648010). The cell suspension was added to a cryovial and placed in a Nalgene Mr Frosty freezing container at −80ºC and then transferred to a liquid nitrogen tank.

When recovered, the frozen organoids were thawed in a 37ºC water bath. The thawed organoids were added to a tube with 4 mL wash medium and centrifuged at 350 x *g* for 5 min at 4ºC. The supernatant was removed and then the pellet was resuspended in 100 µL BME2/Matrigel and seeded in two wells of a 24-well plate. The plate was flipped and incubated for 20 min at 37ºC before adding the required pre-warmed medium supplemented with 10 µM Y-27632.

For liver organoids starting medium (Table 2.3) was used after thawing and until organoids had formed (approximately 7 days). Starting medium consists of Advanced DMEM/F12 supplemented with 10 mM HEPES, 1X GlutaMAX, 10% R-Spondin-1, 30% WNT3A, 1.25 mM N-acetyl-L-cysteine, 25 ng/mL HGF, 50 ng/mL recombinant human EGF, 100 ng/mL FGF-10, 10 nM Gastrin, 25 ng/mL Noggin, 1X B27 (without vitamin A), 5 µM A83-01, 1X N2, 10 µM Forskolin, 10 mM nicotinamide, 10 µM Y-27632 and 1X hES cell cloning and recovery supplement (Stemgent, #01-0014-500) (Broutier et al., 2016).

2.2.4 Liver organoid differentiation

Liver organoids were seeded as described in Section 2.2.2 and grown in liver growth medium supplemented with 25 ng/mL BMP7 (Peprotech, #OP1 120-03) for 5 days. After day 5 the medium was changed to liver organoid differentiation medium (Table 2.3) consisting of Advanced DMEM/F12 with 10 mM HEPES, 1X GlutaMAX, 1.25 mM *N*-acetyl-L-cysteine, 25 ng/mL HGF, 50 ng/mL recombinant human EGF, 100 ng/mL

FGF-19 (R&D, #969-FG-025), 10 nM Gastrin, 1X B27 (with vitamin A), 0.5 µM A83-01, 1X N2, 10 µM DAPT (Sigma, #D5942), 3 µM dexamethasone (Sigma, #D4902), 25 ng/mL BMP7. Organoids were cultured for 10 days in liver differentiation medium, after which organoids were ready for further experimentation (Broutier et al., 2016). A timeline of the process can be seen in Figure 2.1.

Table 2.3. Liver starting and differentiation media recipes

Medium component	Final concentration	
	Liver Starting	Liver Differentiation
Advanced DMEM/F12	√	√
HEPES	10 mM	10 mM
Glutamax	1X	1X
WNT3A CM	30%	-
R-Spondin-1 CM	10%	-
N-acetyl cysteine	1.25 mM	1.25 mM
Human Noggin	25 ng/mL	-
Recombinant Human EGF	50 ng/mL	50 ng/mL
FGF-10	100 ng/mL	-
HGF	25 ng/mL	25 ng/mL
Gastrin I human	10 nM	10 nM
FGF-19	-	100 ng/mL
B27 Supplement (+ Vitamin A)	-	1X
B27 Supplement (- Vitamin A)	1X	-
A83-01	5 µM	0.5 µM
N2 Supplement	1X	1X
Forskolin	10 µM	-
Nicotinamide	10 mM	-
DAPT	-	10 µM
Dexamethasone	-	3 µM
BMP7	-	25 ng/mL
Y-27632	10µM	-
hES Cell Cloning and Recovery	1X	-

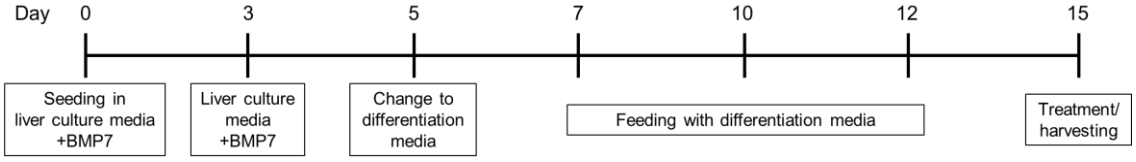

Figure 2.1. Liver organoid differentiation timeline from seeding to treatment or analysis.

2.2.5 Treatment with carcinogens

Organoids were seeded in 96-well or 24-well plates 48 to 72 hr before treatment. Carcinogens were diluted in organoid medium to the desired final concentrations. Organoids were treated for 48 hr at a range of concentrations: 0-50 µM BaP; 0-200 µM AAI; 0-150 µM AFB_1; 0-250 µM PhIP; or 0-20 µM *N*-OH-PhIP. Controls were treated with solvent only at the same final percentage used in the carcinogen treatments (*i.e.,* DMSO or water).

2.3 Measurement of cell viability

After treatment cell viability was assessed using the CellTiter-Glo 3D Cell Viability Assay (Promega, G9683), which determines the amount of viable cells based on the quantitation of ATP present. This assay relies on the luciferase reaction between luciferin and ATP that generates a luminescent signal that is measured using a plate reader (Figure 2.2).

Organoids were seeded in 96-well plates at 20% density, cultured for 48-72 hr and then treated with the carcinogen of interest for 48 hr at concentrations indicated in Section 2.2.5. Each treatment was performed at least in triplicate. After treatment, the plate and CellTiter-Glo reagent were allowed to equilibrate to room temperature for approximately 30 min. If wells contained more than 75 µL medium, the excess was removed. The remaining 75 µL medium was mixed with the reagent at a 2:1 ratio by pipetting up and down. The mixture was then incubated at room temperature in the dark for 20 min, and briefly mixed again before 50 µL was transferred to a white assay plate. Luminescence was measured using a GloMax Explorer microplate reader (Promega).

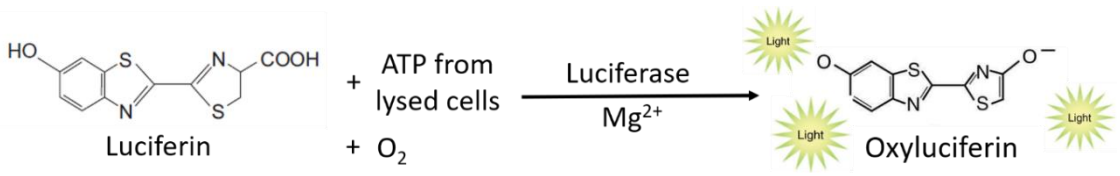

Figure 2.2. CellTiter-Glo Assay reaction. Luciferin reacts with ATP from the lysed cells in the presence of luciferase to produce oxyluciferin, which emits light (peak at 560 nm) that is then measured using a plate reader. The level of luminescence is proportional to the number of viable cells.

2.4 Protein expression analysis

2.4.1 Preparation of organoid lysates

For Western blotting organoids were seeded in 24-well plates. Organoids were treated for 48 hr once they reached a density of 70-80% and 3 wells per sample were pooled. Each treatment was carried out at least in duplicate. After treatment, organoids were harvested by adding cold wash medium to the wells. These were then transferred to a 15-mL Falcon tube and centrifuged at 500 x *g* for 5 min at 4ºC. To break down the BME2, the supernatant was removed, and cold wash media added to the pellet, which was then incubated for 10 min on ice and centrifuged. After removing the supernatant, the pellet was resuspended in 1 mL TrypLE and incubated at 37ºC for 10 min and then pipetted vigorously 3 times before adding cold wash medium and centrifuging again. The organoid pellet was transferred into a 1.5-mL Eppendorf tube, washed with PBS and centrifuged at 4000 rpm for 3 min at 4ºC. The supernatant was removed, and the pellet was lysed with 90 µL lysis buffer (62.5 mM Tris [pH 6.8; Thermo Scientific, #17926], 1 mM EDTA [pH 8; Sigma, EDS500G], 2% sodium dodecyl sulfate [SDS; AppliChem GmbH, #A0767,0250], 10% glycerol [Sigma, #G7757], 1X HaltTM Protease and Phosphatase Inhibitor Cocktail [Thermo Fisher Scientific, #78442]). Cell lysates were sonicated twice at 20% amplitude, 0 pulse for 10 sec with a Sonic Dismembrator (Fisher Scientific, #FB-120).

2.4.2 Protein quantitation

The protein content was quantified with the Pierce Bicinchoninic Acid (BCA) Protein Assay (Thermo Fisher Scientific, #23225). This assay uses the reduction of Cu^{2+} to Cu^{+} by protein in alkaline conditions and the highly sensitive colorimetric detection of the Cu^{1+} cation, which reacts with two molecules of BCA (Thermo Scientific, 2011). The BCA assay was carried out according to manufacturer's instructions by pipetting 5 µL of diluted bovine serum albumin (BSA) standard (0-2 mg/mL) and each sample in duplicate on a clear 96-well plate and then 195 µL of BCA working solution in a 50:1 ratio of Reagent A to Reagent B. The plate was then incubated for 20 to 30 min at 37ºC, and the

absorption assessed at 595 nm using a BioTek ELx800 plate reader. Samples were normalised to the lowest concentration by adding appropriate amounts of lysis buffer. β-Mercaptoethanol (0.1% v/v; Sigma, M3148) and bromophenol blue (0.01% w/v; Sigma, #B0126) were added to each lysate prior to denaturation at 95ºC for 5 min. Lysates were then stored at −20ºC until analysis.

2.4.3 Sodium dodecyl sulphate polyacrylamide gel electrophoresis (SDS-PAGE)

Proteins were separated by size using SDS-PAGE, with the smaller proteins migrating faster through the gel. Equal amounts of protein (10-15 µg) and 5 µL of SeeBlue Plus2 Pre-stained Protein Ladder (Life Technologies, #LC5925) were loaded on 15- or 26-well precast 4-12% gradient bis(2-hydroxyethyl)amino-tris(hydroxymethyl)methane-HCl, (bis-tris) gels (Invitrogen, #NP0336BOX or #WG1403BOX). The gel was run for 75 min at 150 V for 15-well gels or 90 min at 130V for 26-well gels in an Invitrogen or Bio-Rad electrophoresis chamber, respectively, with 1X NuPAGE MES SDS running buffer (Thermo Fisher Scientific, #NP0002).

A lysate of human induced pluripotent stem cells (the cBOB line) treated with 3.125 µM cisplatin was used as a positive control. These cells were derived at the Wellcome Trust Sanger Institute, Hinxton and used as previously described (Kucab et al., 2019).

2.4.4 Western blot analysis

After SDS-PAGE proteins were then transferred onto a 0.2 µm nitrocellulose membrane (Bio-Rad, #162-0112) using a Bio-Rad transfer chamber for 90 min at 110 V for 15-well gels or 100V for 26-well gels. The chamber was filled with cold transfer buffer, which for 15-well gels consisted of: 10% methanol + 10X transfer buffer stock diluted to 1X with diH_2O (250 mM Tris base [Fisher Scientific, #BP152-1], 1.92 M glycine [Santa Cruz, #sc-29096] and diH_2O up to 1 L for 10X transfer buffer); and for 26-well gels: 10% methanol + 20x NuPAGE transfer buffer diluted to 1X with diH_2O (Invitrogen, #NP00061). The chamber was put in an ice box and a cooling block placed inside the chamber to

keep it cold throughout the process. After blotting, successful transfer was assessed by staining the membrane with Ponceau Red (Sigma, #P7170). The membrane was then washed with water followed by a wash in 1X TBST (10x tris-buffered saline diluted to 1X with diH_2O [TBS: 10X stock 10 mM Tris base, 150 mM NaCl and diH_2O up to 2 L, pH 7.3-7.5] plus 0.1% Tween-20 [Sigma, #P1379]). Membranes were cut at 28 kDa and blocked in 3% non-fat dry milk (Marvel) in TBST for 1 hr at room temperature or up to 24 hr at 4ºC to minimise non-specific binding.

The following primary antibodies diluted in blocking solution and 0.1% sodium azide (Sigma, #S8032) were used: anti-p21 (1:2000; BD Bioscience, #BD556431), anti-phospho-H2AX (pH2AX; Ser139, 1:1000; Cell Signalling, #9718S), anti-phospho-CHK2 (pCHK2; T68, 1:1000; Cell Signalling, #2197S), anti-phospho-p53 (p-p53; Ser15, 1:2000; Cell Signalling, #9284S) and anti-GAPDH (1:25000; Chemicon, #MAB374). All primary antibodies were incubated overnight at 4ºC, except the loading control, GAPDH, which was incubated for 30 min at room temperature. After incubation with the primary antibody membranes were washed in TBST for 30 min with agitation and then incubated in species-specific secondary antibodies linked to horseradish peroxidase (HRP; anti-mouse/rabbit, Bio-Rad, #170-5046/7) for 1 hr at room temperature. Then membranes were washed again with agitation in TBST for 40 min.

The proteins were detected using enhanced chemiluminescence (ECL) solution (Amersham GE Healthcare, #RPN2106). The working reagent was prepared in a 1:1 ratio for reagents A and B, added onto the membrane to cover it for 1 min and then the membranes were wrapped in plastic and placed in a film cassette. The ECL solution reacts with the HRP on the secondary antibody to produce light, which is then captured by photographic films (Amersham Hyperfilm ECL; GE Healthcare Life Sciences, #28906836). The film was processed using a film processor (Konica, #SRX-101A). The membranes were then washed with TBST and stored in TBST at 4ºC for short-term, −20ºC for long-term or re-probed with another primary antibody.

2.5 DNA adduct analysis

2.5.1 Preparation of organoid samples

For DNA adduct analysis organoids were seeded in 24-well plates and exposed to the carcinogens for 48 hr, with 4 wells pooled together per sample after treatment. Each treatment was carried out in at least triplicate. After treatment, organoids were harvested by adding cold wash medium to the wells and transferring them into a 15-mL Falcon, which was centrifuged at 500 x *g* for 5 min at 4ºC. The supernatant was removed, and cold wash media added to the pellet, which was then incubated for 10 min on ice and centrifuged. After removing the supernatant, the pellet was transferred into a 1.5-mL Eppendorf tube and centrifuged at 3000 rpm for 3 min. The supernatant was removed, and the pellets were stored at −20ºC until DNA extraction.

2.5.2 DNA extraction by phenol-chloroform

DNA was extracted using a phenol-chloroform extraction method. The organoid pellets were resuspended in 300 µL of 1 mM EDTA/50 mM Tris and 9 µL RNase mix (4.5 µL of 10 mg/mL RNase A [Sigma, #R4875] + 4.5 µL of 50 KU RNase T1 [Sigma, #R1003]). The pellets were lysed by adding 40 µL of 10% SDS in 10 mM EDTA, followed by vortexing and incubation at 37°C at 450 rpm for 30 min. After this 40 µL of 10 mg/mL proteinase K (Sigma, #P6556) were added and the samples incubated overnight at 37°C at 450 rpm. DNA was extracted by adding 400 µL of phenol (Sigma, #P4557) followed by vigorous shaking for 5 min and centrifugation for 5 min at maximum speed. The upper layer was transferred to a new 1.5-mL Eppendorf tube and the step repeated with 400 µL phenol:chloroform:isoamyl alcohol (25:24:1) saturated with Tris-HCl (Invitrogen, #15593031). The top layer was transferred to a new tube and 500 µL of SEVAG (chloroform:isoamyl alcohol, 24:1) were added; the shaking and centrifugation steps were then repeated. After transferring the upper layer to a new tube, 1/10th of the sample volume of 5 mM NaCl was added and mixed by vortexing. DNA was precipitated by adding 2 volumes of 100% ice-cold ethanol and shaking by hand and then vortexing. The DNA was then pelleted by centrifugation at maximum speed for 5 min. The ethanol

was removed, and the DNA pellet washed by adding 300 µL of 70% ice-cold ethanol followed by centrifugation for 2 min at maximum speed. All ethanol was removed, and the DNA was resuspended in 30-100 µL TE buffer (10 mM Tris-HCl, 1 mM EDTA, pH 8.0) according to pellet size. The pellets were dissolved at 4°C overnight and then mixed for 2-3 hr at 37°C at 400 rpm. The DNA concentration and purity were measured by spectrophotometry at 230, 260 and 280 nm using the NanoDrop 2000 Spectrophotometer. The DNA was stored at –20°C until further analysis.

2.5.3 DNA adduct analysis by LC-ESI-MS/MS after treatment with BaP

Samples were evaporated to dryness using a SpeedVac concentrator (SVC-100, Savant) and were shipped at room temperature to the Masonic Cancer Center at the University of Minnesota (Minneapolis, Minnesota, USA). Liquid chromato-graphy-electrospray ionization tandem mass spectrometry (LC-ESI-MS/MS) analysis was performed by Dr Silvia Balbo and Andrew Floeder as previously described (Villalta et al., 2017). A diagram of the process is shown in Figure 2.3. DNA purification was carried out by dissolving 20 µg in 50 µL of water. This solution was then loaded onto an Amicron Ultra 10K Centrifugal Filter (0.5 mL). The sample was centrifuged for 20 min at 14000 x *g* and 24°C. The filter was then washed twice with 400 µL of 400 mM $(NH_4)_2HCO_2$ (pH 9.0) and 5 mM $N(NH_4)_2HCO_2$ (pH 8.0) and the DNA recovered by inverting the filter into a new centrifuge tube and centrifuging for 2 min at 1000 x *g* at 24°C. Then 30 µL of the DNA solution were transferred to insert vials with 35 µL of 10 mM $MgCl_2$ and 0.1 mM $ZnCl_2$ in 400 mM $(NH_4)_2HCO_2$ digestion buffer. The samples then underwent enzymatic hydrolysis by adding 5 µL of Benzonase® (1 U/µL in water) and heating to 37°C in a water bath for 1 hr. This was followed by the addition of 3.2 µL of phosphodiesterase (1 mU/µL in water) and 4 µL of alkaline phosphatase (10 mU/µL in 400 mM $(NH_4)_2HCO_2$) and heated overnight in a 37°C water bath.

The quantitation of dG was then performed to determine the amount of DNA in each sample and confirm its complete hydrolysis. A 10 µL aliquot from each sample was taken and 2 µL were injected onto a Dionex UltiMate 3000 RSLCnano UPLC system with UV

detection at 254 nm and a Luna C18 (250 mm × 0.5 mm, 5 µm, 100 Å) HPLC column. The LC solvents were (A) water and (B) methanol. The HPLC column was equilibrated at 15 µL/min with 5% B for 20 min. This was followed by a linear mixed gradient starting at 5% B for 1 min, increasing to 25% B over 10 min, then to 95% B over 3 min and remaining constant at 95% B for 5 min before decreasing to 5% B for an 11 min equilibration for the next injection. The dG was quantified using a calibration curve (0.0625 ng/µL – 32 ng/µL).

A two-step liquid-liquid butanol extraction was carried out to isolate the dG-N^2-BPDE adducts. First, the internal standard (5 fmol of [$^{13}C_{10}$](±)BPDE−N^2-dG in 5 µL of 50% acetonitrile) was added to the samples. A water-saturated butanol solution was prepared by combining 2 mL of butanol and 1 mL of water, and vortexing for 30 sec; this was left to stand overnight until the layers separated. The bottom layer (water) was discarded and only the water-saturated butanol was left. Then 80 µL of water-saturated butanol was added to each sample. The biphasic samples were then vortexed for 30 sec and centrifuged for 2 min at 248 x *g* to separate the layers. The newly formed bottom aqueous layer was removed with a 100 µL airtight Hamilton syringe. Then 500 µL of water was added to the samples to remove any residual salts. The samples were vortexed for 30 sec, centrifuged and the water layer was discarded as described above. The remaining butanol solution was dried in a SpeedVac and the residue reconstituted by vortexing the samples with 20 µL of 10% acetonitrile. The samples were centrifuged and 2 µL of the sample was injected onto a LC-ESI-MS/MS system for analysis.

The dG-N^2-BPDE adducts were quantified by positive ion targeted MS^2 (tMS^2) analysis using a Lumos Orbitrap Tribrid mass spectrometer (Thermo Scientific, Waltham, Massachusetts, USA). Isolation of the parent ions of the analyte and internal standard (*m/z* 570.1983 and *m/z* 580.2318, respectively) was performed using the quadrupole mass filter with an isolation window of *m/z* 1.5 and underwent “beam-type” fragmentation with a higher-energy C-trap dissociation collision energy of 15%. Quantitation of the analyte and internal standard was performed by chromatographic peak integration of the

extraction ion chromatograms of the fragment ion masses of *m/z* 454.1510 ± 5 ppm and *m/z* 459.1678 ± 5 ppm, respectively. The Easy-IC internal mass calibration feature was used to ensure maximum mass accuracy to sub-ppm levels. The tMS^2 method had a maximum Orbitrap inject time of 246 msec, a normalized automatic gain control target of 2000%, a scan range (*m/*z) 100-600, and at a resolution of 120000. A full scan with a maximum Orbitrap inject time of 50 msec, normalised automatic gain control target of 250%, scan range (*m/z*) 100-1000, and resolution 15000 was performed to monitor all ionisable constituents present during the chromatographic runs. Positive mode ionisation was performed using a Nanoflex nanospray ion source (Thermo Scientific) with the following parameters: spray voltage of 2200 V, ion transfer tube temperature of 300°C, and a radio frequency lens setting of 60%.

The chromatographic separation was performed using a Dionex UltiMate 3000 RSLCnano UPLC system coupled to the nanospray ion source containing a capillary column (75 µm i.d., 15 cm length, 10 µm orifice) created by hand-packing a commercially available fused-silica emitter (New Objective, Woburn, Massachusetts, USA) with Luna C18(2) (5 µm particle size, 100 Å pore size) stationary phase (Phenomenex, Torrance California, USA). The LC solvents were (A) 0.05% acetic acid in water and (B) acetonitrile. The column was equilibrated at 1 µL/min for 5 min at initial gradient conditions. Two µL of each sample were injected. A linear gradient was used starting with a 5% B hold for 5.5 min to push the sample out of the 5 µL autosampler loop and onto the column. The flow rate was decreased to 0.3 µL/min over 1 min, with switching of the injection valve to remove the injection loop from the flow path. The percent of B was increased to 95% over 19 min and kept constant for 2 min. Data analysis was performed using FreeStyle™ 1.4 from Thermo Fisher Scientific.

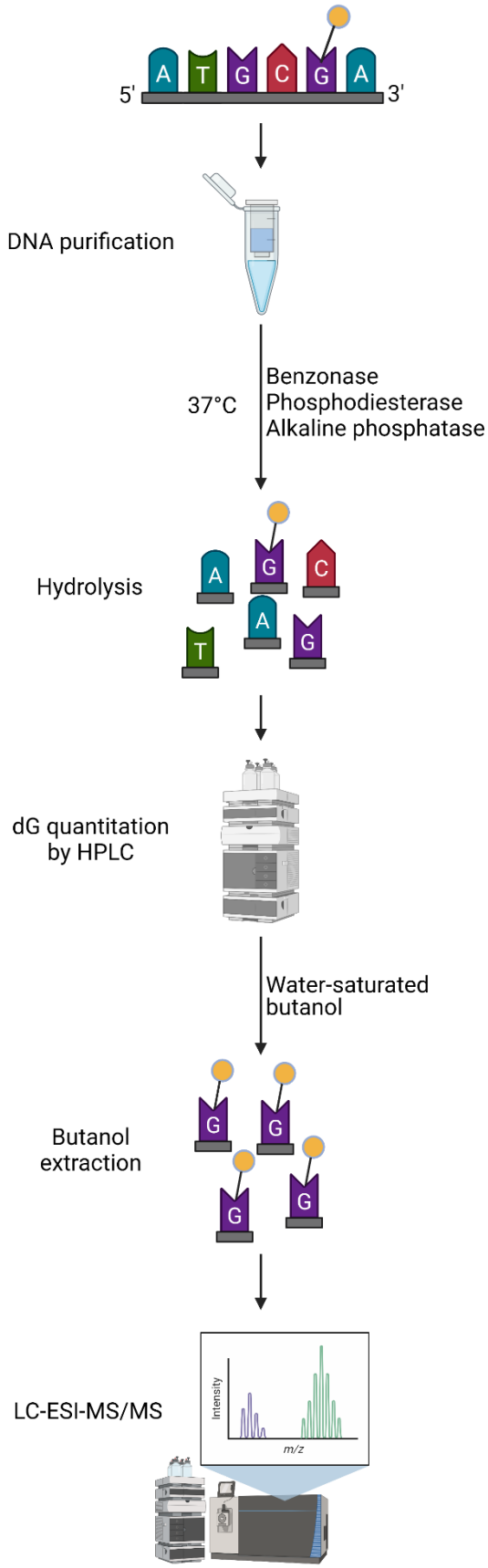

Figure 2.3. Diagram of the analysis of BaP-DNA adducts by LC−ESI-MS/MS. Yellow label represents the DNA adduct (modified DNA base). See text for details. Created with BioRender.com.

2.5.4 DNA adduct analysis by UPLC-ESI/MS^3 after treatment with AAI, PhIP or *N*-OH-PhIP

Frozen DNA samples were shipped on dry ice to the Masonic Cancer Center at the University of Minnesota (Minneapolis, Minnesota, USA). The ultra-performance liquid chromatography coupled with electrospray ionisation tandem mass spectrometry (UPLC-ESI/MS^3) analysis was performed by Drs Madjda Bellamri, Lihua Yaol, and Robert Turesky as previously described (Nauwelaers et al., 2011). A scheme of the process is shown in Figure 2.4. Samples from the same organoid donor treated with AAI (5 µg) or *N*-OH-PhIP (5 µg) were pooled and digested simultaneously (*e.g.*, D95 AAI-treated with D95 *N*-OH-PhIP treated). PhIP-treated samples (5 µg) were analysed separately. Each sample was resuspended in LC/MS water to a final volume of 94 µL. Each sample (pooled or not) was spiked with 2 µL of labelled internal standard ($^{15}N_3$-dA-AL-I and/or $^{13}C_{10}$-dG-C8-PhIP) at a level of 5x10^8 bases. To this 3.5 µL of Master mix I (2.5 µL of pH 7.1, 200 mM Bis-Tris and 1 µL of 1M $MgCl_2$) and 6 µL of Master mix II (5 µL of 1 mg/mL DNase I and 1 µL of 0.5 mg/mL nuclease P1), the samples were mixed gently by vortexing and incubated at 37°C at 950 rpm for 3.5 hrs. After 4 hr of incubation, 3 µL of Master mix III (2 µL of 1 mg/mL alkaline phosphatase and 1 µL of 50 ng/mL phosphodiesterase I) was added and the samples incubated for 18 hr at 37°C at 950 rpm. After digestion, the DNA was dried under vacuum at room temperature. The dried DNA was resuspended in 28 µL of water:DMSO (1:1), and then vortexed and sonicated for 5 min. This was followed by centrifugation for 10 min at 21000 x *g*. Twenty-five µL of each sample were transferred into a LC/MS vial.

The DNA adducts were measured by UPLC-ESI/MS^3 employing a Dionex Ultimate 3000 LC (Thermo Fisher, San Jose, California, USA) equipped with a Thermo Acclaim PepMap trap cartridge RP C18 (0.3 mm × 5 mm, 5 µm particle size, 100 Å), a Michrom Magic C18 AQ column (0.1 mm × 150 mm, 3 µm particle size), and a Michrom Captive Spray source (Auburn, CA) interfaced with a linear ion trap mass spectrometer Velos Pro (Thermo Scientific, San Jose, CA). The LC mobile phases were (A) 0.01% formic acid

and (B) 95% acetonitrile containing 0.01% formic acid. The DNA digest was injected onto the trapping column and washed with mobile phase A for 6 min at a flow rate of 12 µL/min. Then the adducts were back-flushed onto the Magic C18 AQ column at a flow rate of 1 µL/min. A linear gradient of 1–99% B over 10 min was applied for the separation, followed by 3 min of washing at 99% B. Analyses were conducted in the positive ionization mode. Optimized instrument tuning parameters were as follows: capillary temperature: 270°C; source spray voltage: 1.8 kV; injection time: 10 ms, activation Q: 0.35, and a normalized collision energy: 25 and 40 for MS^2 and MS^3 respectively. The ions monitored at the MS^3 scan stage were as follows: dA-AL-I (*m/z* 543.3 > 427.2 > 292.1, 293.1, 412.1), $^{15}N_5$-dA-AL-I (*m/z* 548.3 > 432.2 > 292.1, 293.1, 417.1), dG-C8-PhIP (*m/z* 490.1 > 374.1 > 250.1, 304.1, 329.1, 357.1) and $^{13}C_{10}$-dG-C8-PhIP (*m/z* 500.1 > 379.1 > 251.1, 307.1, 333.1, 362.1).

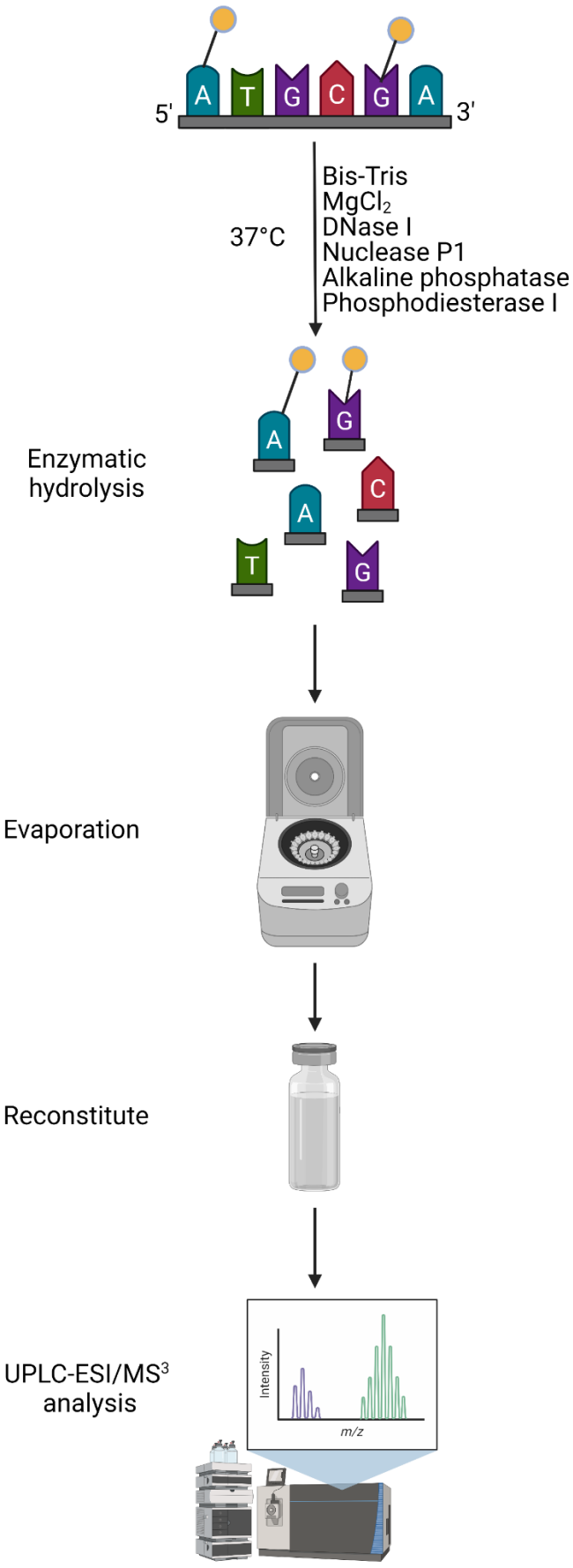

Figure 2.4. Diagram of the analysis of AAI and PhIP-DNA adducts by UPLC-ESI/MS^3. Yellow label represents the DNA adduct (modified DNA base). See text for details. Created with BioRender.com.

2.5.5 DNA adduct analysis by LC-MS/MS after treatment with AFB_1

DNA samples were evaporated using a SpeedVac. The samples were shipped at room temperature to the Johns Hopkins Bloomberg School of Public Health (Baltimore, Maryland, USA). The analysis was carried out by Dr John Groopman using liquid chromatography tandem mass spectrometry (LC-MS/MS) (Coskun et al., 2019; Egner et al., 2006; Woo et al., 2011), a scheme is shown in Figure 2.5. The internal standard AFB_1-FapyGua-$^{15}N_5$ was added at 0.6 pmol to 3-30 µg dried DNA sample. The samples were then dissolved in 100 µL of 0.1 mol/L HCl and were heated at 95°C for 1 hr. After cooling the samples, they were freeze-dried. The dried samples were dissolved in 100 µL of water before LC-MS/MS analysis.

A Thermo-Scientific Finnigan TSQ Quantum Ultra AM triple quadrupole MS/MS system with an installed heated electrospray-ionization source, was used for LC-MS/MS analysis. An Zorbax Extend C18 narrow-bore LC column (2.1 mm × 100 mm, 1.8 µm particle size) (Agilent Technologies, Wilmington, Delaware, USA) with an attached Agilent Eclipse XDB-C8 guard column (2.1 mm × 12.5 mm, 5 µm particle size) was used to analyse the cis-AFB_1-FapyGua, and trans-AFB_1-FapyGua adducts. The mobile phases used for analysis were: A: 98% water, 2% acetonitrile and 0.1% formic acid, and B: acetonitrile with 0.1% formic acid. An initial gradient of 4% of B/min starting from 100% A was used. After 10 min, mobile phase B was increased to 90% in 0.5 min and kept at this level for 5 min and then another 15 min at 8% to equilibrate the column. The flow rate was 0.3 mL/min, and the total analysis time was 25 min.

MS/MS was conducted using the following parameters: spray voltage at 3.5 kV; tube lens offsets at 89 V for Q1 and Q3; vaporizer temperature at 250°C; capillary temperature at 340°C; sheath gas (nitrogen) pressure at 50 arbitrary units; auxiliary gas (nitrogen) pressure at 30 arbitrary units; collision gas (argon) pressure at 6.67 × 10−5 Pa (5 mTorr). Selected reaction monitoring data were acquired in the positive ionization mode at a mass range of *m/z* 100 to *m/z* 1500 with scan width *m/z* 2.000 and scan time 0.10 sec.

The data obtained were normalised to the amount of DNA used in the analysis.

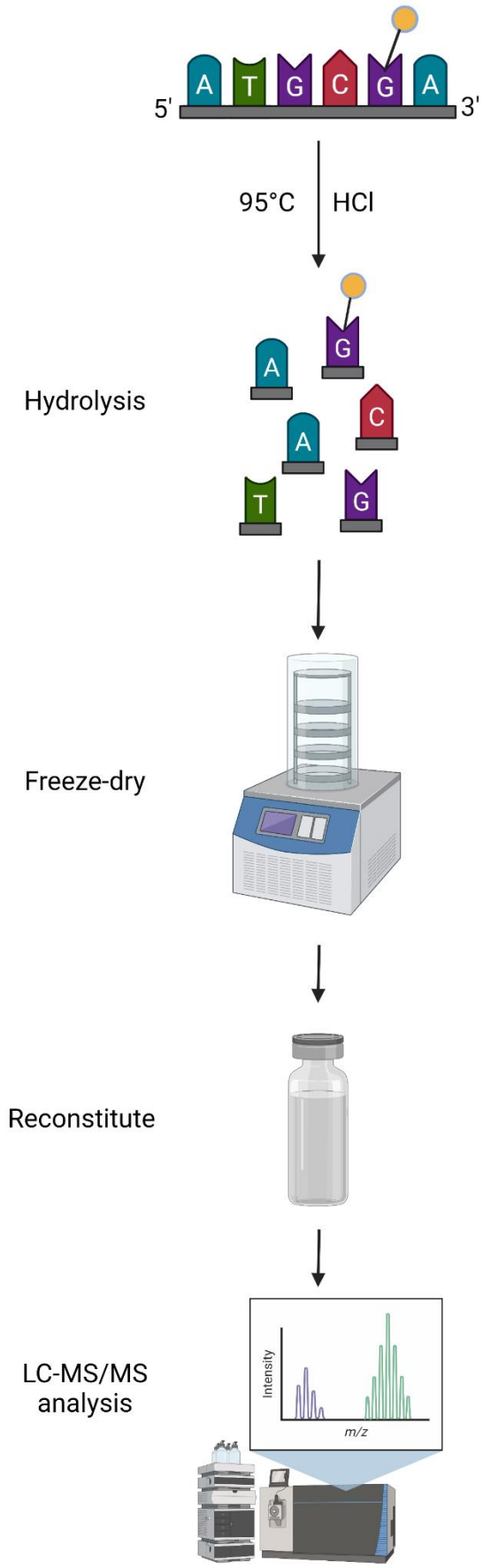

Figure 2.5. Diagram of the analysis of AFB_1-DNA adducts by LC-MS/MS. Yellow label represents the DNA adduct (modified DNA base). See text for details. Created with BioRender.com.

2.6 Gene expression analysis

2.6.1 Preparation of organoid samples

To assess the relative gene expression of various genes of interest, organoids were seeded in 24-well plates. Organoids were treated when they reached a density of 70-80% and 3 wells were pooled together per sample after treatment. Each treatment was carried out in at least triplicate. After treatment, organoids were harvested as described in section 2.5.1, and the pellets lysed with 350 µL RLT buffer (RNeasy Mini Kit; Qiagen, #74104) with 10 µL/mL β-mercaptoethanol. Lysates were homogenised by centrifuging through QIAshredder columns (Qiagen, #79654) for 2 min at 9600 x *g*. The homogenised lysates were stored at −80°C until RNA isolation.

2.6.2 RNA extraction

Total RNA was isolated using the RNeasy Mini Kit (Qiagen) according to the manufacturer's instructions. Briefly, the homogenised lysates were thawed, and an equal volume of 70% ethanol was added and mixed by pipetting. The sample was then transferred to a RNeasy Mini Spin column, to which RNA binds; this was centrifuged for 15 sec at 8000 x *g*. The flow-through was discarded and the column washed by adding 350 µL of RW1 buffer to the column and spinning for 15 sec at 8000 x *g*. When DNase treatment was required, 80 µL DNase I mix (10 µL DNase I stock + 70 µL RDD buffer; Qiagen, #79254) was added to the column and incubated at room temperature for 15 min before adding 350 µL of RW1 buffer to the column and spinning for 15 sec at 8000 x *g*. The flow-through was discarded and a second wash with 500 µL RPE buffer followed by a centrifugation step was carried out. The flow-through was discarded and the RPE buffer wash repeated but with a 2-min centrifugation step. After discarding the flow-through the column was centrifuged again for 15 sec at 8000 x *g* to remove any liquid remaining on the outside of the column. To elute the RNA the column was placed in a new 1.5 mL Eppendorf tube and 30 µL RNase-free water was added directly to the membrane. The column was left to stand for 1 min before centrifuging for 1 min at 8000 x *g*. RNA was placed on ice and the concentration and purity were measured by

spectrophotometry at 230, 260 and 280 nm with a NanoDrop 2000 Spectrophotometer. RNA samples were stored at −80°C until further use.

2.6.3 cDNA synthesis

Reverse transcription into cDNA of total RNA was carried out using the High-Capacity RNA-to-cDNA Kit (Applied Biosystems, #4387406) or the High-Capacity cDNA Reverse Transcription Kit (Applied Biosystems, #4368814), which use the MultiScribe reverse transcriptase and random primers, according to the manufacturer's instructions (Tables 2.4 and 2.5, respectively). An Eppendorf Mastercycler (Sigma, Z316091) was used to incubate the reactions; the programmes can be found in Table 2.6. The cDNA was stored at −20°C until further use.

2.6.4 Real time quantitative polymerase chain reaction (RT-qPCR)

First, the Universal Probe Library (UPL) Assay Design Centre (Roche, Basel, Switzerland) was used to design and select intron-spanning primers and probes for each gene of interest and the housekeeping gene, *GAPDH* (Table 2.7). Then, the cDNA was diluted to 4.5 ng/µL for *GAPDH* or 18 ng/µL for all other genes and used as a template in 20 µL or 10 µL RT-qPCR reactions, including TaqMan Gene Expression Master Mix (Applied Biosystems, #4369016), as described in Table 2.8. Each reaction was run in at least triplicate using ABI Fast optical 96-well (Applied Biosystems, #4346907) or 384-well reaction plates on an ABI Prism 7500 or 7900HT Fast Real-Time PCR machine (Applied Biosystems). Standard conditions for fluorescence-base RT-qPCR were used (20 sec at 50ºC, 10 min at 95ºC and 40 cycles of 15 sec at 95ºC and 1 min at 60ºC).

Table 2.4. High-Capacity RNA-to-cDNA Kit reaction components

Component	Volume/Reaction (µL)
2X RT Buffer	10
20X Enzyme Mix	1
RNA	Up to 9 (1-2 µg)
Nuclease-free H_2O	As required
Total per Reaction	20

Table 2.5. High-Capacity cDNA Reverse Transcription Kit reaction components

Component	Volume/Reaction (µL)
10X RT Buffer	2
25X dNTP Mix (100 mM)	0.8
10X RT Random Primers	2
MultiScribe Reverse Transcriptase	1
Nuclease-free H_2O	4.2
RNA	10 (1-2 µg)
Total per Reaction	20

Table 2.6. Cycling parameters for cDNA synthesis

High-Capacity RNA-to-cDNA Kit				
	Step 1	**Step 2**	**Step 3**	
Temperature (°C)	37	95	4	
Time	60 min	5 min	∞	
High-Capacity cDNA Reverse Transcription Kit				
	Step 1	**Step 2**	**Step 3**	**Step 4**
Temperature (°C)	25	37	85	4
Time	10 min	120 min	5 min	∞

Table 2.7. List of primers and probes used for gene expression analysis

Primer name	Primer sequence (5' to 3')	UPL Probe #
GAPDH_Forward	AGC CAC ATC GCT CAG ACA C	60
GAPDH_Reverse	GCC CAA TAC GAC CAA ATC C	
CYP1A1_Forward	TCC AAG AGT CCA CCC TTC C	30
CYP1A1_Reverse	AAG CAT GAT CAG TGT AGG GAT CT	
NQO1_Forward	CAG CTC ACC GAG AGC CTA GT	21
NQO1_Reverse	GAG TGA GCC AGT ACG ATC AGT G	
CYP3A4_Forward	GAT GGC TCT CAT CCC AGA CTT	2
CYP3A4_Reverse	AGT CCA TGT GAA TGG GTT CC	
CYP1A2_Forward	CAG CAA GAA GGG GCC TAG A	2
CYP1A2_Reverse	ATG GCT GTG GTG ACT GTG TC	
ALB_Forward	AAT GTT GCC AAG CTG CTG A	27
ALB_Reverse	CTT CCC TTC ATC CCG AAG TT	
HNF4_Forward	TGA CAA CCT GTT GCA GGA GA	3
HNF4_Reverse	CGT TGG TTC CCA TAT GTT CC	

Table 2.8. RT-qPCR reaction components

Reagent	Stock concentration	Final concentration	Volume (µL) 96-well plate	Volume (µL) 384-well plate
Forward primer	20 µM	400 nM	0.4	0.2
Reverse primer	20 µM	400 nM	0.4	0.2
Probe	10 µM	100 nM	0.2	0.1
TaqMan master mix	2X	1X	10	5
cDNA	4.5-18 ng/µL	18-72 ng/µL	4	2
Water	-	-	5	2.5

2.6.5 Quantification of relative gene expression using the ΔΔCt method

The comparative threshold cycle ($\Delta\Delta C_T$) method was used to calculate the relative gene expression between the control and treated samples. In this method the relative fold change in expression, or $2^{-\Delta\Delta Ct}$, is calculated as follows: first ΔC_T is obtained by subtracting the average C_T value of the housekeeping gene (*GAPDH*) from the average C_T of the gene of interest, then $\Delta\Delta C_T$ is calculated by subtracting the ΔC_T of the treated sample from the ΔC_T of the control sample. This value can then be used to quantify the relative fold change as mentioned previously.

2.7 High-throughput (HT) RT-qPCR

2.7.1 Sample preparation and cDNA synthesis

Organoids samples were prepared as described in Section 2.6.1 and RNA extracted as in Section 2.6.2. Frozen RNA samples were shipped in dry ice to the Karlsruhe Institute of Technology (Karlsruhe, Germany) for HT RT-qPCR analysis, which was performed by Dr Matthias Hufnagel and Franziska Fischer as described previously (Fischer et al., 2016; Piberger et al., 2018). RNA concentration was determined on a NanoQuant plate (Tecan) and the volume for 1 µg RNA was calculated. The reverse transcription of RNA into cDNA was carried out using the iScript cDNA synthesis kit (Bio-Rad, #1708890) by adding 1 µg RNA to 1 µL iScript reverse transcriptase, 4 µL 5X reaction mix and water for a 20-µL reaction. The tubes were centrifuged for 15 sec then vortexed briefly and centrifuged again for 15 sec. The cDNA reactions were incubated in a Bio-Rad Thermocycler as shown in Table 2.9. cDNA was stored at −20°C until further use.

Table 2.9. Cycling parameters for iScript cDNA synthesis.

	Step 1	Step 2	Step 3	Step 4
Temperature (°C)	25	42	85	4
Time	5 min	30 min	5 min	∞

2.7.2 Specific target amplification (STA) and exonuclease digestion

For pre-amplification primers (stock 100 µM) were pooled in a tube as follows: 1 µL of each primer (x95) and 105 µL of DNA suspension buffer (TEKnova, #T0221; final concentration 500 nM). The target genes included can be found in Table 2.10 (additional information in Supplementary Table 2). A pre-mix for the STA reaction was set up as shown in Table 2.11. The STA reactions were then set up in 8-strip PCR tubes by adding 3.75 µL of the pre-mix and 1.25 µL cDNA to each tube for a 5-µL reaction. A water control and noRT (reverse transcription) control were included. The tubes were centrifuged for 15 sec, vortexed for 15 sec and centrifuged again. The STA reaction temperature programme used was as shown in Table 2.12.

The exonuclease was diluted as follows: 168 µL of water, 24 µL Exonuclease I Reaction Buffer and 48 µL Exonuclease I (20 U/µL; New England BioLabs, #M0293). After the STA was completed, the exonuclease solution was mixed by pipetting and 2 µL (4 U/µL) was added directly to each sample. The samples were digested for 40 min at 37°C followed by a 15-min inactivation step at 80°C after which the samples were kept at 4°C. The digested STA samples were then diluted 5-fold by adding 18 µL of TE buffer (TEKnova, #T0224). The samples were then centrifuged for 15 sec, vortexed for 30 sec and centrifuged again for 15 sec, twice. Samples were stored at −20°C until further use.

Table 2.10. List of target genes classified by pathway.

Gene classification by pathway and cellular process					
Transcription factors	**DNA damage response and repair**	**Apoptosis**	**Proliferation and cell cycle control**	**Oxidative stress response**	**Xenobiotic metabolism**
AXIN2	*APEX1*	*APAF1*	*CCND1*	*CAT*	*ABCB1*
BTRC	*ATM*	*BAX*	*CDKN1A*	*FTH1*	*ABCC1*
JUN	*ATR*	*BBC3*	*CDKN1B*	*G6PD*	*ADH1B*
KEAP1	*BRCA1*	*BCL2*	*CDKN2B*	*GCLC*	*ALDH1A1*
MAP3K5	*BRCA2*	*BCL2L1*	*E2F1*	*GPX1*	*CYP1A1*
MDM2	*DDB1*	*PMAIP1*	*EGFR*	*GPX2*	*EPHX1*
NFE2L2	*DDB2*	*TNFRSF10B*	*IL8*	*GSR*	*GSTP1*
NFKB1	*DDIT3*	*XIAP*	*MYC*	*HMOX1*	*NAT1*
NFKB2	*ERCC1*		*PLK3*	*HSPA1A*	*NQO1*
NFKBIA	*ERCC2*		*PPM1D*	*MT1X*	*SULT1A1*
TP53	*ERCC4*		*SIRT2*	*MT2A*	*UGT1A*
SLC30A1	*ERCC5*			*PRDX1*	
VEGFA	*GADD45A*			*SEPP1*	
	LIG1			*SOD1*	
	LIG3			*SOD2*	
	MGMT			*TFRC*	
	MLH1			*TXN*	
	MSH2			*TXNRD1*	
	OGG1				
	PARP1				
	PCNA				
	POLB				
	POLD1				
	RAD50				
	RAD51				
	RRM2B				
	XPA				
	XPC				
	XRCC5				

Adapted from (Fischer et al., 2016)

Table 2.11. STA pre-mix components

Component	Volume/Reaction (µL)	Volume for 96 Reactions + additional volume (µL)
2X TaqMan PreAmp Master Mix (Applied BioSystems, #4391128)	2.5	280
50 nM (10x) pooled primer mix	0.5	56
Water	0.75	84

Table 2.12. STA temperature programme

		12 Cycles		
Temperature (°C)	95	95	60	4
Time	10 min	15 sec	4 min	∞

2.7.3 HT RT-qPCR

Primers were diluted by mixing 22.5 µL of DNA suspension buffer, 25 µL of 2X assay loading reagent (Fluidigm, #85000736) and 2.5 µL of 100 µM forward and reverse primer mixture (or water for no reagent control) for a 50 µL total and a final primer concentration of 5 µM. This primer mix was then centrifuged for 30 sec, vortexed for 30 sec and centrifuged again for 30 sec, and the process was repeated. Then a sample pre-mix was prepared for the 96.96 Dynamic Array IFC (integrated fluidic circuit; 120 samples) by adding 360 µL of 2X Sso Fast EvaGreen Supermix with Low Rox (Bio-Rad, #172-5211) and 36 µL of 20X DNA Binding Dye Sample Loading Reagent (Fluidigm, #100-3738). To finish sample preparation 3.3 µL of the sample pre-mix and 2.7 µL of the diluted STA and exonuclease-treated samples (or water for no reagent control) were added to 8-strip PCR tubes. The tubes were then centrifuged for 30 sec, vortexed for 30 sec and centrifuged again for 30 sec, twice.

To load the 96.96 chip (Figure 2.6), the accumulators were first filled with Control Line Fluid, then the protective film was removed from the bottom and the chip placed in the IFC controller. The “select prime” programme was run for approximately 30 min. The samples and assays (primers) were loaded within 2 hr, a total of 5 µL of each were pipetted into their respective inlets (Figure 2.6) making sure there were no bubbles. The chip was placed back in the controller and the programme “Select load mix” was run for around 90 min. While the programme was running, the Biomark (Fluidigm) was prepared

by pre-heating the lamp. The Biomark data collection software was set up indicating the passive reference (ROX), the probe type (EvaGreen), the detection (autoexposure) and the thermal cycling protocol (Table 2.13). Once the “select load mix” run was over, any dust particles were carefully removed from the detection surface, the chip was loaded onto the instrument and the run started. After the first 40 min of thermal mixing, the device was checked to ensure the camera had passed successfully through the automatic exposure.

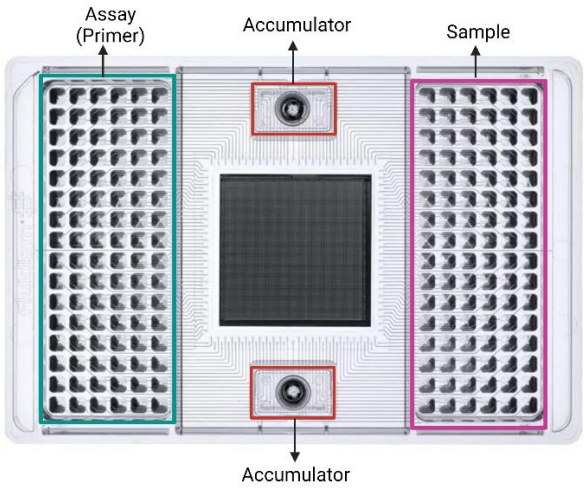

Figure 2.6. Diagram of the 96.96 Dynamic Array IFC chip. The accumulators, which need to be filled with Control Line Fluid, are at the top and bottom of the chip (red). The assay or primer inlets are shown on the left of the chip (green) and the sample inlets are on the right (pink). Adapted from Fluidigm.com (2021), created with BioRender.com.

Table 2.13. Thermal cycling protocol for the 96.96 chip

Segment	Type	Temperature (°C)	Time	BioMark Ramp Rate (°C/s)
1	Thermal Mix	70	40 min	2
		60	30 sec	2
2	Hot Start	95	1 min	2
3	PCR (30 cycles)	96	5 sec	2
		60	20 sec	2
4	Melting Curve	60	3 sec	1
		60-95		1°C/3 sec

2.7.4 Analysis of HT RT-qPCR

The chip was then analysed using the Fluidigm Real-Time PCR Analysis software (Fluidigm) using the Ct-threshold method. Data were then processed using the GenEx software (MultiD Analyses). A quality control process was carried out to detect any outliers. During this process any genes having Ct values higher than 28 more than twice were removed as these were considered nonreproducible. If only individual samples exceeded this cut-off, the values were replaced by a replicate, providing the Ct values of the reference genes of the two samples were similar. All values were replaced making sure no Ct values above 28 remained. To identify the appropriate reference genes the geNorm tool was used to calculate M-values or gene expression stability values, here genes with more stable expression (M-values lower than 0.5) were identified. The NormFinder tool was then used to determine the number of reference genes. A subtraction of gDNA background or RT-correction was carried out, when necessary, followed by a normalisation against the reference genes. The technical replicates were then averaged, and the relative quantities calculated. Data was log2 transformed for statistical analysis.

2.8 Metabolite analysis by high performance liquid chromatography (HPLC)

Growth media from organoids exposed to BaP was collected and stored at −20ºC for metabolite analysis. Before extraction, 5 µL of 1 mM phenacetin (Fluka, #PHR1249) in HPLC grade methanol (Fisher, #M/4056/17) was added to 1-mL aliquots of the media as internal standard and vortexed. The extraction was carried out by adding 900 µL of ethyl acetate (VWR, #23882.296) to the media aliquots, shaking at 1400 rpm for 2 min and centrifuging for 3 min at 13000 rpm. The upper ethyl acetate layer was transferred to a new Eppendorf tube. Another 900 µL of ethyl acetate were added to the media and the process repeated. Both extracts were combined before the ethyl acetate was evaporated to dryness using a SpeedVac and the samples stored at −20ºC.

Dried extracts were then resuspended in 30 µL methanol, vortexed and centrifuged for 30 sec at full speed before injecting 25 µL onto the HPLC machine. HPLC was performed

on a HPLC Agilent 1100 System (Agilent Technologies) with a SunFire™ C18 reverse phase column (250 × 4.6 mm, 5 µm with a column guard; Waters). Conditions used for the chromatographic separation of BaP metabolites were as follows: mobile phase A: 100% HPLC water, mobile phase B: 100% acetonitrile (Fisher, #A/0627/17). The separation started with an isocratic elution of 50% of mobile phase B for 50 sec. Then a linear gradient to 95% of mobile phase B in 33 min was followed by isocratic elution for 7 min, a linear gradient from 95% to 50% of mobile phase B in 5 min, followed by an isocratic elution for 5 min. Total run time was 50 min at a flow rate of 1 mL/min. The metabolites were detected by fluorescence detection (0-6 min at excitation 341 nm and emission 381 nm, and 6-48 min at excitation 380 nm and emission 431 nm). Standards of (±)-trans-7,8-dihydroxy-7,8-dihydrobenzo[*a*]pyrene (BaP-t-7,8-dihydrodiol) and (±)-r-7,t-8,t-9,c-10-tetrahydroxy-7,8,9,10-tetrahydrobenzo[*a*]pyrene (BaP-tetrol-I-1; both synthesised at the Biochemical Institute for Environmental Carcinogens, Lurup, Germany) were used to identify BaP metabolites. The peak areas of the metabolites were calculated relative to the peak area of the internal standard phenacetin and expressed as relative peak areas.

2.9 Statistical analysis

Results are shown as mean with standard deviation (± SD). Sample size is indicated in each section. *GraphPad Prism versions 8.4.3 and 9* software (GraphPad Software Inc., La Jolla, California, USA) was used to perform all statistical analysis. Relative mRNA expression data were log2 transformed in order to calculate and compare fold changes and normalise the data, and a one sample *t*-test with Bonferroni correction against the control mean of 0 (*p<0.05; **p<0.01; ***p<0.001, different from control). Groups of two were compared by two-sample *t*-test assuming unequal variances.

Chapter 3 Metabolic activation and cellular responses to benzo[*a*]pyrene

3.1 Introduction

The well-characterised human carcinogen BaP is prevalent in the environment as it is found in air (including cigarette smoke), water, soil, food, and some pharmaceutical products (IARC, 2012a). BaP belongs to the PAH family, and it is often used as representative for PAH exposure when effects of PAHs are investigated in humans (Boström et al., 2002; Boysen and Hecht, 2003). This environmental carcinogen induces tumour formation at multiple sites in many species, including in the lung, liver, forestomach, skin, lymphoid tissues and sarcomas in mice; lung, mammary glands and sarcomas in rats; and lung, trachea, larynx, forestomach and sarcomas in hamsters (IARC, 2012a).

In humans, lung cancer is most commonly associated to BaP exposure due to its presence in cigarette smoke and air pollution (Alexandrov et al., 2006; Balansky et al., 2007; Phillips, 2002), however, for most humans, the main source of BaP is the diet (Phillips, 1999). Although studies have shown associations between BaP exposure, increased risk of development and/or progression of other cancers including pancreas, liver and breast, epidemiological evidence for a causal relationship in humans is still very limited (Amadou et al., 2021; Anderson et al., 2005; Li et al., 2007; Malik et al., 2018; Su et al., 2014).

BaP requires metabolic activation to exert its biological effects, including genotoxicity. The formation of BaP covalent DNA adducts has been reported in cell lines and animal tissues, including in lung, liver, colon, forestomach, glandular stomach, kidney, pancreas, and spleen tissues (Alexandrov et al., 1996, 2006; Jin Kang et al., 2011; Krais et al., 2016a; Motwani et al., 2020; Zuo et al., 2014). DNA adduct formation has been identified as an initiation event, leading to mutagenesis and ultimately carcinogenesis, however, more changes are required for tumour formation. Some of these changes have

been investigated in mice and human cell lines, where BaP treatment induces differential expression of a number of genes and miRNAs, as well as epigenetic alterations (Caiment et al., 2015; Chang et al., 2019; Labib et al., 2012; Tryndyak et al., 2018; Zuo et al., 2014). These studies provide information to help understand tissue-specific responses to BaP, however, not all may be relevant to humans. Thus, a major aim of this study was to determine if human organoids can bioactivate BaP and therefore serve as a model to investigate its organotropism.

Recently, human bronchial 3D cultures were used to examine the toxicity of BaP and other PAHs, helping to identify chemical-specific transcriptional patterns (Chang et al., 2019). Here, normal human tissue organoids from stomach, pancreas, liver, colon, and kidney tissues were treated with BaP to investigate its toxicity. The metabolic potential of the organoids was also evaluated by looking at the formation of metabolites and DNA adducts. In addition, this study looked at differences between possible target (pancreas and liver) and non-target (stomach, colon and kidney) tissues of BaP carcinogenicity. As lung organoids were not available at the time this study was carried out, the pancreas and liver were chosen as possible targets as increased BaP exposure has been linked to increased risk of these cancers (Li et al., 2007; Su et al., 2014). Tissue-specific responses were investigated by evaluating DDR protein induction and mRNA expression changes of genes involved in different pathways including DDR, apoptosis, cell cycle regulation and xenobiotic metabolism.

3.2 Materials and methods

Organoids from stomach, pancreas, liver, kidney, and colon human tissues were cultured as described in Section 2.2. Gastric organoids were cultured in Schlaermann media (Section 2.2.1.1), and liver organoids were differentiated as described in Section 2.2.4. Liver organoids were characterised using RT-qPCR (Section 2.6) to quantify the mRNA expression of hepatocyte markers (*ALB, HNF4 and CYP3A4*). Organoids were treated with BaP as described in Section 2.2.5; controls were treated with vehicle only (0.5% DMSO). Cell viability was assessed using the CellTiter-Glo assay as explained in Section

2.3. Gene expression analysis was carried out to measure the induction of the XMEs *CYP1A1* and *NQO1* (Section 2.6), and HT RT-qPCR was performed to investigate further gene expression changes (Section 2.7; these investigations were partly conducted by Dr Matthias Hufnagel and Franziska Fischer at the Karlsruhe Institute of Technology, Karlsruhe, Germany). DNA adduct formation was assessed by LC-ESI-MS/MS (Section 2.5.3; these investigations were partly conducted by Dr Silvia Balbo and Andrew Floeder at the Masonic Cancer Center, Minneapolis, USA). The formation of BaP metabolites, BaP-t-7,8-dihydrodiol and BaP-tetrol-I-1, was assessed by HPLC analysis (Section 2.8; gastric, pancreas and liver analyses were performed by an MSci Biochemistry student, Krishshan Gobalakrishnan, at King's College London). The induction of different DDR markers (p-p53, pCHK2, p21 and γ-H2AX) was investigated by Western blotting (Section 2.4).

3.3 Results

3.3.1 Liver organoid differentiation and characterisation

Liver organoids derived from adult stem cells consist of ductal cells only (Huch et al., 2015), therefore they lack hepatocytes, the major cell type involved in liver metabolism. Due to the importance of hepatocytes, liver organoids were differentiated into this cell type by changing the growth conditions. The removal of R-Spondin-1 and addition of dexamethasone and BMP7 to the culture medium facilitated the differentiation of the organoids into hepatocytes by inhibiting Notch, an inducer of ductal morphogenesis (Broutier et al., 2016). Organoid morphology was monitored throughout the process and images were taken at various points (Figure 3.1 A). Undifferentiated and differentiated organoids had spheroid-like shapes and similar sizes from the time of seeding (data not shown) until day 5, when the media on the differentiated organoids was changed to differentiation media. After day 5, differentiated organoids started to become smaller and darker than undifferentiated organoids and these differences increased with time (Figure 3.1 A). At day 15, when the organoids were either treated with BaP or collected for analysis, most of the differentiated organoids had become dark and small while most of

the undifferentiated had continued growing and were still bright (Figure 3.1 A). In addition, to test the outcome of the differentiation process, organoids were characterised by looking at the mRNA expression of three hepatocyte cell markers, *CYP3A4*, albumin (*ALB*) and *HNF4* (hepatocyte nuclear factor 4) by RT-qPCR. The expression of these genes was investigated after day 15 in both undifferentiated (ductal cells) and differentiated (hepatocytes) organoids grown at the same time. Differentiated organoids showed higher levels of expression of the three markers, however, although the changes were significant, they were also very variable (Figure 3.1 B). In order to further evaluate the differences between undifferentiated and differentiated liver organoids, both types of culture were used in all the experiments carried out in this study.

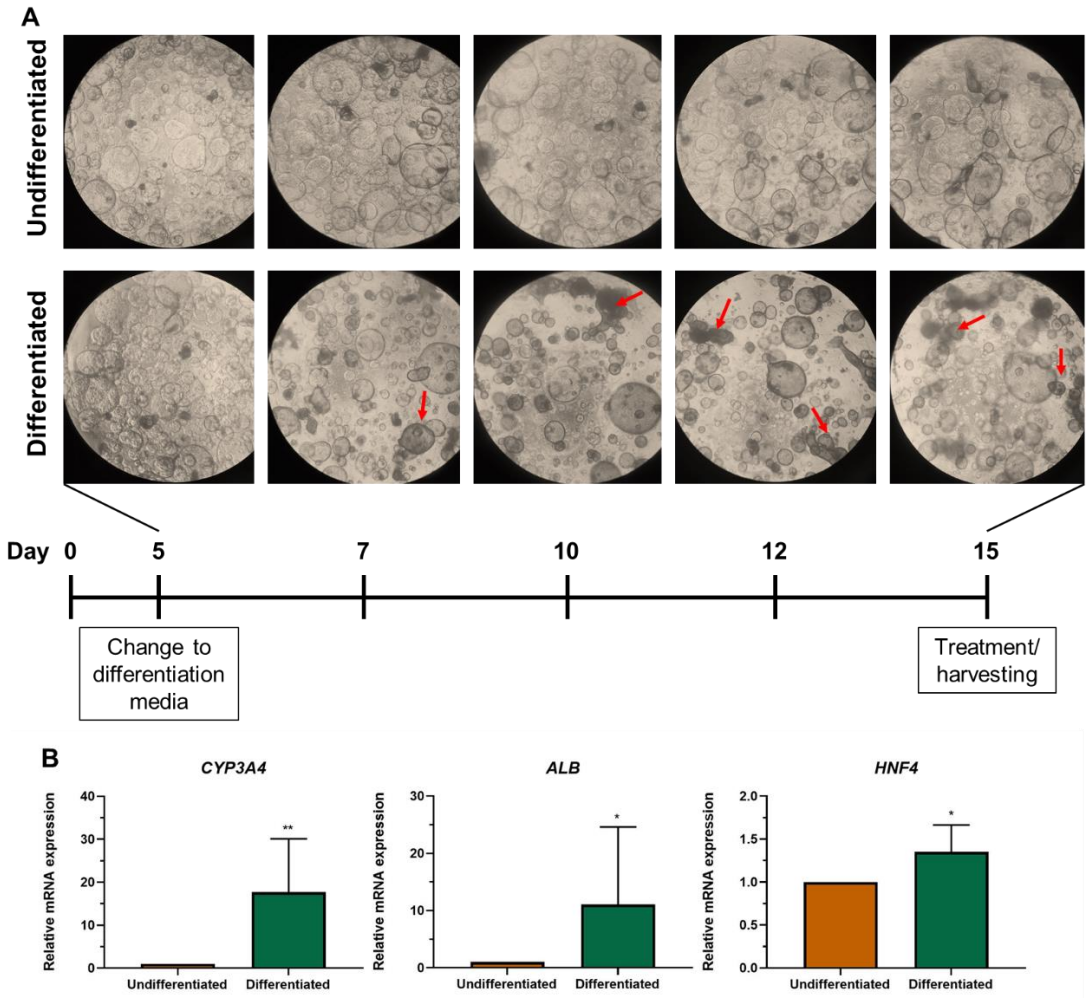

Figure 3.1. Morphology of the liver organoids during differentiation and their characterisation. Liver organoids were differentiated from ductal cells (undifferentiated) to hepatocytes (differentiated). (**A**) Representative images of undifferentiated (top) and differentiated (bottom) organoids were taken at the indicated stages of the differentiation process. Differentiated organoids became smaller and darker than undifferentiated organoids during the

differentiation process (red arrows). (**B**) Liver organoids were characterised by determining the relative gene expression of hepatocytes markers *CYP3A4, ALB* and *HNF4* by RT-qPCR and the $2^{-\Delta\Delta CT}$ method. Values are shown as mean ± SD (n≥4). Values were normalised to mRNA expression of *GAPDH* and are relative to the undifferentiated control. Statistical analysis was performed by log2 transforming the data and a one sample *t*-test with Bonferroni correction against the undifferentiated mean of 0 (*p<0.05; **p<0.01).

3.3.2 Cell viability assessment of organoids after BaP treatment

Cell viability after treatment with a range of BaP concentrations (0-50 µM) for 48 hr was determined using the CellTiter-Glo assay. Differences were seen between different tissues and in some cases between donor cultures. Gastric organoids from culture D95 were more susceptible to BaP, with an IC_{50} of 12.8 µM, than those from donor culture D88, which had an IC_{50} close to 50 µM (Figure 3.2 A). Although both pancreatic organoid donor cultures had IC_{50} values greater than 50 µM, D39 was less susceptible to BaP-induced cytotoxicity than D44 (Figure 3.2 B). Similarly, kidney organoids showed little response to BaP treatment (IC_{50} ≥ 50 µM); however, culture D21 was slightly more susceptible than D50 (Figure 3.2 C). Colon organoids had a more pronounced decrease in viability after BaP treatment, with D311 and D351 having IC_{50} values of 44.2 µM and 34.5 µM, respectively (Figure 3.2 D). Finally, liver organoids from donor D4 were assessed in both their undifferentiated and differentiated forms, and as shown in Figure 3.2 E; there was no cytotoxic response to BaP in either.

Based on the cell viability results, three concentrations were chosen for subsequent experiments for each culture. When possible, a concentration close to the IC_{50}, one above (~30% viability) and one below (~80% viability) were chosen. When there was no IC_{50}, as was the case with the pancreatic, kidney and liver organoids, the highest concentration selected was 50 µM, as well as two lower concentrations (12.5 µM and 25 µM).

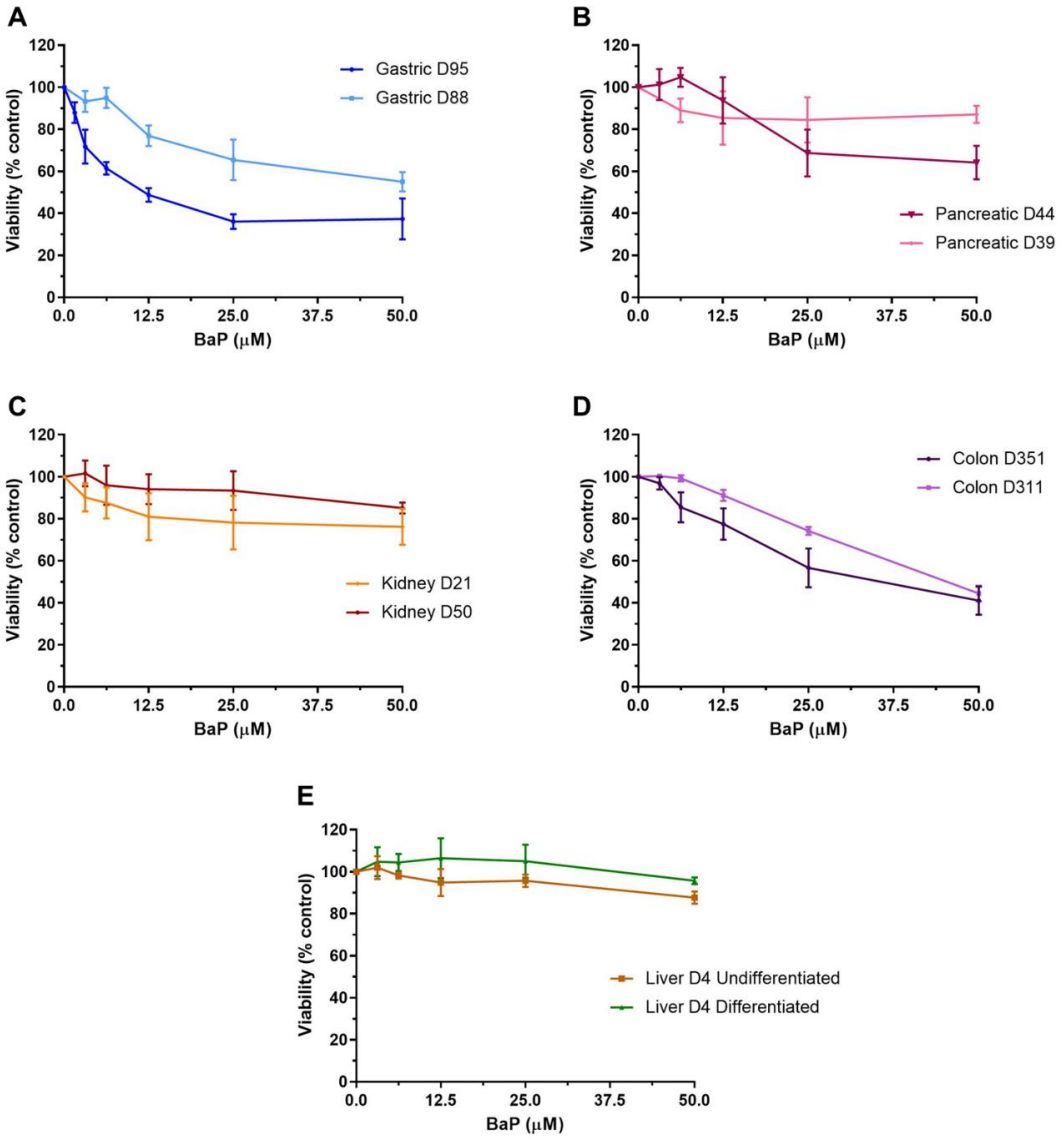

Figure 3.2. Cell viability in human tissue organoids after treatment with BaP. Organoids from normal human stomach (**A**; D95 and D88), pancreas (**B**; D39 and D44), kidney (**C**; D50 and D21), colon (**D**; D351 and D311), and liver (**E**; D4 undifferentiated and differentiated) tissues were treated with various concentrations (0-50 μM) of BaP for 48 hr. A vehicle control (0.5% DMSO) was included. Cell viability (% control) was measured using the CellTiter-Glo assay. Results are shown as mean ± SEM (n≥3).

3.3.3 Xenobiotic-metabolising enzyme expression after treatment with BaP

As the ability of the organoids to metabolically activate BaP had not been previously assessed, gene expression levels of main XMEs involved in BaP metabolism, *CYP1A1* and *NQO1*, were investigated after treatment in all organoid types by RT-qPCR. In general, there was a concentration-dependent induction of *CYP1A1* and *NQO1* in all

organoid donor cultures (Figures 3.3 and 3.4).

The expression of *CYP1A1* in both gastric organoid cultures, D95 and D88, had similar levels at the highest concentrations selected (IC_{50} values, 12.5 µM and 50 µM, respectively), with almost a 2000-fold increase compared to the control. At the lower concentrations, induction was also significant, although at much lower levels, 11.4-fold for D95 and 180-fold for D88 (Figure 3.3 A). The induction levels between pancreatic donor cultures were more distinct as D39 had much higher levels than D44 at both concentrations. D39 had an increase of almost 5000-fold at 50 µM and around 800-fold at 12.5 µM, whilst D44 showed an induction of around 900-fold at 50 µM and 90-fold at 12.5 µM (Figure 3.3 B). Although the induction at 50 µM in D50 was greater than in D21, the expression levels of *CYP1A1* in kidney organoids were higher than in any other organoid type, having inductions of almost 30000 and 19000-fold, respectively, and of about 1500-fold at 12.5 µM (Figure 3.3 C). Colon organoids showed the lowest *CYP1A1* induction levels overall. Gene expression levels in D311 and D351 were quite similar, showing increases between 300- and 400-fold at the highest concentration and around 200-fold at the lowest (Figure 3.3 D). Lastly, the expression levels of *CYP1A1* in the differentiated liver D4 control were significantly higher (24-fold) than those in the undifferentiated D4 control. After treatment, the induction at 50 µM in the differentiated liver organoids was around twice that in the undifferentiated (approximately 4500 and 2000-fold, respectively), relative to the undifferentiated liver control. At 12.5 µM, induction was only significant in the differentiated organoids, with a 287-fold change compared to the undifferentiated control. Induction of *CYP1A1* was also significant at both concentrations compared to the differentiated control (Figure 3.3 E).

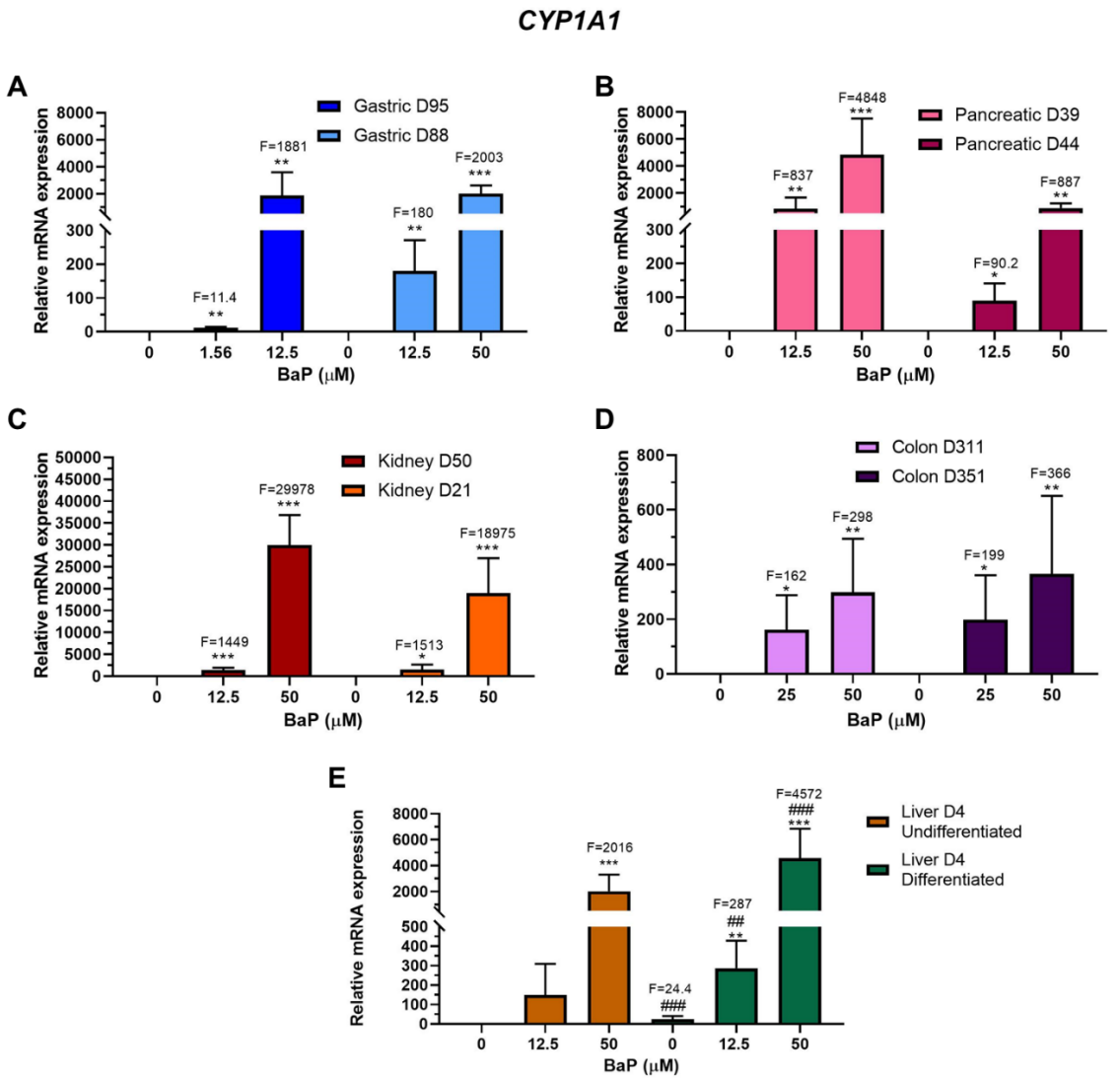

Figure 3.3. Relative gene expression of *CYP1A1* in human tissue organoids after treatment with BaP. Gastric (D95 and D88; **A**), pancreatic (D39 and D44; **B**), kidney (D50 and D21; **C**), colon (D311 and D351; **D**) and liver undifferentiated and differentiated (D4; **E**) organoids were treated with the indicated concentrations of BaP for 48 hr. *CYP1A1* expression was determined by RT-qPCR and the $2^{-\Delta\Delta CT}$ method. Values are shown as mean ± SD (n≥3). Values were normalised to mRNA expression of the housekeeping gene *GAPDH* and are relative to the control (DMSO); for liver organoids the values are relative to the undifferentiated control. Statistical analysis was performed by log2 transforming the data and a one sample *t*-test with Bonferroni correction against the control mean of 0: *p<0.05; **p<0.01; ***p<0.001 compared to untreated control; $^{\#\#}$p<0.01; $^{\#\#\#}$p<0.001 compared to undifferentiated liver control.

Overall, *NQO1* expression was low across all the organoid types and donor cultures. In gastric organoids, significant changes were seen only at the highest concentrations with fold increases of 2.1 and 1.6 for D95 and D88, respectively (Figure 3.4 A). Both pancreatic organoid cultures had very similar levels of induction; at 50 µM they had approximately a 3.5-fold increase, while at 12.5 µM only D44 had a significant induction of 1.7-fold (Figure 3.4 B). As with *CYP1A1*, the higher induction levels were seen in kidney organoids, with significant increases in expression levels of around 10-fold at 50 µM in both donor cultures, however, at 12.5 µM induction was only significant in D50 with 2.8-fold (Figure 3.4 C). *NQO1* expression was significantly increased at both concentrations for both colon organoid donor cultures, with around 1.5 and 2.5-fold at 25 µM and 50 µM, respectively (Figure 3.4 D). As seen in *CYP1A1*, differentiated liver organoids had significantly higher levels of *NQO1* in the control than undifferentiated organoids with a 2.6-fold increase. However, the induction after BaP treatment was only significant at 50 µM, with a 2.1-fold increase for undifferentiated organoids and a 3.7-fold increase for the differentiated organoids compared to the liver undifferentiated control. Differentiated organoids also had a significant induction at 50 µM relative to the differentiated control (Figure 3.4 E).

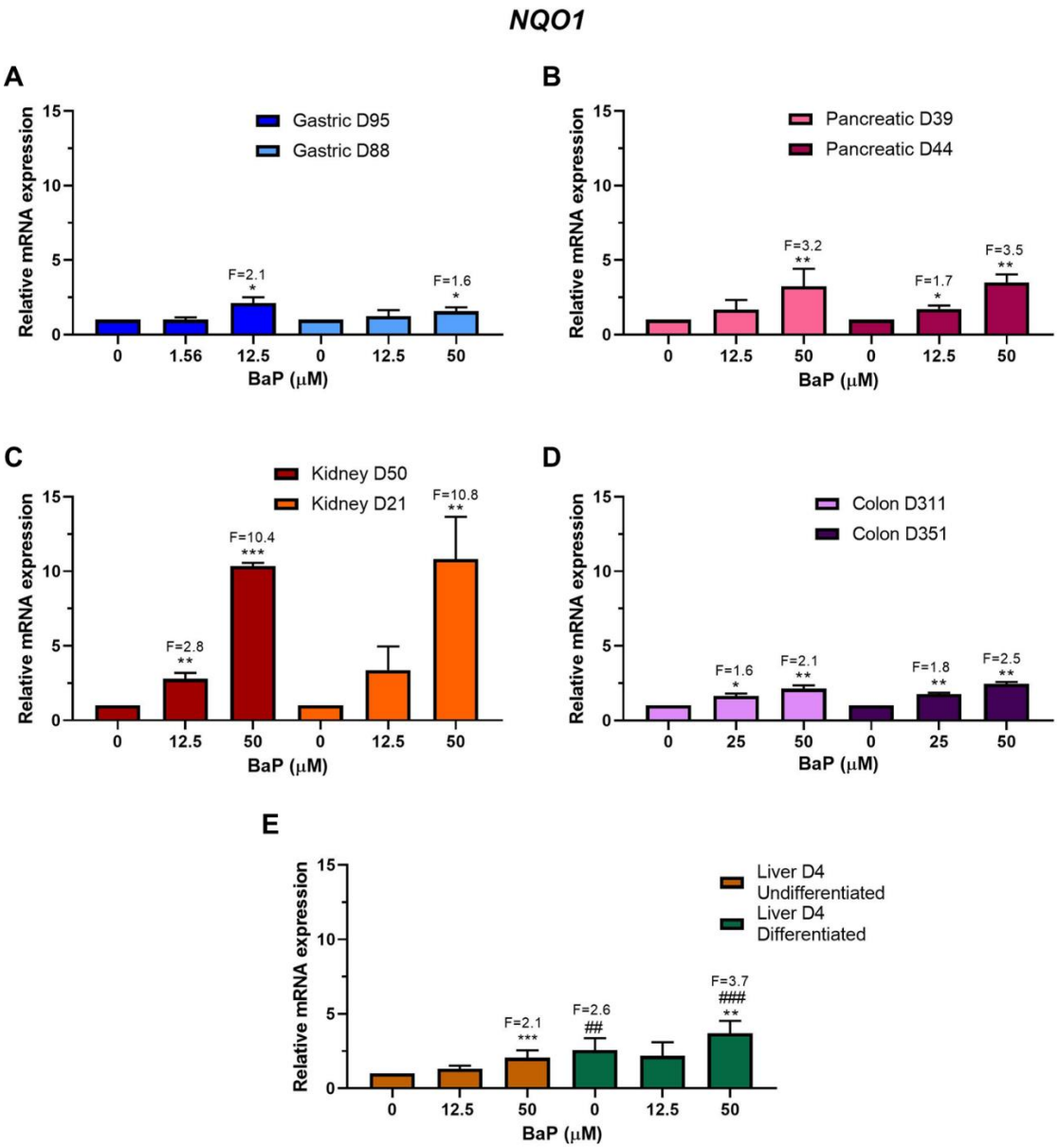

Figure 3.4 Relative gene expression of *NQO1* in human tissue organoids after treatment with BaP. Gastric (D95 and D88; **A**), pancreatic (D39 and D44; **B**), kidney (D50 and D21; **C**), colon (D311 and D351; **D**) and liver undifferentiated and differentiated (D4; **E**) organoids were treated with various concentrations of BaP for 48 hr. *NQO1* expression was determined by RT-qPCR and the $2^{-\Delta\Delta CT}$ method. Values are shown as mean ± SD (n≥3). Values were normalised to mRNA expression of the housekeeping gene *GAPDH* and are relative to the DMSO control; for liver organoids the values are relative to the undifferentiated control. Statistical analysis was performed by log2 transforming the data and a one sample t-test with Bonferroni correction against the control mean of 0: *p<0.05; **p<0.01; ***p<0.001 compared to untreated control; $^{\#\#}$p<0.01; $^{\#\#\#}$p<0.001 compared to undifferentiated liver control.

3.3.4 Induction of DDR proteins after BaP treatment

To further evaluate the effects of BaP in the organoids, induction of DDR proteins (p-p53, pCHK2, p21 and γ-H2AX) was investigated after treatment with BaP for 48 hr by Western blotting. The expression and induction of these proteins varied across organoid types and donor cultures. Cultures from the same organoid type were run on the same gel. As shown in Figure 3.5 A, there was expression and induction of all the DDR proteins in both gastric cultures, however, for pCHK2 and p21, expression was higher in D88 than in D95. Additionally, induction of γ-H2AX was also slightly stronger in D88 as it showed a concentration-dependent increase. Although pancreatic organoids showed an induction in all proteins, culture D44 had very low levels of expression, and no induction in p21, compared to D39, as it can be seen in Figure 3.5 B. Culture D39 showed a concentration-dependent induction in all DDR proteins except p21, where the induction remained constant in all treatments. Kidney organoids showed expression and induction of all DDR proteins (Figure 3.5 C). Expression levels of p-p53 were higher in D21 than in D50 and the induction had a concentration-dependent pattern, whilst pCHK2 showed the highest induction at 12.5 μM which then decreased at the highest concentrations tested. p21 was induced at all concentrations, however, it remained constant in D50 and in D21 it slightly decreased at the highest concentration tested. There was γ-H2AX induction in both donor cultures, but the induction seemed to stay fairly constant across treatments (Figure 3.5 C). Expression of most DDR proteins was seen in colon organoids; however, induction could only be seen for pCHK2 and γ-H2AX in both donor cultures, and p-p53 and p21 in D311 (Figure 3.5 D). Liver organoids had higher expression levels of all DDR proteins in undifferentiated than in differentiated organoids. Undifferentiated liver organoids showed induction of pCHK2 and γ-H2AX, while p-p53 levels seemed to decrease. Differentiated organoids had low expression of all DDR proteins and only induction of γ-H2AX (Figure 3.5 E).

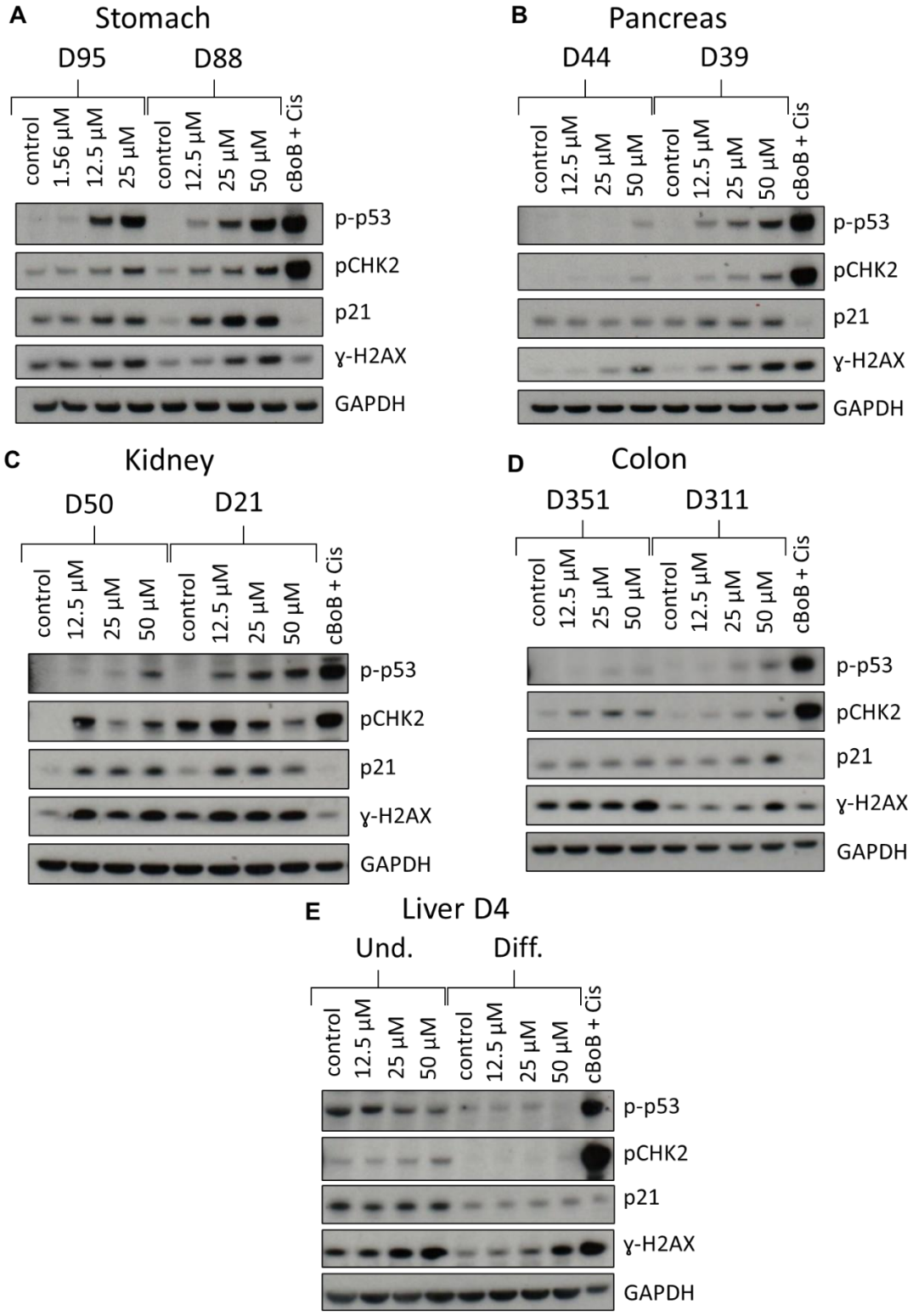

Figure 3.5. Expression of DDR proteins in normal human tissue organoids after treatment with BaP. Organoids from gastric (D95 and D88; **A**), pancreatic (D39 and D44; **B**), kidney (D50 and D21; **C**), colon (D351 and D311; **D**) and liver (D4 undifferentiated and differentiated; **E**) tissues were exposed to the indicated concentrations of BaP for 48 hr, and lysates were prepared for Western blot analysis. Various DDR proteins (p-p53, pCHK2, p21 and γ-H2AX) were detected and GAPDH was used as a loading control. Organoids from the same tissue were run on one gel to allow direct comparison. cBoB + Cis (cBoB treated with 3.125 µM cisplatin) was used as a positive control. Representative blots are shown (n=2).

3.3.5 Analysis of BaP metabolites after BaP treatment

In order to assess the capability of the organoids to metabolise BaP, the levels of two main BaP metabolites, BaP-t-7,8-dihydrodiol (diol; precursor of BPDE) and BaP-tetrol-l-1 (tetrol; hydrolysis product of BPDE) which are released into the culture media were measured by HPLC fluorescence detection (Baker et al., 2018). Metabolites were detected in media samples from all organoid types treated with BaP for 48 hr, showing a concentration-dependent increase (Figure 3.6). Although both metabolites were detected in gastric organoids, there were not significant differences between concentrations (Figure 3.6 A and B). Media from pancreatic organoids showed the presence of the diol and tetrol; however, only D44 had significant differences of diol metabolites levels between the concentrations tested (Figure 3.6 C and D). In kidney organoids both diol and tetrol metabolites were detected in media from both D50 and D21 donor cultures, and significant differences were found between 12.5 and 50 μM (Figure 3.6 E and F). Unlike D311, colon culture D351 had significant differences in diol levels between concentrations, the levels of tetrol for both donor cultures were not significant (Figure 3.6 G and H). While the BaP metabolites were found in both undifferentiated and differentiated liver organoids, only the diol levels in differentiated liver organoids were significantly different between concentrations (Figure 3.6 I and J).

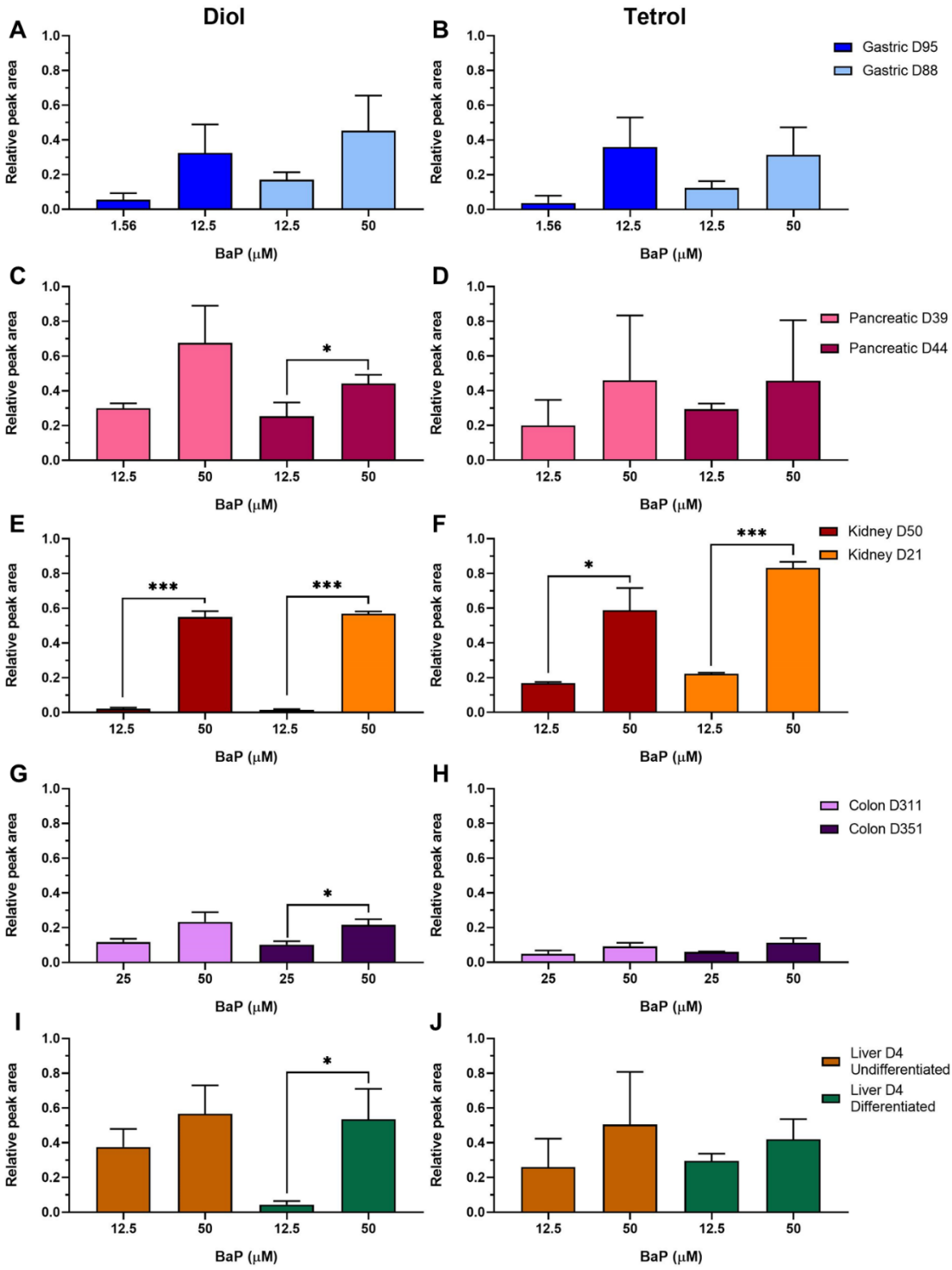

Figure 3.6. BaP metabolite levels in human tissue organoids after BaP exposure. Gastric (D95 and D88; **A and B**), pancreatic (D39 and D44; **C and D**), kidney (D50 and D21; **E and F**), colon (D311 and D351; **G and H**) and liver undifferentiated and differentiated (D4; **I and J**) organoids were treated with various concentrations of BaP for 48 hr. DMSO controls (not shown) were included. The formation of BaP-t-7,8-dihydrodiol (left) and BaP-tetrol-l-1 (right) was determined by HPLC analysis. Metabolite levels are presented as peak area relative to phenacetine (arbitrary units) and as mean ± SD (n≥3). Statistical analysis was performed by *t*-test between treatments of the same culture assuming unequal variances (*p<0.05; ***p<0.001 compared between concentrations tested).

3.3.6 Formation of DNA adducts after treatment with BaP

To further assess the metabolic activation and DNA damage induced by BaP treatment the formation of DNA adducts was evaluated by LC-ESI-MS/MS. Although adducts were detected in the controls the levels were very low (data not shown). Levels of dG-*N*^{2}-BPDE are shown in Figure 3.7. Overall, dG-*N*^{2}-BPDE adducts were formed in a concentration-dependent manner and the levels varied between organoid types and donor cultures. Gastric D95 had lower dG-*N*^{2}-BPDE adduct levels than gastric D88 at the IC_{50} values, with D95 having 295 adducts per 10^7 nucleosides (12.5 µM) and D88 463 adducts per 10^7 nucleosides (50 µM). Similarly, at the lower concentrations tested culture D95 had 34.1 adducts per 10^7 nucleosides while D88 had 182 adducts per 10^7 nucleosides, however the concentration used to treat D88 was slightly more toxic than that for D95 (Figure 3.7 A). Pancreatic organoids had higher dG-*N*^{2}-BPDE adduct levels with D39 having the highest with 889 and 275 adducts per 10^7 nucleosides at 50 and 12.5 µM, respectively. Culture D44 had 617 adducts per 10^7 nucleosides at 50 µM and 220 adducts per 10^7 nucleosides at 12.5 µM (Figure 3.7 B). Kidney D21 had higher adduct levels than D50, however, the concentrations tested were also slightly more toxic in D21 than in D50. Culture D21 had 182 adducts per 10^7 nucleosides at 12.5 µM and 738 adducts per 10^7 nucleosides at 50 µM, while D50 had 159 and 481 adducts per 10^7 nucleosides at 12.5 and 50 µM, respectively (Figure 3.7 C). Colon organoids had the lowest dG-*N*^{2}-BPDE adduct levels of all the organoid types with colon D351 having lower levels than D311. Culture D351 had 137 adducts per 10^7 nucleosides and D311 had 188 adducts per 10^7 nucleosides at 50 µM. At 25 µM, D351 and D311 had 81.0 and 126 adducts per 10^7 nucleosides, respectively, although this concentration was more toxic in D351 (Figure 3.7 D). Lastly, undifferentiated liver organoids had much higher levels of dG-*N*^{2}-BPDE than the differentiated liver organoids, with the former having 131 adducts per 10^7 nucleosides and the latter having 37.0 adducts per 10^7 nucleosides at 12.5 µM. At 50 µM, the undifferentiated liver had 844 adducts per 10^7 nucleosides and the differentiated had 295 adducts per 10^7 nucleosides (Figure 3.7 E).

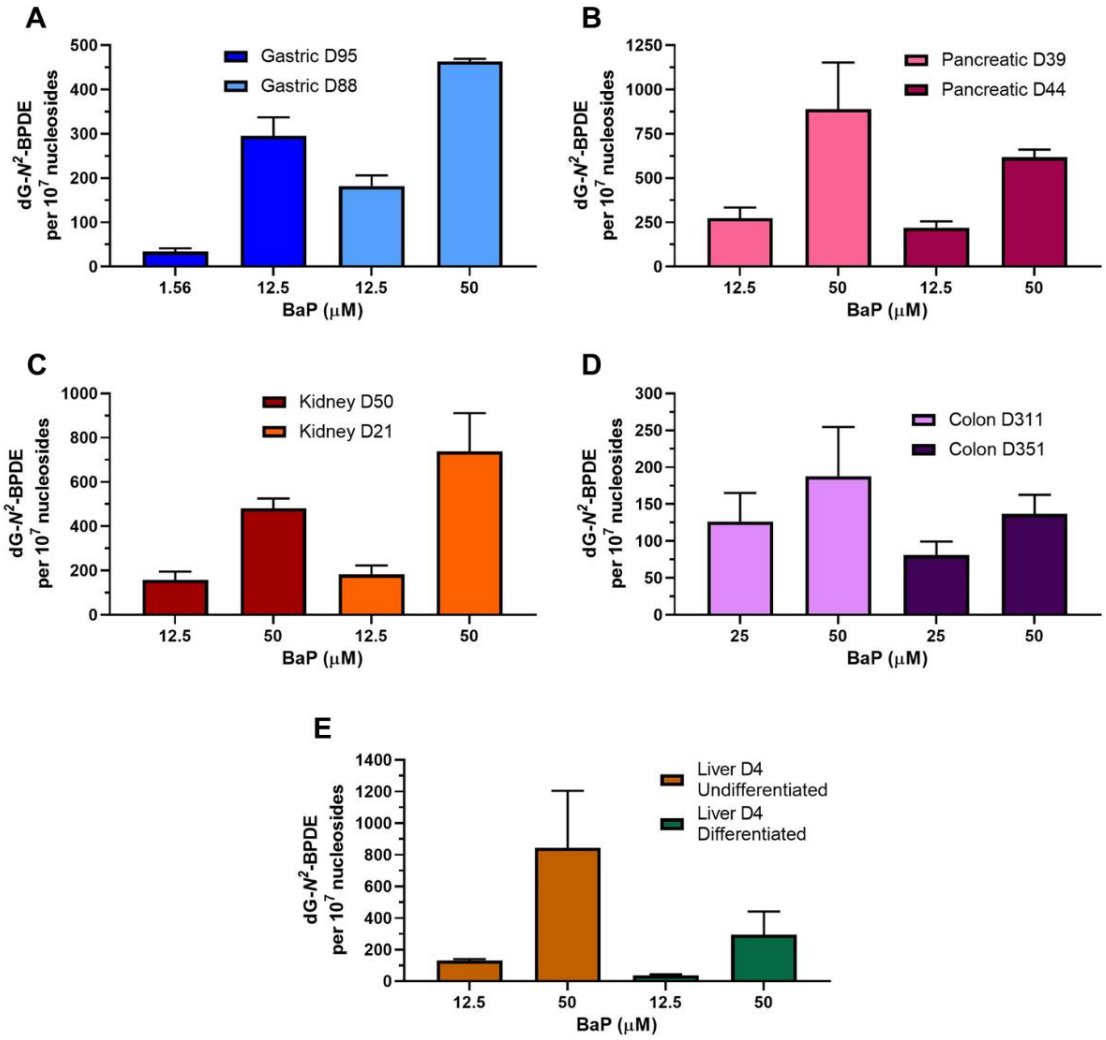

Figure 3.7. DNA adduct formation in human tissue organoids after treatment with BaP. Gastric (**A**; D95 and D88), pancreatic (**B**; D39 and D44), kidney (**C**; D50 and D21), colon (**D**; D311 and D351) and liver (**E**; D4 undifferentiated and differentiated) organoids were treated with the indicated concentrations of BaP for 48 hr. dG-N^2-BPDE adduct formation was quantified using LC-ESI-MS/MS. Very low adduct levels were detected in the untreated controls (<0.5 per 10^7 nucleosides for gastric, kidney, colon and liver, and <5 per 10^7 nucleosides for pancreatic organoids). Results are shown as mean ± SD, n=3.

3.3.7 Gene expression analysis by high throughput RT-qPCR

The expression of 90 genes involved in different cellular pathways was investigated by HT RT-qPCR after treatment with BaP for 48 hr. The panel of genes was selected based on their relevance and involvement in genomic instability, DNA damage response and repair, oxidative stress response, apoptosis, cell cycle arrest and proliferation, and xenobiotic metabolism (Fischer et al., 2016). Unfortunately, the analysis of some genes was not possible as they had to be removed during the quality control process due to their Ct values being higher than 28 as there is lack of reproducibility above this value

(*ABCB1*-Gastric; *CYP1A1* and *BCL2*-Gastric, pancreas and liver). During analysis, genes with log2-fold values higher than 1 (expression doubled) or lower than -1 (expression halved) compared to the untreated control were considered biologically relevant. Overall, several differences in gene expression were seen between organoid types and donor cultures. Pancreas, kidney, and colon organoids had the most relevant changes, and although gene expression between donor cultures of these tissues appeared consistent, slight differences were seen in some cases. Changes between gastric donor cultures, and undifferentiated and differentiated liver organoids had more notable differences, as gastric organoid D88 and undifferentiated liver had more relevant changes compared to gastric organoid D95 and differentiated liver. Concentration-dependent differences were also seen, with the highest concentration having more pronounced changes for some genes (Figure 3.8).

Downregulation of a number of DNA damage and repair genes such as *MGMT, BRCA1/2* and *RAD51* was seen across most organoid types; in contrast, other genes like *GADD45A*, *DDB2* and *RRM2B* were upregulated (Figure 3.8, DDR). Most of the genes involved in xenobiotic metabolism (XM) appeared to be upregulated; however, this was only significant for *NQO1* and *UGT1A* (Figure 3.8, XM). In the apoptosis (AP) group, genes like *BAX, PMAIP1* and *BBC3* were upregulated in all organoid types, although the levels of expression varied between donor cultures and tissues (Figure 3.8, AP). The most pronounced changes in the proliferation and cell cycle control (PCC) gene group were seen in *CDKN1A* for which expression levels increased after treatment in all organoid donor cultures. Upregulation of *CDKN2B* and *PLK3* was also seen in most organoid types (Figure 3.8, PCC). The upregulation of *MDM2* and *TXNRD1* were the most noticeable gene expression changes in the transcription factor (TF) and oxidative stress response (OS) gene groups, respectively (Figure 3.8, TF and OS).

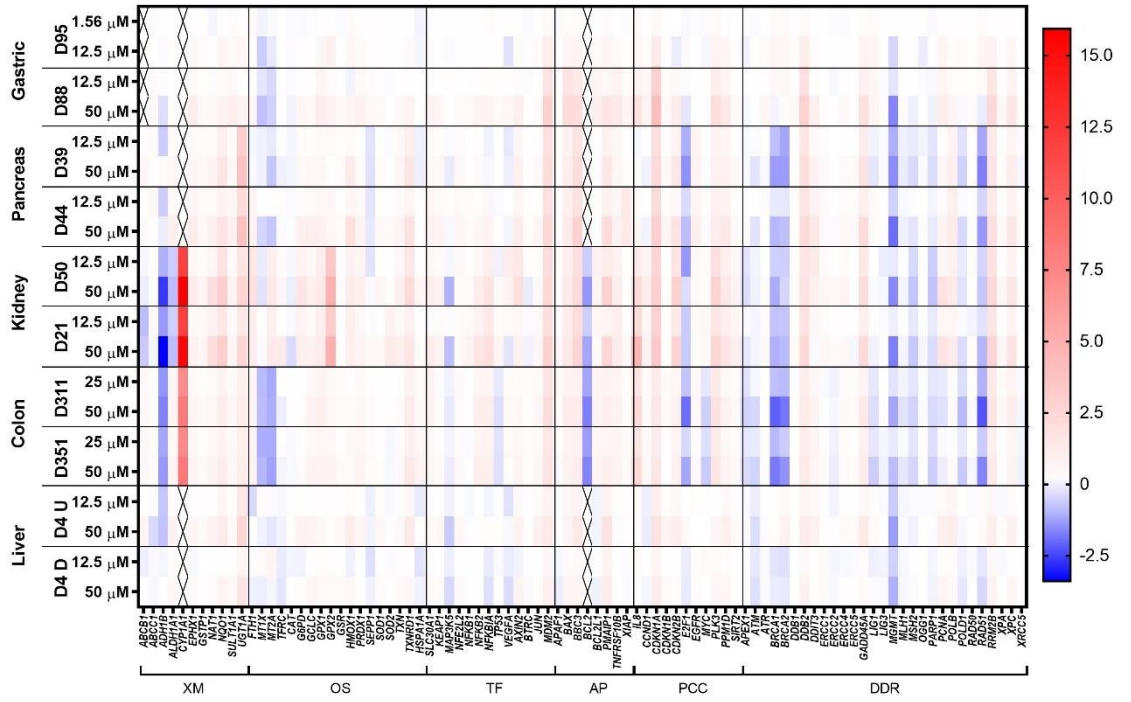

Figure 3.8. Heatmap of the relative gene expression in human organoids after BaP treatment. HT RT-qPCR was carried out with samples from gastric (D95 and D88), pancreas (D39 and D44), kidney (D50 and D21), colon (D311 and D351) and liver (D4 undifferentiated and differentiated) organoids after treatment with BaP for 48 hr. Upregulated and downregulated genes are shown in red and blue, respectively. Genes that were not analysed are displayed as X. XM: Xenobiotic metabolism; OS: Oxidative stress response; TF: Transcription factors; AP: Apoptosis; PCC: Proliferation and cell cycle control; DDR: DNA damage response and repair. Results shown are log2 transformed and relative to the DMSO control (n=3).

Although *CYP1A1* analysis was only possible in kidney and colon organoids, the levels of expression from the HT RT-qPCR followed the same trend as those presented in Section 3.3.3. The results showed a concentration-dependent upregulation and the kidney had much higher expression levels than the colon (Figure 3.9 A). This was also the case for *NQO1*, which showed similar levels of expression in all organoid types except kidney, which had higher fold-change values. However, the results were only biologically relevant (*i.e.*, >2-fold) for the pancreas, colon and undifferentiated liver at the highest concentrations, and for the kidney at both concentrations (Figure 3.9 B). *UGT1A*, involved in BaP detoxification (Shimada, 2006), was upregulated in all organoids, however, the pancreatic organoids had the highest expression followed by the kidney organoids. The lowest fold changes for *UGT1A* were seen in the gastric organoids, which were not biologically significant (Figure 3.9 C).

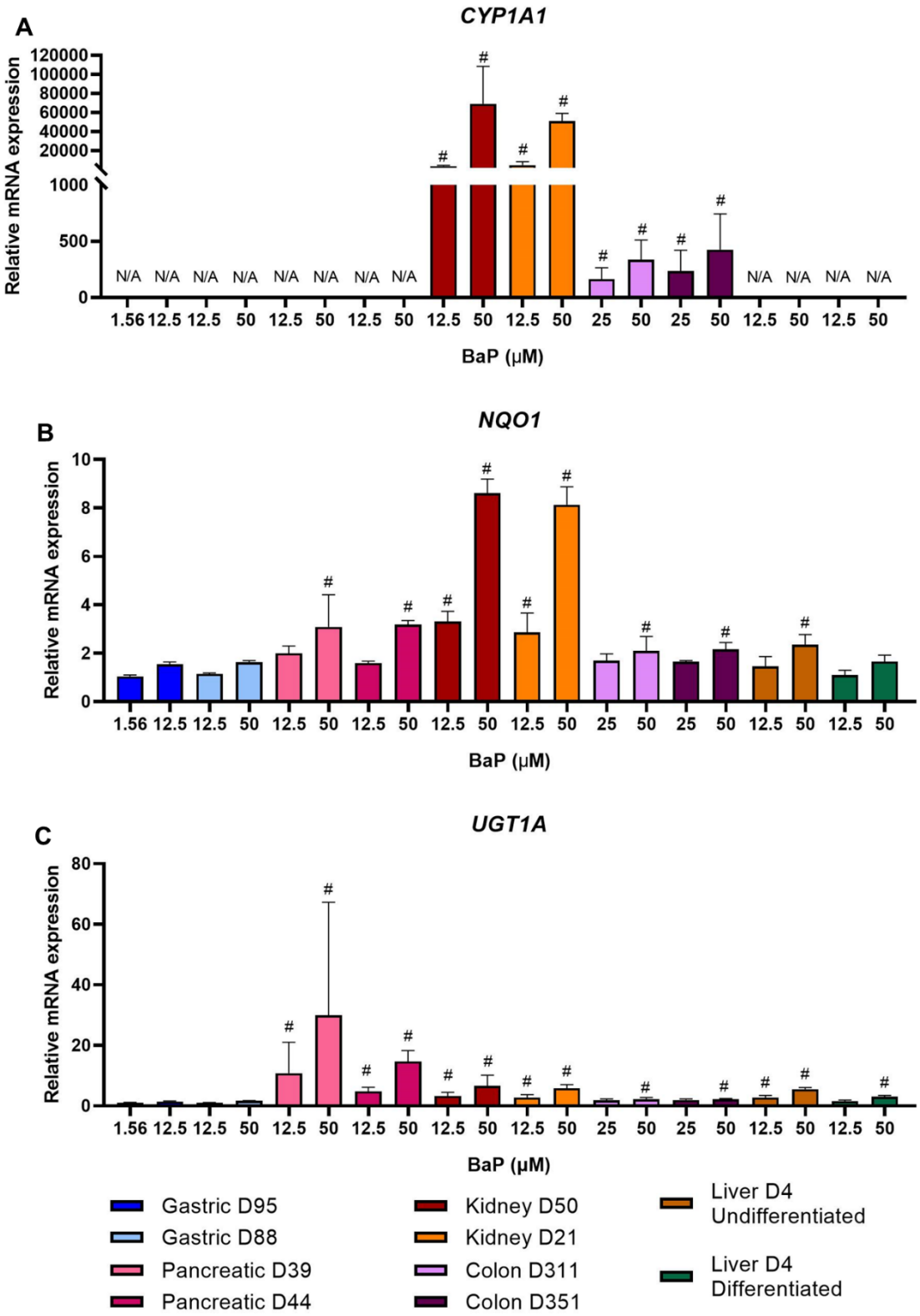

Figure 3.9. Effects of BaP in the gene expression of XMEs measured by HT RT-qPCR. Human tissue organoids were treated with the indicated concentrations of BaP for 48 hr. Linear fold-changes for (**A**) *CYP1A1*, (**B**) *NQO1* and (**C**) *UGT1A* are shown as mean ± SD (n=3). Log2 values ±1 were considered biologically relevant (#), compared to the DMSO control. N/A, Not analysed.

When looking at the genes with the most relevant changes from the DDR group, *MGMT* was downregulated in all organoids following a concentration-dependent decrease in expression (Figure 3.10 A). *GADD45A* was upregulated in a concentration-dependent manner across all organoids and the highest levels were seen in the kidney, pancreas and gastric D88 organoids (Figure 3.10 B). For both *MGMT* and *GADD45A*, gene expression changes were not observed for gastric D95 and at the low concentrations of most of the other donor cultures. In the case of *DDB2* and *RRM2B*, upregulation was biologically relevant in almost all cultures and conditions, except for gastric D95 and differentiated liver at both concentrations, and at the low concentration in undifferentiated liver, and colon D351 for *RRM2B* only (Figure 3.10 C and D).

As mentioned above, *CDKN1A* was the gene in the PCC group with the most relevant changes. This gene, which encodes for the cyclin-dependent kinase inhibitor p21, was upregulated in all organoids but its levels of expression were much higher in the gastric D88 than in other organoids. The lowest levels were seen in gastric D95, and in the colon and liver organoids (Figure 3.11 A). *MDM2*, a major regulator of the p53 pathway (Malmlöf et al. 2008), was selected as the most relevant gene in the TF group. This gene was upregulated and had relevant changes in all organoids except the differentiated liver (Figure 3.11 B). The pro-apoptotic gene *BBC3* showed the greater expression changes in the kidney, pancreatic and gastric D88 organoids, upregulation was not observed in gastric D95 and differentiated liver (Figure 3.11 C). The expression of *TXNRD1*, which is part of the OS group, increased in all organoids, however, this was only biologically relevant in the pancreas, colon, undifferentiated liver, and kidney organoids (Figure 3.11 D).

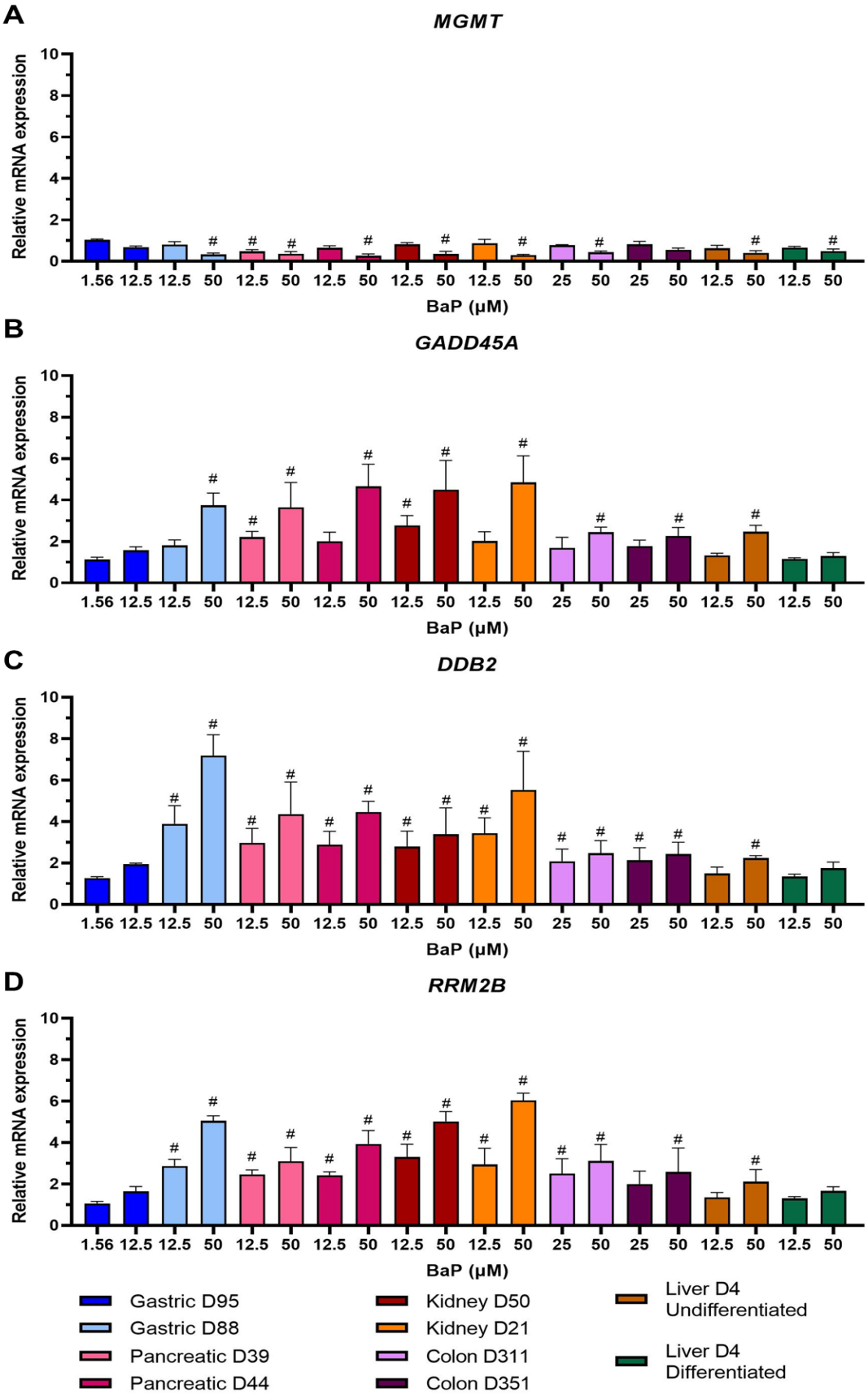

Figure 3.10. Effects of BaP in the expression of genes involved in DDR measured by HT RT-qPCR. Human tissue organoids were treated with the indicated concentrations of BaP for 48 hr. Linear fold-changes for (**A**) *MGMT*, (**B**) *GADD45A*, (**C**) *DDB2* and (**D**) *RRM2B* are shown as mean ± SD (n=3). Log2 values ±1 were considered biologically relevant (#), compared to the DMSO control.

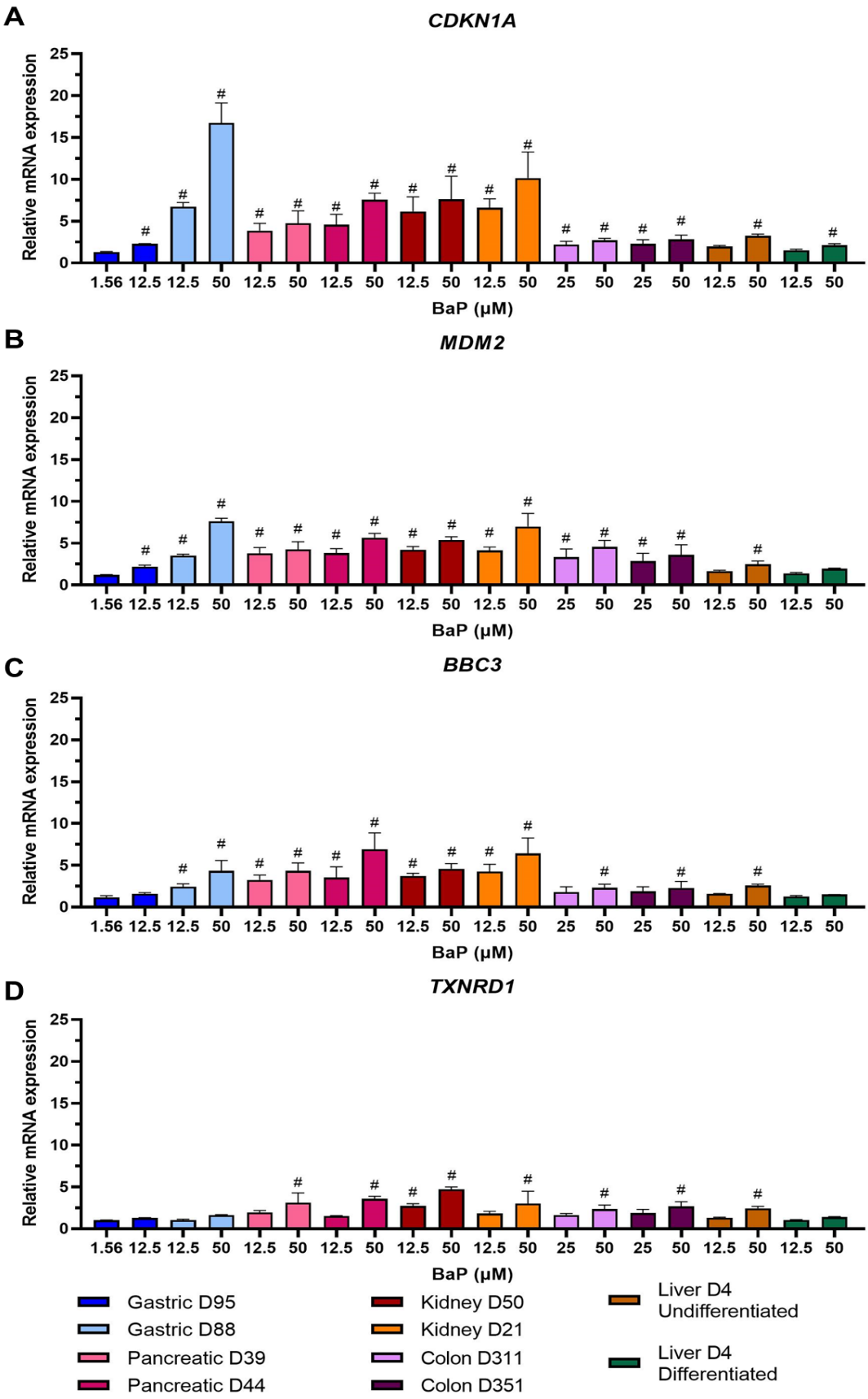

Figure 3.11. Effects of BaP in the expression of genes in the PCC, TF, OS and AP groups measured by HT RT-qPCR. Human tissue organoids were treated with the indicated concentrations of BaP for 48 hr. Linear fold-changes for (**A**) *CDKN1A*, (**B**) *MDM2*, (**C**) *BBC3* and (**D**) *TXNRD1* are shown as mean ± SD (n=3). Log2 values ±1 were considered biologically relevant (#), compared to the DMSO control.

3.4 Discussion

The main objective of this chapter was to investigate the ability of human tissue organoids to bioactivate BaP. Additionally, the tissue-specific responses to BaP were evaluated by treating organoids from possible target organs for cancer (pancreas and liver) and non-target organs (kidney, colon and gastric). Different responses were expected in different organoid types after BaP treatment, highlighting differences between organoids from target and non-target organs.

First, the differentiation of the ductal liver organoids into hepatocyte organoids was carried out, and the morphology of the organoids and expression of hepatocyte markers was assessed (Figure 3.1). Differentiated liver organoids changed their morphology after the differentiation media was added, becoming smaller and darker than the undifferentiated organoids. This could be due to the differentiated organoids having a lower level of the stem cell marker *LGR5* and therefore a lower amount of stem cells and proliferation (Huch et al., 2013b, 2015). However, as some dark organoids were also seen in the undifferentiated wells, the long-term culture of the organoids without passaging may have also led to the collapse of some of the organoid cysts resulting in dark clumps of cells. In line with the findings published by Huch et al. (2015), who reported higher expression of *CYP3A4* and *ALB* in differentiated organoids compared to undifferentiated, as well as higher CYP3A4 activity and ALB secretion in differentiated organoids (Huch et al., 2013b), here the expression of these markers was higher in the differentiated organoids. Additionally, *HNF4* expression was also higher in differentiated organoids, which has been shown previously to be at low levels in undifferentiated liver organoids and increase after differentiation (Broutier et al., 2016; Huch et al., 2013b). *HNF4* expression was also seen in hepatocyte-derived organoids, and it decreased after these were converted to cholangiocyte organoids (Hu et al., 2018). These results are consistent with the idea ductal liver organoids (undifferentiated) were successfully differentiated into hepatocyte liver organoids (differentiated).

The cell viability assessment after BaP treatment showed different responses between organoid types and donor cultures. Gastric D95 cultures were the most susceptible to BaP cytotoxicity with an IC_{50} concentration around 4-fold lower (*i.e.*, 12.8 µM) than gastric D88, pancreatic, kidney and liver organoids (*i.e.*, ≤50 µM), and around 3-fold lower than colon organoids (*i.e.*, 44.2 and 34.5 µM) (Figure 3.2). Although treatment conditions differ, only low cytotoxic responses have been reported after BaP treatment in a number of cell lines, including human colon HCT116, human hepatocellular carcinoma HepG2 and human breast adenocarcinoma MCF-7 and MDA-MB-231 cells (Alotaibi et al., 2021; Hockley et al., 2006; Malik et al., 2018; Štampar et al., 2019; Tung et al., 2014). Similarly, treatment of human bronchial epithelial cells cultured in an air-liquid interface did not affect cell viability (Chang et al., 2019). In contrast, Krais et al. (2015) found that cell viability of murine embryonic stem cells and embryonic fibroblasts decreased by 50% after BaP treatment for 48 hr at concentrations up to 10 µM. In addition, a study by Theobald et al. (2018) reported high toxicity in HepG2 cells and low toxicity in the kidney HEK293 cells under static conditions; however, effects on cell viability seemed marginal when treated in a liver-kidney organ-on-chip. Furthermore, high toxicity in HepG2 cells, as well as in human lymphoblastoid MCL-5 cells, was reported by Shah et al. (2016) in a comparative study testing the effects of BaP on four different human cell lines (as both cell lines express high levels of CYP1A).

The potential of the organoids to metabolically activate BaP was evaluated by examining the gene expression levels of *CYP1A1* and *NQO1*. Overall, the mRNA levels for both enzymes were induced in a concentration-dependent manner in all organoid types and donor cultures. The highest levels were seen in the kidney organoids and the lowest in the colon organoids (Figures 3.3 and 3.4). Induction of mRNA expression of these enzymes after BaP treatment has been reported in different experimental models, including mice and rats as well as cultured human and animal cells (Alotaibi et al., 2021; Arlt et al., 2015; Chang et al., 2019; Dračínská et al., 2021; Hamouchene et al., 2011; Hockley et al., 2006; Krais et al., 2015; Shah et al., 2016; Štampar et al., 2019; Zuo et

al., 2014). This upregulation correlates with the increase in CYP1A1 activity that has been seen in human cell lines (Gearhart-Serna et al., 2020; Shah et al., 2016) and the increased NQO1 activity in mice after treatment (Arlt et al., 2015).

The induction of XME gene expression indicates that organoids are capable of bioactivating BaP. To further corroborate this, the expression of DDR proteins was investigated, showing activation of DDR pathways in all organoid types after BaP treatment (Figure 3.5). Although levels differed, a concentration-dependent response was seen in p-p53 expression in both gastric and kidney cultures, pancreatic D39 and colon D311, while pancreatic culture D44 only showed induction at the highest concentration, and colon D351 and liver undifferentiated organoids had no induction. Interestingly, undifferentiated liver organoids showed a reduction of p-p53 expression, which could be due to cell death unrelated to BaP toxicity. Induction of the p53 downstream target p21 was also observed in gastric and kidney organoids, pancreatic D39 and colon D311 organoids. Induction of p-CHK2 in all organoids, except differentiated liver organoids, further suggests activation of the ATM pathway. This is supported by previous reports showing the induction and activation of p53, p21 and CHK2 by BaP and its reactive metabolite BPDE in human and murine cells (Christmann et al., 2016; Hamouchene et al., 2011; Hockley et al., 2006; Krais et al., 2015; Kucab et al., 2019; Liamin et al., 2017). Expression of γ-H2AX increased after BaP treatment in all organoids, which is in line with the induction seen in human and murine cell lines as well as in human primary and stem cells (Christmann et al., 2016; Jamin et al., 2013; Kucab et al., 2019; Liamin et al., 2017).

Moreover, the activation of BaP was confirmed by determining the formation of two main BaP metabolites: BaP-t-7,8-dihydrodiol and BaP-tetrol-I-1. Although differences between metabolite levels were not significant in all organoids at the concentrations tested, they all showed a concentration-dependent increase (Figure 3.6). BaP metabolite levels varied between organoid types, and similarly to the *CYP1A1* expression results, colon organoids had the lowest levels. The gastric and liver organoids had intermediate levels

of BaP metabolites, while kidney and pancreatic organoids had the highest tetrol and diol levels, respectively. Many studies have evaluated BaP metabolite formation in different experimental systems identifying different amounts of these and other BaP metabolites. Studies using hepatic microsomes from BaP pre-treated wild-type, Hepatic Reductase Null (HRN) and Hepatic cytochrome b_5/P450 reductase null (HBRN) mice showed a significant increase in diol levels when comparing microsomes of untreated and BaP treated mice (Reed et al., 2018; Stiborová et al., 2014). Similarly, the presence of the diol metabolite was found after BaP incubation of microsomes from *Trp53*(+/+) mice pre-treated with BaP, and the levels increased in *Trp53*(+/-) and *Trp53*(-/-) (Krais et al., 2016a). The generation of BaP metabolites was also studied in F258 rat liver epithelial and mouse hepatoma Hepa1c1c7 cell lines, where the BaP-t-7,8-dihydrodiol was formed in both with Hepa1c1c7 having higher levels and BaP-tetrol-l-1 formation was only seen in Hepa1c1c7 (Holme et al., 2007).

Additionally, different dG-N^2-BPDE adduct levels, measured by LC-ESI-MS/MS, were seen in all organoid types and donor cultures (Figure 3.7). The highest adduct levels were seen in pancreatic D39, followed by liver undifferentiated and kidney D21 organoids; intermediate levels were seen in pancreatic D44, followed by kidney D50, gastric D88 and D95, and liver differentiated; the lowest levels were seen in the colon. As with *CYP1A1* expression and BaP metabolite formation, colon organoids had the lowest levels of DNA adducts and there was a difference of 1.5-2-fold between concentrations. BaP-induced DNA adduct formation has been reported in several studies using a variety of methods and testing different biological systems, including mice and rats, cell lines and *in vitro* cell-free systems (Arlt et al., 2008; Dračínská et al., 2021; Hockley et al., 2006, 2007; Krais et al., 2015; Long et al., 2018; Stiborová et al., 2014). Krais et al. (2016a) measured DNA adduct levels in different organs of mice treated by intraperitoneal injection with BaP or BPDE. In wild-type mice treated with BaP the liver had higher average adduct levels than the kidney, while treatment with BPDE led to more adducts in the kidney. In contrast to the results presented in this chapter, the colon had

higher levels of dG-N^2-BPDE than the liver, kidney and glandular stomach. Here, gastric D95 had the same amount of adducts as the differentiated liver organoids which correlates with the results from the glandular stomach and the liver as they had similar adduct levels (Krais et al., 2016a). High levels of adducts in the liver of Muta™ Mouse were seen across different BaP doses; these were more than double those seen in the glandular stomach, which is similar to what was seen between the undifferentiated liver and gastric organoids (Lemieux et al., 2011). A recent study by Long et al., (2018) in which adult male Muta™ Mouse were orally exposed to BaP at various doses showed tissue-specific differences in DNA adduct levels. In line with what was seen in this chapter, the highest increase was seen in the liver, followed by the kidney and the glandular stomach. Similarly, higher adduct levels in the liver compared to the glandular stomach and the colon were seen in male and female mice administered BaP by oral gavage (Zuo et al., 2014). In a study by Arlt et al. (2008), DNA adduct levels were investigated in wild-type mice after intraperitoneal injection with BaP for 1 or 5 days showing higher adduct levels after 5 days of exposure and higher adduct levels in the glandular stomach and kidney compared to the colon and liver. Overall, there are conflicting data on the levels of adduct formation in individual tissues between studies, but some similarities can be found. Unfortunately, no data were found comparing adduct levels in the pancreas to other tissues, although adducts have been reported to be formed in pancreatic cell systems (Jin Kang et al., 2011).

Lastly, to investigate tissue-specific responses in more depth an analysis of gene expression changes of genes involved in different pathways was carried out using HT RT-qPCR. Overall, significant changes were seen across all organoid types and the six gene group classifications (Figure 3.8). Similar studies have been carried out in mice, fish, and human cell lines, where the expression profiles after BaP or BPDE treatment were investigated. These studies have highlighted the alteration of phase I and II metabolic enzymes, DNA damage response, pro-apoptotic and oxidative stress response genes (Labib et al., 2012; Piberger et al., 2018; Yuan et al., 2014; Zuo et al.,

2014). Additionally, some of these studies compared responses between target and non-target organs and although the modulation of some genes seemed to be significantly different, there were still overlaps between target and non-target organs (Zuo et al., 2014). The results presented here show a lot of overlap between organoids from possible BaP target organs for cancer (pancreas and liver) and non-target (colon, stomach, and kidney) organs, as the alterations tend to follow the same trend but with different levels of expression.

Some of the genes with the most significant changes in the XM group were *CYP1A1*, *NQO1* and *UGT1A.* The upregulation of *CYP1A1* and *NQO1* followed a similar pattern to that seen in the analysis of XMEs presented in Section 3.3.3, and *UGT1A* had the highest upregulation in the pancreatic organoids (Figure 3.9). Upregulation of *CYP1A1* and *NQO1* has been reported in previous studies as mentioned previously. *UGT1A* has been found to be significantly induced by BaP in 3D culture of HepG2 cells, in which *CYP1A1* was also induced but at much higher levels (Štampar et al., 2019). Additionally, *UGT1A* expression was differentially regulated in MCF-7 cells (Hamouchene et al., 2011). Some of the DDR genes with the most significant changes were *MGMT*, *GADD45A*, *DDB2* and *RRM2B* (Figure 3.10). In contrast to what was seen here, the expression of *MGMT* has been found to be upregulated in the forestomach and lungs of BaP-treated mice (Labib et al., 2012, 2013). A study by Piberger et al. (2018) investigating the transcriptional response to BPDE in the human lymphoblasts TK6 cells found *GADD45A, DDB2* and *RRM2B* to be induced at a range of BPDE concentrations. This is in line with what was seen here and also reported in HepG2 spheroids, primary human T lymphocytes, human lung fibroblasts and MCF-7 cells (Christmann et al., 2016; Dreij et al., 2010; Hockley et al., 2006; Liamin et al., 2017; Štampar et al., 2019). The PCC gene *CDKN1A* was upregulated (Figure 3.11 A), which partly correlates with what was seen in DDR protein expression where p21 was induced in most organoid cultures, and with what has been reported in studies involving different human cells (Christmann et al., 2016; Dreij et al., 2010; Hockley et al., 2006, 2007; Liamin et al., 2017; Piberger

et al., 2018; Štampar et al., 2019) and in BaP-treated mice (Labib et al., 2012). The TF, OS and AP genes, *MDM2*, *TXNRD1* and *BBC3*, respectively, were upregulated after BaP treatment (Figure 3.11 B, C and D). The upregulation of *MDM2* has also been reported in the TK6 cell line, human primary T lymphocytes and mouse lung and forestomach tissues. In contrast, no change was seen in HepG2 spheroids (Labib et al., 2012, 2013; Liamin et al., 2017; Piberger et al., 2018; Štampar et al., 2019). There was no significant upregulation of *BBC3* mRNA expression in human T lymphocytes; however, ≥2-fold induction was seen in TK6 and MCF-7 cells (Hamouchene et al., 2011; Liamin et al., 2017; Piberger et al., 2018), while *TXNRD1* was upregulated in HepG2 and MCF-7 cells (Hockley et al., 2006, 2007).

To conclude, organoids derived from normal human stomach, colon, pancreas, kidney and liver tissues were all capable of activating BaP, leading to different cytotoxic and genotoxic effects. This was confirmed by the induction of XMEs, DDR proteins, BaP metabolite and BaP-DNA adduct formation. Although no clear differences between organoids from possible target and non-target organs were identified several changes were seen when looking at the HT RT-qPCR analysis of the 90-gene panel. The induction of some of these genes including *CDKN1A*, *MDM2* and *GADD45A* as well as the expression of p-p53 and p21 proteins indicate the involvement of the p53 pathway in response to BaP treatment. Although a follow-up of these findings is required (discussed in Chapter 7), the results described in this chapter suggest human tissue organoids are an interesting system to investigate the cellular responses to BaP treatment and its organotropism.

Chapter 4 Metabolic activation and cellular responses to aflatoxin B_1

4.1 Introduction

Aflatoxins are a group of mycotoxins found in various crops such as cereals, legumes, and nuts; therefore, the main source of human exposure is the diet. Aflatoxin contamination of food products is common, particularly in regions with tropical climates; however, due to movement of food from these regions into other countries, aflatoxins are prevalent worldwide (IARC, 1993). Aflatoxins have been linked not only to human cancer, but also to acute and chronic toxicity, or aflatoxicosis (Williams et al., 2004). There are four types of aflatoxins, AFB_1, AFB_2, AFG_1 and AFG_2, of which AFB_1 is the most common and toxic (Wild et al., 2015).

Several epidemiological and animal studies have shown evidence linking AFB_1 exposure to liver cancer, mainly hepatocellular carcinoma; therefore, AFB_1 has been classified as a human carcinogen (Hamid et al., 2013; IARC, 2012a; Rushing and Selim, 2019). The metabolic activation of AFB_1 occurs in the liver by the action of CYP enzymes to produce the highly reactive metabolite AFBO, which can react with DNA to form the DNA adduct, AFB_1-N^7-Gua, which in turn can be converted to the persistent and highly mutagenic ring-opened adduct AFB_1-FapyGua (Section 1.4.2) (Groopman et al., 1981; Rushing and Selim, 2019; Smela et al., 2002). The presence of DNA adducts in urine and liver samples from animals and humans exposed to AFB_1 has been widely reported (Asim et al., 2011; Chawanthayatham et al., 2015; Coskun et al., 2019; Egner et al., 2001, 2006; Woo et al., 2011), but they have also been detected in other tissues including the kidney and colon (Cupid et al., 2004; Harrison et al., 1993; Hsieh and Hsieh, 1993; Kolars et al., 1994).

It is well known that adduct formation is only an initiation step in the oncogenesis process and that the events that follow are key in tumour formation. Aflatoxin-specific mutations in the *TP53* gene have been identified in liver tumours (Besaratinia et al., 2009; Gouas

et al., 2009; Hussain et al., 2007; Kirk et al., 2000); however, there are still many factors that remain unknown. Studies investigating AFB_1-induced changes in human liver cell lines have found a number of differentially expressed genes, including transcription factors and genes associated with cell cycle, proliferation, DNA replication and repair, and cellular movement, growth and organisation (Smit et al., 2017; Tryndyak et al., 2018). Additionally, epigenetic alterations in several regions of the genome have been reported; however, only a few of them were found to affect genes that could be involved in carcinogenicity (Rieswijk et al., 2016; Tryndyak et al., 2018).

The need for more physiologically relevant models for genotoxicity testing has led to the development of 3D models like spheroids from different cell lines, including the human liver HCC cell line HepG2. This particular 3D model had higher sensitivity than the monolayer culture of the same cells, and also showed it was useful for identifying gene expression changes (Štampar et al., 2019). Here, organoids, another 3D cell culture model, were used to assess the effects of AFB_1. The aim of this chapter was to investigate tissue-specific responses in human tissue organoids that represent target (liver) and non-target (gastric and kidney) organs for AFB_1 carcinogenicity. For this purpose, the ability of these organoids to metabolise the compound was tested and the cytotoxic responses were measured. The activation of the DDR pathway and the formation of AFB_1-DNA adducts were also investigated.

4.2 Materials and methods

Normal human tissue organoids from gastric, kidney and liver tissues were grown as explained in Section 2.2. Gastric organoids were cultured in Bartfeld media (Section 2.2.1.1), and liver organoids were differentiated into hepatocytes as detailed in section 2.2.4. Treatment of organoids with AFB_1 was carried out as mentioned in Section 2.2.5; controls were treated with vehicle only (0.5% DMSO). The CellTiter-Glo assay was used to measure cell viability after treatment (Section 2.3), and the expression and induction of DDR proteins (p-p53, pCHK2, p21 and γ-H2AX) was assessed by Western blotting (Section 2.4; kidney and liver experiments were performed by the MSc Biomedical and

Molecular Sciences student Andrew Breen at King's College London). *CYP3A4* and *CYP1A2* gene expression after AFB_1 treatment was investigated by RT-qPCR (Section 2.6) and DNA adduct formation was determined by LC-MS/MS (Section 2.5.5; conducted partly by Dr John Groopman at the Johns Hopkins Bloomberg School of Public Health, Baltimore, USA).

4.3 Results

4.3.1 Cell viability assessment of organoids treated with AFB_1

Gastric, kidney and liver organoids were treated for 48 hr with a range of concentrations of AFB_1 (0-150 µM). Cell viability was assessed using the CellTiter-Glo assay and IC_{50} values were calculated when possible. Overall, AFB_1 treatment led to a decrease in cell viability in all organoids; however, different levels of cytotoxicity were seen between organoid types. Gastric culture D95 was the most susceptible to AFB_1 as it reached the IC_{50} at a concentration of 22 µM, while culture D88 had an IC_{50} of 126 µM (Figure 4.1 A). Kidney organoids were less susceptible to treatment with IC_{50} values over 150 µM, the highest concentration possible (due to solubility). Culture D50 had an IC_{50} close to 150 µM, while D21's IC_{50} was estimated at 213 µM (Figure 4.1 B). As explained in Section 3.3.1, liver organoids were differentiated into hepatocytes as these are the main metabolic units of the liver. Cell viability assessment of both undifferentiated and differentiated liver organoids showed the IC_{50} values for both were greater than 150 µM. Even though the undifferentiated liver cells seemed to have a more toxic response than the differentiated ones at 100 µM, their cell viability increased to the levels of the differentiated liver at 150 µM (Figure 4.1 C).

Based on the cytotoxicity assessment, the following concentrations were chosen for subsequent experiments. As the only culture with an IC_{50} lower than 150 µM, *i.e.*, 22 µM, was gastric D95, a concentration close to this value (25 µM), one higher (50 µM; ~30% viability) and one lower (6.25 µM; ~80% viability) were chosen. For all other organoids the highest (150 µM) and two lower (37.5 µM and 75 µM) concentrations were selected.

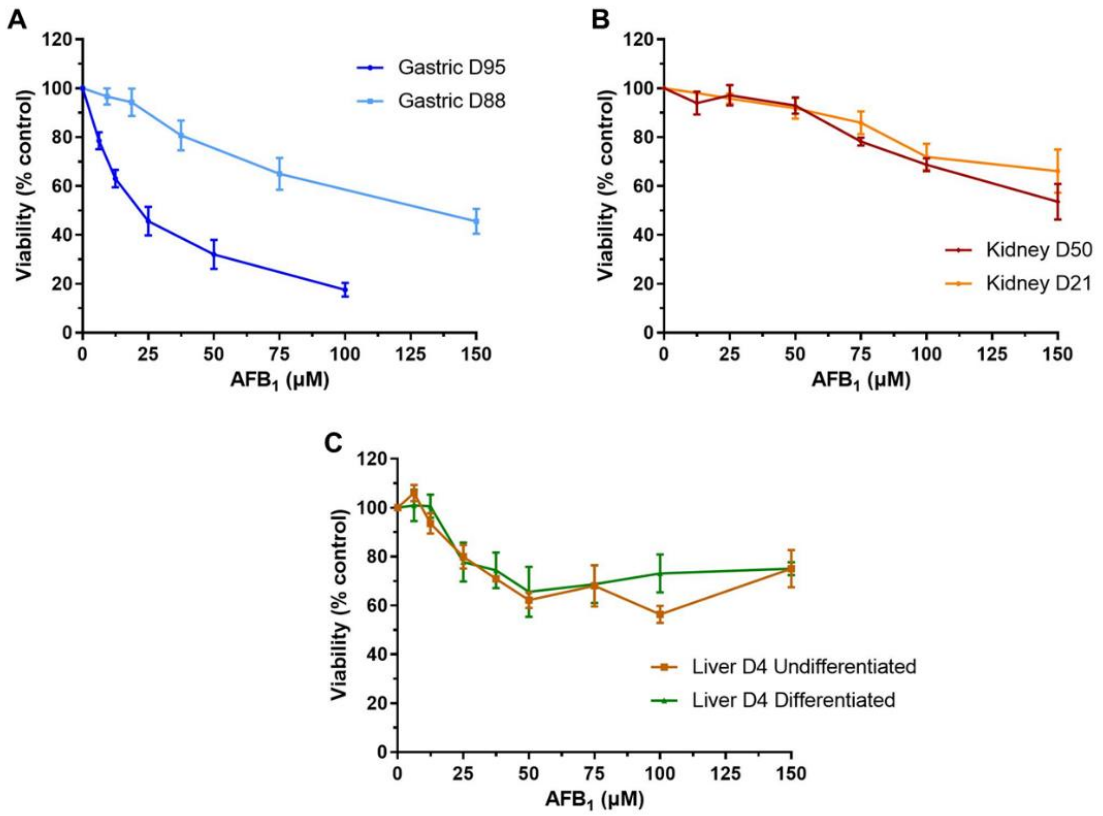

Figure 4.1. Cell viability in human tissue organoids after AFB_1 treatment. Organoids from normal gastric (D95 and D88; **A**), kidney (D50 and D21; **B**) and liver (D4 undifferentiated and differentiated; **C**) tissues were treated with various concentrations of AFB_1 (0-150 µM) for 48 hr. A DMSO control was included. Cell viability (% control) was measured using the CellTiter-Glo assay. Results are shown as mean ± SEM, n≥3.

4.3.1 Xenobiotic-metabolising enzyme expression after AFB_1 treatment

To investigate the ability of organoids to bioactivate AFB_1, gene expression levels of *CYP3A4* and *CYP1A2*, XMEs involved in AFB_1 metabolism, were analysed by RT-qPCR. In all organoids, except gastric D95, an increase in *CYP3A4* expression was seen at the lowest concentration, which then decreased at the highest (Figure 4.2). The lowest *CYP3A4* levels were seen in gastric D95, where there was no increase in expression at the lowest concentration and at the highest concentration there was a slight decrease in expression (Figure 4.2 A). Although gastric D88 had an increase in expression at 37.5 µM, this was not significant, however, at 150 µM there was a significant induction of ~2.2-fold compared to the control (Figure 4.2 A). Both kidney organoid cultures, D50 and D21, showed a significant increase of 30.4 and 17.4-fold, respectively, at 37.5 µM (Figure 4.2 B). Undifferentiated liver organoids only had a small increase in *CYP3A4*

expression at 37.5 µM. In contrast, the differentiated liver control had significantly higher levels of expression compared to the undifferentiated liver control with a fold increase of 26.3. The differentiated liver organoids had a 25.2-fold increase at 37.5 µM compared to the undifferentiated control, but there was no induction compared to the differentiated control. As seen in other organoid types, *CYP3A4* expression decreased at the highest concentration in both undifferentiated and differentiated liver organoids, compared to the levels at 37.5 µM in undifferentiated and differentiated organoids, respectively (Figure 4.2 C).

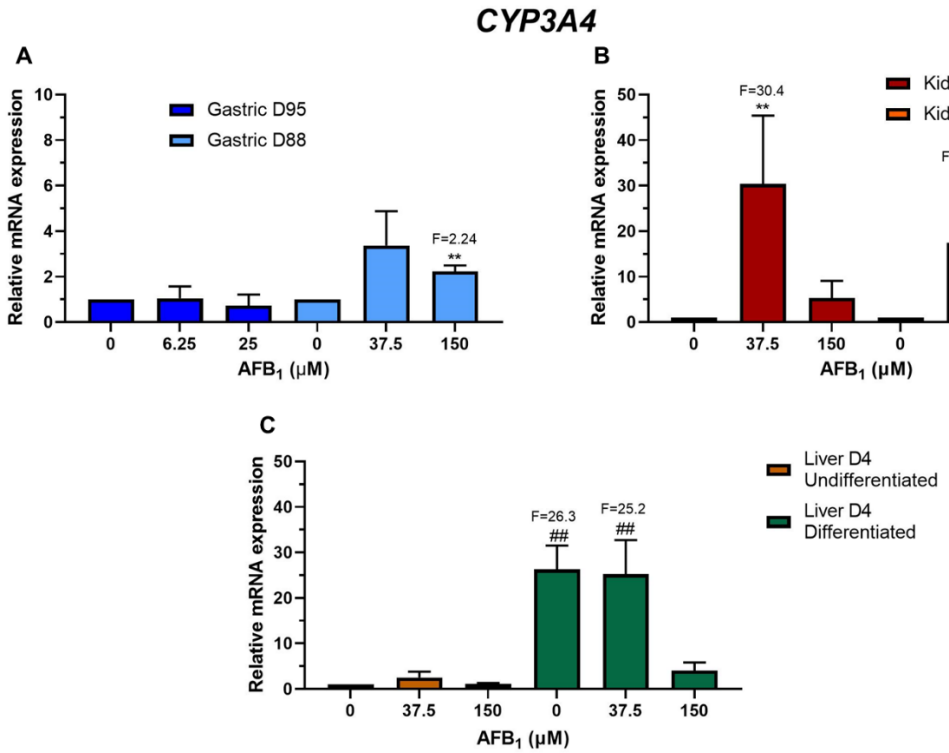

Figure 4.2. Relative gene expression of *CYP3A4* in normal human tissue organoids after AFB_1 treatment. Organoids from stomach (D95 and D88; **A**), kidney (D50 and D21; **B**) and liver (D4, undifferentiated and differentiated; **C**) tissues were treated with the indicated concentrations of AFB_1 for 48 hr. *CYP3A4* expression was analysed by RT-qPCR and the $2^{-\Delta\Delta CT}$ method. Values are shown as mean ± SD (n=3). Values were normalised to mRNA expression of the housekeeping gene *GAPDH* and are relative to the DMSO control; for liver organoids the values are relative to the undifferentiated control. Statistical analysis was performed by log2 transforming the data and a one sample *t*-test with Bonferroni correction against the control mean of 0: *p<0.05; **p<0.01 compared to untreated control; ## p<0.01 compared to liver undifferentiated control.

Expression of *CYP1A2* increased in a concentration-dependent manner after treatment of AFB_1 in all organoid types. As with CYP3A4, gastric D95 had the lowest expression levels of *CYP1A2*, and although D88 levels were slightly higher, the induction was not significant (Figure 4.3 A). In the case of the kidney organoids, D50 seemed to have higher levels of expression than D21; however, the changes were not significant due to variation, while D21 had significant changes in expression at both 37.5 and 150 µM with ~5.7 and 30-fold increases, respectively (Figure 4.3 B). Lastly, undifferentiated liver organoids had a significant increase in expression at 150 µM, while the differentiated did not show any significant changes (Figure 4.3 C).

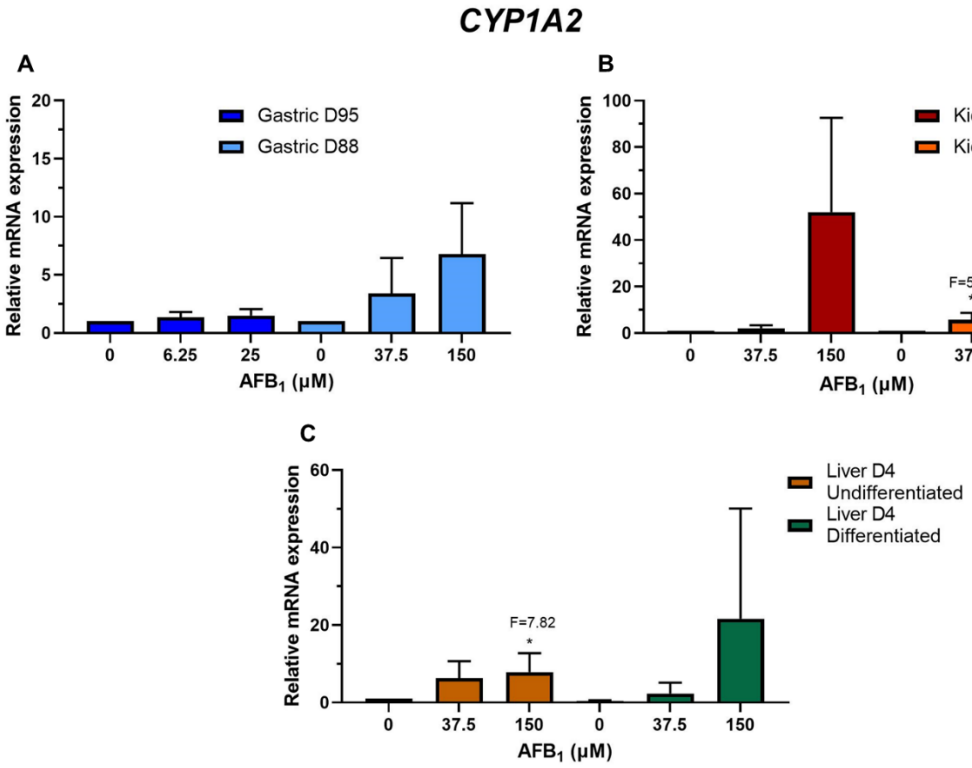

Figure 4.3. Relative gene expression of *CYP1A2* in normal human organoids after AFB_1 treatment. Organoids from normal stomach (D95 and D88; **A**), kidney (D50 and D21; **B**) and liver (D4, undifferentiated and differentiated; **C**) tissues were treated with the indicated concentrations of AFB_1 for 48 hr. *CYP1A2* expression was analysed by RT-qPCR and the $2^{-\Delta\Delta CT}$ method. Values are shown as mean ± SD (n=3). Values were normalised to mRNA expression of the housekeeping gene *GAPDH* and are relative to the DMSO control; for liver organoids the values are relative to the undifferentiated control. Statistical analysis was performed by log2 transforming the data and a one sample *t*-test with Bonferroni correction against the control mean of 0: *p<0.05 compared to untreated control. No statistical differences were observed between differentiated and undifferentiated liver organoids (D4).

Basal levels of *CYP3A4* and *CYP1A2* expression were compared between kidney, liver and gastric organoids showing that differentiated liver organoids had significantly higher levels of *CYP3A4* expression than kidney and gastric organoids. In the case of *CYP1A2*, undifferentiated liver and gastric D88 organoids had the highest levels of expression in the control, intermediate in the differentiated liver and the kidney cultures and the gastric D95 having the lowest expression (Figure 4.4).

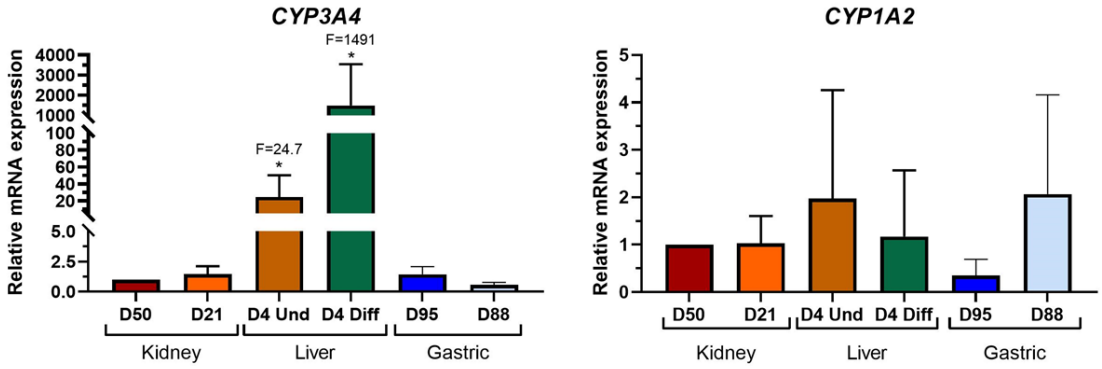

Figure 4.4. Relative gene expression of *CYP3A4* and *CYP1A2* in normal human organoids. *CYP3A4* and *CYP1A2* expression of controls from normal kidney (D50 and D21), liver (D4, undifferentiated and differentiated) and gastric (D95 and D88) tissue organoids was analysed by RT-qPCR and the $2^{-\Delta\Delta CT}$ method after 48 hr of incubation in vehicle control (0.5% DMSO). Values are shown as mean ± SD (n=3). Values were normalised to mRNA expression of the housekeeping gene *GAPDH* and are relative to kidney D50. Gastric organoids were analysed in a separate plate. Statistical analysis was performed by log2 transforming the data and a one sample *t*-test with Bonferroni correction against the control mean of 0: *p<0.05 compared to D50.

4.3.2 Induction of DDR proteins after AFB_1 treatment

Expression and induction of the DDR markers p-p53, pCHK2, p21 and γ-H2AX was assessed after AFB_1 treatment for 48 hr by Western blotting. To allow comparison, protein extracts from the same organoid type were run on the same gel. Overall, although differences between cultures were seen, there was induction in all the proteins tested (Figure 4.5). Both gastric organoids showed a dose-dependent response of γ-H2AX, while the other proteins seemed to have a higher expression at the lower concentrations compared to the highest treatment concentration. For D95, p-p53 and pCHK2 had the highest induction at 25 µM, while p21 had higher induction at 6.25 and 25 µM when compared to 50 µM. For D88, induction of pCHK2 and p21 appeared constant across

the concentrations tested, while p-p53 increased slightly at 150 µM (Figure 4.5 A). Kidney organoid cultures had similar induction patterns, γ-H2AX had a concentration-dependent increase, while p-p53 and pCHK2 showed the highest expression at 75 µM. The highest induction of p21 was seen at 37.5 µM; this decreased slightly at 75 µM and at 150 µM expression levels were similar to those in the control (Figure 4.5 B). Undifferentiated liver organoids had higher expression of these proteins than the differentiated organoids. Although γ-H2AX was induced in both liver organoids, a stronger concentration-dependent increase was seen in the undifferentiated. As seen in other organoid types, p21 expression was the highest at 37.5 µM and then decreased to control levels at 150 µM. While undifferentiated organoids had induction of p-p53 at 37.5 µM and 75 µM, and pCHK2 at all concentrations, expression of p-p53 and pCHK2 in the differentiated liver was very low (Figure 4.5 C).

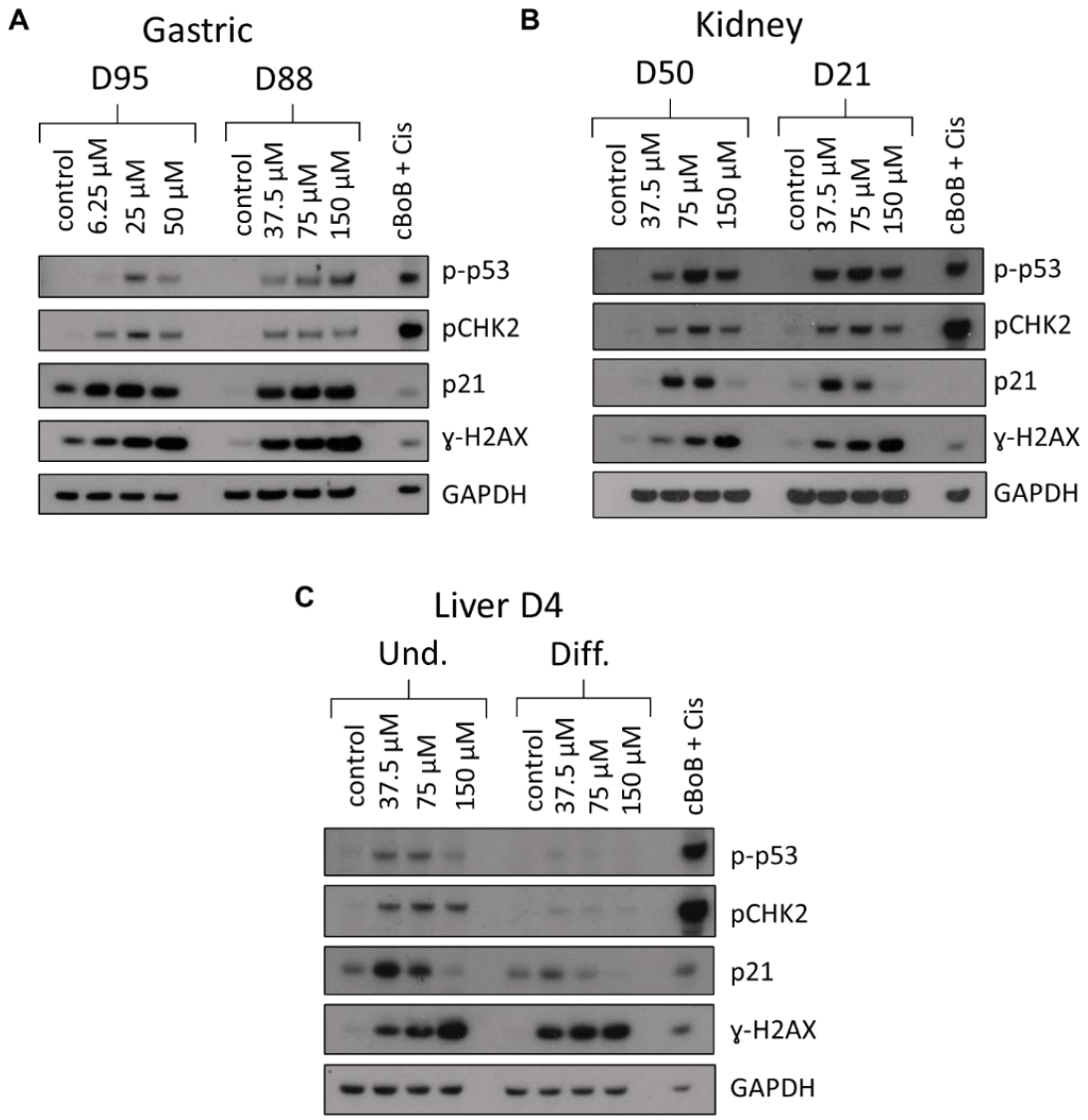

Figure 4.5. Expression of DDR proteins in human organoids after treatment with AFB_1. Organoids from normal gastric (D95 and D88; **A**), kidney (D50 and D21; **B**) and liver (D4 undifferentiated and differentiated; **C**) tissues were treated with the indicated concentrations of AFB_1 for 48 hr. Different DDR proteins (p-p53, pCHK2, p21 and γ-H2AX) were detected and GAPDH was used as a loading control. Organoids from the same tissue were loaded on one gel to allow direct comparison. cBoB + Cis (cBoB treated with 3.125 µM cisplatin) was used as a positive control. Representative blots are shown (n=2).

4.3.3 DNA adduct formation after AFB_1 exposure

To further evaluate the metabolic activation and genotoxicity of AFB_1, formation of AFB_1-DNA adducts was investigated by LC-MS/MS. Generally, levels of AFB_1-N^7-Gua adducts were low in all samples (data not shown); however, high levels of AFB_1-FapyGua adducts were observed. Levels of total-AFB_1-FapyGua formation are shown in Figure 4.6. Overall, adduct formation in a concentration-dependent manner was seen in all

organoid types, with the liver, particularly the undifferentiated liver, having a significantly higher level of adducts than the kidney and the gastric organoids in all conditions tested. Gastric organoids had the lowest levels of adducts of the three organoid types tested, with culture D95 having lower levels than D88. At the IC_{50} concentration D95 had 150.5 adducts per 10^7 nucleosides while D88 had 341.8 adducts per 10^7 nucleosides. At the lowest concentrations D95 and D88 had 38.4 and 102.9 adducts per 10^7 nucleosides, respectively (Figure 4.6 A). Kidney organoids had much higher levels of adducts than the gastric, and less differences between cultures. Kidney D50 had slightly lower adduct levels than D21 at both concentrations tested. D50 had 1079.5 and 383.1 adducts per 10^7 nucleosides at 150 and 37.5 µM, respectively, while D21 had 1176.6 and 426.1 adducts per 10^7 nucleosides at the same concentrations. It is worth highlighting that the levels of toxicity at 150 µM were slightly higher in the D50 culture (Figure 4.6 B). Lastly, the highest levels of adducts were detected in undifferentiated liver organoids, which had 5547 and 1467.2 adducts per 10^7 nucleosides at 150 and 37.5 µM, respectively. Differentiated liver organoids also had high levels of adducts, however, at 150 µM these were about half of those in the undifferentiated (2719.8 adducts per 10^7 nucleosides). At 37.5 µM differentiated liver organoids had 1297.8 adducts per 10^7 nucleosides (Figure 4.6 C).

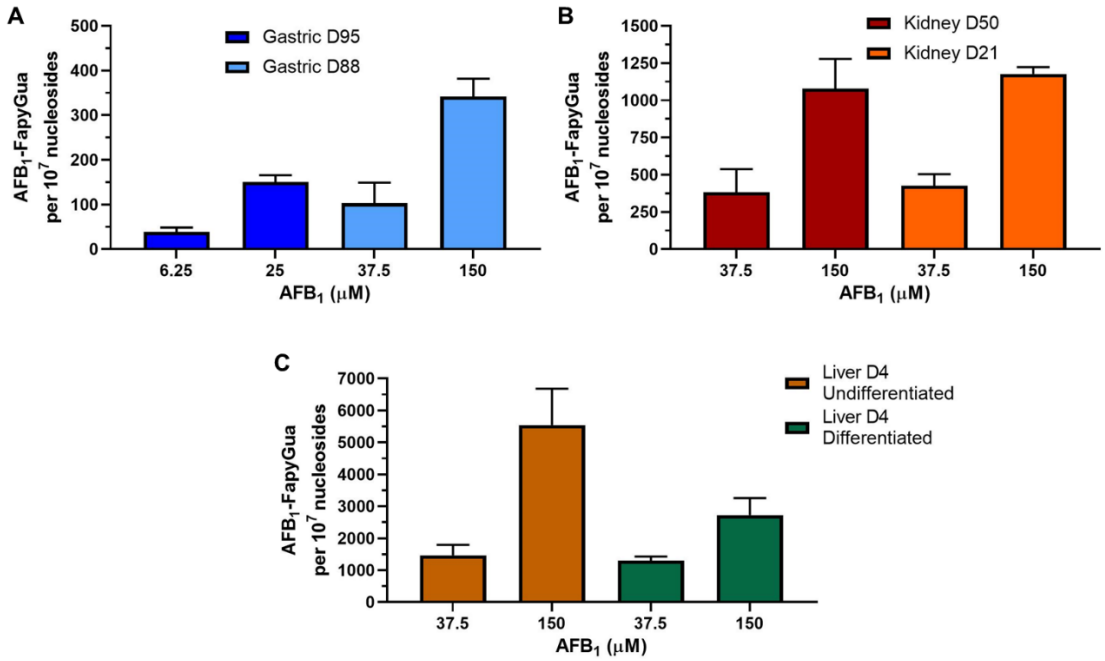

Figure 4.6. DNA adduct formation in human tissue organoids after treatment with AFB_1. Gastric (**A**; D95 and D88), kidney (**B**; D50 and D21) and liver (**C**; D4 undifferentiated and differentiated) organoids were treated with the indicated concentrations of AFB_1 for 48 hr. AFB_1-FapyGua adduct formation was quantified using LC-MS/MS. No adducts were detected in the untreated controls. Results are shown as mean ± SD, n≥3.

4.4 Discussion

The main objective of this chapter was to investigate if human tissue organoids can bioactivate AFB_1 and to assess tissue-specific responses in liver (target tissue), kidney and gastric (non-target tissues) organoids, in order to shed some light on the organotropism of this well-characterised carcinogen. Different responses were hypothesised to occur in organoids of target and non-target tissues, including different levels of adduct formation.

The cell viability assessment showed different responses between organoid types. Gastric D95 were the most susceptible organoids to AFB_1 toxicity with an IC_{50} almost 6-fold lower (*i.e.*, 22 µM) than that of the gastric D88 culture, and the kidney and liver organoids for which IC_{50} values were ≤150 µM (Figure 4.1). To some extent these findings correlate with histopathological observations published in a recent study where AFB_1 exposure of Wistar rats lead to higher levels of damage, including inflammatory cellular infiltration, necrosis, oedemas and haemorrhages, in the gastric mucosa than in

the liver (Akinrinde et al., 2020). *In vivo* liver and kidney toxicity was also reported in mice, where their organ/body weight ratios were significantly affected after being fed with AFB_1-contaminated foods for 40 days (Luo et al., 2018). A liver-kidney-on-chip model was recently used to model primary and secondary AFB_1 toxicity, showing that toxicity in renal HEK293 cells increases after primary exposure of hepatoma HepG2 cells to AFB_1. The latter study also showed that cells in the microfluidic system have higher declines in cell viability than those in static cultures (Theobald et al., 2018). Furthermore, other *in vitro* studies with animal and human cells have shown different effects of AFB_1 treatment on cell viability. Some of them had small reductions in cell viability, while others reported big declines in cell survival (Loquet and Wiebel, 1982; Mace et al., 1997; Smit et al., 2017; Štampar et al., 2019). However, many factors differed between these studies, including the concentrations and times of exposure, and methods used to test cell viability, making comparisons difficult. In other studies, the co-treatment with S9 mix was required to reach IC_{50} values in mouse embryonic fibroblasts and stem cells (Besaratinia et al., 2009; Kucab et al., 2019).

The bioactivation of AFB_1 into reactive metabolites occurs by the action of *CYP1A2* and *CYP3A4*. The results presented here show that, although at different levels, all organoids tested express these AFB_1 metabolising enzymes. However, significant induction of these enzymes after treatment was not seen in every culture (Figures 4.2 and 4.3). As the hepatocytes carry out the main metabolic activities of the liver, it was expected for the undifferentiated liver organoids (ductal cells) to have lower induction levels of the CYP enzymes than the differentiated liver organoids (hepatocytes). This was the case for both enzymes; however, because the induction of *CYP1A2* in differentiated liver had high variability the difference did not reach statistical significance. Although gastric culture D95 had the highest cytotoxic response, it had the lowest levels of induction of both enzymes, followed by gastric D88. Interestingly, *CYP3A4* induction did not have a concentration-dependent response having the highest induction at the lowest concentration tested, while *CYP1A2* expression followed a concentration-dependent

pattern. Several studies have looked at the involvement of these enzymes in AFB_1 metabolism (Gallagher et al., 1996; Kamdem et al., 2006); however, investigations of the effects of AFB_1 treatment on their expression in different tissues or cell types have been limited. Only a small induction of these XMEs in HepG2 spheroids has been reported (Štampar et al., 2019), and the *CYP3A4* pattern seen in this study has not been previously published, but it could be caused by increased toxicity at the highest concentrations. The higher levels of *CYP1A2* induction in the kidney organoids may be due to this enzyme having a more important role in extra-hepatic metabolism of AFB_1 (McCullough and Lloyd, 2019). As kidney and differentiated liver organoids had high levels of *CYP3A4* induction, the basal levels of expression of the enzyme were assessed as this might influence responses to AFB_1 treatment. Overall basal levels of *CYP3A4* were the highest in the differentiated liver organoids and levels of *CYP1A2* were highest in the undifferentiated liver organoids (Figure 4.4). These findings are in concordance with studies done on tissue distribution of human CYP isoforms (Nishimura et al., 2003).

To further analyse the effects of AFB_1 on the organoids, the activation of the DDR pathway was investigated. Overall, all organoids showed an induction of all the tested proteins with different levels of expressions, except differentiated liver organoids, which did not show p-p53 or pCHK2 expression (Figure 4.5). The induction of p53 and CHK2 indicates the activation of the ATM pathway, a response previously seen after AFB_1 treatment (Engin and Engin, 2019). A dose-dependent induction of γ-H2AX was seen in all organoids, while expression of p21, p-p53 and pCHK2 followed a similar pattern to *CYP3A4* mRNA expression, where the highest induction was seen at the lowest concentrations and then declined at the highest concentration tested in gastric D95, kidney and undifferentiated liver organoids. Gastric D88 had a concentration-dependent induction of p-p53 and a constant level of induction of pCHK2 and p21 at all concentrations. As mentioned previously, the decrease in the expression of these markers may be due to increased toxicity; however, the precise reason is unclear. Induction of these markers at mRNA and protein levels has been reported, however, a

lack of CHK2 and p53 activation after AFB_1 treatment has also been seen, which correlates with the failure of the differentiated liver organoids to activate p53 and CHK2 (Gursoy-Yuzugullu et al., 2011; Kucab et al., 2019; Smit et al., 2017; Yang et al., 2013; Yin et al., 2016).

The analysis of DNA adduct formation confirmed the metabolic activation of AFB_1 in the organoids as low levels of AFB_1-N^7-Gua, and AFB_1-FapyGua adducts were detected in all cultures (Figure 4.6). It has been shown that the half-life of the initial adduct AFB_1-N^7-Gua is around 7.5 hr, which is gradually converted into the persistent AFB_1-FapyGua adduct, with approximately 20% of the original adduct converted after 24 hr and 70% removed from the DNA (Croy and Wogan, 1981), and approximately 10% of the peak level of AFB_1-N^7-Gua adducts remaining after 48 hr (Woo et al., 2011). The decrease in AFB_1-N^7-Gua adducts may also be due to enzymatic removal by repair enzymes (Woo et al., 2011). This was also seen in the livers of new-born wild-type mice injected with AFB_1, where there was a significant decrease in AFB_1-N^7-Gua adducts between 6 and 48 hr and higher levels of AFB_1-FapyGua at 48 hr compared to AFB_1-N^7-Gua were detected (McCullough and Lloyd, 2019). Therefore, due to the 48-hr treatment used here, at the moment of analysis only a small amount of AFB_1-N^7-Gua remains. The levels of AFB_1-FapyGua adducts detected in the organoids were highest in the liver organoids, intermediate in the kidney and lowest in the gastric (Figure 4.6). This finding is in line with a study in male Fischer rats in which the levels of AFB_1-N^7-Gua adducts in liver were much higher than those in kidney and other tissues including colon (Cupid et al., 2004). Similarly, the prevalence of AFB_1-FapyGua adducts in the liver has been shown in human subjects. Adducts were also found in human colon, rectum, pancreas, breast and cervix samples but at lower levels (Harrison et al., 1993).

The distribution of the adduct formation between the organoid types correlated with the induction of the XMEs. The gastric organoids had the lowest responses, followed by the kidney, which although high levels of XMEs induction were seen, had basal levels of these enzymes lower than those of the liver organoids, which had the highest responses.

This association was also seen between gastric cultures, as D95 had lower levels of XMEs expression and adducts than D88. However, this was not the case for kidney and liver organoid cultures, as kidney cultures had similar levels of adduct formation, but different levels of XME induction, with D50 having higher levels than D21; similarly, differentiated liver organoids formed fewer adducts than undifferentiated liver cultures, but had higher levels of induction of XMEs, particularly *CYP3A4*.

In conclusion, this study showed that gastric, liver and kidney organoids have the metabolic competence to bioactivate AFB_1. The results shown here also support the hypothesis that there are differences between the target (liver) and the non-target (kidney and gastric) organs, not only in DNA adduct levels, but also in XMEs and DDR protein expression. Moreover, the high level of adducts formed in the liver organoids relative to the other organoid types, agrees with the susceptibility of this organ to AFB_1-induced carcinogenesis. However, these results reflect only early events in the carcinogenesis process and cannot reflect the long-term changes associated with neoplastic transformation. Although further investigations will be required to understand the organotropism of this compound, this study indicated that human tissue organoids are an interesting model to study mechanisms of AFB_1 carcinogenicity.

Chapter 5 Metabolic activation and cellular responses to aristolochic acid

5.1 Introduction

The potent human carcinogen AAI is a component of the plant extract from the *Aristolochia* species, which have been used in traditional herbal medicines for centuries (IARC, 2012b). AAI has been directly linked to chronic renal diseases, such as aristolochic acid nephropathy (AAN) and Balkan endemic nephropathy (BEN), which are associated with cancers of the upper urinary tract (Hoang et al., 2016; Turesky et al., 2016). Although most medicinal products containing AAI have been banned in many countries, exposure to this compound is still common in some areas of the world (Han et al., 2019) because it has continued to be used in herbal remedies for a range of conditions (Yang et al., 2014). Furthermore, in BEN areas contamination of flour with seeds of *Aristolochia* plants during wheat harvesting may also still continue (Jelaković et al., 2019; Stefanović and Polenaković, 2009).

AAI requires metabolic activation to its reactive intermediate *N*-hydroxyaristolactam I to be able to react with DNA and form DNA adducts (Arlt et al., 2002). AAI-DNA adducts are considered biomarkers for AAI exposure, as several studies have shown their presence in various tissues of patients with AAN and BEN (Arlt et al., 2004, 2007; Grollman et al., 2007; Stiborová et al., 2017). However, tumours are not formed in every tissue, in humans and rodents: the kidney is one of the main targets of AAI carcinogenicity, particularly renal proximal tubule cells (Arlt et al., 2002; Gökmen et al., 2013; Shibutani et al., 2007). Tissue-specific responses such as increased mutation frequencies and characteristic mutations in specific genes like *TP53* (in humans) and H-*ras* (in rodents) have been identified in target tissues (Arlt et al., 2002, 2007; Stiborová et al., 2016; Wang et al., 2012). Other studies *in vivo* and *in vitro* have shown that AAI also alters gene expression profiles, which differ between target and non-target tissues (Arlt et al., 2011a; Chen et al., 2006; Sborchia et al., 2019a; Simões et al., 2008, 2018).

As with other compounds, different responses are seen in different models, and not all are relevant to humans. A recent study using a liver-kidney organ-on-chip model investigated the mechanisms of toxicity of AAI, demonstrating that prior bioactivation in the liver leads to greater toxicity in the kidney (Chang et al., 2017). This study highlighted the importance and the need to carry out studies in models that are more relevant to human physiology. Therefore, here organoids from kidney (target) and gastric (non-target) human tissues were treated with different concentrations of AAI to assess its toxicity. The aim of the experiments described in this chapter was first to evaluate the potential of human tissue organoids to metabolically activate AAI, and ultimately to investigate the tissue-specific responses triggered by this compound by analysing the gene expression of XMEs, the induction of DDR markers and DNA adduct formation.

5.2 Materials and methods

Organoids from gastric and kidney normal human tissues were cultured as described in Section 2.2; gastric organoids were grown in Bartfeld media (Section 2.2.1.1). Treatment with AAI was carried out as described in Section 2.2.5, controls were treated with vehicle only (0.1-1% water). Cell viability was measured using the CellTiter-Glo assay as indicated in Section 2.3. To assess the bioactivation of AAI, the induction of the XMEs *CYP1A1/2* and *NQO1* was investigated by RT-qPCR (Section 2.6) and the expression and induction of DDR markers p-p53, pCHK2, p21 and γ-H2AX was analysed by Western blotting (Section 2.4). To further investigate AAI-induced DNA damage, the formation of DNA adducts was assessed by UPLC-ESI/MS^3 (Section 2.5.4; these investigations were conducted partly by Drs Madjda Bellamri, Lihua Yaol, and Robert Turesky at the Masonic Cancer Center, Minneapolis, USA).

5.3 Results

5.3.1 Cell viability assessment of organoids after AAI treatment

The cell viability of gastric and kidney organoids was assessed after treatment with range of AAI concentrations (0-200 µM) for 48 hr. Gastric organoids had different responses to this compound; D95 was less susceptible and was treated with concentrations up to 100 µM, while D88 only had to be treated with concentrations up to 25 µM to reach a viability close to 0%. The IC_{50} values for D95 and D88 were 38.5 and 5.4 µM, respectively (Figure 5.1 A). Kidney organoids were less susceptible than gastric organoids and had to be treated with up to 200 µM AAI to induce toxicity. D21 was slightly more sensitive than D50 with an estimated IC_{50} of 234 and 259 µM, respectively (Figure 5.1 B).

Based on the cytotoxicity results, three concentrations were chosen for subsequent experiments. For gastric organoids, concentrations close to the IC_{50} and one above (20% viability) and one below (80% viability) were chosen. For D95 these were 12.5, 50 and 75 µM and for D88 1.56, 6.25 and 12.5 µM. As the kidney organoids had IC_{50} values close to 200 µM, this and two lower concentrations were selected (25 and 100 µM).

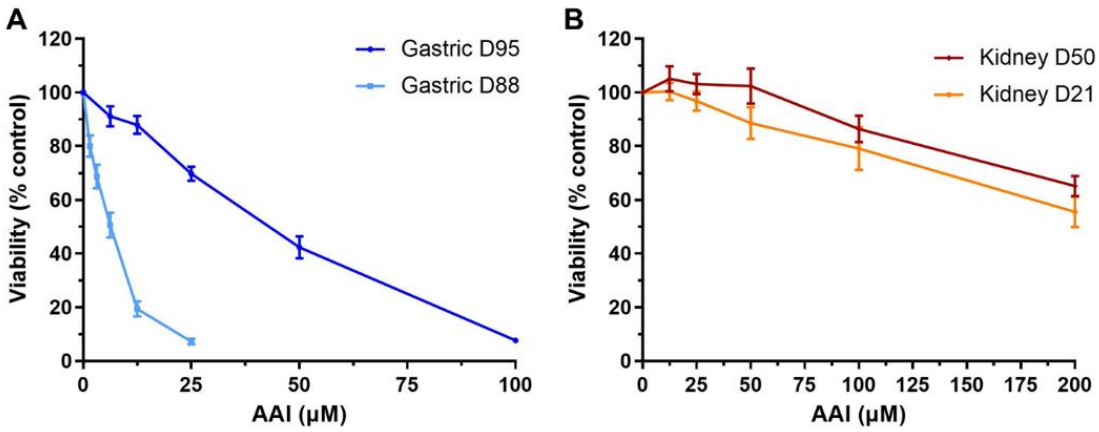

Figure 5.1. Cell viability in human tissue organoids after treatment with AAI. Organoids from normal human stomach (**A**; D95 and D88) and kidney (**B**; D50 and D21) tissues were treated with various concentrations (0-200 µM) of AAI for 48 hr. A water only control was included. Cell viability (% control) was measured using the CellTiter-Glo assay. Results are shown as mean ± SEM, n≥3.

5.3.2 Xenobiotic-metabolising enzyme expression after treatment with AAI

To investigate the metabolic activation of AAI in the organoids, the expression of the main XMEs involved in its metabolism was assessed. Gene expression levels of *CYP1A1, CYP1A2* and *NQO1* were measured by RT-qPCR. Overall, expression levels varied between organoids, but the three enzymes were induced after treatment in most cases. The expression of *CYP1A1* was significantly induced at concentrations close to the IC_{50} in both gastric D95 and D88 with fold increases of 168 and 404, respectively. D88 also had significant induction at the lowest concentration with 311-fold (Figure 5.2 A). Kidney organoid cultures had significant but different levels of expression at 200 µM, with D50 having a much higher induction with 575-fold, while D21 only had 95.8-fold (Figure 5.2 B).

Although the expression levels of *CYP1A2* were lower than those of *CYP1A1*, induction was seen in both gastric and kidney organoids. Gastric organoid culture D95 showed significant induction at 50 µM; however, D88 did not have significant induction at any concentration (Figure 5.2 C). Both kidney D50 and D21 had similar levels of induction of *CYP1A2* with fold increases of 33 and 37, respectively (Figure 5.2 D).

NQO1 expression was significantly induced at the highest concentrations used in all organoid cultures. Gastric D95 had slightly lower levels of induction than D88, with 2.38- and 4.88-fold, respectively (Figure 5.2 E). In the case of the kidney, D21 had higher expression levels with 9.97-fold when compared to D50 with 3.67-fold (Figure 5.2 F).

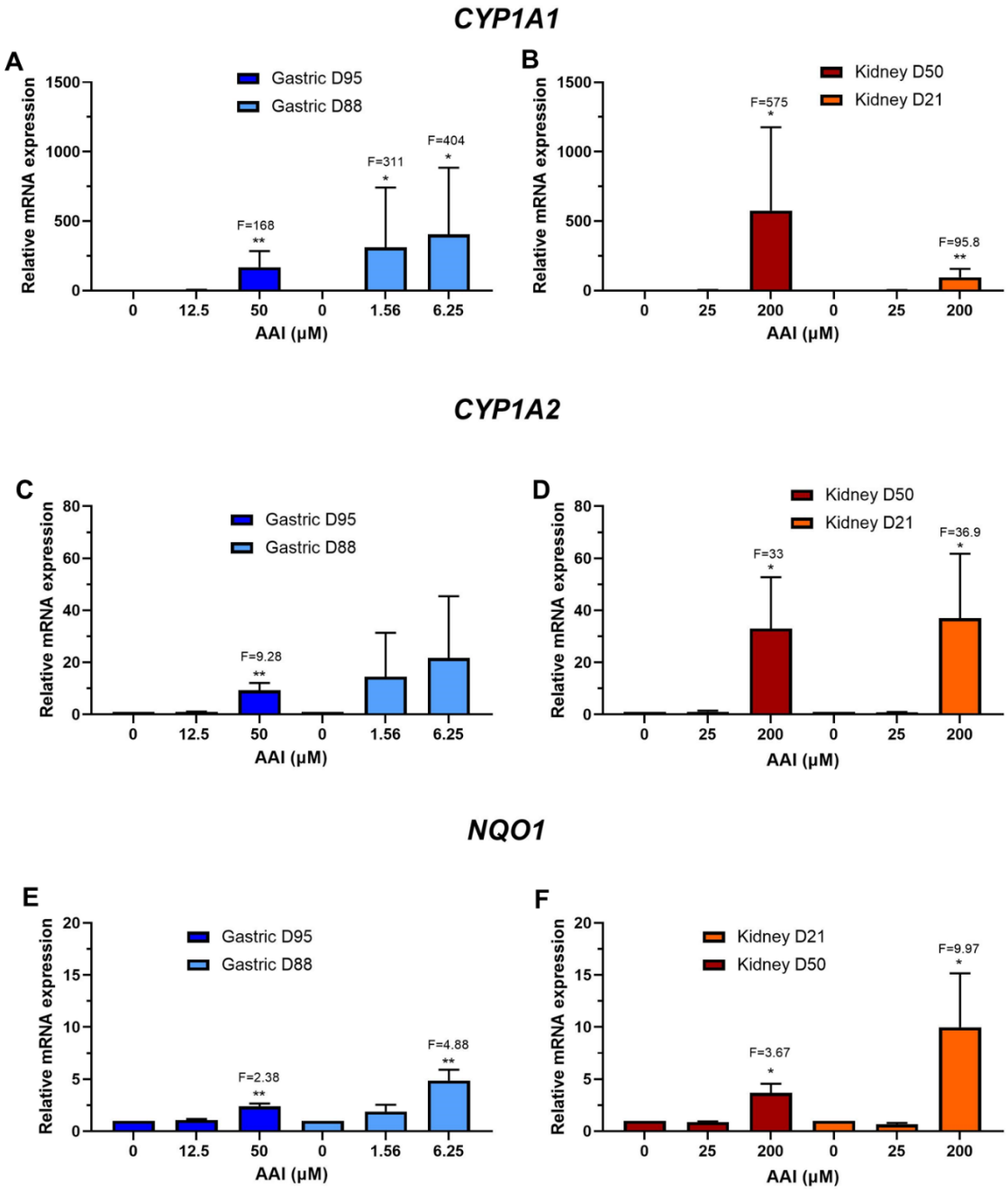

Figure 5.2. Relative gene expression of *CYP1A1, CYP1A2* and *NQO1* in normal human tissue organoids after AAI treatment. Organoids from stomach (D95 and D88) and kidney (D50 and D21) tissues were treated with the indicated concentrations of AAI for 48 hr. *CYP1A1* (**A and B**), *CYP1A2* (**C and D**) and *NQO1* (**E and F**) expression was analysed by RT-qPCR and the $2^{-\Delta\Delta CT}$ method. Values are shown as mean ± SD (n=3). Values were normalised to mRNA expression of the housekeeping gene *GAPDH* and are relative to the water control. Statistical analysis was performed by log2 transforming the data and a one sample *t*-test with Bonferroni correction against the control mean of 0 (*p<0.05; **p<0.01).

5.3.3 Induction of DDR proteins after AAI treatment

Induction of DDR proteins (p-p53, pCHK2, p21 and γ-H2AX) was assessed by Western blotting after treatment with AAI for 48 hr. Overall, there was an induction of all the DDR proteins in both gastric and kidney organoids. Although gastric D88 had slightly higher protein expression than D95, they both showed a dose-dependent response. Both gastric organoid cultures displayed a p-p53 induction at the two highest AAI concentrations. Expression of pCHK2 and γ-H2AX increased at 50 and 75 µM in D95, while D88 had induction at all AAI concentrations. p21 was induced at the highest AAI concentrations in both gastric cultures, but the levels were higher in D88 (Figure 5.3 A). Lastly, kidney organoids (D50 and D21) only had clear induction of p-p53 and pCHK2 at 200 µM, although some expression can be seen at 100 µM. Expression of p21 was seen throughout, however, induction was only seen at 100 and 200 µM, with the highest seen at 100 µM. γ-H2AX was also expressed in all conditions, and it was induced at 100 and 200 µM in a concentration-dependent manner (Figure 5.3 B).

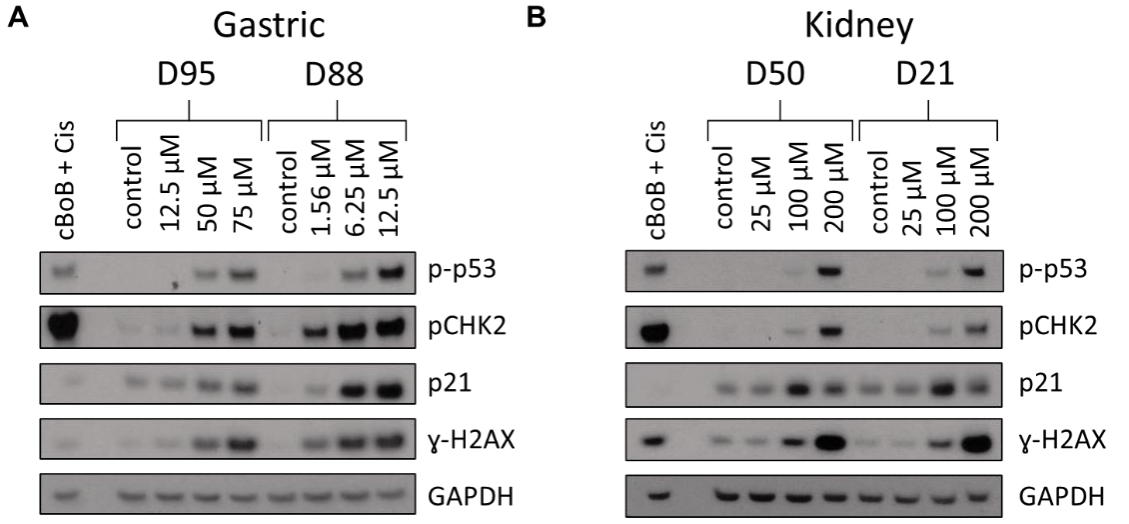

Figure 5.3. Expression of DDR proteins in normal human organoids after AAI treatment. Organoids from gastric (D95 and D88; **A**) and kidney (D50 and D21; **B**) tissues were exposed to the indicated concentrations of AAI for 48 hr. DDR proteins (p-p53, pCHK2, p21 and γ-H2AX) were detected and GAPDH was used as a loading control. Organoids from the same tissue were loaded on the same gel to allow for comparison. cBoB + Cis (cBoB treated with 3.125 µM cisplatin) was used as a positive control. Representative blots are shown (n=2).

5.3.4 DNA adduct formation after AAI treatment

To evaluate genotoxicity after treatment with AAI, formation of dA-AL-I adducts was analysed by UPLC-ESI/MS^3. Representative chromatograms and ion spectra are shown in Figure 5.4. The internal standard, [$^{15}N_5$]-dA-AL-I, produced a peak at 13.3 min (Figure 5.4 D and E). The controls showed no presence of dA-AL-I adducts (Figure 5.4 A), while in the AAI-treated organoids the adducts were detected at a retention time of 13.3 min (Figure 5.4 B). Figure 5.4 shows examples of the MS spectra of dA-AL-I (C) and [$^{15}N_5$]-dA-AL-I (F) obtained at *m/z* 412.1, 395.1 and 292 and *m/z* 417.1, 400.1 and 292.1, respectively.

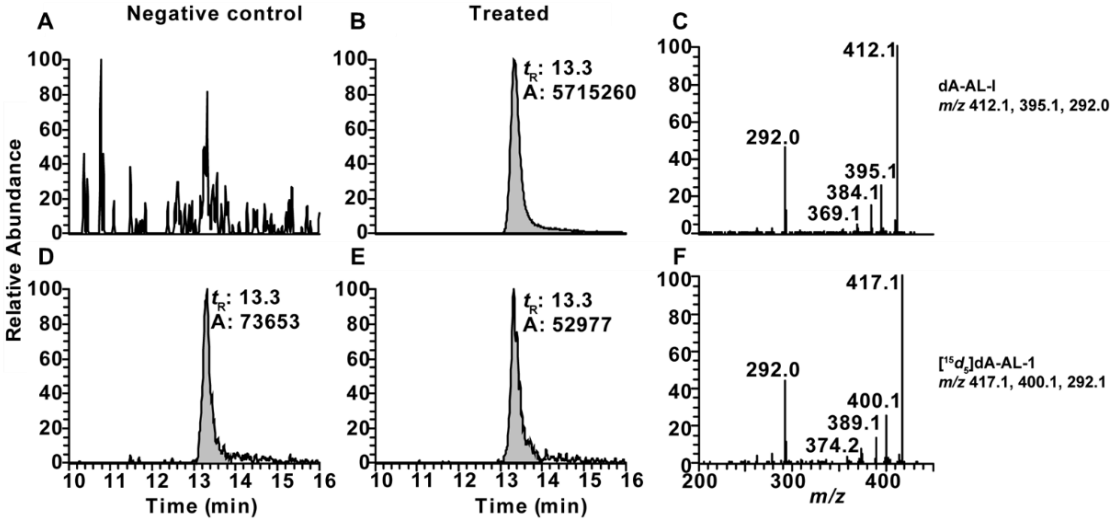

Figure 5.4. Representative chromatograms and product ion spectra from the UPLC-ESI/MS^3 analysis. Chromatograms of the untreated control (**A**) and the dA-AL-I in the AAI-treated organoids (**B**), and of the internal standard, [$^{15}N_5$]-dA-AL-I, in the control (**D**) and treated samples (**E**). MS^3 ion spectra of dA-AL-I (**C**) and [$^{15}N_5$]-dA-AL-I (**F**). t_R: Retention time; A: Area under the peak.

Treatment with AAI led to the formation of dA-AL-I adduct in a concentration-dependent manner. Adducts were detected in all organoids tested (Figure 5.5). Overall, gastric organoids had lower levels of adducts than kidney organoids at the concentrations close to the IC_{50} values, with the kidney having 1.5- to 3-fold higher DNA adduct levels. Higher level of adducts were found in gastric D88 compared to gastric D95 which correlated with higher cytotoxicity and higher levels of XMEs seen in D88. At the lowest concentrations tested D88 had 192.7 adducts per 10^7 nucleosides compared to 55.7 adducts per 10^7

nucleosides in D95. At the IC_{50} values D95 and D88 had 412 and 843 adducts per 10^7 nucleosides, respectively (Figure 5.5 A). Although kidney D21 had slightly higher levels of adducts than D50, which correlated with higher levels of *NQO1* and *CYP1A2* in this donor culture, both kidney cultures had similar levels of adducts. At 25 µM they had around 20 adducts per 10^7 nucleosides and at 200 µM around 1200 adducts per 10^7 nucleosides (Figure 5.5 B).

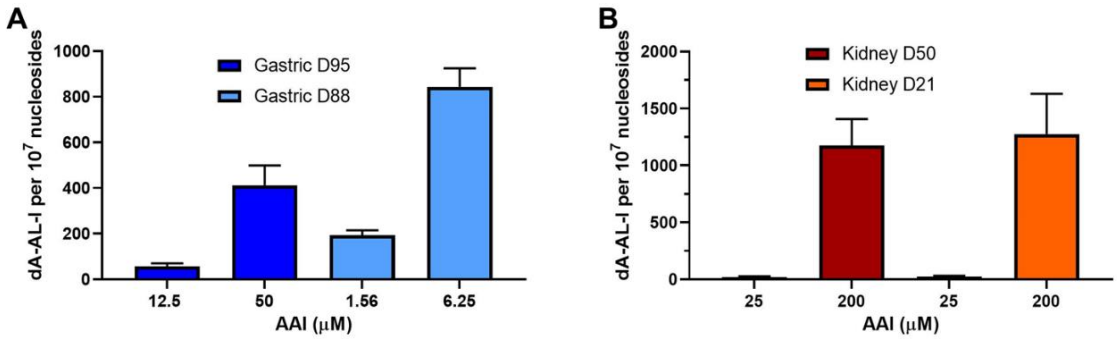

Figure 5.5. DNA adduct formation in human tissue organoids after treatment with AAI. Gastric (**A**; D95 and D88) and kidney (**B**; D50 and D21) organoids were treated with the indicated concentrations of AAI for 48 hr. dA-AL-I adduct formation was quantified using UPLC-ESI/MS^3. No dA-AL-I adducts were detected in the untreated controls. Results are shown as mean ± SD, n=3.

5.4 Discussion

The aim of the studies described in this chapter was to assess the metabolic potential of human tissue organoids to bioactivate AAI and to investigate tissue-specific responses in target (kidney) and non-target (stomach) tissues for AAI carcinogenicity in humans. It has been shown that target and non-target tissues have different responses to AAI treatment, including gene expression profiles and mutation frequencies (Arlt et al., 2002, 2011a; Chen et al., 2006), therefore it was hypothesised that the responses of kidney organoids would differ from those of the gastric organoids.

Firstly, the cytotoxicity assessment of AAI in kidney and gastric organoids showed very different responses between donor cultures and organoid types. The biggest differences between donor cultures were seen in the gastric organoids where D95 was much less susceptible than D88 with an IC_{50} dose around 6-fold higher. Gastric organoids were more susceptible to cytotoxic damage than kidney organoids, as the kidney organoids

required the highest possible dose (200 µM) to approach the IC_{50} (Figure 5.1). Chang et al. (2017) used a liver-kidney organ-on-chip to compare nephrotoxic responses with and without prior hepatic metabolism, showing that AAI-induced cell death in the kidney was significantly increased by prior hepatic metabolism. This could explain the low cytotoxic response seen in the kidney organoids.

The metabolic ability of the organoids was evaluated by assessing the expression of the XMEs involved in the activation and/or detoxication of AAI. Induction of protein and gene expression as well as activity of these enzymes after AAI treatment has been reported several times in various models (Arlt et al., 2011a, 2017; Bárta et al., 2014; Krais et al., 2015; Nitzsche et al., 2013; Simões et al., 2008, 2018). In line with this, these results show that *NQO1*, *CYP1A1* and *CYP1A2* are expressed at different levels in kidney and gastric organoids and were induced in a concentration-dependent manner after AAI treatment. Gastric D88 organoids had higher induction levels of all enzymes at the IC_{50} concentration than D95 at the equivalent dose, which correlated with the higher susceptibility of this culture to AAI cytotoxicity (Figure 5.2 A, C and E). Similarly, the more susceptible kidney culture, D21, had higher induction of *NQO1* and *CYP1A2* than D50 at 200 µM, however, *CYP1A1* expression was much higher in D50 than in D21 (Figure 5.2 B, D and F). Therefore, this study demonstrated that kidney and gastric organoids from human tissues contain the XMEs required for AAI metabolism.

DDR proteins were found to be induced after treatment with AAI in both gastric and kidney organoids. Following the same pattern observed for the XMEs, the levels of induction in D88 were higher than in D95 when treated with equivalent doses. Both kidney organoid cultures had similar levels of induction of all proteins (Figure 5.3). AAI treatment induced pCHK2, particularly at the highest concentrations, as was previously reported in human HK-2 kidney proximal tubular cells by Romanov et al. (2015). An induction of γ-H2AX was also seen after treatment. Furthermore, gastric organoids showed a concentration-dependent induction of both p-p53 and p21 after AAI treatment, while kidney organoids showed dose-dependent induction of p-p53 but only an induction

of p21 at 100 µM. These data agree with previous publications that reported induction of p-p53 and p21, proteins involved in the maintenance of the G1/S checkpoint, after AAI treatment in a variety of experimental models (Krais et al., 2015; Nitzsche et al., 2013; Simões et al., 2008, 2018; Zhou et al., 2010).

Activation of the p53 pathway has been described as key for AAI carcinogenicity and kidney injury in some studies (Simões et al., 2008, 2018; Zhou et al., 2010). However, a protective role for p53 against AAI-induced nephrotoxicity has been suggested by Sborchia et al. (2019b) who reported that wild-type *Trp53* mouse kidneys had reduced proximal tubule injury following AAI treatment compared with *Trp53*(-/-) mice. Although induction of p-p53 and p21 were not observed *in vivo* in that study, expression of both proteins was shown in *Trp53*(+/+) mouse embryonic fibroblasts treated with AAI (Sborchia et al., 2019b).

The bioactivation of AAI in kidney and gastric organoids was further corroborated by the formation of dA-AL-I adducts (Figure 5.5). Overall, the DNA adduct levels correlated with the levels of expression of the DDR markers and XMEs. Gastric D88 had higher levels of DNA adducts and XMEs expression than D95 by approximately 2-fold at the IC_{50} concentrations. Kidney organoids had similar levels of DNA adducts at both concentrations tested; however, as D21 had slightly more adducts than D50, there was only a linear relationship between *CYP1A2* expression and the adducts levels. Although the induction of *NQO1*, the main AAI activator, was higher in D21, the levels of *CYP1A1* in D50 were at least 6-fold higher than in D21. The high expression of *CYP1A1* may account for the similar levels of adducts in both D21 and D50 to some extent as this gene is also involved in the detoxication of AAI (Arlt et al., 2011b; Dračínská et al., 2016).

The results seen here also relate to what has been seen in target and non-target organs of AAI carcinogenicity, where both present adducts, and in some cases target organs have higher levels than non-targets (Arlt et al., 2004, 2011a). Here, adducts were found in both the kidney (target) and the stomach (non-target). High levels of dA-AL-I adduct formation in kidney tissues of humans and animals have been reported numerous times

(Arlt et al., 2007, 2011a; Dračínská et al., 2016; Shibutani et al., 2007). Adduct formation has also been seen in the glandular stomach and forestomach of rodents (Arlt et al., 2011a; Shibutani et al., 2007), however these are lower than in the kidney and there is little evidence of AA-DNA adduct formation in human stomach (Arlt et al., 2004). This correlates with the higher levels of adducts seen in the kidney organoids than in the gastric organoids.

As previously mentioned, adduct formation is only one of the initiation events for tumour formation, therefore the events that follow are key in carcinogenesis (Stiborová et al., 2017). Studies in Muta^{TM}Mouse of the mutagenic activity of AA showed that target organs, such as kidney and bladder, had increased mutation frequencies compared to non-targets like liver and glandular stomach after intragrastric treatment with AA (Arlt et al., 2002). Additionally, studies of gene expression in target and non-target tissues have found tissue-specific responses like alterations in genes related to apoptosis, cell cycle, stress response, immune system and inflammatory response in the kidney (Arlt et al., 2011a; Chen et al., 2006). Sborchia et al. (2019a) also demonstrated AAI treatment leads to gene expression alterations in mouse kidneys, affecting the pathways mentioned previously and other processes such as tissue damage, cell adhesion and development, metabolism, and cancer-related processes. Although it was not possible to carry out an assessment of a large panel of genes in the present study, the results with regards to XMEs indicate that there are differences in gene expression between the kidney and the stomach after AAI treatment.

In summary, the present study found that kidney and gastric organoids are capable of metabolising AAI as they express the required XMEs: *NQO1*, *CYP1A1* and *CYP1A2*. AAI also activated DDR pathways in both organoid types and induced DNA adduct formation. Kidney organoids, the target tissue, had higher levels of enzyme expression and DNA adducts compared to the non-target tissue, the stomach. In addition, culture-specific differences were also seen. In conclusion, the results support the hypothesis and indicate that human tissue organoids are an interesting model for AAI

toxicity and the study of its organotropism. However, additional work is required to fully understand the utility of this model.

Chapter 6 Metabolic activation and cellular responses to *N*-hydroxy-2-amino-1-methyl-6-phenylimidazo[4,5-*b*]pyridine

6.1 Introduction

The possible human carcinogen PhIP is formed during the cooking of meat (beef, chicken, fish and pork) at high temperatures, and is also found in cigarette smoke (IARC, 1993; Lauber and Gooderham, 2007). PhIP is the most abundant mutagen in meat, and exposure to this compound can be frequent, depending on lifestyle and diet (Lauber and Gooderham, 2007). As a procarcinogen PhIP requires metabolic activation to *N*-OH-PhIP, which can itself react with DNA or be further activated by phase II enzymes to reactive intermediates that can form bulky DNA adducts (Turesky, 2002).

The mutagenic and carcinogenic potential of PhIP has been shown in rats and mice, where it was found to cause tumours in colon, prostate and breast tissues (Andreassen et al., 2001; Ito et al., 1991; Shirai et al., 1997; Wang et al., 2016). Various epidemiological studies have shown a link between meat consumption and an increased risk of these cancers in humans (Malfatti et al., 2006; Wu et al., 2006; Xiao et al., 2016). Additionally, PhIP-DNA adducts have been detected in a number of human tissues including the colon, breast, prostate and pancreas (Gorlewska-Roberts et al., 2002; Malfatti et al., 2006; Tang et al., 2007; Xiao et al., 2016; Zhu et al., 2006). Short-term mutational studies in the Muta^{TM}Mouse model have also shown an increase in mutation frequency after oral gavage treatment with PhIP in the large and small intestines and the liver (Lynch et al., 1996).

Different studies have shown that DNA adduct formation alone is not sufficient for tumour formation. Treatment of Syrian hamsters with PhIP led to adduct formation in several tissues but not tumours (Fretland et al., 2001a, 2001b). Similarly, analyses of DNA adduct formation in human samples have shown the presence of adducts not only in tumours but also in normal tissues, and in some cases at similar levels (Tang et al., 2007; Xiao et al., 2016; Zhu et al., 2006). The study of tissue-specific responses to PhIP has

shown that hormones may be key to identify tumour targets (Lauber et al., 2004). Furthermore, PhIP-induced gene expression changes in genes involved in different processes like transcription regulation, inflammation, proliferation and cancer have been identified (Rogers et al., 2016; Shan et al., 2004).

The experiments described in this chapter aimed to investigate the potential of human tissue organoids to metabolise PhIP, as well as the tissue-specific responses of PhIP in colon (target) and gastric (non-target) human tissue organoids. This was done by evaluating cytotoxicity, DDR responses and DNA adduct formation after PhIP treatment. Additionally, the effects on these end points after treatment with the reactive intermediate *N*-OH-PhIP were studied in gastric and kidney organoids. Unfortunately, due to time constrains and organoid availability at the time these experiments were performed, PhIP could not be tested in the kidney and *N*-OH-PhIP could not be tested in the colon.

6.2 Materials and methods

Normal human organoids from stomach, colon and kidney tissues were cultured as explained in Section 2.2; gastric organoids were grown in Bartfeld media (Section 2.2.1.1). Treatments with PhIP and *N*-OH-PhIP were carried out as stated in Section 2.2.5, controls were treated with vehicle only, 1% and 0.1% DMSO, respectively. The CellTiter-Glo assay was used to determine the cell viability after treatment with the compounds for 48 hr (Section 2.3), and Western blotting analysis was carried out to investigate the induction and expression of DDR markers, p-p53, pCHK2, p21 and γ-H2AX (Section 2.4). Finally, DNA adduct formation was assessed using UPLC-ESI/MS^3 (Section 2.5.4; these investigations were partly conducted by Drs Madjda Bellamri, Lihua Yaol, and Robert Turesky at the Masonic Cancer Center, Minneapolis, USA).

6.3 Results

6.3.1 Cell viability assessment of organoids after PhIP treatment

Cell viability after treatment with a range of PhIP concentrations (0-250 µM) for 48 hr was assessed using the CellTiter-Glo assay. Gastric organoids showed very little toxicity after

treatment with 250 µM, having only ~20% decrease in viability, hence, both gastric cultures had IC_{50} values higher than 250 µM (Figure 6.1 A). Colon organoids were more susceptible to cytotoxicity, D350 and D311 had IC_{50} values of 250 and 222 µM, respectively (Figure 6.1 B).

Based on the cytotoxicity results two concentrations were selected for subsequent experiments. As the IC_{50} for all organoid cultures was close to or higher than 250 µM, this concentration and a lower one, 187.5 µM, were chosen.

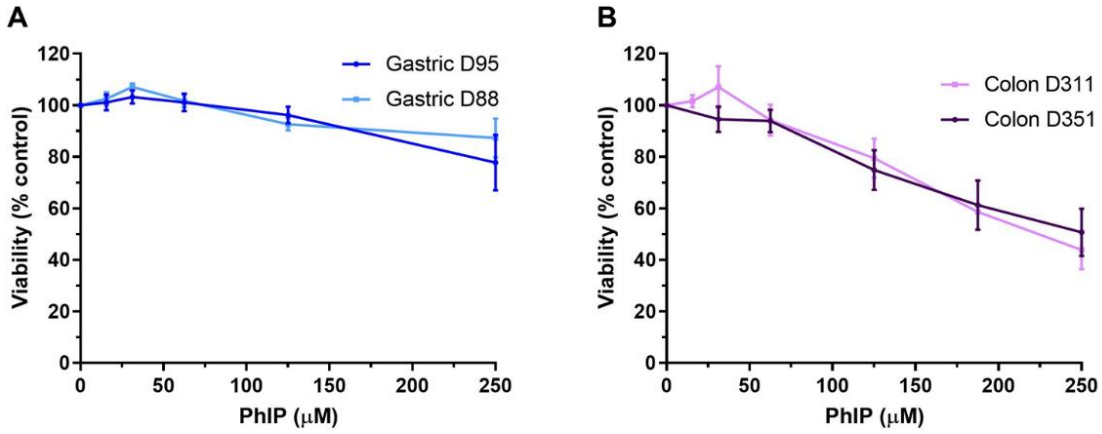

Figure 6.1. Cell viability in human tissue organoids after treatment with PhIP. Organoids from normal human stomach (**A**; D95 and D88) and colon (**B**; D311 and D351) tissues were treated with various concentrations (0-250 µM) of PhIP for 48 hr. A DMSO control was included. Cell viability (% control) was measured using the CellTiter-Glo assay. Results are shown as mean ± SEM, n≥3.

6.3.2 Induction of DDR proteins after PhIP treatment

The expression and induction of DDR markers p-p53, pCHK2, p21 and γ-H2AX after PhIP treatment were investigated by Western blotting. Gastric organoids had similar patterns of expression, but some proteins appeared to be slightly more induced in D95 than in D88. There was no expression of p-p53 in either of the gastric cultures, and pCHK2 expression was very low, but it was induced slightly at 250 µM in D95. p21 expression seemed to be dose-dependent, with D95 having higher levels than D88 in all conditions. Similarly, γ-H2AX was induced in both donor cultures, but the induction was stronger in the D95 than in the D88 (Figure 6.2 A). Colon organoids had no expression of p-p53. Although both cultures expressed all the other proteins, not all of them were

induced. pCHK2 and γ-H2AX were only induced in D311, while in D351 pCHK2 remained constant and γ-H2AX seemed to decrease. p21 was expressed and induced slightly in both donors, but D351 had higher expression than D311 in all conditions (Figure 6.2 B).

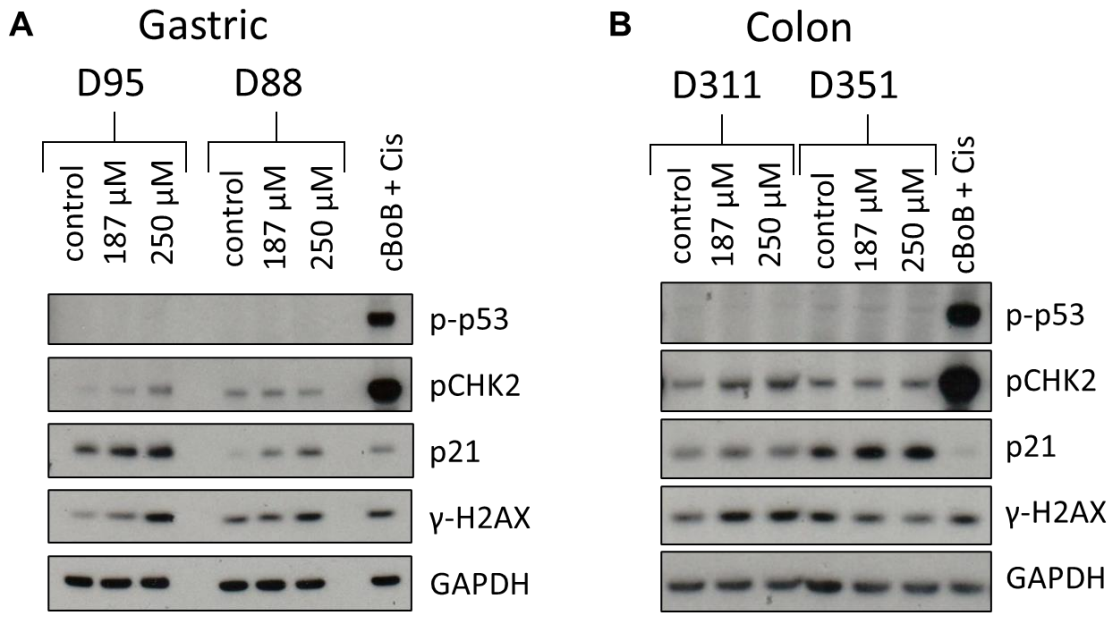

Figure 6.2. Expression of DDR proteins in normal human organoids after PhIP treatment. Organoids from gastric (D95 and D88; **A**) and colon (D311 and D351; **B**) tissues were exposed to the indicated concentrations of PhIP for 48 hr. DDR markers (p-p53, pCHK2, p21 and γ-H2AX) were detected and GAPDH was used as a loading control. Organoids from the same tissue were loaded on the same gel to allow for comparison. cBoB + Cis (cBoB treated with 3.125 µM cisplatin) was used as a positive control. Representative blots are shown (n=2).

6.3.3 Cell viability assessment of organoids after *N*-OH-PhIP treatment

As the gastric organoids had a limited response to PhIP, maybe due to the lack of bioactivation of the compound, they were treated with *N*-OH-PhIP, its reactive metabolite. Kidney organoids showed no cytotoxic response to PhIP in a test carried out by another member of the laboratory (results not shown), therefore, they were also treated with *N*-OH-PhIP to analyse their responses. All organoids were susceptible to toxicity after treatment with this compound, with the gastric D95 showing the highest toxicity with an IC_{50} of 3.26 µM. Gastric D88 was slightly less susceptible with an IC_{50} of 14.7 µM (Figure 6.3 A). Although kidney D50 were slightly more susceptible, kidney organoids had similar responses to *N*-OH-PhIP with IC_{50} values of 10.65 µM for D21 and 8.47 µM for D50 (Figure 6.3 B).

Based on the cytotoxicity results, three concentrations were selected for subsequent experiments, with one being close to the IC_{50} value.

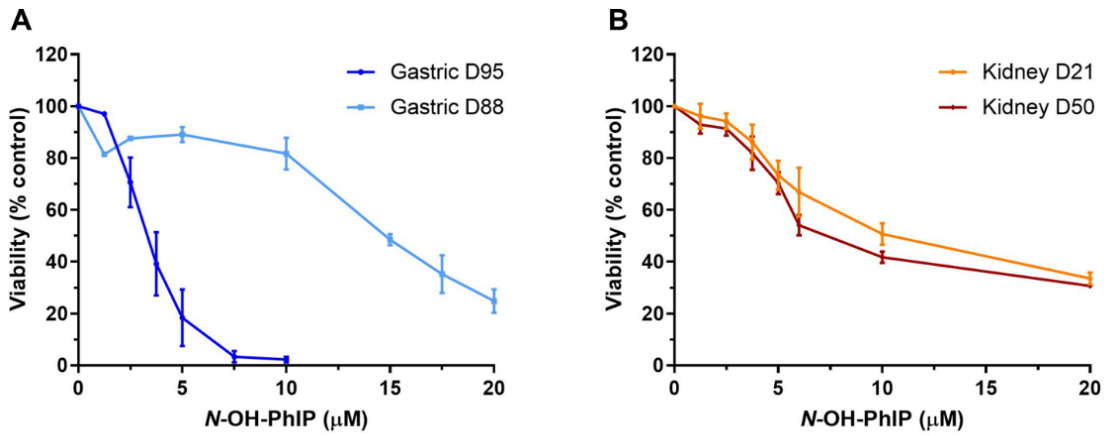

Figure 6.3. Cell viability in human tissue organoids after treatment with *N*-OH-PhIP. Organoids from normal human stomach (**A**; D95 and D88) and kidney (**B**; D50 and D21) tissues were treated with various concentrations (0-20 µM) of *N*-OH-PhIP for 48 hr. A DMSO control was included. Cell viability (% control) was measured using the CellTiter-Glo assay. Results are shown as mean ± SEM, n≥3.

6.3.4 Induction of DDR proteins after *N*-OH-PhIP treatment

The induction of DDR markers after treatment with selected concentrations of *N*-OH-PhIP was assessed by Western blotting. Gastric organoids had low expression of p-p53, which was induced in D95 at the highest *N*-OH-PhIP concentration tested. Both gastric cultures showed induction of pCHK2, p21 and γ-H2AX, however this remained constant with the exception of small increases of p21 and γ-H2AX at the highest *N*-OH-PhIP concentrations for D95 (Figure 6.4 A). All markers were induced in kidney organoids, and donor cultures displayed the same pattern of expression for all proteins. They had low p-p53 expression, but it was induced in a dose-dependent manner. The induction of γ-H2AX, followed the same pattern, and showed a much higher induction at 10 µM. The expression of pCHK2 and p21 increased at 5 and 6 µM and decreased at 10 µM (Figure 6.4 B).

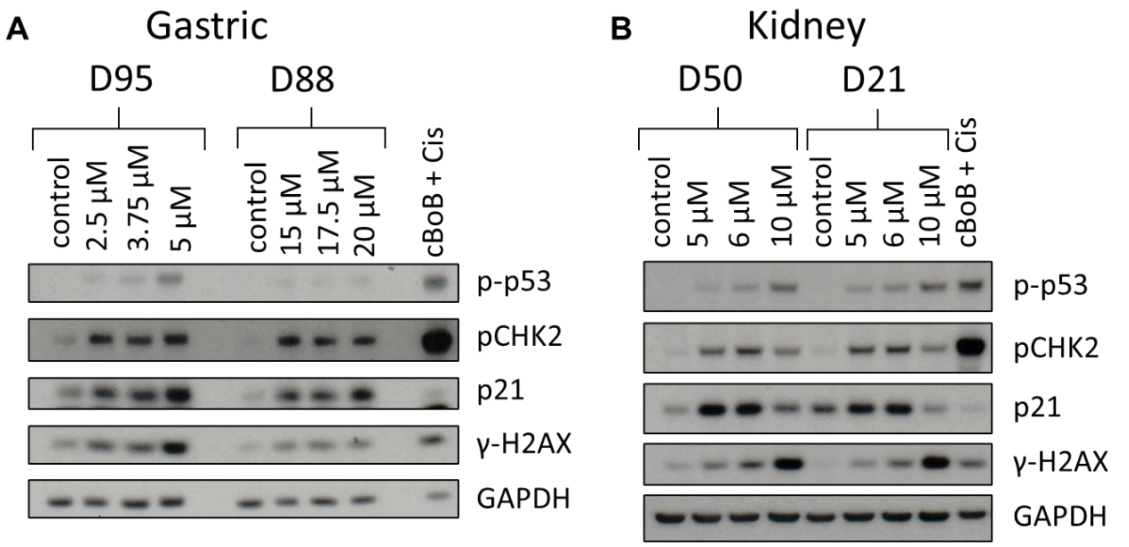

Figure 6.4. Expression of DDR proteins in normal human organoids after *N*-OH-PhIP treatment. Organoids from gastric (D95 and D88; **A**) and kidney (D50 and D21; **B**) tissues were exposed to the indicated concentrations of *N*-OH-PhIP for 48 hr. DDR markers (p-p53, pCHK2, p21 and γ-H2AX) were detected and GAPDH was used as a loading control. Organoids from the same tissue were loaded on the same gel to allow for comparison. cBoB + Cis (cBoB treated with 3.125 µM cisplatin) was used as a positive control. Representative blots are shown (n=2).

6.3.5 DNA adduct formation after PhIP and *N*-OH-PhIP treatment

To evaluate the DNA damage induced by PhIP and *N*-OH-PhIP treatment, the formation of the dG-C8-PhIP adduct was assessed by UPLC-ESI/MS^3. Representative chromatograms showed a peak at 11.3 min for the internal standard, [$^{13}C_{10}$]-dG-C8-PhIP, (Figure 6.5 D and E). dG-C8-PhIP was detected in treated organoids and showed a peak at a retention time of 11.3 min (Figure 6.5 B), while *N*-OH-PhIP controls showed no presence of adducts (Figure 6.5 A). Ions were monitored at *m/z* 250.2, 329.2 and 357.2 for dG-C8-PhIP and *m/z* 251.2, 333.2 and 362.2 for [$^{13}C_{10}$]-dG-C8-PhIP. Representative spectra are shown in Figure 6.5 C and F.

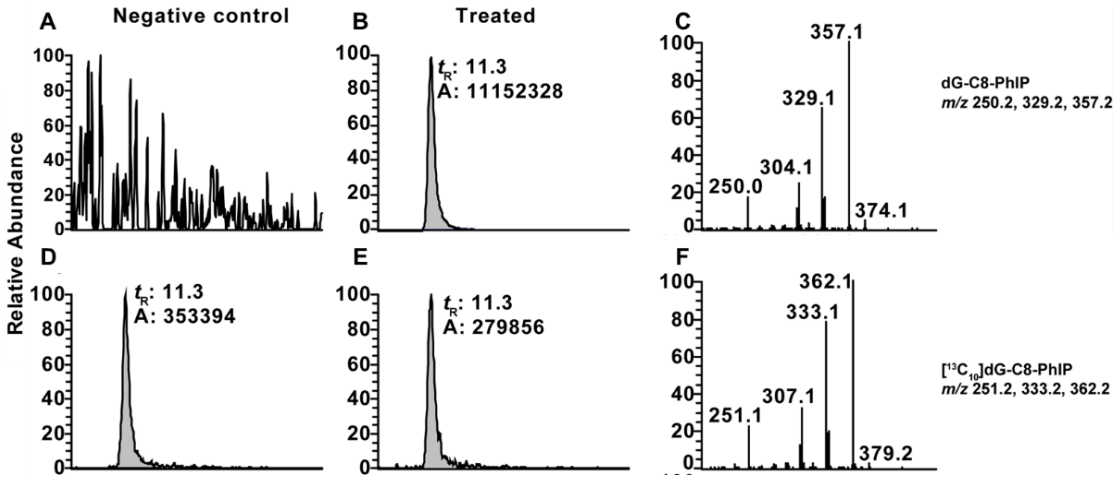

Figure 6.5. Representative chromatograms and product ion spectra from the UPLC-ESI/MS^3 analysis. Chromatograms of the untreated control (**A**) and the dG-C8-PhIP in the treated organoids (**B**), and of the internal standard, [$^{13}C_{10}$]-dG-C8-PhIP, in the control (**D**) and treated samples (**E**). MS^3 ion spectra of dG-C8-PhIP (**C**) and [$^{13}C_{10}$]-dG-C8-PhIP (**F**). t_R: Retention time; A: Area under the peak.

As the induction of DDR markers was low after PhIP treatment, DNA adduct formation was only assessed at 250 µM. Although dG-C8-PhIP adducts were detected in all organoids, colon organoids had 2-4-fold higher levels than gastric organoids. Gastric D95 had higher levels than gastric D88 with 1.2 and 0.57 adducts per 10^7 nucleosides, respectively (Figure 6.6 A). Colon D351 showed slightly higher levels of adducts than D311, with 2.7 and 2.2 adducts per 10^7 nucleosides, respectively (Figure 6.6 B).

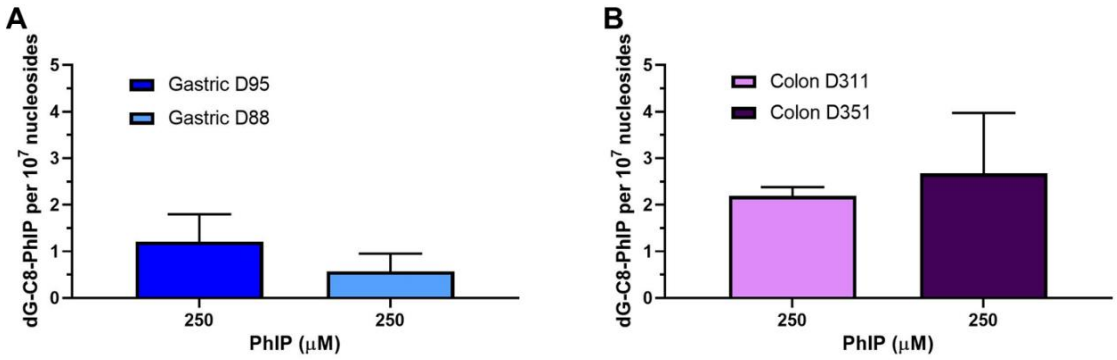

Figure 6.6. DNA adduct formation in human organoids after treatment with PhIP. Gastric (D95 and D88; **A**) and colon (D311 and D351; **B**) organoids were treated with 250 µM PhIP for 48 hr. dG-C8-PhIP adduct formation was quantified using UPLC-ESI/MS^3. Background dG-C8-PhIP adducts detected in the DMSO controls (<0.3 per 10^7 nucleosides) were subtracted from dG-C8-PhIP levels in the treated samples. Results are shown as mean ± SD, n=3.

Treatment with *N*-OH-PhIP led to DNA adduct formation in a dose-dependent manner. Compared to the adduct levels induced by PhIP treatment, gastric organoids had much higher levels of adduct formation after *N*-OH-PhIP treatment, however, the toxicity at the concentrations tested was also higher. Gastric D95 treatment with 2.5 and 3.75 µM resulted in 21.3 and 48.2 adducts per 10^7 nucleosides, respectively. The levels of adducts in D88 were slightly higher with 42.6 adducts per 10^7 nucleosides at 17.5 µM and 56.8 adducts per 10^7 nucleosides after treatment with 20 µM (Figure 6.7 A). The highest levels of dG-C8-PhIP adducts were detected in kidney D21 with 814.3 adducts per 10^7 nucleosides at 10 µM and 73.6 adducts per 10^7 nucleosides at 5 µM. Treatment of D50 with the same *N*-OH-PhIP concentrations 5 and 10 µM resulted in 107.6 and 589.3 adducts per 10^7 nucleosides, respectively (Figure 6.7 B).

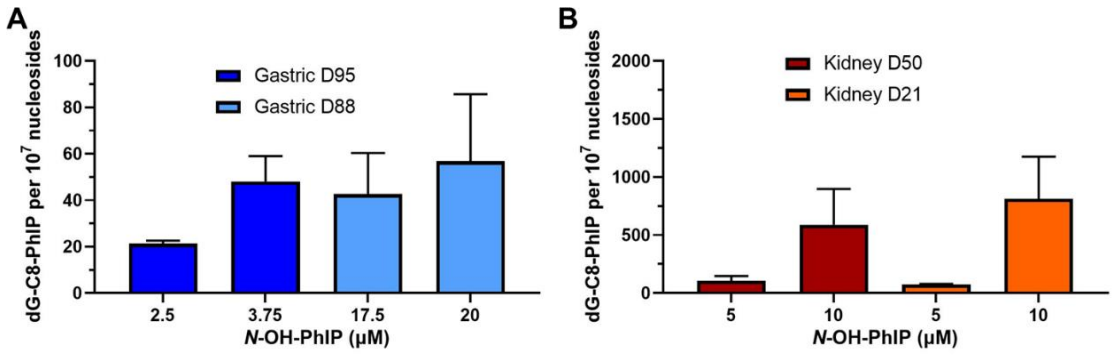

Figure 6.7. DNA adduct formation in human organoids after treatment with *N*-OH-PhIP. Gastric (D95 and D88; **A**) and kidney (D50 and D21; **B**) organoids were treated with the indicated concentrations of *N*-OH-PhIP for 48 hr. dG-C8-PhIP adduct formation was quantified using UPLC-ESI/MS3. No dG-C8-PhIP adducts were detected in the DMSO controls. Results are shown as mean ± SD, n=3.

6.4 Discussion

The main objective of this chapter was to evaluate the effects of PhIP on human tissue organoids to investigate their ability to metabolise the compound and to study tissue-specific responses by comparing colon (target) and gastric (non-target) organoids. It was hypothesised that DNA adducts would form in both tissue organoid types, but differences in adduct levels and DDR responses would be seen between target and non-target organoids. A higher level of DNA adducts was also expected in organoids treated with the reactive metabolite *N*-OH-PhIP.

The treatment of colon organoids with PhIP led to a decrease in cell viability of approximately 50% at the highest concentration tested (250 µM). In contrast, gastric organoids had only a small decrease in cell viability (~20%) at the same concentration (Figure 6.1). These results correlate with previous studies in human and mouse cell lines from different tissue origins (colon, liver, breast and lung) that have shown low cytotoxic responses to PhIP in both 2D and 3D cultures (HepG2 spheroids) (Alotaibi et al., 2021; Gooderham et al., 2007; Hölzl-Armstrong et al., 2020; Jamin et al., 2013; Štampar et al., 2019). In a number of studies, co-culture with other metabolically active cells or the addition of S9 mix was required to see an effect (Gooderham et al., 2007; Hölzl-Armstrong et al., 2020; Kucab et al., 2019).

The low cytotoxic responses seen in the organoids match the low induction of DDR proteins. As with the cytotoxicity, gastric culture D95 had stronger responses than D88 and more proteins were induced in colon D311 than in D351 cultures (Figure 6.2). Although Yang et al. (2021) showed that p53 is activated after PhIP treatment in mice, and the importance of the p53 genotype in PhIP bioactivation using *Trp53(+/+)*, *Trp53(+/-)* and *Trp53(-/-)* mice has been reported (Krais et al., 2016b), no induction of p-p53 was seen in the organoids used here. This correlates with findings by Hölzl-Armstrong et al. (2020), where murine FE1 lung epithelial cells treated with PhIP and without the addition of S9 mix had no induction of DDR markers. In the present study, small inductions of p21, pCHK2 and γ-H2AX were seen in some gastric and colon organoid cultures; in line with other published results showing induction of p21 and γ-H2AX following PhIP treatment of human and hamster cells (Gooderham et al., 2007; Mimmler et al., 2016).

The results of the DNA adduct analysis of PhIP-treated gastric organoids followed the same pattern seen in previous experiments. Gastric culture D95 had higher levels of dG-C8-PhIP adducts than D88 (Figure 6.7 A). Interestingly, although colon organoids had very similar levels of adducts, colon culture D351 had higher adduct levels than D311, despite D311 having slightly stronger cytotoxic and DDR responses (Figure 6.7

B). Overall, colon organoids had higher levels of adduct formation than gastric organoids; these results are in line with previous findings in mice where PhIP-DNA adduct formation was higher in the colon compared to the glandular stomach (Arlt et al., 2011c; Krais et al., 2016b).

Due to the low responses seen following PhIP treatment, the reactive metabolite *N*-OH-PhIP was tested. Unfortunately, due to time constrains and organoid availability *N*-OH-PhIP responses could only be tested in gastric and kidney organoids. The cytotoxicity assessment showed a dose-dependent decrease in all gastric and kidney organoid cultures (Figure 6.3). As expected, gastric organoids had a greater response to *N*-OH-PhIP than to PhIP, and as seen with PhIP, D95 was more susceptible to *N*-OH-PhIP than D88. This agrees with previous studies where cell viability was not affected after PhIP treatment but after treatment with *N*-OH-PhIP the same or lower concentrations led to a decrease in viability (Bellamri et al., 2018; Hölzl-Armstrong et al., 2020).

Treatment with *N*-OH-PhIP led to the induction of all DDR proteins in all the organoid cultures tested (Figure 6.4). Gastric organoids had similar induction levels at all concentrations, and D95 had slightly stronger responses than D88 at the equivalent concentrations. Kidney organoid cultures had similar levels of expression between them, with dose-dependent inductions of p-p53 and γ-H2AX. In contrast, the induction of pCHK2 and p21 did not follow this pattern and it decreased at the highest concentration. This response could be due to increased cell death; however, it is unlikely as it does not occur for all proteins. A similar response was seen in FE1 cells treated with PhIP in the presence of rat liver S9 mix (Hölzl-Armstrong et al., 2020). Activation of p-p53 and p21 via the ATM-CHK2 pathway following *N*-OH-PhIP has been reported previously (Mimmler et al., 2016). This was accompanied by the activation of the ATR-CHK1 pathway which also leads to p53 phosphorylation (Hölzl-Armstrong et al., 2020, 2021; Mimmler et al., 2016); however, the latter was not tested here.

As *N*-OH-PhIP can react directly with DNA and because of the high toxicity it induced, it was anticipated that *N*-OH-PhIP would lead to higher adduct formation in gastric organoids than PhIP. This is consistent with previous studies on the human prostate cancer cell line LNCaP where no adduct formation was seen following PhIP treatment and lower concentrations of *N*-OH-PhIP led to adduct formation (Bellamri et al., 2018). Kidney organoids had much higher levels of dG-C8-PhIP adducts than gastric organoids after *N*-OH-PhIP treatment, and they both showed a dose-dependent response. Gastric D88 had higher levels of adducts than D95, however, the concentrations used were also slightly more toxic. Kidney D21 had more adducts than D50 at 10 µM, although DDR responses seemed equal in both cultures and toxicity was slightly higher in D50. Studies in mice have shown that kidney tissues accumulate higher levels of dG-C8-PhIP adducts than glandular stomach, however, this was tested with PhIP (Arlt et al., 2011c; Krais et al., 2016b). The low levels of adducts detected in the untreated controls of the PhIP experiments (and blank samples) were due to carry-over of dG-C8-PhIP after the analysis of the *N*-OH-PhIP-treated samples, this background was subtracted from the treated samples.

In summary, the presence of dG-C8-PhIP adducts and induction of DDR markers following PhIP treatment indicate that gastric and colon organoids can metabolise the compound. However, the observed adduct levels may indicate that the expression of the XMEs required for its metabolism (mainly CYP1A2) may be low. Additionally, it has been shown that liver metabolism is important for PhIP activation (Boobis et al., 1994), therefore it would be advantageous to study its effect on this organoid type. The results presented here also showed differences in PhIP-induced responses between tissues, with the target tissue (*i.e.,* colon organoids) having higher levels of DNA adducts than the non-target tissue (*i.e.,* gastric organoids). However, DDR markers were induced in both organoid types and no big differences in the pattern of induction were seen between them. Additional investigations with *N*-OH-PhIP showed tissue-specific responses as adduct levels and DDR induction patterns were different in both kidney and gastric

organoids. As expected, higher dG-C8-PhIP adduct levels were seen after *N*-OH-PhIP treatment due to this metabolite directly reacting with DNA, but further metabolism by the organoids is also possible. Therefore, an analysis of the expression of phase I and II XMEs is required to better understand the responses seen here which could not be achieved due to time constrains. Furthermore, investigating the effects of *N*-OH-PhIP on colon organoids would also be beneficial to this study. Unfortunately, as these were the last experiments carried out, due to the deadlines to send DNA samples to collaborators and the low availability of colon organoids in culture at that moment, this was not possible. Overall, this study showed that organoids can be a useful model to study the metabolic activation and target specificity of PhIP. However, the ability of the organoids to recapitulate certain aspects of PhIP biology, such as its hormonal activity, was not investigated in this study, which may be key in the understanding of its tissue-specific responses, therefore, work is required in this area.

Chapter 7 General discussion

The increase of cancer cases and deaths over the years is a great cause for concern. Many cases are attributed to environmental factors and life-style choices and thus, could be prevented to some extent. Therefore, it is important to understand the way carcinogens work at physiological and molecular levels in order to develop preventative strategies. For many environmental carcinogens the modes of action have been studied extensively; however, the changes they cause at a molecular level have not been fully characterised for most of them. Studies in different *in vivo* and *in vitro* models have provided important mechanistic information on many of these processes. However, limitations such as species-specific responses, including different tumour targets and metabolism, and the limited extent to which 2D cell cultures reproduce physiological conditions *in vivo* have shown the need for more relevant experimental models for studying human physiology (Kolenda et al., 2018; Ruggeri et al., 2014). This study addresses this need by using human organoids derived from normal tissues to investigate the metabolic activation and cellular responses to four environmental carcinogens: BaP, AFB_1, AAI and PhIP. Additionally, this project assessed the tissue-specificity of these compounds, as it has been shown that molecular events such as DNA adduct formation can occur in both target and non-target tissues, hence the continuing need to understand why tumour formation only happens in target tissues.

In Chapter 3, the bioactivation of BaP was confirmed in all organoid types with the activation of DDR pathways, induction of *CYP1A1* and *NQO1*, and formation of BaP metabolites and DNA adducts. Figure 7.1A compared the levels of dG-N^2-BPDE adducts formed in all organoid types showing that gastric culture D95 and pancreatic D39 at 12.5 µM and D39 at 50 µM had the highest levels of DNA adducts. When the induction of *CYP1A1* was compared between all organoids, similar levels were seen in gastric D95, pancreatic D39 and both kidney donors at 12.5 µM, and at 50 µM the kidney organoids had the highest induction. *NQO1* levels were the highest in kidney organoids

at both concentrations (Figure 7.1B and C). Overall, there was no correlation between adduct levels and the induction of XMEs in the organoids.

When looking at the tissue-specific responses there were no clear differences between organoids from possible BaP target (pancreas and liver) and non-target (stomach, colon and kidney) tissues in metabolite, XME and adduct levels. Furthermore, the HT RT-qPCR analysis of gene expression changes after BaP treatment showed alterations in genes that have been linked to the development of cancer such as *MDM2* (Hou et al., 2019), *TXNRD1* (Bhatia et al., 2016), *RRM2B* (Iqbal et al., 2021) and *DDB2* (Gilson et al., 2019); however, this analysis did not identify any target-specific changes.

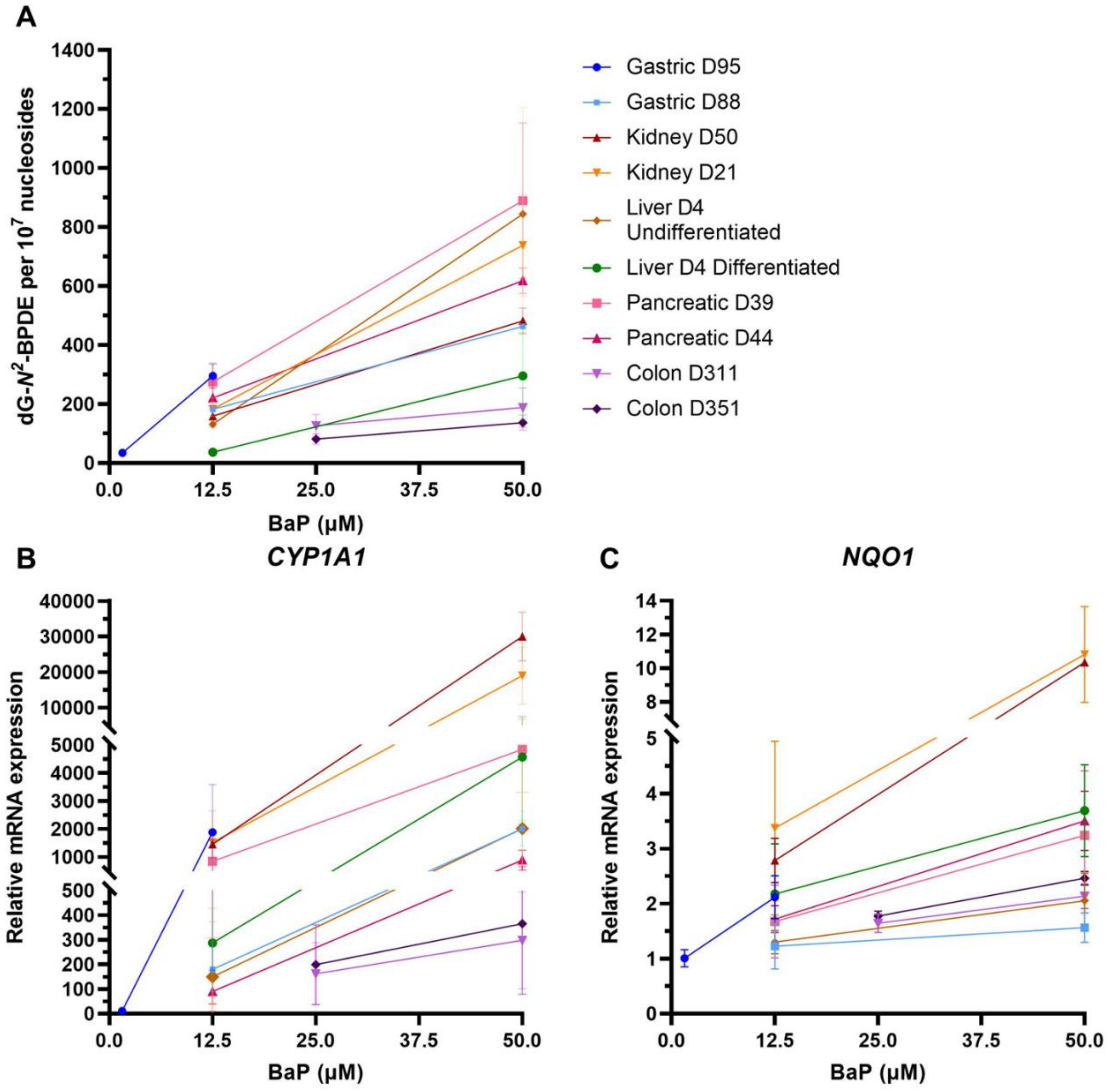

Figure 7.1. dG-*N*^{2}-BPDE adduct levels and relative mRNA expression of *CYP1A1* and *NQO1* in human tissue organoids. DNA adduct levels (**A**) and mRNA levels of *CYP1A1* (**B**) and *NQO1* (**C**) in organoids from gastric, kidney, liver, pancreatic and colon tissues after BaP treatment at the indicated concentrations. Results are shown as mean ± SD (n≥3).

Chapter 4 showed the activation of AFB_1 in gastric, kidney and liver organoids. Similar to what was seen in response to BaP treatment, there was no correlation between adduct formation and the induction of XMEs, as the two liver organoid cultures (target) had the highest adduct levels and lower XME induction than non-target organoids, particularly the kidney. This is shown in Figure 7.2, where it can be seen that undifferentiated liver organoids had the highest levels of adducts and the greatest increase between the concentrations tested (Figure 7.2A), while kidney culture D50 had the highest levels of XME expression and undifferentiated liver had one of the lowest levels of *CYP3A4* and intermediate levels of *CYP1A2* expression (Figure 7.2B and C).

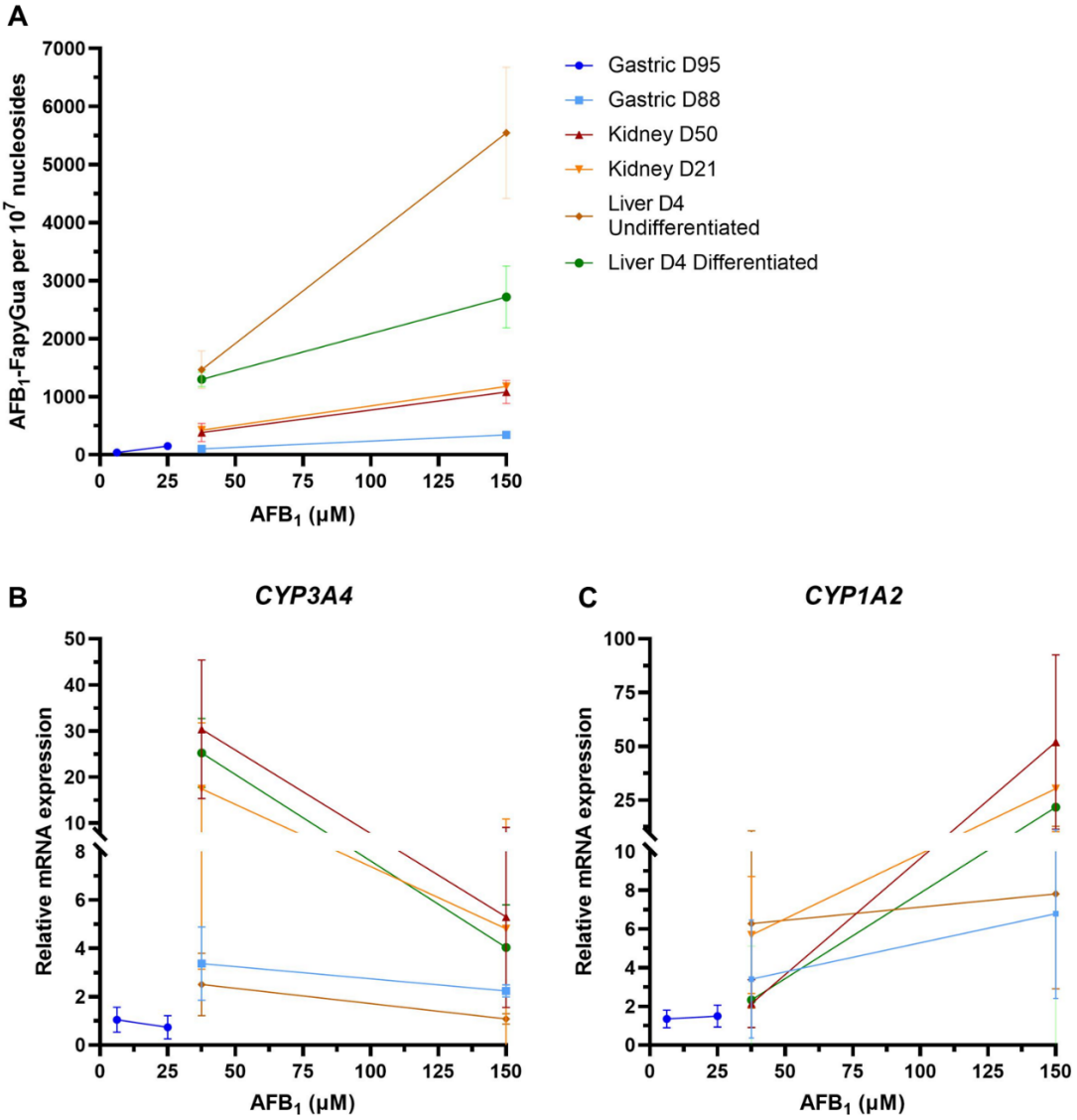

Figure 7.2. AFB_1-FapyGua adduct levels and relative mRNA expression of *CYP3A4* and *CYP1A2* in human tissue organoids. DNA adduct levels (**A**) and mRNA levels of *CYP3A4* (**B**) and *CYP1A2* (**C**) in organoids from gastric, kidney and liver tissues after AFB_1 treatment at the indicated concentrations. Results are shown as mean ± SD (n≥3).

In Chapter 5 the metabolic activation of AAI by organoids from kidney and gastric tissues was shown. Although there seem to be more tissue-specific responses with pronounced effects in the kidney than in the gastric organoids when comparing events at the same levels of cytotoxicity, the kidney had the lowest adduct levels per µM compound when treated with AAI (Figure 7.3A), although it is a target for AAI carcinogenicity (Arlt et al., 2002). Something similar was seen in the expression of XMEs, where D88 had a higher relative mRNA level per µM AAI than the kidney organoids (Figure 7.3B, C and D). Therefore, although the kidney accumulated a lot of AAI DNA adducts, gastric D88 seemed to activate this compound more readily.

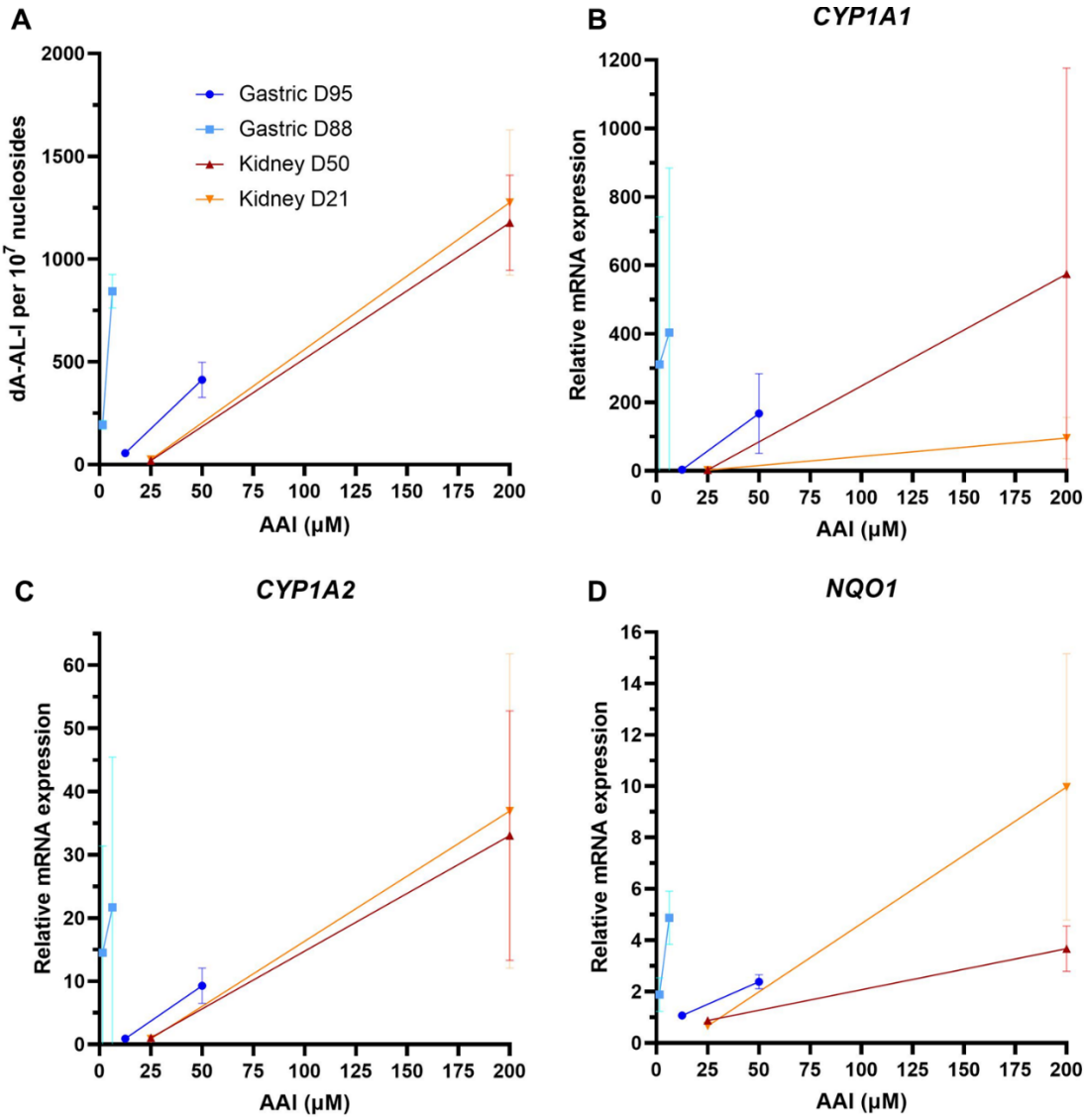

Figure 7.3. dA-AL-I adduct levels and relative mRNA expression of *CYP1A1*, *CYP1A2* and *NQO1* in human tissue organoids. DNA adduct levels (**A**) and mRNA levels of *CYP1A1* (**B**), *CYP1A2* (**C**) and *NQO1* (**D**) in organoids from gastric and kidney tissues after AAI treatment at the indicated concentrations. Results are shown as mean ± SD (n≥3).

Lastly, Chapter 6 showed low levels of PhIP bioactivation, with colon organoids having highest DNA adduct levels at an average of no more than 3 adducts per 10^7 nucleosides (Figure 7.4A). Treatment with the reactive intermediate *N*-OH-PhIP led to higher levels of adduct formation and to activation of the DDR response. Kidney organoids had much higher levels of adducts per µM *N*-OH-PhIP than gastric organoids (Figure 7.4B). As the higher adduct formation seen after *N*-OH-PhIP may be due to some of the phase I enzymes required for PhIP activation not being present at high enough levels in the organoids, treating the organoids with PhIP in the presence of S9 mix could aid PhIP bioactivation as it has been shown in human stem cells and mouse FE1 cells (Hölzl-Armstrong et al., 2020; Kucab et al., 2019).

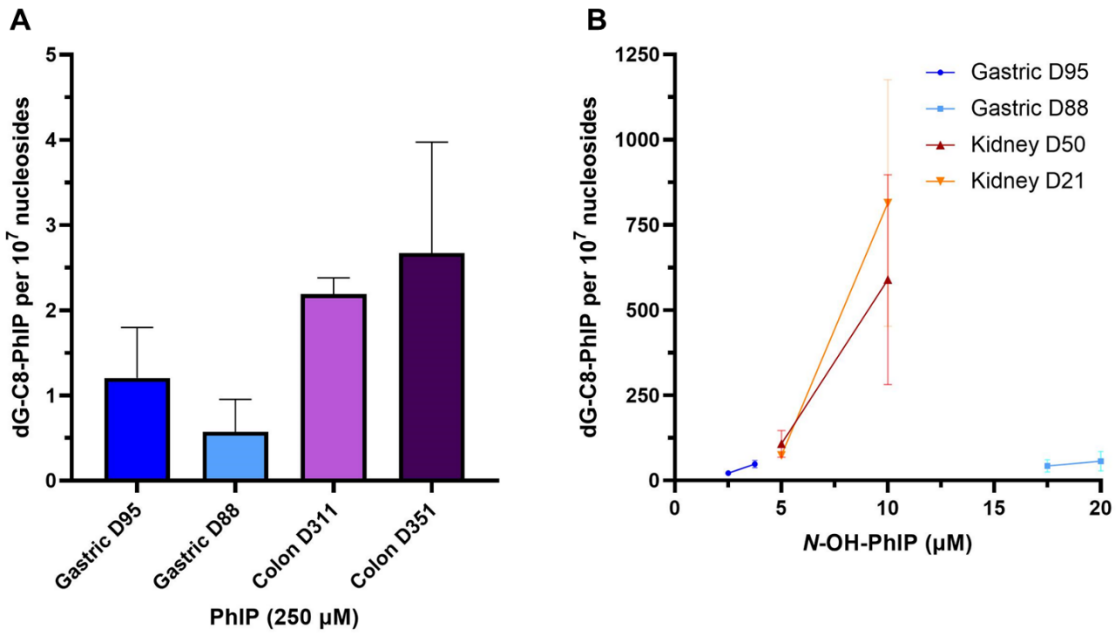

Figure 7.4. dG-C8-PhIP adduct levels in human tissue organoids. DNA adduct levels after PhIP treatment in organoids from gastric and colon tissues (**A**) and after *N*-OH-PhIP treatment in gastric and kidney organoids (**B**), at the indicated concentrations. Results are shown as mean ± SD (n≥3).

This project showed that human tissue organoids express different levels of XMEs as shown in Figure 7.5. When comparing the basal levels of expression of *CYP1A1* it could be seen that levels not only differed significantly between organoid types but also between some organoid donor cultures. Colon D311 had the highest basal levels of *CYP1A1* expression followed by differentiated liver organoids and pancreatic D44. The lowest levels were seen in kidney and undifferentiated liver organoids (Figure 7.5A).

According to the normalised RNA data from human tissue samples available in The Human Protein Atlas (Karlsson et al., 2021; Uhlén et al., 2015), the liver has the highest *CYP1A1* expression between these organs, with hepatocytes expressing almost 5-fold more than ductal cells, which correlates with the higher mRNA levels seen in the differentiated (hepatocytes) organoids compared to the undifferentiated (ductal cells) organoids. In contrast, this database indicates that the colon and the pancreas have some of the lowest levels of *CYP1A1* between these tissues, which was not the case for colon D311 and pancreatic D44 organoids. However, colon D351 and pancreatic D39 followed a trend closer to that seen *in vivo*.

Basal levels of expression of *NQO1* are shown in Figure 7.5B. The highest expression was seen in colon D311, which had double the expression of the donor with the second highest expression, gastric D95. These were followed by differentiated liver and gastric D88. The lowest expression was seen in the kidney organoids. Data from The Human Protein Atlas (Karlsson et al., 2021; Uhlén et al., 2015) indicates that the stomach is the tissue with the highest *NQO1* expression, which is close to what was seen in the organoids. However, it also shows the kidney has the second highest *NQO1* expression, which does not correlate with what was seen in the organoids.

The expression of *CYP3A4* and *CYP1A2* could only be compared between kidney, liver and gastric organoids (Figure 7.5C and D). As mentioned in Chapter 4 differentiated liver organoids had significantly higher levels of *CYP3A4* than kidney and gastric organoids, while undifferentiated liver had the highest levels of *CYP1A2*. This correlates with the *in vivo* data for *CYP3A4* where the liver, particularly the hepatocytes, have the highest levels of these enzymes, with the levels in ductal cells, kidney and stomach tissues being close to zero (Karlsson et al., 2021; Uhlén et al., 2015). Furthermore, the liver has the highest expression of *CYP1A2 in vivo*, with other tissues having no detectable levels, however, the expression is seen in hepatocytes, not ductal cells, which contrasts with that seen in the organoids as the undifferentiated liver had slightly higher levels than the differentiated liver.

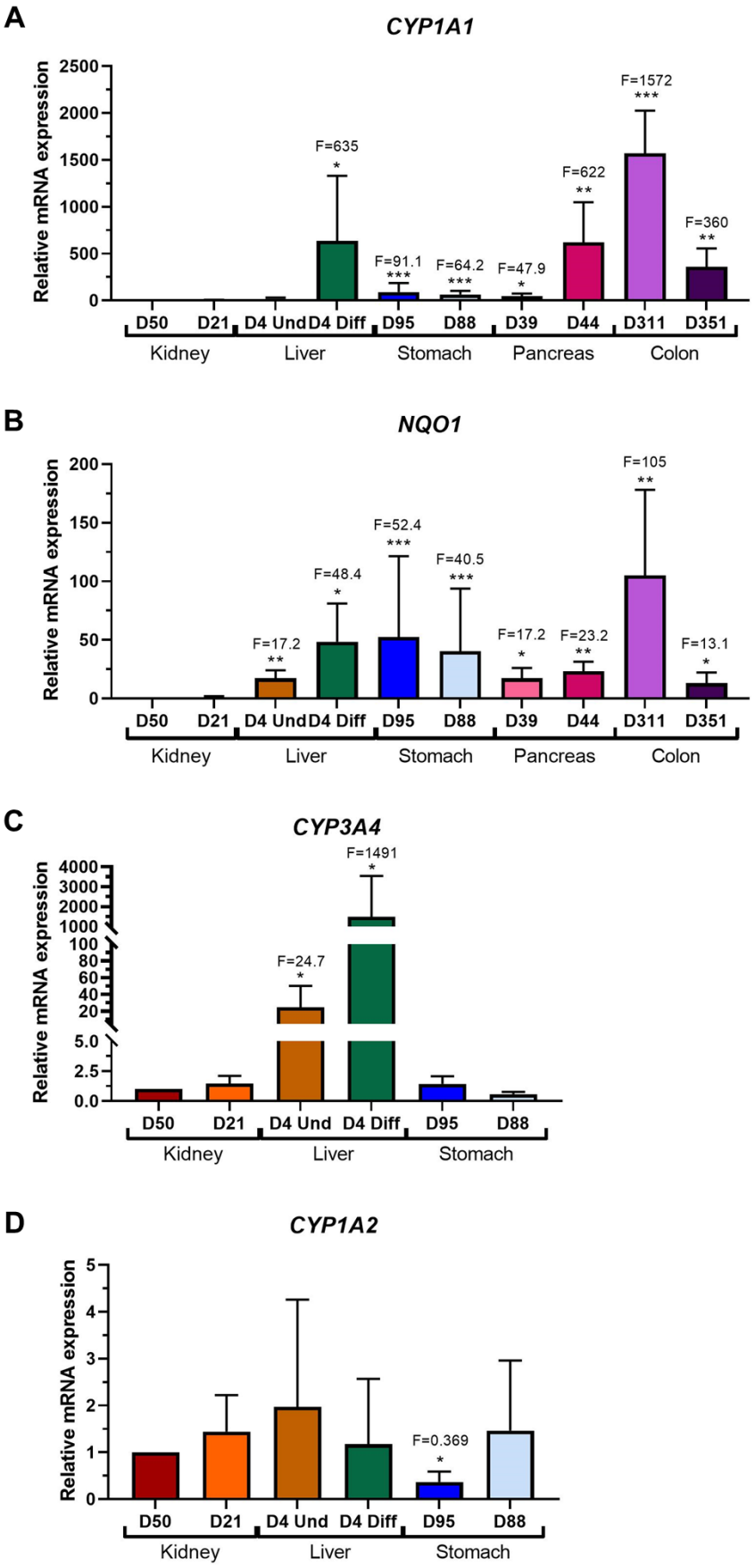

Figure 7.5. Relative mRNA levels of XMEs in normal human tissue organoids. Expression of *CYP1A1* (**A**), *NQO1* (**B**), *CYP3A4* (**C**) and *CYP1A2* (**D**) in vehicle control treated (DMSO or water) organoids from kidney (D50 and D21), liver (D4, undifferentiated and differentiated), stomach (D95 and D88), pancreas (D39 and D44) and colon (D311 and D351) tissues was

analysed by RT-qPCR and the $2^{-\Delta\Delta CT}$ method. Results are shown as mean ± SD (n≥3). Values are normalised to mRNA expression of the housekeeping gene *GAPDH* and are relative to kidney D50. Statistical analysis was performed by log2 transforming the data and a one sample *t*-test with Bonferroni correction against the control mean of 0: *p<0.05; **p<0.01; ***p<0.001 compared to D50.

As mentioned previously, the environmental carcinogens used in this PhD project are known to form bulky DNA adducts, which are repaired by NER, as described in Section 1.2.3. Studies in mouse cells showed that p53 deficiency led to defects in the NER pathway, while p21 deficiency led defects to a lesser extent, therefore indicating that p53 and its downstream genes play a role in NER (Smith et al., 2000). Additionally, it has been shown that in UV-exposed quiescent cells NER can lead to secondary DNA damage leading to SSBs and DSBs, which in turn triggers H2AX phosphorylation and the activation of the ATR and ATM pathways (Wakasugi et al., 2014). This agrees with the results presented in this thesis, which showed that the treatment of human organoids with the test carcinogens leads to the induction of DDR proteins such as p-p53, pCHK2, p21 and γ-H2AX.

Figure 7.6 compares the relative protein levels of the DDR proteins tested in this project between the different organoid types. Overall, there was some variability between blots which could partly be due to differences in passage numbers in the different experiments. When compared to the protein expression information available in The Human Protein Atlas (Uhlén et al., 2015) there is no correlation between the levels of expression seen in tissues and the organoids, however, according to this database these proteins have low tissue-specificity. Additionally, as the analyses of protein and RNA expression carried out here and in The Human Protein Atlas were done differently, these comparisons are only indications of similarities or differences between the organoids and the human tissues and are not directly comparable.

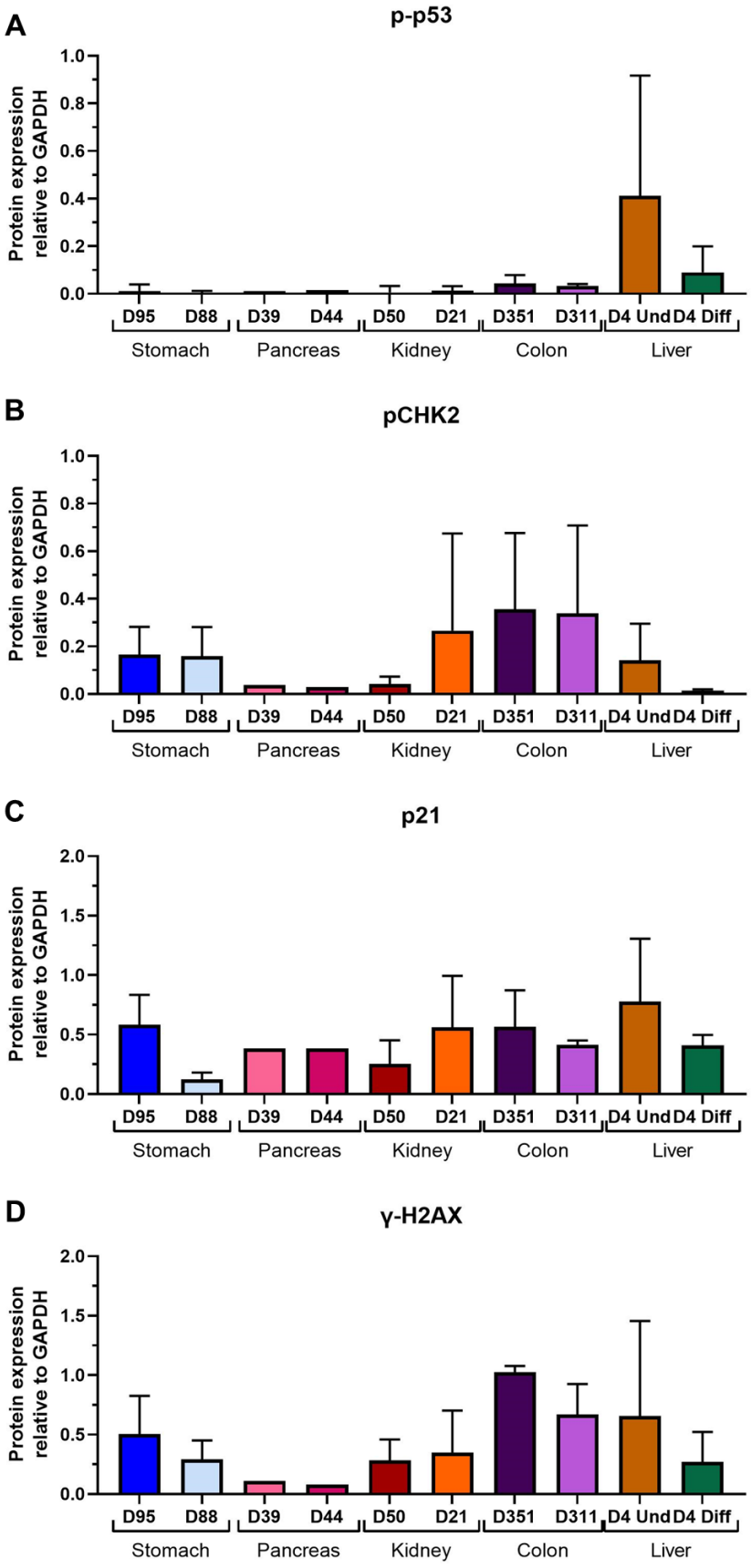

Figure 7.6. DDR protein expression relative to GAPDH in normal human tissue organoids. Expression of p-p53 (**A**), pCHK2 (**B**), p21 (**C**) and γ-H2AX (**D**) in vehicle control treated (DMSO or water) organoids from stomach (D95 and D88), pancreas (D39 and D44), kidney (D50 and D21), colon (D311 and D351) and liver (D4, undifferentiated and differentiated) tissues was

analysed by Western blotting. Densitometric analysis was carried out using ImageJ. Results are shown as mean ± SD (n≥2).

As mentioned previously, this study included donors from different age groups (*i.e*., paediatric and adult) as these were the organoids that were available for the project. It is known that children have a higher drug clearance than adults, which may be in part due to the expression and activity of the XMEs (Zane et al., 2018). Additionally, it has been shown that the expression of CYP enzymes and their related nuclear receptors in rats varies with age, for example, *Cyp1a1* and AhR decreased with ageing, while *Cyp1a2* levels remained high throughout adulthood (Xu et al., 2019). Therefore, as the age differences between donors may influence the metabolism of the compounds, in future studies it would be important to compare between donors from the same age groups (e*.g.,* adults).

This project focused on the tissue-specific responses to events involved in the early stages of carcinogenesis, which are associated with the initiation step. Due to the complexity of cancer development, which is a multistep process, and the long-term changes that are associated with neoplastic transformation and cancer progression, the short-term treatments of the organoids used in this study were not suitable to model many of the factors that are likely to impact cancer susceptibility. The results of these investigations into the organotropism or tissue-specificity of the tested environmental carcinogens were inconclusive, and more work needs to be done in this area. One of the limitations was that the present study did not include organoids from a confirmed target of BaP carcinogenicity, such as the lung (Balansky et al., 2007), as human organoids derived from this tissue were not available at the time this project was planned. The analysis of tissue-specific responses for the other compounds could not be completed, therefore a study with the gene panel used in this project and/or an analysis of a broader set of genes using microarrays or RNA-sequencing would be beneficial to follow-up what was found in this thesis. Additionally, more organoid types and donor samples (including adult donors) could be added to the assessment of these carcinogens, as was initially planned, in order to better compare tissue-specific responses and identify pathways

affected by these compounds. It is known that components of the epigenetic machinery are affected in cancer, this includes DNA methylation, histone-modifying enzymes, histone posttranslational modification readers, miRNAs, etc (Baylin and Jones, 2016). Therefore, an investigation of the epigenetic changes induced by these carcinogens would also add important knowledge to their tissue-specificity (Meng et al., 2021; Rieswijk et al., 2016; Tryndyak et al., 2018). Furthermore, it has been shown that the dysregulation of miRNAs affects different hallmarks of cancer, from uncontrolled cell proliferation to inducing angiogenesis and metastasis, therefore, the study of miRNA changes induced by these compounds would provide useful information of their mechanisms and roles in tumour formation (Chen et al., 2022; Peng and Croce, 2016; Pu et al., 2017).

It is worth mentioning that there were notable differences in the responses of cultures from the same organoid type, with some being more susceptible to damage or more metabolically competent than others. This was mainly noted in the gastric organoid cultures, as D95 required lower concentrations of BaP, AFB_1 and PhIP than D88, while D88 was more susceptible than D95 to AAI. Future experiments could further investigate these differences between donor cultures by looking at polymorphisms in the XMEs. It has been suggested that polymorphisms in certain XME genes, such as *NAT2*, *UGT1A1*, *NQO1* and *CYPs*, may influence the metabolism of the compounds and therefore the susceptibility of an individual to developing cancer (Atanasova et al., 2005; Girard et al., 2005; Metry et al., 2009; Rojas et al., 2000; Stiborová et al., 2017; Zanger and Schwab, 2013). Moreover, the metabolic enzyme activity and protein expression of the XMEs could be tested, as these do not always correlate with the mRNA expression (Arlt et al., 2015). Furthermore, mixtures of compounds, such as BaP and PhIP, as well as chronic treatments with lower concentrations could be tested as these may be more representative of typical human exposure conditions.

Organoids not only provide a more representative model to human physiology, but also may be a way to decrease the number of animals being used for toxicology research.

However, organoids lack certain features like tissue-tissue interactions that may be necessary in processes such as the metabolism of xenobiotics. This limitation of the 'static' culture of the organoids could be overcome by using more complex systems like organ-on-chips and MPS to represent organ-organ interactions (Truskey, 2018). Although the organoids are easy to maintain once the ideal culture conditions have been established, they can be sensitive to small changes in their culture environment. This can be noticed when looking at the high variability between some of the biological replicates, where small variations in the media could be affecting the cell composition of the organoids, as fresh batches of media are prepared every two weeks and the media components need to be prepared every few months. Additionally, due to the non-clonal nature of the organoids the proportion of each cell type may vary between passages, therefore, it would be interesting to analyse their cell composition at different points of their culture as this may affect how the organoids respond to treatments. Moreover, although the differentiation of the liver organoids led to an increase in hepatocyte markers it also had some disadvantages, as the long culture of the organoids without passaging led to some of the cells collapsing and dying, which could have had an effect on the results obtained for this organoid culture. Furthermore, it was not possible to know the percentage of the organoids that were successfully differentiated, which is something that could be investigated in the future by looking at markers (*e.g*., by whole-mount immunostaining) on the individual cells within the organoid.

While organoids have been used to test a range of environmental agents (reviewed in Section 1.6.2.3), the use of organoids derived from human tissues to investigate the effects of environmental carcinogens is still limited. Therefore, this study adds to the efforts to introduce the organoid model as a routine testing system in environmental toxicology research. Additionally, organoids are being used for other applications like the study of mutational signatures, which are the marks left in the genome by different processes like DNA damage and repair and can be associated with exposure to different compounds (Alexandrov et al., 2013). The signatures for several environmental

carcinogens, including the test compounds used in this study, have been examined in different models such as mouse embryo fibroblasts and stem cells (Kucab et al., 2019; Nik-Zainal et al., 2015). Preliminary results from the Phillips lab show that the organoids can replicate the signatures seen in other models, in which the signature for BaP was found to be similar to Signature 4, which was extracted from smoking-associated cancers (Kucab et al., 2019). Similarly, the signature for PhIP or *N*-OH-PhIP was found to contain elements from Signatures 4, 18 (ROS) and 29 (tobacco chewing) (Hölzl-Armstrong et al., 2021). Lastly, the signatures for AFB_1 and AAI are Signatures 22 and 24, respectively (Kucab et al., 2019; Totsuka et al., 2020).

In conclusion, the work presented in this thesis showed that human tissue organoids are potentially a good model for the study of the metabolic activation and genotoxicity induced by environmental carcinogens, as well as other cellular responses. Expanding the list of compounds used in this model will provide a better idea of the metabolic potential of these 3D cultures. Additionally, the use of organoids from several human tissue origins will provide a greater understanding of carcinogen organotropism and, therefore, greater understanding of the aetiology of human cancers.

Appendix

Supplementary Table 1. Role of individual supplements in organoid culture media

Medium component	Function	Reference
A83-01	TGFβ inhibitor, disrupts epithelial to mesenchymal transition (EMT). Enhances cell proliferation.	(Tojo et al., 2005)
Advanced DMEM/F12	Basal media	
B27 Supplement	Chemically defined supplement that optimises cell growth in the absence of serum.	(Crespo et al., 2017)
BMP7	Accelerates hepatocyte proliferation.	(Huch et al., 2015)
DAPT	Notch inhibitor	(Huch et al., 2015)
Dexamethasone	Suppresses growth and induces hepatocyte maturation.	(Michalopoulos et al., 2003)
FGF-10	Regulates cell survival and proliferation. Drives formation of organoids.	(Merker et al., 2016; Rabata et al., 2020)
FGF-19	Increases hepatocyte proliferation.	(Wu et al., 2011)
Forskolin	Agonist of cAMP signalling, induces proliferation of biliary duct cells.	(Huch et al., 2015)
Gastrin I human	Peptide hormone that stimulates proliferation and maturation of gastric epithelial cells.	(Merker et al., 2016)
Glutamax	Alternative to L-glutamine with more stability, improves cell health.	(GlutaMAX Supplement)
HEPES	Buffer, helps maintain neutral pH.	(HEPES)
hES Cell Cloning and Recovery	Improves efficiency of thawing and increases the chances of recovery.	(hES Cell Cloning & Recovery Supplement)
HGF	Required for formation of biliary epithelium.	(Michalopoulos et al., 2003)
N2 Supplement	Chemically defined supplement that optimises cell growth.	(Crespo et al., 2017)
N-acetyl cysteine	Antioxidant. Protects against cell death and enhances cell survival.	(Merker et al., 2016)
Nicotinamide	Promotes organoid formation and increases their lifespan. Reduces oxidative stress.	(Bartfeld et al., 2015)

Medium component	Function	Reference
Noggin	Bone morphogenic protein (BMP) inhibitor. Crucial for maintenance of the stem cell niche.	(Kretzschmar and Clevers, 2016)
PGE2	Prostaglandin E2. Activator of the WNT pathway. Induces growth of cysts and prolongs lifespan.	(Bartfeld et al., 2015; Merker et al., 2016)
Recombinant EGF	Induces cell survival and lineage determination. Important in cell growth and proliferation.	(Merker et al., 2016)
R-Spondin-1 CM	WNT agonist, a ligand of LGR5. Enhances effects of WNT3A, *i.e*. maintain stem cell regeneration.	(Schuijers and Clevers, 2012)
SB202190	Inhibits autophagy and apoptosis (p38 inhibitor). Required for long-term organoid cultures.	(Kretzschmar and Clevers, 2016)
WNT3A CM	Maintains stem cell regeneration. Allows long-term organoid expansion.	(Sato et al., 2011)
Y-27632	ρ-associated protein kinase inhibitor. Prevents anoikis.	(Schlaermann et al., 2016)

Supplementary Table 2. List of genes included in HT qRT-PCR and their names

Gene symbol	Official full name
Transcription factors	
AXIN2	Axin2
BTRC	Beta-Transducin Repeat Containing E3 Ubiquitin Protein Ligase
JUN	Jun proto-oncogene, AP-1 transcription factor subunit
KEAP1	Kelch-like ECH-associated protein 1
MAP3K5	Mitogen-activated protein kinase kinase kinase 5
MDM2	MDM2 proto-oncogene
NFE2L2	NFE2 like bZIP transcription factor 2
NFKB1/2	Nuclear factor kappa B subunit 1/2
NFKBIA	NFKB inhibitor alpha
TP53	Tumour protein p53
SLC30A1	Solute carrier family 30 member 1
VEGFA	Vascular endothelial growth factor A
DNA damage response and repair	
APEX1	Apurinic/apyrimidinic endodeoxyribonuclease 1
ATM	ATM serine/threonine kinase
ATR	ATR serine/threonine kinase
BRCA1/2	BRCA1/2 DNA repair associated

Gene symbol	Official full name
DDB1/2	Damage specific DNA binding protein 1/2
DDIT3	DNA damage inducible transcript 3
ERCC1	ERCC excision repair 1, endonuclease non-catalytic subunit
ERCC2	ERCC excision repair 2, TFIIH core complex helicase subunit
ERCC4	ERCC excision repair 4, endonuclease catalytic subunit
ERCC5	ERCC excision repair 5, endonuclease
GADD45A	Growth arrest and DNA damage inducible alpha
LIG1/3	DNA ligase 1/3
MGMT	O-6-methylguanine-DNA methyltransferase
MLH1	mutL homolog 1
MSH2	mutS homolog 2
OGG1	8-oxoguanine DNA glycosylase
PARP1	Poly(ADP-ribose) polymerase 1
PCNA	Proliferating cell nuclear antigen
POLB	DNA polymerase beta
POLD1	DNA polymerase delta 1, catalytic subunit
RAD50	RAD50 double strand break repair protein
RAD51	RAD51 recombinase
RRM2B	Ribonucleotide reductase regulatory TP53 inducible subunit M2B
XPA	XPA, DNA damage recognition and repair factor
XPC	XPC complex subunit, DNA damage recognition and repair factor
XRCC5	X-ray repair cross complementing 5
Apoptosis	
APAF1	Apoptotic peptidase activating factor 1
BAX	BCL2 associated X, apoptosis regulator
BBC3	BCL2 binding component 3
BCL2	BCL2 apoptosis regulator
BCL2L1	BCL2 like 1
PMAIP1	Phorbol-12-myristate-13-acetate-induced protein 1
TNFRSF10B	TNF receptor superfamily member 10b
XIAP	X-linked inhibitor of apoptosis
Proliferation and cell cycle control	
CCND1	Cyclin D1
CDKN1A/B	Cyclin dependent kinase inhibitor 1A/B
CDKN2B	Cyclin dependent kinase inhibitor 2B
E2F1	E2F transcription factor 1
EGFR	Epidermal growth factor receptor
IL8	Interleukin 8
MYC	MYC proto-oncogene, bHLH transcription factor

Gene symbol	Official full name
PLK3	Polo like kinase 3
PPM1D	Protein phosphatase, Mg^{2+}/Mn^{2+} dependent 1D
SIRT2	Sirtuin 2
Oxidative stress response	
CAT	Catalase
FTH1	Ferritin heavy chain 1
G6PD	Glucose-6-phosphate dehydrogenase
GCLC	Glutamate-cysteine ligase catalytic subunit
GPX1/2	Glutathione peroxidase 1/2
GSR	Glutathione-disulfide reductase
HMOX1	Heme oxygenase 1
HSPA1A	Heat shock protein family A (Hsp70) member 1A
MT1X	Metallothionein 1X
MT2A	Metallothionein 2A
PRDX1	Peroxiredoxin 1
SEPP1	SELENOP (selenoprotein P)
SOD1/2	Superoxide dismutase 1/2
TFRC	Transferrin receptor
TXN	Thioredoxin
TXNRD1	Thioredoxin reductase 1
Xenobiotic metabolism	
ABCB1	ATP binding cassette subfamily B member 1
ABCC1	ATP binding cassette subfamily C member 1
ADH1B	Alcohol dehydrogenase 1B (class I), beta polypeptide
ALDH1A1	Aldehyde dehydrogenase 1 family member A1
CYP1A1	Cytochrome P450 family 1 subfamily A member 1
EPHX1	Epoxide hydrolase 1
GSTP1	Glutathione S-transferase pi 1
NAT1	N-acetyltransferase 1
NQO1	NAD(P)H quinone dehydrogenase 1
SULT1A1	Sulfotransferase family 1A member 1
UGT1A	UDP glucuronosyltransferase family 1 member A complex locus

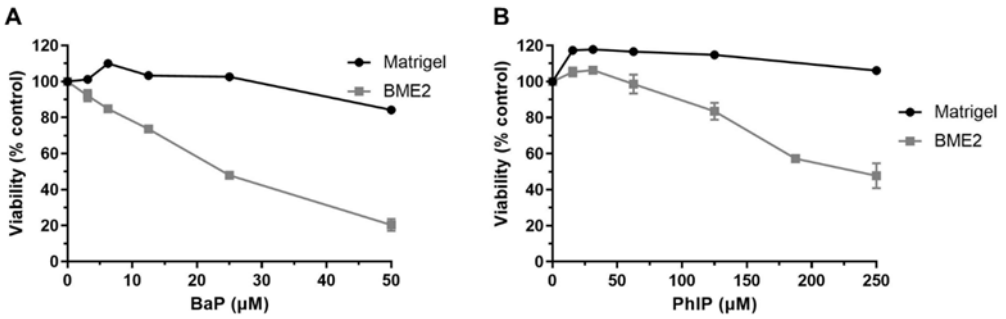

Supplementary Figure 1. Cell viability in human colon organoids seeded in Matrigel vs BME2 after BaP and PhIP treatment. Organoids from normal colon tissue (D311) were seeded in Matrigel and BME2 and were treated with (**A**) BaP (0-50 μM) or (**B**) PhIP (0-250 μM) for 48 hr. A 48 hr recovery period in fresh culture media was included after the 48 hr treatment, after which cytotoxicity was assessed. A DMSO control was included. Cell viability (% control) was measured using the CellTiter-Glo assay. Results are shown as mean ± SD, n=3 technical replicates. Experiments carried out by Jill E. Kucab.

References

Abd, E., Yousef, S.A., Pastore, M.N., Telaprolu, K., Mohammed, Y.H., Namjoshi, S., Grice, J.E., and Roberts, M.S. (2016). Skin models for the testing of transdermal drugs. Clinical Pharmacology: Advances and Applications *8*, 163–176.

Akinrinde, A.S., Ogunbunmi, T., and Akinrinmade, F.J. (2020). Acute aflatoxin B1-induced gastro-duodenal and hepatic oxidative damage is preceded by time-dependent hyperlactatemia in rats. Mycotoxin Research *36*, 443–452.

Alexandrov, K., Rojas, M., Kadlubar, F.F., Lang, N.P., and Bartsch, H. (1996). Evidence of anti-benzo[α]pyrene diolepoxide-DNA adduct formation in human colon mucosa. Carcinogenesis *17*, 2081–2083.

Alexandrov, K., Rojas, M., and Rolando, C. (2006). DNA damage by benzo(a)pyrene in human cells is increased by cigarette smoke and decreased by a filter containing rosemary extract, which lowers free radicals. Cancer Research *66*, 11938–11945.

Alexandrov, L.B., Nik-Zainal, S., Wedge, D.C., Aparicio, S.A.J.R., Behjati, S., Biankin, A. v., Bignell, G.R., Bolli, N., Borg, A., Børresen-Dale, A.L., et al. (2013). Signatures of mutational processes in human cancer. Nature *500*, 415–421.

Alexandrov, L.B., Ju, Y.S., Haase, K., Loo, P. van, Martincorena, I., Nik-Zainal, S., Totoki, Y., Fujimoto, A., Nakagawa, H., Shibata, T., et al. (2016). Mutational signatures associated with tobacco smoking in human cancer. Science (1979) *354*, 618–622.

Alotaibi, A.G., Li, J. v., and Gooderham, N.J. (2021). Tumour necrosis factor-α (TNF-α) enhances dietary carcinogen-induced DNA damage in colorectal cancer epithelial cells through activation of JNK signaling pathway. Toxicology *457*, 152806.

Amadou, A., Praud, D., Coudon, T., Deygas, F., Grassot, L., Faure, E., Couvidat, F., Caudeville, J., Bessagnet, B., Salizzoni, P., et al. (2021). Risk of breast cancer associated with long-term exposure to benzo[a]pyrene (BaP) air pollution: Evidence from the French E3N cohort study. Environment International *149*, 106399.

Amaral, R.L.F., Miranda, M., Marcato, P.D., and Swiech, K. (2017). Comparative analysis of 3D bladder tumor spheroids obtained by forced floating and hanging drop methods for drug screening. Frontiers in Physiology *8*, 605.

Ames, B.N., Lee, F.D., and Durston, W.E. (1973). An improved bacterial test system for the detection and classification of mutagens and carcinogens (Salmonella typhimurium/lipopolysaccharide/frameshift mutations). Proc Natl Acad Sci U S A *70*, 782–786.

Anderson, K.E., Kadlubar, F.F., Kulldorff, M., Harnack, L., Gross, M., Lang, N.P., Barber, C., Rothman, N., and Sinha, R. (2005). Dietary intake of Heterocyclic Amines and Benzo(a)pyrene: Associations with Pancreatic Cancer. Cancer Epidemiology, Biomarkers & Prevention *14*, 2261–2265.

Andreassen, Å., Vikse, R., Steffensen, I.L., Paulsen, J.E., and Alexander, J. (2001). Intestinal tumours induced by the food carcinogen 2-amino-1-methyl-6-phenylimidazo[4,5-b]pyridine in multiple intestinal neoplasia mice have truncation mutations as well as loss of the wild-type Apc+ allele. Mutagenesis *16*, 309–315.

Antoni, D., Burckel, H., Josset, E., and Noel, G. (2015). Three-dimensional cell culture: A breakthrough in vivo. International Journal of Molecular Sciences *16*, 5517–5527.

Arbillaga, L., Vettorazzi, A., Gil, A.G., van Delft, J.H., García-Jalón, J.A., and López de Cerain, A. (2008). Gene expression changes induced by ochratoxin A in renal and hepatic tissues of male F344 rat after oral repeated administration. Toxicology and Applied Pharmacology *230*, 197–207.

Arlt, V.M., Stiborova, M., and Schmeiser, H.H. (2002). Aristolochic acid as a probable human cancer hazard in herbal remedies: a review. Mutagenesis *17*, 265–277.

Arlt, V.M., Alunni-Perret, V., Quatrehomme, G., Ohayon, P., Albano, L., Gaïd, H., Michiels, J.F., Meyrier, A., Cassuto, E., Wiessler, M., et al. (2004). Aristolochic acid (AA)-DNA adduct as marker of AA exposure and risk factor for AA nephropathy-associated cancer. International Journal of Cancer *111*, 977–980.

Arlt, V.M., Stiborová, M., vom Brocke, J., Simões, M.L., Lord, G.M., Nortier, J.L., Hollstein, M., Phillips, D.H., and Schmeiser, H.H. (2007). Aristolochic acid mutagenesis: Molecular clues to the aetiology of Balkan endemic nephropathy-associated urothelial cancer. Carcinogenesis *28*, 2253–2261.

Arlt, V.M., Stiborová, M., Henderson, C.J., Thiemann, M., Frei, E., Aimová, D., Singh, R., Gamboa da Costa, G., Schmitz, O.J., Farmer, P.B., et al. (2008). Metabolic activation of benzo[a]pyrene in vitro by hepatic cytochrome P450 contrasts with detoxification in vivo: experiments with hepatic cytochrome P450 reductase null mice. Carcinogenesis *29*, 656–665.

Arlt, V.M., Zuo, J., Trenz, K., Roufosse, C.A., Lord, G.M., Nortier, J.L., Schmeiser, H.H., Hollstein, M., and Phillips, D.H. (2011a). Gene expression changes induced by the human carcinogen aristolochic acid I in renal and hepatic tissue of mice. International Journal of Cancer *128*, 21–31.

Arlt, V.M., Levová, K., Bárta, F., Shi, Z., Evans, J.D., Frei, E., Schmeiser, H.H., Nebert, D.W., Phillips, D.H., and Stiborová, M. (2011b). Role of P450 1A1 and P450 1A2 in Bioactivation versus detoxication of the renal carcinogen aristolochic acid I: Studies in Cyp1a1(-/-), Cyp1a2(-/-), and Cyp1a1/1a2(-/-) mice. Chemical Research in Toxicology *24*, 1710–1719.

Arlt, V.M., Singh, R., Stiborová, M., Costa, G.G. da, Frei, E., Evans, J.D., Farmer, P.B., Wolf, C.R., Henderson, C.J., and Phillips, D.H. (2011c). Effect of hepatic cytochrome P450 (P450) oxidoreductase deficiency on 2-amino-1-methyl-6-phenylimidazo [4 , 5-b] pyridine- DNA adduct formation in P450 reductase conditional null mice. Drug Metabolism and Disposition *39*, 2169–2173.

Arlt, V.M., Krais, A.M., Godschalk, R.W., Riffo-Vasquez, Y., Mrizova, I., Roufosse, C.A., Corbin, C., Shi, Q., Frei, E., Stiborova, M., et al. (2015). Pulmonary inflammation impacts on CYP1A1-mediated respiratory tract DNA damage induced by the carcinogenic air pollutant benzo[a]pyrene. Toxicological Sciences *146*, 213–225.

Arlt, V.M., Meinl, W., Florian, S., Nagy, E., Barta, F., Thomann, M., Mrizova, I., Krais, A.M., Liu, M., Richards, M., et al. (2017). Impact of genetic modulation of SULT1A enzymes on DNA adduct formation by aristolochic acids and 3-nitrobenzanthrone. Archives of Toxicology *91*, 1957–1975.

Arzua, T., Yan, Y., Jiang, C., Logan, S., Allison, R.L., Wells, C., Kumar, S.N., Schäfer, R., and Bai, X. (2020). Modeling alcohol-induced neurotoxicity using human induced pluripotent stem cell-derived three-dimensional cerebral organoids. Translational Psychiatry *10*, 347.

Asim, M., Sarma, M.P., Thayumanavan, L., and Kar, P. (2011). Role of Aflatoxin B1 as a risk for primary liver cancer in north Indian population. Clinical Biochemistry *44*, 1235–1240.

Atanasova, S.Y., von Ahsen, N., Toncheva, D.I., Dimitrov, T.G., Oellerich, M., and Armstrong, V.W. (2005). Genetic polymorphisms of cytochrome P450 among patients with Balkan endemic nephropathy (BEN). Clinical Biochemistry *38*, 223–228.

Attaluri, S., Bonala, R.R., Yang, I.Y., Lukin, M.A., Wen, Y., Grollman, A.P., Moriya, M., Iden, C.R., and Johnson, F. (2009). DNA adducts of aristolochic acid II: Total synthesis and site-specific mutagenesis studies in mammalian cells. Nucleic Acids Research *38*, 339–352.

Augustyniak, J., Bertero, A., Coccini, T., Baderna, D., Buzanska, L., and Caloni, F. (2019). Organoids are promising tools for species-specific in vitro toxicological studies. Journal of Applied Toxicology *39*, 1–13.

Baird, W.M., Hooven, L.A., and Mahadevan, B. (2005). Carcinogenic polycyclic aromatic hydrocarbon-DNA adducts and mechanism of action. Environmental and Molecular Mutagenesis *45*, 106–114.

Baker, S.C., Arlt, V.M., Indra, R., Joel, M., Stiborová, M., Eardley, I., Ahmad, N., Otto, W., Burger, M., Rubenwolf, P., et al. (2018). Differentiation-associated urothelial

cytochrome P450 oxidoreductase predicates the xenobiotic-metabolizing activity of “luminal” muscle-invasive bladder cancers. Molecular Carcinogenesis *57*, 606–618.

Balansky, R., Ganchev, G., Iltcheva, M., Steele, V.E., D’Agostini, F., and de Flora, S. (2007). Potent carcinogenicity of cigarette smoke in mice exposed early in life. Carcinogenesis *28*, 2236–2243.

Barker, N., van Es, J.H., Kuipers, J., Kujala, P., van den Born, M., Cozijnsen, M., Haegebarth, A., Korving, J., Begthel, H., Peters, P.J., et al. (2007). Identification of stem cells in small intestine and colon by marker gene Lgr5. Nature *449*, 1003–1007.

Barker, N., Huch, M., Kujala, P., van de Wetering, M., Snippert, H.J., van Es, J.H., Sato, T., Stange, D.E., Begthel, H., van den Born, M., et al. (2010). Lgr5+ve Stem Cells Drive Self-Renewal in the Stomach and Build Long-Lived Gastric Units In Vitro. Cell Stem Cell *6*, 25–36.

Barnes, J.L., Zubair, M., John, K., Poirier, M.C., and Martin, F.L. (2018). Carcinogens and DNA damage (Portland Press Ltd).

Bárta, F., Levová, K., Frei, E., Schmeiser, H.H., Arlt, V.M., and Stiborová, M. (2014). The effect of aristolochic acid I on expression of NAD(P)H:quinone oxidoreductase in mice and rats—A comparative study. Mutation Research/Genetic Toxicology and Environmental Mutagenesis *768*, 1–7.

Bartfeld, S., Bayram, T., van de Wetering, M., Huch, M., Begthel, H., Kujala, P., Vries, R., Peters, P.J., and Clevers, H. (2015). In vitro expansion of human gastric epithelial stem cells and their responses to bacterial infection. Gastroenterology *148*, 126-136.e6.

Battilani, P., Toscano, P., van der Fels-Klerx, H.J., Moretti, A., Camardo Leggieri, M., Brera, C., Rortais, A., Goumperis, T., and Robinson, T. (2016). Aflatoxin B 1 contamination in maize in Europe increases due to climate change. Scientific Reports *6*, 1–7.

Baudy, A.R., Otieno, M.A., Hewitt, P., Gan, J., Roth, A., Keller, D., Sura, R., van Vleet, T.R., and Proctor, W.R. (2020). Liver microphysiological systems development guidelines for safety risk assessment in the pharmaceutical industry. Lab on a Chip *20*, 215–225.

Baylin, S.B., and Jones, P.A. (2016). Epigenetic determinants of cancer. Cold Spring Harbor Perspectives in Biology *8*, 1–35.

Bellamri, M., Xiao, S., Murugan, P., Weight, C.J., and Turesky, R.J. (2018). Metabolic activation of the cooked meat carcinogen 2-amino-1-methyl-6-phenylimidazo[4,5-b]pyridine in human prostate. Toxicological Sciences *163*, 543–556.

Benkerroum, N. (2020). Chronic and acute toxicities of aflatoxins: Mechanisms of action. International Journal of Environmental Research and Public Health *17*, 1–28.

Berkers, G., van Mourik, P., Vonk, A.M., de Jonge, H.R., Beekman, J.M., and van Der, C.K. (2019). Rectal Organoids Enable Personalized Treatment of Cystic Fibrosis. Cell Reports *26*, 1701-1708.e3.

Bertram, J.S. (2001). The molecular biology of cancer. Molecular Aspects of Medicine *21*, 167–223.

Besaratinia, A., Kim, S. in, Hainaut, P., and Pfeifer, G.P. (2009). In Vitro Recapitulating of TP53 Mutagenesis in Hepatocellular Carcinoma Associated With Dietary Aflatoxin B1 Exposure. Gastroenterology *137*, 1127–1137.

Bhatia, M., McGrath, K.L., di Trapani, G., Charoentong, P., Shah, F., King, M.M., Clarke, F.M., and Tonissen, K.F. (2016). The thioredoxin system in breast cancer cell invasion and migration. Redox Biology *8*, 68–78.

Blanpain, C., Mohrin, M., Sotiropoulou, P.A., and Passegué, E. (2011). DNA-damage response in tissue-specific and cancer stem cells. Cell Stem Cell *8*, 16–29.

Boj, S.F., Hwang, C. il, Baker, L.A., Chio, I.I.C., Engle, D.D., Corbo, V., Jager, M., Ponz-Sarvise, M., Tiriac, H., Spector, M.S., et al. (2015). Organoid models of human and mouse ductal pancreatic cancer. Cell *160*, 324–338.

Boobis, A.R., Lynch, A.M., Murray, S., de la Torre, R., Solans, A., Farre, M., Segura, J., Gooderham, N.J., and Davies, D.S. (1994). CYPlA2-catalyzed Conversion of Dietary Heterocyclic Amines to Their Proximate Carcinogens Is Their Major Route of Metabolism in Humans. Cancer Research *54*, 89–94.

Boström, C.E., Gerde, P., Hanberg, A., Jernström, B., Johansson, C., Kyrklund, T., Rannug, A., Törnqvist, M., Victorin, K., and Westerholm, R. (2002). Cancer risk assessment, indicators, and guidelines for polycyclic aromatic hydrocarbons in the ambient air. Environmental Health Perspectives *110*, 451–488.

Boysen, G., and Hecht, S.S. (2003). Analysis of DNA and protein adducts of benzo[a]pyrene in human tissues using structure-specific methods. Mutation Research - Reviews in Mutation Research *543*, 17–30.

Branzei, D., and Foiani, M. (2008). Regulation of DNA repair throughout the cell cycle. Nature Reviews Molecular Cell Biology *9*, 297–308.

Brookes, P., and Lawley, P.D. (1964). Evidence for the binding of polynuclear aromatic hydrocarbons to the nucleic acids of mouse skin: Relation between carcinogenic power of hydrocarbons and their binding to deoxyribonucleic acid. Nature *202*, 781–784.

Broutier, L., Andersson-Rolf, A., Hindley, C.J., Boj, S.F., Clevers, H., Koo, B.K., and Huch, M. (2016). Culture and establishment of self-renewing human and mouse adult liver and pancreas 3D organoids and their genetic manipulation. Nature Protocols *11*, 1724–1743.

Brown, K.F., Rumgay, H., Dunlop, C., Ryan, M., Quartly, F., Cox, A., Deas, A., Elliss-brookes, L., Gavin, A., Hounsome, L., et al. (2018). The fraction of cancer attributable to modifiable risk factors in England , Wales , Scotland , Northern Ireland , and the United Kingdom in 2015. British Journal of Cancer *118*, 1130–1141.

Bu, Q., Huang, Y., Li, M., Dai, Y., Fang, X., Chen, K., Liu, Q., Xue, A., Zhong, K., Huang, Y., et al. (2020). Acrylamide exposure represses neuronal differentiation, induces cell apoptosis and promotes tau hyperphosphorylation in hESC-derived 3D cerebral organoids. Food and Chemical Toxicology *144*, 111643.

Caiment, F., Gaj, S., Claessen, S., and Kleinjans, J. (2015). High-throughput data integration of RNA-miRNA-circRNA reveals novel insights into mechanisms of benzo[a]pyrene-induced carcinogenicity. Nucleic Acids Research *43*, 2525–2534.

Caipa Garcia, A.L., Arlt, V.M., and Phillips, D.H. (2022). Organoids for toxicology and genetic toxicology: applications with drugs and prospects for environmental carcinogenesis. Mutagenesis *37*, 143–154.

Calandrini, C., Schutgens, F., Oka, R., Margaritis, T., Candelli, T., Mathijsen, L., Ammerlaan, C., van Ineveld, R.L., Derakhshan, S., de Haan, S., et al. (2020). An organoid biobank for childhood kidney cancers that captures disease and tissue heterogeneity. Nature Communications *11*, 1–14.

Cantwell, M., Mittl, B., Curtin, J., Carroll, R., Potischman, N., Caporaso, N., and Sinha, R. (2004). Relative Validity of a Food Frequency Questionnaire with a Meat-Cooking and Heterocyclic Amine Module. Cancer Epidemiology Biomarkers and Prevention *13*, 293–298.

Chakravarti, D., Venugopal, D., Mailander, P.C., Meza, J.L., Higginbotham, S., Cavalieri, E.L., and Rogan, E.G. (2008). The role of polycyclic aromatic hydrocarbon-DNA adducts in inducing mutations in mouse skin. Mutation Research - Genetic Toxicology and Environmental Mutagenesis *649*, 161–178.

Chang, S.-Y., Weber, E.J., Sidorenko, V.S., Chapron, A., Yeung, C.K., Gao, C., Mao, Q., Shen, D., Wang, J., Rosenquist, T.A., et al. (2017). Human liver-kidney model elucidates the mechanisms of aristolochic acid nephrotoxicity. JCI Insight *2*, e95978.

Chang, Y., Siddens, L.K., Heine, L.K., Sampson, D.A., Yu, Z., Fischer, K.A., Löhr, C. v, and Tilton, S.C. (2019). Comparative mechanisms of PAH toxicity by benzo[a]pyrene

and dibenzo[def,p]chrysene in primary human bronchial epithelial cells cultured at air-liquid interface. Toxicology & Applied Pharmacology *379*, 114644.

Chao, M.-R., Evans, M.D., Hu, C.-W., Ji, Y., Møller, P., Rossner, P., and Cooke, M.S. (2021). Biomarkers of nucleic acid oxidation – A summary state-of-the-art. Redox Biology *42*, 101872.

Chau, D.Y.S., Johnson, C., MacNeil, S., Haycock, J.W., and Ghaemmaghami, A.M. (2013). The development of a 3D immunocompetent model of human skin. Biofabrication *5*, 035011.

Chawanthayatham, S., Thiantanawat, A., Egner, P.A., Groopman, J.D., Wogan, G.N., Croy, R.G., and Essigmann, J.M. (2015). Prenatal exposure of mice to the human liver carcinogen Aflatoxin B 1 reveals a critical window of susceptibility to genetic change. International Journal of Cancer *136*, 1254–1262.

Chen, C.H., Dickman, K.G., Moriya, M., Zavadil, J., Sidorenko, V.S., Edwards, K.L., Gnatenko, D. v., Wu, L., Turesky, R.J., Wu, X.R., et al. (2012). Aristolochic acid-associated urothelial cancer in Taiwan. Proc Natl Acad Sci U S A *109*, 8241–8246.

Chen, J., Yang, S., Li, P., Wu, A., Nepovimova, E., Long, M., Wu, W., and Kuca, K. (2022). MicroRNA regulates the toxicological mechanism of four mycotoxins in vivo and in vitro. Journal of Animal Science and Biotechnology *13*, 1–12.

Chen, L., Devanesan, P.D., Higginbotham, S., Ariese, F., Jankowiak, R., Small, G.J., Rogan, E.G., and Cavalieri, E.L. (1996). Expanded analysis of benzo[a]pyrene-DNA adducts formed in vitro and in mouse skin: Their significance in tumor initiation. Chemical Research in Toxicology *9*, 897–903.

Chen, T., Guo, L., Zhang, L., Shi, L., Fang, H., Sun, Y., Fuscoe, J.C., and Mei, N. (2006). Gene expression profiles distinguish the carcinogenic effects of aristolochic acid in target (kidney) and non-target (liver) tissues in rats. BMC Bioinformatics *7*, 1–13.

Christmann, M., Boisseau, C., Kitzinger, R., Berac, C., Allmann, S., Sommer, T., Aasland, D., Kaina, B., and Tomicic, M.T. (2016). Adaptive upregulation of DNA repair genes following benzo(a)pyrene diol epoxide protects against cell death at the expense of mutations. Nucleic Acids Research *44*, 10727–10743.

Clark, J.M. (2018). The 3Rs in research: a contemporary approach to replacement, reduction and refinement. British Journal of Nutrition *120*, S1–S7.

Clevers, H. (2016). Modeling Development and Disease with Organoids. Cell *165*, 1586–1597.

Clevers, H., Loh, K.M., and Nusse, R. (2014). An integral program for tissue renewal and regeneration: Wnt signaling and stem cell control. Science (1979) *346*, 1248012.

Cogliano, V.J., Baan, R., Straif, K., Grosse, Y., Lauby-Secretan, B., Ghissassi, F. el, Bouvard, V., Benbrahim-Tallaa, L., Guha, N., Freeman, C., et al. (2011). Preventable exposures associated with human cancers. J Natl Cancer Inst *103*, 1827–1839.

Conney, A.H., Miller, E.C., and Miller, J.A. (1956). The metabolism of methylated aminoazo dyes V. Evidence for induction of enzyme synthesis in the rat by 3-methylcholanthrene. Cancer Research *16*, 450–459.

Conway, G.E., Shah, U.-K., Llewellyn, S., Cervena, T., Evans, S.J., al Ali, A.S., Jenkins, G.J., Clift, M.J.D., and Doak, S.H. (2020). Adaptation of the in vitro micronucleus assay for genotoxicity testing using 3D liver models supporting longer-term exposure durations. Mutagenesis *35*, 319–329.

Cook, J.W., Hewett, L., and Hieger, I. (1933). The isolation of a cancer-producing hydrocarbon from coal tar. J Chem Soc *106*, 395–405.

Coskun, E., Jaruga, P., Vartanian, V., Erdem, O., Egner, P.A., Groopman, J.D., Lloyd, R.S., and Dizdaroglu, M. (2019). Aflatoxin-Guanine DNA Adducts and Oxidatively Induced DNA Damage in Aflatoxin-Treated Mice in Vivo as Measured by Liquid

Chromatography-Tandem Mass Spectrometry with Isotope Dilution. Chemical Research in Toxicology *32*, 80–89.

Crespo, M., Vilar, E., Tsai, S.-Y., Chang, K., Amin, S., Srinivasan, T., Zhang, T., Pipalia, N.H., Chen, H.J., Witherspoon, M., et al. (2017). Colonic organoids derived from human induced pluripotent stem cells for modeling colorectal cancer and drug testing. Nature Medicine *23*, 878–884.

Croy, R.G., and Wogan, G.N. (1981). Temporal Patterns Of Covalent Dna Adducts In Rat Liver After Single And Multiple Doses Of Aflatoxin B. Cancer Research *41*, 197–203.

Cupid, B.C., Lightfoot, T.J., Russell, D., Gant, S.J., Turner, P.C., Dingley, K.H., Curtis, K.D., Leveson, S.H., Turteltaub, K.W., and Garner, R.C. (2004). The formation of AFB1-macromolecular adducts in rats and humans at dietary levels of exposure. Food and Chemical Toxicology *42*, 559–569.

Danaei, G., vander Hoorn, S., Lopez, A.D., Murray, C.J.L., Ezzati, M., and Group, C.R.A. collaborating (2005). Causes of cancer in the world: Comparative risk assessment of nine behavioural and environmental risk factors. Lancet *366*, 1784–1793.

David, R.M., and Gooderham, N.J. (2016). Using 3D MCF-7 mammary spheroids to assess the genotoxicity of mixtures of the food-derived carcinogens benzo[a]pyrene and 2-amino-1-methyl-6-phenylimidazo[4,5-b]pyridine. Toxicology Research *5*, 312–317.

Debelle, F.D., Vanherweghem, J.L., and Nortier, J.L. (2008). Aristolochic acid nephropathy: A worldwide problem. Kidney International *74*, 158–169.

Dekkers, J.F., Wiegerinck, C.L., de Jonge, H.R., Bronsveld, I., Janssens, H.M., de Winter-de Groot, K.M., Brandsma, A.M., de Jong, N.W.M., Bijvelds, M.J.C., Scholte, B.J., et al. (2013). A functional CFTR assay using primary cystic fibrosis intestinal organoids. Nature Medicine *19*, 939–945.

Deng, J., Zhao, L., Zhang, N.-Y., Karrow, N.A., Krumm, C.S., Qi, D.-S., and Sun, L.-H. (2018). Aflatoxin B1 metabolism: Regulation by phase I and II metabolizing enzymes and chemoprotective agents. Mutation Research/Reviews in Mutation Research *778*, 79–89.

Devall, M., Jennelle, L.T., Bryant, J., Bien, S., Peters, U., Powell, S., and Casey, G. (2020). Modeling the effect of prolonged ethanol exposure on global gene expression and chromatin accessibility in normal 3D colon organoids. PLoS ONE *15*, e0227116.

Dračínská, H., Bárta, F., Levová, K., Hudecová, A., Moserová, M., Schmeiser, H.H., Kopka, K., Frei, E., Arlt, V.M., Stiborová, M., et al. (2016). Induction of cytochromes P450 1A1 and 1A2 suppresses formation of DNA adducts by carcinogenic aristolochic acid I in rats in vivo. Toxicology *344–346*, 7–18.

Dračínská, H., Indra, R., Jelínková, S., Černá, V., Arlt, V.M., and Stiborová, M. (2021). Benzo[a]pyrene-induced genotoxicity in rats is affected by co-exposure to sudan i by altering the expression of biotransformation enzymes. International Journal of Molecular Sciences *22*, 8062.

Dreij, K., Rhrissorrakrai, K., Gunsalus, K.C., Geacintov, N.E., and Scicchitano, D.A. (2010). Benzo[a]pyrene diol epoxide stimulates an inflammatory response in normal human lung fibroblasts through a p53 and JNK mediated pathway. Carcinogenesis *31*, 1149.

Dundon, M., Madden, O., and Comizzoli, P. (2019). Three-dimensional culture of endometrial cells from domestic cats: A new in vitro platform for assessing plastic toxicity. PLoS ONE *14*, e0217365.

Egner, P.A., Wang, J.-B., Zhu, Y.-R., Zhang, B.-C., Wu, Y., Zhang, Q.-N., Qian, G.-S., Kuang, S.-Y., Gange, S.J., Jacobson, L.P., et al. (2001). Chlorophyllin intervention reduces aflatoxin-DNA adducts in individuals at high risk for liver cancer. Proceedings of the National Academy of Sciences *98*, 14601–14606.

Egner, P.A., Groopman, J.D., Wang, J.S., Kensler, T.W., and Friesen, M.D. (2006). Quantification of aflatoxin-B1-N7-guanine in human urine by high-performance liquid

chromatography and isotope dilution tandem mass spectrometry. Chemical Research in Toxicology *19*, 1191–1195.

Eiraku, M., Takata, N., Ishibashi, H., Kawada, M., Sakakura, E., Okuda, S., Sekiguchi, K., Adachi, T., and Sasai, Y. (2011). Self-organizing optic-cup morphogenesis in three-dimensional culture. Nature *472*, 51–56.

Elje, E., Hesler, M., Rundén-Pran, E., Mann, P., Mariussen, E., Wagner, S., Dusinska, M., and Kohl, Y. (2019). The comet assay applied to HepG2 liver spheroids. Mutation Research - Genetic Toxicology and Environmental Mutagenesis *845*, 403033.

Engin, A.B., and Engin, A. (2019). DNA damage checkpoint response to aflatoxin B1. Environmental Toxicology and Pharmacology *65*, 90–96.

Felton, J.S., Knize, M.G., and Shen, N.H. (1986). Identification of the mutagens in cooked beef. Environmental Health Perspectives *VOL. 67*, 17–24.

Finkbeiner, S.R., Zeng, X.-L., Utama, B., Atmar, R.L., Shroyer, N.F., and Estes, M.K. (2012). Stem Cell-Derived Human Intestinal Organoids as an Infection Model for Rotaviruses. MBio *3*, e00159-12.

Finkbeiner, S.R., Hill, D.R., Altheim, C.H., Dedhia, P.H., Taylor, M.J., Tsai, Y.H., Chin, A.M., Mahe, M.M., Watson, C.L., Freeman, J.J., et al. (2015). Transcriptome-wide Analysis Reveals Hallmarks of Human Intestine Development and Maturation In Vitro and In Vivo. Stem Cell Reports *4*, 1140–1155.

Fischer, B.M., Neumann, D., Piberger, A.L., Risnes, S.F., Köberle, B., and Hartwig, A. (2016). Use of high-throughput RT-qPCR to assess modulations of gene expression profiles related to genomic stability and interactions by cadmium. Archives of Toxicology *90*, 2745–2761.

Flaten, G.E., Palac, Z., Engesland, A., Filipović-Grčić, J., Vanić, Ž., and Škalko-Basnet, N. (2015). In vitro skin models as a tool in optimization of drug formulation. European Journal of Pharmaceutical Sciences *75*, 10–24.

Fluidigm.com (2021). https://store.fluidigm.com/Genomics/ApplicationsGenomics/

GeneExpression/96-96 Dynamic Array™ IFC for Gene Expression

Forsythe, S.D., Devarasetty, M., Shupe, T., Bishop, C., Atala, A., Soker, S., and Skardal, A. (2018). Environmental Toxin Screening Using Human-Derived 3D Bioengineered Liver and Cardiac Organoids. Frontiers in Public Health *6*, 103.

Fretland, A.J., Devanaboyina, U.S., Nangju, N.A., Leff, M.A., Xiao, G.H., Webb, S.J., Doll, M.A., and Hein, D.W. (2001a). DNA adduct levels and absence of tumors in female rapid and slow acetylator congenic hamsters administered the rat mammary carcinogen 2-amino-1-methyl-6-phenylimidazo[4,5-b]pyridine. Journal of Biochemical and Molecular Toxicology *15*, 26–33.

Fretland, A.J., Devanaboyina, U.S., Feng, Y., Leff, M.A., Xiao, G.H., Webb, S.J., and Hein, D.W. (2001b). Oral administration of 2-amino-1-methyl-6-phenylimidazo[4,5-b]pyridine (PhIP) yields PhIP-DNA adducts but not tumors in male syrian hamsters congenic at the n-acetyltransferase 2 (NAT2) locus. Toxicological Sciences *59*, 226–230.

Fujii, M., Matano, M., Toshimitsu, K., Takano, A., Mikami, Y., Nishikori, S., Sugimoto, S., and Sato, T. (2018). Human Intestinal Organoids Maintain Self-Renewal Capacity and Cellular Diversity in Niche-Inspired Culture Condition. Cell Stem Cell *23*, 787-793.e6.

Gallagher, E.P., Kunze, K.L., Stapleton, P.L., and Eaton, D.L. (1996). The kinetics of aflatoxin B1 oxidation by human cDNA-expressed and human liver microsomal cytochromes P450 1A2 and 3A4. Toxicology and Applied Pharmacology *141*, 595–606.

Gearhart-Serna, L.M., Davis, J.B., Jolly, M.K., Jayasundara, N., Sauer, S.J., Giulio, R.T. di, and Devi, G.R. (2020). A polycyclic aromatic hydrocarbon-enriched environmental chemical mixture enhances AhR, antiapoptotic signaling and a proliferative phenotype in breast cancer cells. Carcinogenesis *41*, 1648–1659.

Georgakopoulos, N., Prior, N., Angres, B., Mastrogiovanni, G., Cagan, A., Harrison, D., Hindley, C.J., Arnes-Benito, R., Liau, S.S., Curd, A., et al. (2020). Long-term expansion,

genomic stability and in vivo safety of adult human pancreas organoids. BMC Developmental Biology *20*, 1–20.

Gilson, P., Drouot, G., Witz, A., Merlin, J.L., Becuwe, P., and Harlé, A. (2019). Emerging roles of DDB2 in cancer. International Journal of Molecular Sciences *20*, 5168.

Ginzkey, C., Friehs, G., Koehler, C., Hackenberg, S., Voelker, H.U., Richter, E., and Kleinsasser, N.H. (2010). Nicotine and methyl methane sulfonate in mini organ cultures of human parotid gland tissue. Toxicology Letters *197*, 69–74.

Girard, H., Thibaudeau, J., Court, M.H., Fortier, L.C., Villeneuve, L., Caron, P., Hao, Q., von Moltke, L.L., Greenblatt, D.J., and Guillemette, C. (2005). UGT1A1 polymorphisms are important determinants of dietary carcinogen detoxification in the liver. Hepatology *42*, 448–457.

GlutaMAX^{TM} Supplement (2021). https://www.thermofisher.com/order/catalog/

product/35050061#/35050061

Gökmen, M.R., Cosyns, J.-P., Arlt, V.M., Stiborová, M., Phillips, D.H., Schmeiser, H.H., Simmonds, M.S.J., Cook, H.T., Vanherweghem, J.-L., Nortier, J.L., et al. (2013). The epidemiology, diagnosis, and management of aristolochic acid nephropathy: a narrative review. Annals of Internal Medicine *158*, 469–477.

Gonzalez, F.J., and Kimura, S. (2001). Understanding the role of xenobiotic-metabolism in chemical carcinogenesis using gene knockout mice. Mutation Research *477*, 79–87.

Gooderham, N.J., Creton, S., Lauber, S.N., and Zhu, H. (2007). Mechanisms of action of the carcinogenic heterocyclic amine PhIP. Toxicology Letters *168*, 269–277.

Gorlewska-Roberts, K., Green, B., Fares, M., Ambrosone, C.B., and Kadlubar, F.F. (2002). Carcinogen-DNA adducts in human breast epithelial cells. Environmental and Molecular Mutagenesis *39*, 184–192.

Götz, C., Pfeiffer, R., Tigges, J., Blatz, V., Jäckh, C., Freytag, E.-M.M., Fabian, E., Landsiedel, R., Merk, H.F., Krutmann, J., et al. (2012). Xenobiotic metabolism capacities

of human skin in comparison with a 3D epidermis model and keratinocyte-based cell culture as in vitro alternatives for chemical testing: activating enzymes (Phase I). Experimental Dermatology *21*, 358–363.

Gouas, D., Shi, H., and Hainaut, P. (2009). The aflatoxin-induced TP53 mutation at codon 249 (R249S): Biomarker of exposure, early detection and target for therapy. Cancer Letters *286*, 29–37.

Grabinger, T., Luks, L., Kostadinova, F., Zimberlin, C., Medema, J.P., Leist, M., and Brunner, T. (2014). Ex vivo culture of intestinal crypt organoids as a model system for assessing cell death induction in intestinal epithelial cells and enteropathy. Cell Death and Disease *5*, e1228-10.

Greggio, C., de Franceschi, F., Figueiredo-Larsen, M., Gobaa, S., Ranga, A., Semb, H., Lutolf, M., and Grapin-Botton, A. (2013). Artificial three-dimensional niches deconstruct pancreas development in vitro. Development *140*, 4452–4462.

Grollman, A.P., Shibutani, S., Moriya, M., Miller, F., Wu, L., Moll, U., Suzuki, N., Fernandes, A., Rosenquist, T., Medverec, Z., et al. (2007). Aristolochic acid and the etiology of endemic (Balkan) nephropathy. Proc Natl Acad Sci U S A *104*, 12129.

Groopman, J.D., Croyt, R.G., and Wogan, G.N. (1981). In vitro reactions of aflatoxin B1-adducted DNA (high-pressure liquid chromatography/carcinogen-nucleic acid interactions). Proceedings of the National Academy of Sciences *78*, 5445–5449.

Guengerich, F.P., Johnson, W.W., Shimada, T., Ueng, Y.F., Yamazaki, H., and Langouët, S. (1998). Activation and detoxication of aflatoxin B1. Mutation Research - Fundamental and Molecular Mechanisms of Mutagenesis *402*, 121–128.

Gursoy-Yuzugullu, O., Yuzugullu, H., Yilmaz, M., and Ozturk, M. (2011). Aflatoxin genotoxicity is associated with a defective DNA damage response bypassing p53 activation. Liver International *31*, 561–571.

Guyton, K.Z., Rieswijk, L., Wang, A., Chiu, W.A., and Smith, M.T. (2018a). Key Characteristics Approach to Carcinogenic Hazard Identification. Chemical Research in Toxicology *31*, 1290–1292.

Guyton, K.Z., Rusyn, I., Chiu, W.A., Corpet, D.E., van den Berg, M., Ross, M.K., Christiani, D.C., Beland, F.A., and Smith, M.T. (2018b). Application of the key characteristics of carcinogens in cancer hazard identification. Carcinogenesis *39*, 614–622.

Hackenberg, S., Zimmermann, F.-Z., Scherzed, A., Friehs, G., Froelich, K., ChristianGinzkey, Koehler, C., Burghartz, M., Hagen, R., and Kleinsasser, N. (2011). Repetitive Exposure to Zinc Oxide Nanoparticles Induces DNA Damage in Human Nasal Mucosa Mini Organ Cultures. Environmental AndMolecularMutagenesis *52*, 582–589.

Haerani, H., Apan, A., and Basnet, B. (2020). The climate-induced alteration of future geographic distribution of aflatoxin in peanut crops and its adaptation options. Mitigation and Adaptation Strategies for Global Change *25*, 1149–1175.

Hakem, R. (2008). DNA-damage repair; the good, the bad, and the ugly. EMBO Journal *27*, 589–605.

Hamid, A.S., Tesfamariam, S.G., Zhang, Y., and Zhang, Z.G. (2013). Aflatoxin B1-induced hepatocellular carcinoma in developing countries: Geographical distribution, mechanism of action and prevention (Review). Oncology Letters *5*, 1087–1092.

Hamouchene, H., Arlt, V.M., Giddings, I., and Phillips, D.H. (2011). Influence of cell cycle on responses of MCF-7 cells to benzo[a]pyrene. BMC Genomics *12*, 333.

Han, J., Xian, Z., Zhang, Y., Liu, J., and Liang, A. (2019). Systematic overview of aristolochic acids: Nephrotoxicity, carcinogenicity, and underlying mechanisms. Frontiers in Pharmacology *10*, 648.

Hanahan, D., and Weinberg, R.A. (2000). The Hallmarks of Cancer. Cell *100*, 57–70.

Hanahan, D., and Weinberg, R.A. (2011). Hallmarks of cancer: The next generation. Cell *144*, 646–674.

Harris, J.R., Hjelmborg, J., Adami, H.-O., Czene, K., Mucci, L., Kaprio, J., and Nordic Twin Study of Cancer (NorTwinCan) Collaboration (2019). The Nordic twin study on cancer - NorTwinCan. Twin Research and Human Genetics *22*, 817–823.

Harrison, J.C., Carvajal, M., and Garner', R.C. (1993). Does Aflatoxin Exposure in the United Kingdom Constitute a Cancer Risk? Environmental Health Perspectives *99*, 99–105.

Heinrich, M., Chan, J., Wanke, S., Neinhuis, C., and Simmonds, M.S.J. (2009). Local uses of Aristolochia species and content of nephrotoxic aristolochic acid 1 and 2-A global assessment based on bibliographic sources. Journal of Ethnopharmacology *125*, 108–144.

Henry, S.A. (1946). Occupational cutaneous cancer atributable to certain chemicals in industry. British Medical Bulletin *4*, 389–401.

HEPES (2021). https://www.thermofisher.com/uk/en/home/life-science/cell-culture/mammalian-cell-culture/reagents/hepes.html

Hernández, L.G., van Steeg, H., Luijten, M., and van Benthem, J. (2009). Mechanisms of non-genotoxic carcinogens and importance of a weight of evidence approach. Mutation Research - Reviews in Mutation Research *682*, 94–109.

hES Cell Cloning & Recovery Supplement (2021). https://www.reprocell.com/product-catalog/small-molecules/hes-cell-cloning-recovery-supplement

Hill, J. (1761). Cautions against the immoderate use of snuff: founded on the known qualities of the tobacco plant : and the effects it must produce when this way taken into the body : and enforced by instances of persons who have perished miserably of diseases, occasione.

Hoang, M.L., Chen, C.-H., Chen, P.-C., Roberts, N.J., Dickman, K.G., Yun, B.H., Turesky, R.J., Pu, Y.-S., Vogelstein, B., Papadopoulos, N., et al. (2016). Aristolochic Acid in the Etiology of Renal Cell Carcinoma. Cancer Epidemiology and Prevention Biomarkers *25*, 1600–1609.

Hockley, S.L., Arlt, V.M., Brewer, D., Giddings, I., and Phillips, D.H. (2006). Time-and concentration-dependent changes in gene expression induced by benzo(a)pyrene in two human cell lines, MCF-7 and HepG2. BMC Bioinformatics *7*, 260.

Hockley, S.L., Arlt, V.M., Brewer, D., te Poele, R., Workman, P., Giddings, I., and Phillips, D.H. (2007). AHR- and DNA-damage-mediated gene expression responses induced by benzo(a)pyrene in human cell lines. Chemical Research in Toxicology *20*, 1797–1810.

Holme, J.A., Gorria, M., Arlt, V.M., Øvrebø, S., Solhaug, A., Tekpli, X., Landvik, N.E., Huc, L., Fardel, O., and Lagadic-Gossmann, D. (2007). Different mechanisms involved in apoptosis following exposure to benzo[a]pyrene in F258 and Hepa1c1c7 cells. Chemico-Biological Interactions *167*, 41–55.

Hölzl-Armstrong, L., Nævisdal, A., Cox, J.A., Long, A.S., Chepelev, N.L., Phillips, D.H., White, P.A., and Arlt, V.M. (2020). In vitro mutagenicity of selected environmental carcinogens and their metabolites in MutaMouse FE1 lung epithelial cells. Mutagenesis *35*, 453–463.

Hölzl-Armstrong, L., Moody, S., Kucab, J.E., Zwart, E.P., Bellamri, M., Luijten, M., Turesky, R.J., Stratton, M.R., Arlt, V.M., and Phillips, D.H. (2021). Mutagenicity of 2-hydroxyamino-1-methyl-6-phenylimidazo[4,5-b]pyridine (N–OH-PhIP) in human TP53 knock-in (Hupki) mouse embryo fibroblasts. Food and Chemical Toxicology *147*, 111855.

Hou, H., Sun, D., and Zhang, X. (2019). The role of MDM2 amplification and overexpression in therapeutic resistance of malignant tumors. Cancer Cell International *19*, 216.

Howell, K.J., Kraiczy, J., Nayak, K.M., Gasparetto, M., Ross, A., Lee, C., Mak, T.N., Koo, B.-K., Kumar, N., Lawley, T., et al. (2018). DNA methylation and transcription patterns in intestinal epithelial cells from pediatric patients with inflammatory bowel diseases differentiate disease subtypes and associate with outcome. Gastroenterology *154*, 585–598.

Hsieh, L.-L., and Hsieh, T.T. (1993). Detection of aflatoxin B1-DNA adducts in human placenta and cord blood. Cancer Research *53*, 1278–1280.

Hu, Z., and Wells, P.G. (2004). Human interindividual variation in lymphocyte UDP-Glucuronosyltransferases as a determinant of in vitro benzo[a]pyrene covalent binding and cytotoxicity. Toxicological Sciences *78*, 32–40.

Hu, H., Gehart, H., Artegiani, B., LÖpez-Iglesias, C., Dekkers, F., Basak, O., van Es, J., Chuva de Sousa Lopes, S.M., Begthel, H., Korving, J., et al. (2018). Long-term expansion of functional mouse and human hepatocytes as 3D organoids. Cell *175*, 1591–1606.

Huang, L., Holtzinger, A., Jagan, I., Begora, M., Lohse, I., Ngai, N., Nostro, C., Wang, R., Muthuswamy, L.B., Crawford, H.C., et al. (2015). Ductal pancreatic cancer modeling and drug screening using human pluripotent stem cell- and patient-derived tumor organoids. Nature Medicine *21*, 1364–1371.

Huch, M., Bonfanti, P., Boj, S.F., Sato, T., Loomans, C.J.M., van de Wetering, M., Sojoodi, M., Li, V.S.W., Schuijers, J., Gracanin, A., et al. (2013a). Unlimited in vitro expansion of adult bi-potent pancreas progenitors through the Lgr5/R-spondin axis. EMBO Journal *32*, 2708–2721.

Huch, M., Dorrell, C., Boj, S.F., van Es, J.H., Li, V.S.W., van de Wetering, M., Sato, T., Hamer, K., Sasaki, N., Finegold, M.J., et al. (2013b). In vitro expansion of single Lgr5 + liver stem cells induced by Wnt-driven regeneration. Nature *494*, 247–250.

Huch, M., Gehart, H., van Boxtel, R., Hamer, K., Blokzijl, F., Verstegen, M.M.A., Ellis, E., van Wenum, M., Fuchs, S.A., de Ligt, J., et al. (2015). Long-term culture of genome-stable bipotent stem cells from adult human liver. Cell *160*, 299–312.

Hussain, S.P., Schwank, J., Staib, F., Wang, X.W., and Harris, C.C. (2007). TP53 mutations and hepatocellular carcinoma: Insights into the etiology and pathogenesis of liver cancer. Oncogene *26*, 2166–2176.

IARC (1993). Some naturally occurring substances: Food items and constituents, heterocyclic aromatic amines and mycotoxins. Monographs on the Evaluation of Carcinogenic Risks to Humans *56*.

IARC (2002). Some traditional herbal medicines, some mycotoxins, naphthalene and styrene. Monographs on the Evaluation of Carcinogenic Risks to Humans *82*.

IARC (2012a). Chemical agents and related occupations. Monographs on the Evaluation of Carcinogenic Risks to Humans *100 F*, 111–144.

IARC (2012b). Pharmaceuticals. Monographs on the Evaluation of Carcinogenic Risks to Humans *100A*, 347–361.

Iqbal, W., Demidova, E. v., Serrao, S., ValizadehAslani, T., Rosen, G., and Arora, S. (2021). RRM2B Is Frequently Amplified Across Multiple Tumor Types: Implications for DNA Repair, Cellular Survival, and Cancer Therapy. Frontiers in Genetics *12*, 1–13.

Ito, N., Hasegawa, R., Sano, M., Tamano, S., Esumi, H., Takayama, S., and Sugimura, T. (1991). A new colon and mammary carcinogen in cooked food, 2-amino-l-methyl-6-phenylimidazo[4,5-b]pyridine (PhIP). Carcinogenesis *12*, 1503–1506.

Jäckh, C., Blatz, V., Fabian, E., Guth, K., van Ravenzwaay, B., Reisinger, K., and Landsiedel, R. (2011). Characterization of enzyme activities of Cytochrome P450 enzymes, Flavin-dependent monooxygenases, N-acetyltransferases and UDP-glucuronyltransferases in human reconstructed epidermis and full-thickness skin models. Toxicology in Vitro *25*, 1209–1214.

Jaehn, P., Kaucher, S., Pikalova, L. v., Mazeina, S., Kajüter, H., Becher, H., Valkov, M., and Winkler, V. (2019). A cross-national perspective of migration and cancer: Incidence of five major cancer types among resettlers from the former Soviet Union in Germany and ethnic Germans in Russia. BMC Cancer *19*, 1–9.

Jamin, E.L., Riu, A., Douki, T., Debrauwer, L., Cravedi, J.P., Zalko, D., and Audebert, M. (2013). Combined genotoxic effects of a polycyclic aromatic hydrocarbon (B(a)P) and a heterocyclic amine (PhIP) in relation to colorectal carcinogenesis. PLoS ONE *8*, 1–11.

Janssen, A.W.F., Duivenvoorde, L.P.M., Rijkers, D., Nijssen, R., Peijnenburg, A.A.C.M., van der Zande, M., and Louisse, J. (2020). Cytochrome P450 expression, induction and activity in human induced pluripotent stem cell-derived intestinal organoids and comparison with primary human intestinal epithelial cells and Caco-2 cells. Archives of Toxicology *95*, 907–922.

Janssen, A.W.F., Duivenvoorde, L.P.M., Rijkers, D., Nijssen, R., Peijnenburg, A.A.C.M., van der Zande, M., and Louisse, J. (2021). Correction to: Cytochrome P450 expression, induction and activity in human induced pluripotent stem cell-derived intestinal organoids and comparison with primary human intestinal epithelial cells and Caco-2 cells (Archives of Toxicology, (2021), 95, 3, (9. Archives of Toxicology *95*, 923.

Jelaković, B., Dika, Ž., Arlt, V.M., Stiborova, M., Pavlović, N.M., Nikolić, J., Colet, J.M., Vanherweghem, J.L., and Nortier, J.L. (2019). Balkan Endemic Nephropathy and the Causative Role of Aristolochic Acid. Seminars in Nephrology *39*, 284–296.

Jin Kang, H., bin Hong, Y., Jeong Kim, H., Weon Yi, Y., Nath, R.G., Soo Chang, Y., Cho, H.-C., and Bae, I. (2011). A novel in vitro pancreatic carcinogenesis model. Toxicology Letters *202*, 15–22.

Jun, D., Kim, S.Y., Na, J.C., Lee, H.H., Kim, J., Yoon, Y.E., Hong, S.J., and Han, W.K. (2018). Tubular organotypic culture model of human kidney. PLOS ONE *13*, e0206447.

Kamdem, L.K., Meineke, I., Gödtel-Armbrust, U., Brockmöller, J., and Wojnowski, L. (2006). Dominant contribution of P450 3A4 to the hepatic carcinogenic activation of aflatoxin B1. Chemical Research in Toxicology *19*, 577–586.

Karlsson, M., Zhang, C., Méar, L., Zhong, W., Digre, A., Katona, B., Sjöstedt, E., Butler, L., Odeberg, J., Dusart, P., et al. (2021). A single–cell type transcriptomics map of human tissues. Science Advances *7*, 1–10.

Keating, G.A., and Bogen, K.T. (2004). Estimates of heterocyclic amine intake in the US population. Journal of Chromatography B: Analytical Technologies in the Biomedical and Life Sciences *802*, 127–133.

Kim, J., Koo, B.K., and Knoblich, J.A. (2020). Human organoids: model systems for human biology and medicine. Nature Reviews Molecular Cell Biology *21*, 571–584.

King, R.J.B., and Robins, M.W. (2006). Cancer biology (Harlow, England ; Pearson/Prentice Hall).

King, R.S., Teitel, C.H., Shaddock, J.G., Casciano, D.A., and Kadlubar, F.F. (1999). Detoxification of carcinogenic aromatic and heterocyclic amines by enzymatic reduction of the N-hydroxy derivative. Cancer Letters *143*, 167–171.

Kirk, G.D., Camus-Randon, A.-M., Mendy, M., Goedert, J.J., Merle, P., Trépo, C., Bréchot, C., Hainaut, P., and Montesano, R. (2000). Ser-249 p53 mutations in plasma DNA of patients with hepatocellular carcinoma from The Gambia. J Natl Cancer Inst *92*, 148–153.

Klaunig, J.E., Wang, Z., Pu, X., and Zhou, S. (2011). Oxidative stress and oxidative damage in chemical carcinogenesis. Toxicology and Applied Pharmacology *254*, 86–99.

Kleinsasser, N.H., Juchhoff, J., Wallner, B.C., Bergner, A., Harréus, U.A., Gamarra, F., Bührlen, M., Huber, R.M., and Rettenmeier, A.W. (2004). The use of mini-organ cultures of human upper aerodigestive tract epithelia in ecogenotoxicology. Mutation Research - Genetic Toxicology and Environmental Mutagenesis *561*, 63–73.

Klingenberg, M. (1958). Pigments of rat liver microsomes. Archives of Biochemistry and Biophysics *75*, 376–386.

Knight, E., and Przyborski, S. (2015). Advances in 3D cell culture technologies enabling tissue-like structures to be created in vitro. Journal of Anatomy *227*, 746–756.

Kolars, J.C., Benedict, P., Schmiedlin-Ren, P., and Watkins, P.B. (1994). Aflatoxin BI-Adduct Formation in Rat and Human Small Bowel Enterocytes. Gastroenterology *106*, 433–439.

Kolenda, T., Kapałczyńska, M., Przybyła, W., Zajączkowska, M., Teresiak, A., Filas, V., Ibbs, M., Bliźniak, R., Łuczewski, Ł., and Lamperska, K. (2018). 2D and 3D cell cultures-a comparison of different types of cancer cell cultures. Arch Med Sci *14*, 910–919.

Kondo, N., Takahashi, A., Ono, K., and Ohnishi, T. (2010). DNA damage induced by alkylating agents and repair pathways. Journal of Nucleic Acids 1–7.

Kopnin, B.P. (2000). Targets of oncogenes and tumor suppressors: Key for understanding basic mechanisms of carcinogenesis. Biochemistry (Moscow) *65*, 2–27.

Krais, A.M., Mühlbauer, K.-R., Kucab, J.E., Chinbuah, H., Cornelius, M.G., Wei, Q.-X., Hollstein, M., Phillips, D.H., Arlt, V.M., and Schmeiser, H.H. (2015). Comparison of the metabolic activation of environmental carcinogens in mouse embryonic stem cells and mouse embryonic fibroblasts. Toxicology in Vitro *29*, 34–43.

Krais, A.M., Speksnijder, E.N., Melis, J.P.M., Indra, R., Moserova, M., Godschalk, R.W., van Schooten, F.J., Seidel, A., Kopka, K., Schmeiser, H.H., et al. (2016a). The impact of p53 on DNA damage and metabolic activation of the environmental carcinogen benzo[a]pyrene: effects in Trp53(+/+), Trp53(+/–) and Trp53(−/−) mice. Archives of Toxicology *90*, 839–851.

Krais, A.M., Speksnijder, E.N., Melis, J.P.M., Singh, R., Caldwell, A., Gamboa Da Costa, G., Luijten, M., Phillips, D.H., and Arlt, V.M. (2016b). Metabolic activation of 2-amino-1-methyl-6-phenylimidazo [4,5-b]pyridine and DNA adduct formation depends on p53:

Studies in Trp53(+/+),Trp53(+/-) and Trp53(-/-) mice. International Journal of Cancer *138*, 976–982.

Krais, A.M., Singh, R., and Arlt, V.M. (2019). Carcinogen-DNA adducts. Encyclopedia of Cancer *3*, 282–295.

Kretzschmar, K., and Clevers, H. (2016). Organoids: Modeling Development and the Stem Cell Niche in a Dish. Developmental Cell *38*, 590–600.

Kucab, J.E., Zou, X., Morganella, S., Joel, M., Nanda, A.S., Nagy, E., Gomez, C., Degasperi, A., Harris, R., Jackson, S.P., et al. (2019). A compendium of mutational signatures of environmental agents. Cell *177*, 821-836.e16.

Kurian, J.R., Chin, N.A., Longlais, B.J., Hayes, K.L., and Trepanier, L.A. (2006). Reductive detoxification of arylhydroxylamine carcinogens by human NADH cytochrome b5 reductase and cytochrome b5. Chemical Research in Toxicology *19*, 1366–1373.

Labib, S., Yauk, C., Williams, A., Arlt, V.M., Phillips, D.H., White, P.A., and Halappanavar, S. (2012). Subchronic oral exposure to benzo(a)pyrene leads to distinct transcriptomic changes in the lungs that are related to carcinogenesis. Toxicological Sciences *129*, 213–224.

Labib, S., Guo, C.H., Williams, A., Yauk, C.L., White, P.A., and Halappanavar, S. (2013). Toxicogenomic outcomes predictive of forestomach carcinogenesis following exposure to benzo(a)pyrene: Relevance to human cancer risk. Toxicology and Applied Pharmacology *273*, 269–280.

Lancaster, M.A., and Huch, M. (2019). Disease modelling in human organoids. Disease Models & Mechanisms *12*, dmm039347.

Lancaster, M.A., and Knoblich, J.A. (2014). Organogenesis in a dish: Modeling development and disease using organoid technologies. Science (1979) *345*, 1247125.

Landi, S., Gemignani, F., Moreno, V., Gioia-Patricola, L., Chabrier, A., Guino, E., Navarro, M., de Oca, J., Capella, G., Canzian, F., et al. (2005). A comprehensive

analysis of phase I and phase II metabolism gene polymorphisms and risk of colorectal cancer. Pharmacogenetics and Genomics *15*, 535–546.

Langhans, S.A. (2018). Three-dimensional in vitro cell culture models in drug discovery and drug repositioning. Frontiers in Pharmacology *9*, 6.

Lauber, S.N., and Gooderham, N.J. (2007). The cooked meat-derived genotoxic carcinogen 2-amino-3-methylimidazo[4,5-b] pyridine has potent hormone-like activity: Mechanistic support for a role in breast cancer. Cancer Research *67*, 9597–9602.

Lauber, S.N., Ali, S., and Gooderham, N.J. (2004). The cooked food derived carcinogen 2-amino-1-methyl-6-phenylimidazo[4,5-b] pyridine is a potent oestrogen: A mechanistic basis for its tissue-specific carcinogenicity. Carcinogenesis *25*, 2509–2517.

Lemieux, C.L., Douglas, G.R., Gingerich, J., Phonethepswath, S., Torous, D.K., Dertinger, S.D., Phillips, D.H., Arlt, V.M., and White, P.A. (2011). Simultaneous measurement of benzo[a]pyrene-induced Pig-a and lacZ mutations, micronuclei and DNA adducts in MutaTMmouse. Environmental and Molecular Mutagenesis *52*, 756–765.

Li, D., Day, R.S., Bondy, M.L., Sinha, R., Nguyen, N.T., Evans, B., Abbruzzese, J.L., and Hassan, M.M. (2007). Dietary Mutagen Exposure and Risk of Pancreatic Cancer. Cancer Epidemiology Biomarkers & Prevention *16*, 655–661.

Li, L., Knutsdottir, H., Hui, K., Weiss, M.J., He, J., Philosophe, B., Cameron, A.M., Wolfgang, C.L., Pawlik, T.M., Ghiaur, G., et al. (2019). Human primary liver cancer organoids reveal intratumor and interpatient drug response heterogeneity. JCI Insight *4*, e121490.

Li, X., Francies, H.E., Secrier, M., Perner, J., Miremadi, A., Galeano-Dalmau, N., Barendt, W.J., Letchford, L., Leyden, G.M., Goffin, E.K., et al. (2018). Organoid cultures recapitulate esophageal adenocarcinoma heterogeneity providing a model for clonality studies and precision therapeutics. Nature Communications *9*, 2983.

Li, Z., Araoka, T., Wu, J., Liao, H.K., Li, M., Lazo, M., Zhou, B., Sui, Y., Wu, M.Z., Tamura, I., et al. (2016). 3D Culture Supports Long-Term Expansion of Mouse and Human Nephrogenic Progenitors. Cell Stem Cell *19*, 516–529.

Liamin, M., Boutet-Robinet, E., Jamin, E.L., Fernier, M., Khoury, L., Kopp, B., le Ferrec, E., Vignard, J., Audebert, M., and Sparfel, L. (2017). Benzo[a]pyrene-induced DNA damage associated with mutagenesis in primary human activated T lymphocytes. Biochemical Pharmacology *137*, 113–124.

Lichtenstein, P., Holm, N. v., Verkasalo, P.K., Iliadou, A., Kaprio, J., Koskenvuo, M., Pukkala, E., Skytthe, A., and Hemminki, K. (2000). Environmental and heritable factors in the causation of cancer: Analyses of cohorts of twins from Sweden, Denmark, and Finland. The New England Journal of Medicine *343*, 78–85.

Lin, R.Z., and Chang, H.Y. (2008). Recent advances in three-dimensional multicellular spheroid culture for biomedical research. Biotechnology Journal *3*, 1172–1184.

Liu, Y., and Wu, F. (2010). Global burden of Aflatoxin-induced hepatocellular carcinoma: A risk assessment. Environmental Health Perspectives *118*, 818–824.

Liu, Z., Hergenhahn, M., Schmeiser, H.H., Wogan, G.N., Hong, A., and Hollstein, M. (2004). Human tumor p53 mutations are selected for in mouse embryonic fibroblasts harboring a humanized p53 gene. Proc Natl Acad Sci U S A *101*, 2963–2968.

Long, A.S., Wills, J.W., Krolak, D., Guo, M., Dertinger, S.D., Arlt, V.M., and White, P.A. (2018). Benchmark dose analyses of multiple genetic toxicity endpoints permit robust, cross-tissue comparisons of MutaMouse responses to orally delivered benzo[a]pyrene. Archives of Toxicology *92*, 967–982.

Loomans, C.J.M., Williams Giuliani, N., Balak, J., Ringnalda, F., van Gurp, L., Huch, M., Boj, S.F., Sato, T., Kester, L., de Sousa Lopes, S.M.C., et al. (2018). Expansion of adult human pancreatic tissue yields organoids harboring progenitor cells with endocrine differentiation potential. Stem Cell Reports *10*, 1088–1101.

Loquet, C., and Wiebel, F.J. (1982). Geno-and cytotoxidty of nitrosamines, aflatoxin B pyrene in continuous cultures of rat hepatoma cells and benzo[a]pyrene in continuous cultures of rat hepatoma cells.

Lord, G.M., Hollstein, M., Arlt, V.M., Roufosse, C., Pusey, C.D., Cook, T., and Schmeiser, H.H. (2004). DNA adducts and p53 mutations in a patient with aristolochic acid-associated nephropathy. Am J Kidney Dis *43*, e18.1-e18.7.

Lou, Y.R., and Leung, A.W. (2018). Next generation organoids for biomedical research and applications. Biotechnology Advances *36*, 132–149.

Lu, W., Rettenmeier, E., Paszek, M., Yueh, M.-F.F., Tukey, R.H., Trottier, J., Barbier, O., and Chen, S. (2017). Crypt Organoid Culture as an in Vitro Model in Drug Metabolism and Cytotoxicity Studies. DRUG METABOLISM AND DISPOSITION Drug Metab Dispos *45*, 748–754.

Luch, A. (2005). Nature and nurture – lessons from chemical carcinogenesis. Nature Reviews Cancer *5*, 113–125.

Luch, A., and Baird, W.M. (2005). Metabolic activation and detoxification of polycyclic aromatic hydrocarbons.

Luo, X., Li, K., Xing, J., Qi, L., Yang, M., Wang, R., Wang, L., Li, Y., and Chen, Z. (2018). In vivo toxicity assessment of aflatoxin B1-contaminated corn after ozone degradation. Food Additives and Contaminants *35*, 341–350.

Lynch, A.M., Gooderham, N.J., and Boobis, A.R. (1996). Organ distinctive mutagenicity in Muta^{TM}Mouse after short-term exposure to PhIP. Mutagenesis *11*, 505–509.

Lynch, S., Pridgeon, C.S., Duckworth, C.A., Sharma, P., Park, B.K., and Goldring, C.E.P.P. (2019). Stem cell models as an in vitro model for predictive toxicology. Biochemical Journal *476*, 1149–1158.

Mace, K., Aguilar, F., Wang, J.-S., Vautravers, P., Gomez-Lechon, M., Gonzalez, F.J., Groopman, J., Harris, C.C., and Pfeifer, A.M.A. (1997). Aflatoxin B1-induced DNA adduct

formation and p53 mutations in CYP450-expressing human liver cell lines. Carcinogenesis *18*, 1291–1297.

Malfatti, M.A., Dingley, K.H., Nowell-Kadlubar, S., Ubick, E.A., Mulakken, N., Nelson, D., Lang, N.P., Felton, J.S., and Turteltaub, K.W. (2006). The urinary metabolite profile of the dietary carcinogen 2-amino-1-methyl-6-phenylimidazo[4,5-b]pyridine is predictive of colon DNA adducts after a low-dose exposure in humans. Cancer Research *66*, 10541–10547.

Malik, D., David, R.M., and Gooderham, N.J. (2018). Mechanistic evidence that benzo[a]pyrene promotes an inflammatory microenvironment that drives the metastatic potential of human mammary cells. Archives of Toxicology 2018 92:10 *92*, 3223–3239.

Malmlöf, M., Pääjärvi, G., Högberg, J., and Stenius, U. (2008). Mdm2 as a sensitive and mechanistically informative marker for genotoxicity induced by benzo[a]pyrene and dibenzo[a,l]pyrene. Toxicological Sciences *102*, 232–240.

Manabe, S., Tohyama, K., Wada, O., and Aramaki, T. (1991). Detection of a carcinogen, 2-amino-1-methyl-6-phenylimidazo [4,5-b]pyridine (PhIP), in cigarette smoke condensate. Carcinogenesis *12*, 1945–1947.

Marchese, S., Polo, A., Ariano, A., Velotto, S., Costantini, S., and Severino, L. (2018). Aflatoxin B1 and M1: Biological Properties and Their Involvement in Cancer Development. Toxins (Basel) *10*, 214.

Mazzoleni, G., di Lorenzo, D., and Steimberg, N. (2009). Modelling tissues in 3D: The next future of pharmaco-toxicology and food research? Genes and Nutrition *4*, 13–22.

McCracken, K.W., Catá, E.M., Crawford, C.M., Sinagoga, K.L., Schumacher, M., Rockich, B.E., Tsai, Y.-H., Mayhew, C.N., Spence, J.R., Zavros, Y., et al. (2014). Modelling human development and disease in pluripotent stem-cell-derived gastric organoids. Nature *516*, 400–404.

McCullough, A.K., and Lloyd, R.S. (2019). Mechanisms underlying aflatoxin-associated mutagenesis – Implications in carcinogenesis. DNA Repair *77*, 76–86.

McDonald, J.T., Farnworth, M., and Liu, Z. (2017). Cancer and the healthy immigrant effect: a statistical analysis of cancer diagnosis using a linked Census-cancer registry administrative database. BMC Public Health *17*, 1–14.

Mei, N., Arlt, V.M., Phillips, D.H., Heflich, R.H., and Chen, T. (2006). DNA adduct formation and mutation induction by aristolochic acid in rat kidney and liver. Mutation Research *602*, 83–91.

Meinl, W., Pabel, U., Osterloh-Quiroz, M., Hengstler, J.G., and Glatt, H. (2006). Human sulphotransferases are involved in the activation of aristolochic acids and are expressed in renal target tissue. International Journal of Cancer *118*, 1090–1097.

Melis, J.P.M., Luijten, M., Mullenders, L.H.F., and van Steeg, H. (2011). The role of XPC: Implications in cancer and oxidative DNA damage. Mutation Research *728*, 107–117.

Meng, H., Li, G., Wei, W., Bai, Y., Feng, Y., Fu, M., Guan, X., Li, M., Li, H., Wang, C., et al. (2021). Epigenome-wide DNA methylation signature of benzo[a]pyrene exposure and their mediation roles in benzo[a]pyrene-associated lung cancer development. Journal of Hazardous Materials *416*, 125839.

Merker, S.R., Weitz, J., and Stange, D.E. (2016). Gastrointestinal organoids: How they gut it out. Developmental Biology *420*, 239–250.

Metry, K.J., Neale, J.R., Bendaly, J., Smith, N.B., Pierce, W.M., and Hein, D.W. (2009). Effect of N-acetyltransferase 2 polymorphism on tumor target tissue DNA adduct levels in rapid and slow acetylator congenic rats administered 2-amino-1-methyl-6-phenylimidazo[4,5-b]pyridine or 2-amino-3,8-dimethylimidazo-[4,5-f]quinoxaline. Drug Metab Dispos *37*, 2123–2126.

Michalopoulos, G.K., Bowen, W.C., Mulè, K., and Luo, J. (2003). HGF-, EGF-, and Dexamethasone-Induced Gene Expression Patterns During Formation of Tissue in Hepatic Organoid Cultures. Gene Expression *11*, 55–75.

Miller, E.C. (1951). Studies on the formation of protein-bound derivatives of 3,4-benzpyrene in the epidermal fraction of mouse skin. Cancer Research *11*, 100–108.

Miller, E.C., and Miller, J.A. (1947). The presence and significance of bound aminoazo dyes in the livers of rats fed p-dimethylaminoazobenzene. Cancer Research *7*, 468–480.

Mimmler, M., Peter, S., Kraus, A., Stroh, S., Nikolova, T., Seiwert, N., Hasselwander, S., Neitzel, C., Haub, J., Monien, B.H., et al. (2016). DNA damage response curtails detrimental replication stress and chromosomal instability induced by the dietary carcinogen PhIP. Nucleic Acids Research *44*, 10259–10276.

Min, S., Kim, S., and Cho, S.-W. (2020). Gastrointestinal tract modeling using organoids engineered with cellular and microbiota niches. Experimental & Molecular Medicine *52*, 227–237.

Mithal, A., Capilla, A., Heinze, D., Berical, A., Villacorta-Martin, C., Vedaie, M., Jacob, A., Abo, K., Szymaniak, A., Peasley, M., et al. (2020). Generation of mesenchyme free intestinal organoids from human induced pluripotent stem cells. Nature Communications *11*, 215.

Mohammad, S., Kashfi, H., Almozyan, S., Jinks, N., Koo, B.-K., and Nateri, A.S. (2018). Morphological alterations of cultured human colorectal matched tumour and healthy organoids. Oncotarget *9*, 10572–10584.

Morizane, R., Lam, A.Q., Freedman, B.S., Kishi, S., Valerius, M.T., and Bonventre, J. v. (2015). Nephron organoids derived from human pluripotent stem cells model kidney development and injury. Nature Biotechnology *33*, 1193–1200.

Moserovä, M., Kotrbovä, V., Aimovä, D., Šulc, M., Frei, E., and Stiborovä, M. (2009). Analysis of benzo[a]pyrene metabolites formed by rat hepatic microsomes using high

pressure liquid chromatography: Optimization of the method. Interdisciplinary Toxicology *2*, 239–244.

Motwani, H. v., Westberg, E., Lindh, C., Abramsson-Zetterberg, L., and Törnqvist, M. (2020). Serum albumin adducts, DNA adducts and micronuclei frequency measured in benzo[a]pyrene-exposed mice for estimation of genotoxic potency. Mutation Research - Genetic Toxicology and Environmental Mutagenesis *849*, 503127.

Mueller, G.C., and Miller, J.A. (1948). The metabolism of 4-dimethylaminoazobenzene by rat liver homogenates. J Biol Chem *176*, 535–544.

Mun, S.J., Ryu, J.S., Lee, M.O., Son, Y.S., Oh, S.J., Cho, H.S., Son, M.Y., Kim, D.S., Kim, S.J., Yoo, H.J., et al. (2019). Generation of expandable human pluripotent stem cell-derived hepatocyte-like liver organoids. Journal of Hepatology *71*, 970–985.

Múnera, J.O., Sundaram, N., Rankin, S.A., Hill, D., Watson, C., Mahe, M., Vallance, J.E., Shroyer, N.F., Sinagoga, K.L., Zarsozo-Lacoste, A., et al. (2017). Differentiation of human pluripotent stem cells into colonic organoids via transient activation of BMP signaling. Cell Stem Cell *21*, 51–64.

Nagao, M., and Sugimura, T. (1993). Carcinogenic factors in food with relevance to colon cancer development. Mutation Research *290*, 43–51.

Narod, S.A., and Foulkes, W.D. (2004). BRCA1 and BRCA2: 1994 and beyond. Nature Reviews Cancer *4*, 665–676.

Naruse, M., Masui, R., Ochiai, M., Maru, Y., Hippo, Y., and Imai, T. (2020). An organoid-based carcinogenesis model induced by in vitro chemical treatment. Carcinogenesis *20*, 1–10.

Nauwelaers, G., Bessette, E.E., Gu, D., Tang, Y., Rageul, J., Erie Fessard, V., Yuan, J.-M., Yu, M.C., Langou€, S., and Turesky, R.J. (2011). DNA Adduct Formation of 4-Aminobiphenyl and Heterocyclic Aromatic Amines in Human Hepatocytes. Chem. Res. Toxicol *24*, 913–925.

Nebert, D.W. (1997). Polymorphisms in drug-metabolizing enzymes: What is their clinical relevance and why do they exist? American Journal of Human Genetics *60*, 265–271.

Nebert, D.W., and Dalton, T.P. (2006). The role of cytochrome P450 enzymes in endogenous signalling pathways and environmental carcinogenesis. Nature Reviews Cancer *6*, 947–960.

Nebert, D.W., Wikvall, K., and Miller, W.L. (2013). Human cytochromes P450 in health and disease. Philosophical Transactions of the Royal Society B: Biological Sciences *368*.

Netzlaff, F., Lehr, C.-M., Wertz, P.W., and Schaefer, U.F. (2005). The human epidermis models EpiSkin®, SkinEthic® and EpiDerm®: An evaluation of morphology and their suitability for testing phototoxicity, irritancy, corrosivity, and substance transport. European Journal of Pharmaceutics and Biopharmaceutics *60*, 167–178.

Nik-Zainal, S., Kucab, J.E., Morganella, S., Glodzik, D., Alexandrov, L.B., Arlt, V.M., Weninger, A., Hollstein, M., Stratton, M.R., and Phillips, D.H. (2015). The genome as a record of environmental exposure. Mutagenesis *30*, gev073.

Nishimura, M., Yaguti, H., Yoshitsugu, H., Naito, S., and Satoh, T. (2003). Tissue distribution of mRNA expression of human cytochrome P450 isoforms assessed by high-sensitivity real-time reverse transcription PCR. The Pharmaceutical Society of Japan *123*, 369–375.

Nitzsche, D., Melzig, M.F., and Arlt, V.M. (2013). Evaluation of the cytotoxicity and genotoxicity of aristolochic acid I – A component of Aristolochiaceae plant extracts used in homeopathy. Environmental Toxicology and Pharmacology *35*, 325–334.

Nortier, J.L., Muniz Martinez, M.-C., Schmeiser, H.H., Arlt, V.M., Bieler, C.A., Petein, M., Depierreux, M.F., Pauw, L. de, Abramowicz, D., Vereerstraeten, P., et al. (2000). Urothelial carcinoma associated with the use of a chinese herb (Aristolochia Fangchi). The New England Journal of Medicine *342*, 1549–1556.

Olson, H., Betton, G., Robinson, D., Thomas, K., Monro, A., Kolaja, G., Lilly, P., Sanders, J., Sipes, G., Bracken, W., et al. (2000). Concordance of the toxicity of pharmaceuticals in humans and in animals. Regulatory Toxicology and Pharmacology *32*, 56–67.

Omiecinski, C.J., vanden Heuvel, J.P., Perdew, G.H., and Peters, J.M. (2011). Xenobiotic Metabolism, Disposition, and Regulation by Receptors: From Biochemical Phenomenon to Predictors of Major Toxicities. Toxicological Sciences *120*, S49–S75.

Omura, T., and Sato, R. (1962). A new cytochrome in liver microsomes. The Journal of Biological Chemistry *237*, 1375–1376.

Ooms, A.H.A.G., Calandrini, C., de Krijger, R.R., and Drost, J. (2020). Organoid models of childhood kidney tumours. Nature Reviews Urology *17*, 311–313.

Otteneder, M., and Lutz, W.K. (1999). Correlation of DNA adduct levels with tumor incidence: Carcinogenic potency of DNA adducts. Mutation Research *424*, 237–247.

Pamies, D., Block, K., Lau, P., Gribaldo, L., Pardo, C.A., Barreras, P., Smirnova, L., Wiersma, D., Zhao, L., Harris, G., et al. (2018). Rotenone exerts developmental neurotoxicity in a human brain spheroid model. Toxicology and Applied Pharmacology *354*, 101–114.

Pampaloni, F., Reynaud, E.G., and Stelzer, E.H.K. (2007). The third dimension bridges the gap between cell culture and live tissue. Nature Reviews Molecular Cell Biology *8*, 839–845.

Park, E., Kim, H.K., Jee, J., Hahn, S., Jeong, S., and Yoo, J. (2019). Development of organoid-based drug metabolism model. Toxicology and Applied Pharmacology *385*, 114790.

Pendergraft, S.S., Sadri-Ardekani, H., Atala, A., and Bishop, C.E. (2017). Three-dimensional testicular organoid: a novel tool for the study of human spermatogenesis and gonadotoxicity in vitro. Biology of Reproduction *96*, 720–732.

Peng, Y., and Croce, C.M. (2016). The role of microRNAs in human cancer. Signal Transduction and Targeted Therapy *1*, 15004.

Peng, W.C., Logan, C.Y., Fish, M., Anbarchian, T., Aguisanda, F., Álvarez-Varela, A., Wu, P., Jin, Y., Zhu, J., Li, B., et al. (2018). Inflammatory cytokine TNFα promotes the long-term expansion of primary hepatocytes in 3D culture. Cell *175*, 1607-1619.e15.

Peto, J. (2001). Cancer epidemiology in the last century and the next decade. Nature *411*, 390–395.

Petruseva, I.O., Evdokimov, A.N., and Lavrik, O.I. (2014). Molecular mechanism of global genome nucleotide excision repair. Acta Naturae *6*, 23–34.

Pfuhler, S., van Benthem, J., Curren, R., Doak, S.H., Dusinska, M., Hayashi, M., Heflich, R.H., Kidd, D., Kirkland, D., Luan, Y., et al. (2020a). Use of in vitro 3D tissue models in genotoxicity testing: Strategic fit, validation status and way forward. Report of the working group from the 7th International Workshop on Genotoxicity Testing (IWGT). Mutation Research - Genetic Toxicology and Environmental Mutagenesis *850–851*, 503135.

Pfuhler, S., Pirow, R., Downs, T.R., Haase, A., Hewitt, N., Luch, A., Merkel, M., Petrick, C., Said, A., Schäfer-Korting, M., et al. (2020b). Validation of the 3D reconstructed human skin Comet assay, an animal-free alternative for following-up positive results from standard in vitro genotoxicity assays. Mutagenesis *20*, 1–17.

Phillips, D.H. (1983). Fifty years of benzo(a)pyrene. Nature *303*, 468–472.

Phillips, D.H. (1999). Polycyclic aromatic hydrocarbons in the diet. Mutation Research *443*, 139–147.

Phillips, D.H. (2002). Smoking-related DNA and protein adducts in human tissues. Carcinogenesis *23*, 1979–2004.

Phillips, D.H. (2005). DNA adducts as markers of exposure and risk. Mutation Research - Fundamental and Molecular Mechanisms of Mutagenesis *577*, 284–292.

Phillips, D.H., and Arlt, V.M. (2009). Genotoxicity: damage to DNA and its consequences. In Molecular, Clinical and Environmental Toxicology. Experientia Supplementum, pp. 87–110.

Piberger, A.L., Krüger, C.T., Strauch, B.M., Schneider, B., and Hartwig, A. (2018). BPDE-induced genotoxicity: relationship between DNA adducts, mutagenicity in the in vitro PIG-A assay, and the transcriptional response to DNA damage in TK6 cells. Archives of Toxicology *92*, 541–551.

Pitot, H.C. (1993). The molecular biology of carcinogenesis. Cancer *72*, 962–970.

Poirier, M.C. (2016). Linking DNA adduct formation and human cancer risk in chemical carcinogenesis. Environmental and Molecular Mutagenesis *57*, 499–507.

Poirier, M.C., and Beland, F.A. (1994). DNA adduct measurements and tumor incidence during chronic carcinogen exposure in rodents. Environmental Health Perspectives *102*, 161–165.

Poirier, M.C., Santella, R.M., and Weston, A. (2000). Carcinogen macromolecular adducts and their measurement. Carcinogenesis *21*, 353–359.

Poon, S.L., Pang, S.T., McPherson, J.R., Yu, W., Huang, K.K., Guan, P., Weng, W.H., Siew, E.Y., Liu, Y., Heng, H.L., et al. (2013). Genome-wide mutational signatures of aristolochic acid and its application as a screening tool. Science Translational Medicine *5*, 1–11.

Pott, P. (1775). Chirurgical observations relative to the cataract, the polypus of the nose, the cancer of the scrotum, the different kinds of ruptures, and the mortification of the toes and feet.

Pupovac, A., Senturk, B., Griffoni, C., Maniura-Weber, K., Rottmar, M., and McArthur, S.L. (2018). Toward Immunocompetent 3D Skin Models. Advanced Healthcare Materials *7*, 1–11.

Rabata, A., Fedr, R., Soucek, K., Hampl, A., and Koledova, Z. (2020). 3D Cell Culture Models Demonstrate a Role for FGF and WNT Signaling in Regulation of Lung Epithelial Cell Fate and Morphogenesis. Frontiers in Cell and Developmental Biology *8*, 1–16.

Rajan, S.A.P., Aleman, J., Wan, M.M., Pourhabibi Zarandi, N., Nzou, G., Murphy, S., Bishop, C.E., Sadri-Ardekani, H., Shupe, T., Atala, A., et al. (2020). Probing prodrug metabolism and reciprocal toxicity with an integrated and humanized multi-tissue organ-on-a-chip platform. Acta Biomaterialia *106*, 124–135.

Reed, L., Mrizova, I., Barta, F., Indra, R., Moserova, M., Kopka, K., Schmeiser, H.H., Wolf, C.R., Henderson, C.J., Stiborova, M., et al. (2018). Cytochrome b5 impacts on cytochrome P450-mediated metabolism of benzo[a]pyrene and its DNA adduct formation: studies in hepatic cytochrome b5/P450 reductase null (HBRN) mice. Archives of Toxicology *92*, 1625–1638.

Reisinger, K., Blatz, V., Brinkmann, J., Downs, T.R., Fischer, A., Henkler, F., Hoffmann, S., Krul, C., Liebsch, M., Luch, A., et al. (2018). Validation of the 3D Skin Comet assay using full thickness skin models: Transferability and reproducibility. Mutation Research - Genetic Toxicology and Environmental Mutagenesis *827*, 27–41.

Rendic, S., and Guengerich, F.P. (2012). Contributions of Human Enzymes in Carcinogen Metabolism. Chemical Research in Toxicology *25*, 1316–1383.

Renner, M., Lancaster, M.A., Bian, S., Choi, H., Ku, T., Peer, A., Chung, K., and Knoblich, J.A. (2017). Self-organized developmental patterning and differentiation in cerebral organoids. The EMBO Journal *36*, 1316–1329.

Rieswijk, L., Claessen, S.M.H., Bekers, O., van Herwijnen, M., Theunissen, D.H.J., Jennen, D.G.J., de Kok, T.M.C.M., Kleinjans, J.C.S., and van Breda, S.G.J. (2016). Aflatoxin B1 induces persistent epigenomic effects in primary human hepatocytes associated with hepatocellular carcinoma. Toxicology *350–352*, 31–39.

Robbana-Barnat, S., Rabache, M., Rialland, E., and Fradin, J. (1996). Heterocyclic amines: Ocurrence and prevention in cooked food. Environ Health Perspectives *104*, 280–288.

Rocco, S.A., Koneva, L., Middleton, L.Y.M., Thong, T., Solanki, S., Karram, S., Nambunmee, K., Harris, C., Rozek, L.S., Sartor, M.A., et al. (2018). Cadmium Exposure Inhibits Branching Morphogenesis and Causes Alterations Consistent With HIF-1α Inhibition in Human Primary Breast Organoids. Toxicological Sciences *164*, 592–602.

Rogers, L.J., Basnakian, A.G., Orloff, M.S., Ning, B., Yao-Borengasser, A., Raj, V., and Kadlubar, S. (2016). 2-amino-1-methyl-6-phenylimidazo(4,5-b) pyridine (PhIP) induces gene expression changes in JAK/STAT and MAPK pathways related to inflammation, diabetes and cancer. Nutrition and Metabolism *13*, 1–11.

Rohrmann, S., Zoller, D., Hermann, S., and Linseisen, J. (2007). Intake of heterocyclic aromatic amines from meat in the European Prospective Investigation into Cancer and Nutrition (EPIC)-Heidelberg cohort. British Journal of Nutrition *98*, 1112–1115.

Rojas, M., Cascorbi, I., Alexandrov, K., Kriek, E., Auburtin, G., Mayer, L., Kopp-Schneider, A., Roots, I., and Bartsch, H. (2000). Modulation of benzo[a]pyrene diolepoxide-DNA adduct levels in human white blood cells by CYP1A1, GSTM1 and GSTT1 polymorphism. Carcinogenesis *21*, 35–41.

Romanov, V., Whyard, T.C., Waltzer, W.C., Grollman, A.P., and Rosenquist, T. (2015). Aristolochic acid-induced apoptosis and G2 cell cycle arrest depends on ROS generation and MAP kinases activation. Arch Toxicol *89*, 47–56.

Roos, W.P., Thomas, A.D., and Kaina, B. (2016). DNA damage and the balance between survival and death in cancer biology. Nature Reviews Cancer *16*, 20–33.

Rosenquist, T.A., and Grollman, A.P. (2016). Mutational signature of aristolochic acid: Clue to the recognition of a global disease. DNA Repair *44*, 205–211.

Ross, D., and Siegel, D. (2004). NAD(P)H:Quinone Oxidoreductase 1 (NQO1, DT-Diaphorase), Functions and Pharmacogenetics. Methods in Enzymology *382*, 115–144.

Ross, D., Kepa, J.K., Winski, S.L., Beall, H.D., Anwar, A., and Siegel, D. (2000). NAD(P)H:quinone oxidoreductase 1 (NQO1): Chemoprotection, bioactivation, gene regulation and genetic polymorphisms. Chemico-Biological Interactions *129*, 77–97.

Rossi, G., Manfrin, A., and Lutolf, M.P. (2018). Progress and potential in organoid research. Nature Reviews Genetics *19*, 671–687.

Rossi, G., Boni, A., Guiet, R., Girgin, M., Kelly, R.G., and Lutolf, M.P. (2019). Embryonic organoids recapitulate early heart organogenesis. BioRxiv 802181.

Ruggeri, B.A., Camp, F., and Miknyoczki, S. (2014). Animal models of disease: Pre-clinical animal models of cancer and their applications and utility in drug discovery. Biochemical Pharmacology *87*, 150–161.

Rushing, B.R., and Selim, M.I. (2019). Aflatoxin B1: A review on metabolism, toxicity, occurrence in food, occupational exposure, and detoxification methods. Food and Chemical Toxicology *124*, 81–100.

Sachs, N., Papaspyropoulos, A., Ommen, D.D.Z., Heo, I., Böttinger, L., Klay, D., Weeber, F., Huelsz-Prince, G., Iakobachvili, N., Amatngalim, G.D., et al. (2019). Long-term expanding human airway organoids for disease modeling. The EMBO Journal *38*, e100300.

Saito, Y., Muramatsu, T., Kanai, Y., Ojima, H., Sukeda, A., Hiraoka, N., Arai, E., Sugiyama, Y., Matsuzaki, J., Uchida, R., et al. (2019). Establishment of Patient-Derived Organoids and Drug Screening for Biliary Tract Carcinoma. Cell Reports *27*, 1265-1276.e4.

Sampaio, G.R., Guizellini, G.M., Silva, S.A. da, Almeida, A.P. de, Pinaffi-Langley, A.C.C., Rogero, M.M., Camargo, A.C. de, and Torres, E.A.F.S. (2021). Polycyclic aromatic hydrocarbons in foods: Biological effects, legislation, occurrence, analytical methods,

and strategies to reduce their formation. International Journal of Molecular Sciences *22*, 6010.

Sato, T., Vries, R.G., Snippert, H.J., van de Wetering, M., Barker, N., Stange, D.E., van Es, J.H., Abo, A., Kujala, P., Peters, P.J., et al. (2009). Single Lgr5 stem cells build crypt-villus structures in vitro without a mesenchymal niche. Nature *459*, 262–265.

Sato, T., Stange, D.E., Ferrante, M., Vries, R.G.J., van Es, J.H., van den Brink, S., van Houdt, W.J., Pronk, A., van Gorp, J., Siersema, P.D., et al. (2011). Long-term expansion of epithelial organoids from human colon, adenoma, adenocarcinoma, and Barrett's epithelium. Gastroenterology *141*, 1762–1772.

Sborchia, M., Keun, H.C., Phillips, D.H., and Arlt, V.M. (2019a). The Impact of p53 on Aristolochic Acid I-Induced Gene Expression In Vivo. International Journal of Molecular Sciences *20*.

Sborchia, M., Prez, E.G. de, Antoine, M.-H., Bienfait, L., Indra, R., Valbuena, G., Phillips, D.H., Nortier, J.L., Stiborová, M., Keun, H.C., et al. (2019b). The impact of p53 on aristolochic acid I-induced nephrotoxicity and DNA damage in vivo and in vitro. Archives of Toxicology *93*, 3345.

Schärer, O.D. (2013). Nucleotide excision repair in Eukaryotes. Cold Spring Harbor Perspectives in Biology *5*, 1–19.

Schlaermann, P., Toelle, B., Berger, H., Schmidt, S.C., Glanemann, M., Ordemann, J., Bartfeld, S., Mollenkopf, H.J., and Meyer, T.F. (2016). A novel human gastric primary cell culture system for modelling Helicobacter pylori infection in vitro. Gut *65*, 202–213.

Schmeiser, H.H., Nortier, J.L., Singh, R., Gamboa Da Costa, G., Sennesael, J., Cassuto-Viguier, E., Ambrosetti, D., Rorive, S., Pozdzik, A., Phillips, D.H., et al. (2014). Exceptionally long-term persistence of DNA adducts formed by carcinogenic aristolochic acid i in renal tissue from patients with aristolochic acid nephropathy. International Journal of Cancer *135*, 502–507.

Schneeberger, K., Sánchez-Romero, N., Ye, S., van Steenbeek, F.G., Oosterhoff, L.A., Palacin, I.P., Chen, C., van Wolferen, M.E., van Tienderen, G., Lieshout, R., et al. (2020). Large-scale production of LGR5-positive bipotential human liver stem cells. Hepatology *72*, 257–270.

Schuijers, J., and Clevers, H. (2012). Adult mammalian stem cells: the role of Wnt, Lgr5 and R-spondins. The EMBO Journal *31*, 2685–2696.

Schut, H.A.J., and Snyderwine, E.G. (1999). DNA adducts of heterocyclic amine food mutagens: Implications for mutagenesis and carcinogenesis. Carcinogenesis *20*, 353–368.

Schutgens, F., Rookmaaker, M.B., Margaritis, T., Rios, A., Ammerlaan, C., Jansen, J., Gijzen, L., Vormann, M., Vonk, A., Viveen, M., et al. (2019). Tubuloids derived from human adult kidney and urine for personalized disease modeling. Nature Biotechnology *37*, 303–313.

Schwank, G., Koo, B.-K., Sasselli, V., Dekkers, J.F., Heo, I., Demircan, T., Sasaki, N., Boymans, S., Cuppen, E., van der Ent, C.K., et al. (2013). Functional Repair of CFTR by CRISPR/Cas9 in Intestinal Stem Cell Organoids of Cystic Fibrosis Patients. Stem Cell *13*, 653–658.

Shah, U.K., Seager, A.L., Fowler, P., Doak, S.H., Johnson, G.E., Scott, S.J., Scott, A.D., and Jenkins, G.J.S. (2016). A comparison of the genotoxicity of benzo[a]pyrene in four cell lines with differing metabolic capacity. Mutation Research - Genetic Toxicology and Environmental Mutagenesis *808*, 8–19.

Shah, U.K., Mallia, J. de O., Singh, N., Chapman, K.E., Doak, S.H., and Jenkins, G.J.S. (2018). A three-dimensional in vitro HepG2 cells liver spheroid model for genotoxicity studies. Mutation Research - Genetic Toxicology and Environmental Mutagenesis *825*, 51–58.

Shan, L., Yu, M., Schut, H.A.J., and Snyderwine, E.G. (2004). Susceptibility of rats to mammary gland carcinogenesis by the food-derived carcinogen 2-amino-1-methyl-6-

phenylimidazo[4,5-b]pyridine (PhIP) varies with age and is associated with the induction of differential gene expression. Am J Pathol *165*, 191–202.

Shibutani, S., Dong, H., Suzuki, N., Ueda, S., Miller, F., and Grollman, A.P. (2007). Selective Toxicity of Aristolochic Acids I and II. Drug Metabolism and Disposition *35*, 1217–1222.

Shimada, T. (2006). Xenobiotic-metabolizing enzymes involved in activation and detoxification of carcinogenic polycyclic aromatic hydrocarbons. Drug Metabolism and Pharmacokinetics *21*, 257–276.

Shirai, T., Sano, M., Tamano, S., Takahashi, S., Hirose, M., Futakuchi, M., Hasegawa, R., Imaida, K., Matsumoto, K., Wakabayashi, K., et al. (1997). The Prostate:A target for carcinogemcity of 2-Amino-1-methyl-6-phenylimidazo[4,5-b]pyridine (PhIP) derived from cooked foods. Cancer Research *57*, 195–198.

Siddiqui, I.A., Sanna, V., Ahmad, N., Sechi, M., and Mukhtar, H. (2015). Resveratrol nanoformulation for cancer prevention and therapy. Ann N Y Acad Sci *1348*, 20–31.

Sidorenko, V.S., Attaluri, S., Zaitseva, I., Iden, C.R., Dickman, K., Johnson, F., and Grollman, A.P. (2014). Bioactivation of the human carcinogen aristolochic acid. Carcinogenesis *35*, 1814–1822.

Silva-Almeida, C., Ewart, M.-A.A., and Wilde, C. (2020). 3D gastrointestinal models and organoids to study metabolism in human colon cancer. Seminars in Cell & Developmental Biology *98*, 98–104.

Simões, M.L., Hockley, S.L., Schwerdtle, T., Gamboa da Costa, G., Schmeiser, H.H., Phillips, D.H., and Arlt, V.M. (2008). Gene expression profiles modulated by the human carcinogen aristolochic acid I in human cancer cells and their dependence on TP53. Toxicology and Applied Pharmacology *232*, 86–98.

Simões, M.L., Hockley, S.L., Schwerdtle, T., Gamboa da Costa, G., Schmeiser, H.H., Phillips, D.H., and Arlt, V.M. (2018). Erratum to “Gene expression profiles modulated by

the human carcinogen aristolochic acid I in human cancer cells and their dependence on TP53" [Toxicol. Appl. Pharmacol. 232(1) (2008) 86–98]. Toxicology and Applied Pharmacology *344*, 75.

Smela, M.E., Hamm, M.L., Henderson, P.T., Harris, C.M., Harris, T.M., and Essigmann, J.M. (2002). The aflatoxin B1 formamidopyrimidine adduct plays a major role in causing the types of mutations observed in human hepatocellular carcinoma. Proceedings of the National Academy of Sciences *99*, 6655–6660.

Smit, E., Souza, T., Jennen, D.G.J., Kleinjans, J.C.S., and van den Beucken, T. (2017). Identification of essential transcription factors for adequate DNA damage response after benzo(a)pyrene and aflatoxin B1 exposure by combining transcriptomics with functional genomics. Toxicology *390*, 74–82.

Smith, M.L., Ford, J.M., Hollander, M.C., Bortnick, R.A., Amundson, S.A., Seo, Y.R., Deng, C.-X., Hanawalt, P.C., and Fornace, A.J. (2000). p53-mediated DNA repair responses to UV radiation: Studies of mouse cells lacking p53 , p21 , and/or gadd45 genes. Molecular and Cellular Biology *20*, 3705–3714.

Smith, M.T., Guyton, K.Z., Gibbons, C.F., Fritz, J.M., Portier, C.J., Rusyn, I., DeMarini, D.M., Caldwell, J.C., Kavlock, R.J., Lambert, P.F., et al. (2016). Key characteristics of carcinogens as a basis for organizing data on mechanisms of carcinogenesis. Environmental Health Perspectives *124*, 713–721.

Smith, M.T., Guyton, K.Z., Kleinstreuer, N., Borrel, A., Cardenas, A., Chiu, W.A., Felsher, D.W., Gibbons, C.F., Goodson III, W.H., Houck, K.A., et al. (2020). The key characteristics of carcinogens: Relationship to the hallmarks of cancer, relevant biomarkers, and assays to measure them. Cancer Epidemiol Biomarkers Prev *29*, 1887–1903.

Spence, J.R., Mayhew, C.N., Rankin, S.A., Kuhar, M., Vallance, J.E., Tolle, K., Hoskins, E.E., Kalinichenko, V. v, Wells, S.I., Zorn, A.M., et al. (2011). Directed differentiation of human pluripotent stem cells into intestinal tissue in vitro. Nature *470*, 105–109.

Srinivas, U.S., Tan, B.W.Q., Vellayappan, B.A., and Jeyasekharan, A.D. (2019). ROS and the DNA damage response in cancer. Redox Biology *25*, 1–9.

Štampar, M., Tomc, J., Filipič, M., and Žegura, B. (2019). Development of in vitro 3D cell model from hepatocellular carcinoma (HepG2) cell line and its application for genotoxicity testing. Archives of Toxicology *93*, 3321–3333.

Stanley, L.A. (2017). Drug Metabolism. Pharmacognosy: Fundamentals, Applications and Strategy 527–545.

Stefanović, V., and Polenaković, M. (2009). Fifty Years of Research in Balkan Endemic Nephropathy: Where Are We Now? Nephron Clinical Practice *112*, c51–c56.

Stiborová, M., Frei, E., Sopko, B., ara Sopkov, K., ira Markov, V., Lan kov, M., Kumst yr ov, T., Wiessler, M., and HSchmeiser, H. (2003). Human cytosolic enzymes involved in the metabolic activation of carcinogenic aristolochic acid: evidence for reductive activation by human NAD(P)H:quinone oxidoreductase. Carcinogenesis *24*, 1695–1703.

Stiborová, M., Frei, E., Arlt, V.M., and Schmeiser, H.H. (2008a). Metabolic activation of carcinogenic aristolochic acid, a risk factor for Balkan endemic nephropathy. Mutation Research - Reviews in Mutation Research *658*, 55–67.

Stiborová, M., Frei, E., and Schmeiser, H.H. (2008b). Biotransformation enzymes in development of renal injury and urothelial cancer caused by aristolochic acid. Kidney International *73*, 1209–1211.

Stiborova, M., Mares, J., Frei, E., Arlt, V.M., Martinek, V., and Schmeiser, H.H. (2011). The human carcinogen aristolochic acid I is activated to form DNA adducts by humanNAD(P)H:quinone oxidoreductase without the contribution of acetyltransferases or sulfotransferases. Environmental and Molecular Mutagenesis *52*, 448–459.

Stiborová, M., Levová, K., Bárta, F., Shi, Z., Frei, E., Schmeiser, H.H., Nebert, D.W., Phillips, D.H., and Arlt, V.M. (2012). Bioactivation versus detoxication of the urothelial

carcinogen aristolochic acid i by human cytochrome P450 1A1 and 1A2. Toxicological Sciences *125*, 345–358.

Stiborová, M., Moserová, M., Černá, V., Indra, R., Dračínský, M., Šulc, M., Henderson, C.J., Wolf, C.R., Schmeiser, H.H., Phillips, D.H., et al. (2014). Cytochrome b5 and epoxide hydrolase contribute to benzo[a]pyrene-DNA adduct formation catalyzed by cytochrome P450 1A1 under low NADPH:P450 oxidoreductase conditions. Toxicology *318*, 1–12.

Stiborová, M., Arlt, V.M., and Schmeiser, H.H. (2016). Balkan endemic nephropathy: an update on its aetiology. Archives of Toxicology *90*, 2595–2615.

Stiborová, M., Arlt, V.M., and Schmeiser, H.H. (2017). DNA adducts formed by aristolochic acid are unique biomarkers of exposure and explain the initiation phase of upper urothelial cancer. International Journal of Molecular Sciences *18*.

Stratton, M.R., Campbell, P.J., and Futreal, P.A. (2009). The cancer genome. Nature *458*, 719–724.

Su, Y., Zhao, B., Guo, F., Bin, Z., Yang, Y., Liu, S., Han, Y., Niu, J., Ke, X., Wang, N., et al. (2014). Interaction of benzo[a]pyrene with other risk factors in hepatocellular carcinoma: A case-control study in Xiamen, China. Annals of Epidemiology *24*, 98–103.

Sung, H., Ferlay, J., Siegel, R.L., Laversanne, M., Soerjomataram, I., Jemal, A., and Bray, F. (2021). Global Cancer Statistics 2020: GLOBOCAN Estimates of Incidence and Mortality Worldwide for 36 Cancers in 185 Countries. CA: A Cancer Journal for Clinicians *71*, 209–249.

Taguchi, A., Kaku, Y., Ohmori, T., Sharmin, S., Ogawa, M., Sasaki, H., and Nishinakamura, R. (2014). Redefining the In Vivo Origin of Metanephric Nephron Progenitors Enables Generation of Complex Kidney Structures from Pluripotent Stem Cells. Cell Stem Cell *14*, 53–67.

Takasato, M., Er, P.X., Becroft, M., Vanslambrouck, J.M., Stanley, E.G., Elefanty, A.G., and Little, M.H. (2014). Directing human embryonic stem cell differentiation towards a renal lineage generates a self-organizing kidney. Nature Cell Biology *16*, 118–126.

Takasato, M., Er, P.X., Chiu, H.S., Maier, B., Baillie, G.J., Ferguson, C., Parton, R.G., Wolvetang, E.J., Roost, M.S., Chuva de Sousa Lopes, S.M., et al. (2015). Kidney organoids from human iPS cells contain multiple lineages and model human nephrogenesis. Nature *526*, 564–568.

Takasato, M., Er, P.X., Chiu, H.S., and Little, M.H. (2016). Generating kidney organoids from human pluripotent stem cells. Nature Protocols *11*, 1681–1692.

Takebe, T., Sekine, K., Enomura, M., Koike, H., Kimura, M., Ogaeri, T., Zhang, R.R., Ueno, Y., Zheng, Y.W., Koike, N., et al. (2013). Vascularized and functional human liver from an iPSC-derived organ bud transplant. Nature *499*, 481–484.

Tang, D., Liu, J.J., Rundle, A., Neslund-Dudas, C., Savera, A.T., Bock, C.H., Nock, N.L., Yang, J.J., and Rybicki, B.A. (2007). Grilled Meat Consumption and PhIP-DNA Adducts in Prostate Carcinogenesis. Cancer Epidemiology Biomarkers & Prevention *16*, 803–808.

Tanigawa, S., Taguchi, A., Sharma, N., Perantoni, A.O., and Nishinakamura, R. (2016). Selective In Vitro Propagation of Nephron Progenitors Derived from Embryos and Pluripotent Stem Cells. CellReports *15*, 801–813.

Terashima, J., Goto, S., Hattori, H., Hoshi, S., Ushirokawa, M., Kudo, K., Habano, W., and Ozawa, S. (2015). CYP1A1 and CYP1A2 expression levels are differentially regulated in three-dimensional spheroids of liver cancer cells compared to two-dimensional monolayer cultures. Drug Metabolism and Pharmacokinetics *30*, 434–440.

Theobald, J., Ghanem, A., Wallisch, P., Banaeiyan, A.A., Andrade-Navarro, M.A., Taškova, K., Haltmeier, M., Kurtz, A., Becker, H., Reuter, S., et al. (2018). Liver-kidney-on-chip to study toxicity of drug metabolites. ACS Biomaterials Science & Engineering *4*, 78–89.

Thermo Scientific (2011). Pierce BCA Protein Assay Kit, 1296.9. Pierce Biotechnology *0747*, 1–7.

Tojo, M., Hamashima, Y., Hanyu, A., Kajimoto, T., Saitoh, M., Miyazono, K., Node, M., and Imamura, T. (2005). The ALK-5 inhibitor A-83-01 inhibits Smad signaling and epithelial-to-mesenchymal transition by transforming growth factor-β. Cancer Science *96*, 791–800.

Totsuka, Y., Watanabe, M., and Lin, Y. (2020). New horizons of DNA adductome for exploring environmental causes of cancer. Cancer Science 1–9.

Truskey, G.A. (2018). Human microphysiological systems and organoids as in vitro models for toxicological studies. Frontiers in Public Health *6*, 185.

Tryndyak, V., Kindrat, I., Dreval, K., Churchwell, M.I., Beland, F.A., and Pogribny, I.P. (2018). Effect of aflatoxin B1, benzo[a]pyrene, and methapyrilene on transcriptomic and epigenetic alterations in human liver HepaRG cells. Food and Chemical Toxicology *121*, 214–223.

Tung, E.W.Y., Philbrook, N.A., Belanger, C.L., Ansari, S., and Winn, L.M. (2014). Benzo[a]pyrene increases DNA double strand break repair in vitro and in vivo: A possible mechanism for benzo[a]pyrene-induced toxicity. Mutation Research/Genetic Toxicology and Environmental Mutagenesis *760*, 64–69.

Turesky, R.J. (2002). Heterocyclic aromatic amine metabolism, DNA adduct formation, mutagenesis, and carcinogenesis. Drug Metabolism Reviews *34*, 625–650.

Turesky, R.J. (2007). Formation and biochemistry of carcinogenic heterocyclic aromatic amines in cooked meats. Toxicology Letters *168*, 219–227.

Turesky, R.J., and le Marchand, L. (2011). Metabolism and Biomarkers of Heterocyclic Aromatic Amines in Molecular Epidemiology Studies: Lessons Learned from Aromatic Amines. Chem Res Toxicol *24*, 1169–1214.

Turesky, R.J., Yun, B.H., Brennan, P., Mates, D., Jinga, V., Harnden, P., Banks, R.E., Blanche, H., Bihoreau, M.T., Chopard, P., et al. (2016). Aristolochic acid exposure in Romania and implications for renal cell carcinoma. British Journal of Cancer *114*, 76–80.

Uhlén, M., Fagerberg, L., Hallström, B.M., Lindskog, C., Oksvold, P., Mardinoglu, A., Sivertsson, Å., Kampf, C., Sjöstedt, E., Asplund, A., et al. (2015). Tissue-based map of the human proteome. Science (1979) *347*, 1260419.

Valko, M., Rhodes, C.J., Moncol, J., Izakovic, M., and Mazur, M. (2006). Free radicals, metals and antioxidants in oxidative stress-induced cancer. Chemico-Biological Interactions *160*, 1–40.

Vanherweghem, J.L., Depierreux, M., Tielemans, C., Abramowicz, D., Dratwa, M., Jadoul, M., Richard, C., Vandervelde, D., Verbeelen, D., Vanhaelen-Fastre, R., et al. (1993). Rapidly progressive interstitial renal fibrosis in young women: Association with slimming regimen including Chinese herbs. Lancet *341*, 387–391.

Venitt, S. (1994). Mechanisms of carcinogenesis and individual susceptibility to cancer. Clin. Chem. *40*, 1421–1425.

Villalta, P.W., Hochalter, J.B., and Hecht, S.S. (2017). 12735−12742 Downloaded via. Anal. Chem *89*, 50.

Vogelstein, B., and Kinzler, K.W. (2004). Cancer genes and the pathways they control. Nature Medicine *10*, 789–799.

Vogelstein, B., Papadopoulos, N., Velculescu, V.E., Zhou, S., Diaz, L.A., and Kinzler, K.W. (2013). Cancer genome landscapes. Science (1979) *339*, 1546–1558.

Wakasugi, M., Sasaki, T., Matsumoto, M., Nagaoka, M., Inoue, K., Inobe, M., Horibata, K., Tanaka, K., and Matsunaga, T. (2014). Nucleotide excision repair-dependent DNA double-strand break formation and ATM signaling activation in mammalian quiescent cells. Journal of Biological Chemistry *289*, 28730–28737.

van der Wal, J.M., Bodewes, A., Agyemang, C., and Kunst, A. (2019). A population-based retrospective study comparing cancer mortality between Moluccan migrants and the general Dutch population: Equal risk 65 years after immigration? BMJ Open *9*, 1–8.

Wang, H., Zhou, H., Liu, A., Guo, X., and Yang, C.S. (2016). Genetic analysis of colon tumors induced by a dietary carcinogen PhIP in CYP1A humanized mice: Identification of mutation of β-catenin/Ctnnb1 as the driver gene for the carcinogenesis. Molecular Carcinogenesis *54*, P1264-1274.

Wang, Y., Arlt, V.M., Roufosse, C.A., McKim, K.L., Myers, M.B., Phillips, D.H., and Parsons, B.L. (2012). ACB-PCR Measurement of H-ras Codon 61 CAA-CTA Mutation Provides an Early Indication of Aristolochic Acid I Carcinogenic Effect in Tumor Target Tissues. Environmental and Molecular Mutagenesis *53*, 495–504.

Wang, Y., Wang, L., Zhu, Y., and Qin, J. (2018). Human brain organoid-on-a-chip to model prenatal nicotine exposure. Lab on a Chip *18*, 843–990.

Watson, C.L., Mahe, M.M., Múnera, J., Howell, J.C., Sundaram, N., Poling, H.M., Schweitzer, J.I., Vallance, J.E., Mayhew, C.N., Sun, Y., et al. (2014). An in vivo model of human small intestine using pluripotent stem cells. Nature Medicine *20*, 1310–1314.

Webb, D.R. (2014). Animal models of human disease: Inflammation. Biochemical Pharmacology *87*, 121–130.

Weeber, F., Ooft, S.N., Dijkstra, K.K., and Voest, E.E. (2017). Tumor Organoids as a Pre-clinical Cancer Model for Drug Discovery. Cell Chemical Biology *24*, 1092–1100.

van de Wetering, M., Francies, H.E., Francis, J.M., Bounova, G., Iorio, F., Pronk, A., van Houdt, W., van Gorp, J., Taylor-Weiner, A., Kester, L., et al. (2015). Prospective derivation of a living organoid biobank of colorectal cancer patients. Cell *161*, 933–945.

Wheeler, G.P., and Skipper, H.E. (1957). Studies with mustards. III. In vivo fixation of C14 from nitrogen mustard-C14H3 in nucleic acid fractions of animal tissues. Archives of Biochemistry and Biophysics *72*, 465–475.

Wild, C.P., Miller, J.D., and Groopman, J.D. (2015). Mycotoxin control in low- and middle-income countries.

Wild, C.P., Weiderpass, E., and Stewart, B.W. (2020). World Cancer report: Cancer research for cancer prevention (Lyon, France).

Williams, J.H., Phillips, T.D., Jolly, P.E., Stiles, J.K., Jolly, C.M., and Aggarwal, D. (2004). Human aflatoxicosis in developing countries: a review of toxicology, exposure, potential health consequences, and interventions. The American Journal of Clinical Nutrition *80*, 1106–1122.

Williams, K.E., Lemieux, G.A., Hassis, M.E., Olshen, A.B., Fisher, S.J., and Werb, Z. (2016). Quantitative proteomic analyses of mammary organoids reveals distinct signatures after exposure to environmental chemicals. Proc Natl Acad Sci U S A *113*, E1343-51.

Woo, L.L., Egner, P.A., Belanger, C.L., Wattanawaraporn, R., Trudel, L.J., Croy, R.G., Groopman, J.D., Essigmann, J.M., and Wogan, G.N. (2011). Aflatoxin B1-DNA adduct formation and mutagenicity in livers of neonatal male and female B6C3F1 mice. Toxicological Sciences *122*, 38–44.

Wu, A.-L., Coulter, S., Liddle, C., Wong, A., and Eastham-Anderson, J. (2011). FGF19 Regulates Cell Proliferation, Glucose and Bile Acid Metabolism via FGFR4-Dependent and Independent Pathways. PLoS ONE *6*.

Wu, F., Wu, D., Ren, Y., Huang, Y., Feng, B., Zhao, N., Zhang, T., Chen, X., Chen, S., and Xu, A. (2019). Generation of hepatobiliary organoids from human induced pluripotent stem cells. Journal of Hepatology *70*, 1145–1158.

Wu, K., Giovannucci, E., Byrne, C., Platz, E.A., Fuchs, C., Willett, W.C., and Sinha, R. (2006). Meat mutagens and risk of distal colon adenoma in a cohort of U.S. men. Cancer Epidemiology and Prevention Biomarkers *15*, 1120–1125.

Xiao, S., Guo, J., Hwa Yun, B., Villalta, P.W., Krishna, S., Tejpaul, R., Murugan, P., Weight, C.J., and Turesky, R.J. (2016). Biomonitoring DNA adducts of cooked meat carcinogens in human prostate by nano liquid chromatography-high resolution tandem mass spectrometry: Identification of 2-Amino-1-methyl-6-phenylimidazo[4,5-b]pyridine DNA adduct. Anal Chem *88*, 12508–12515.

Xu, H., Jiao, Y., Qin, S., Zhao, W., Chu, Q., and Wu, K. (2018). Organoid technology in disease modelling, drug development, personalized treatment and regeneration medicine. Experimental Hematology & Oncology *7*, 30.

Xu, S.F., Hu, A.L., Xie, L., Liu, J.J., Wu, Q., and Liu, J. (2019). Age-associated changes of cytochrome P450 and related phase-2 gene/proteins in livers of rats. PeerJ *7*.

Yamagiwa, K., and Ichikawa, K. (1918). Experimental study of the pathogenesis of carcinoma. Journal of Cancer Research *3*, 1–29.

Yang, H.-Y., Chen, P.-C., and Wang, J.-D. (2014). Chinese Herbs Containing Aristolochic Acid Associated with Renal Failure and Urothelial Carcinoma: A Review from Epidemiologic Observations to Causal Inference. BioMed Research International 1–9.

Yang, X., Zhang, Z., Wang, X., Wang, Y., Zhang, X., Lu, H., and Wang, S.L. (2013). Cytochrome P450 2A13 enhances the sensitivity of human bronchial epithelial cells to aflatoxin B1-induced DNA damage. Toxicology and Applied Pharmacology *270*, 114–121.

Yang, X., Peng, H., Luo, Z., Luo, A., Cai, M., Xu, L., and Wang, H. (2021). The dietary carcinogen PhIP activates p53-dependent DNA damage response in the colon of CYP1A-humanized mice. BioFactors *47*, 612–626.

Yen, Y.-T., Chien, M., Lai, Y.-C., Chen, D.-P., Chuong, C.-M., Hung, M.-C., and Hung, S.-C. (2020). PP2A deficiency enhances carcinogenesis of LGR5+ intestinal stem cells both in organoids and in vivo. Cells *9*, 90.

Yin, Y., and Zhou, D. (2018). Organoid and Enteroid Modeling of Salmonella Infection. Frontiers in Cellular and Infection Microbiology *8*, 102.

Yin, H., Jiang, M., Peng, X., Cui, H., Zhou, Y., He, M., Zuo, Z., Ouyang, P., Fan, J., and Fang, J. (2016). The molecular mechanism of G2/M cell cycle arrest induced by AFB1 in the jejunum. Oncotarget *7*, 35592–35606.

Yuan, L., Lv, B., Zha, J., Wang, W., and Wang, Z. (2014). Basal and benzo[a]pyrene-induced expression profile of phase I and II enzymes and ABC transporter mRNA in the early life stage of Chinese rare minnows (Gobiocypris rarus). Ecotoxicology and Environmental Safety *106*, 86–94.

Yun, B.H., Guo, J., Bellamri, M., and Turesky, R.J. (2020). DNA adducts: formation, biological effects, and new biospecimens for mass spectrometric measurements in humans. Mass Spectrometry Reviews *39*, 55–82.

Zane, N.R., Chen, Y., Wang, M.Z., and Thakker, D.R. (2018). Cytochrome P450 and flavin-containing monooxygenase families: Age-dependent differences in expression and functional activity. Pediatric Research *83*, 527–535.

Zanger, U.M., and Schwab, M. (2013). Cytochrome P450 enzymes in drug metabolism: Regulation of gene expression, enzyme activities, and impact of genetic variation. Pharmacology and Therapeutics *138*, 103–141.

Zeiger, E. (2019). The test that changed the world: The Ames test and the regulation of chemicals. Mutation Research - Genetic Toxicology and Environmental Mutagenesis *841*, 43–48.

Zhang, C., Zhang, Q., Li, J., Yu, L., Li, F., Li, W., Li, Y., Peng, H., Zhao, J., Carmichael, P.L., et al. (2020). Integration of in vitro data from three dimensionally cultured HepaRG cells and physiologically based pharmacokinetic modeling for assessment of acetaminophen hepatotoxicity. Regulatory Toxicology and Pharmacology *114*, 104661.

Zhou, L., Fu, P., Huang, X.R., Liu, F., Lai, K.N., and Lan, H.Y. (2010). Activation of p53 promotes renal injury in acute aristolochic acid nephropathy. Journal of the American Society of Nephrology *21*, 31–41.

Zhu, J., Rashid, A., Cleary, K., Abbruzzese, J.L., Friess, H., Takahashi, S., Shirai, T., and Li, D. (2006). Detection of 2-amino-1-methyl-6-phenylimidazo[4,5-b]-pyridine (PhIP)-DNA adducts in human pancreatic tissues. Biomarkers *11*, 319–328.

Zuo, J., Brewer, D.S., Arlt, V.M., Cooper, C.S., and Phillips, D.H. (2014). Benzo[a]pyrene-induced DNA adducts and gene expression profiles in target and non-target organs for carcinogenesis in mice. BMC Genomics *15*, 880.

Publications and presentations

Published review

Angela L Caipa Garcia, Volker M Arlt, David H Phillips, Organoids for toxicology and genetic toxicology: applications with drugs and prospects for environmental carcinogenesis, Mutagenesis, 2021; geab023, https://doi.org/10.1093/mutage/geab023

Oral presentations

Angela L. Caipa Garcia, Jill E. Kucab, Halh Al-Serori, Rebekah S. S. Beck, Volker M. Arlt and David H. Phillips (September 2020) DNA Damage and Gene Expression in Human Gastric and Pancreatic Tissue Organoids Treated with Benzo[*a*]pyrene. EMGS (Environmental Mutagenesis and Genomics Society) 2020 virtual conference.

Angela L. Caipa Garcia, Jill E. Kucab, Halh Al-Serori, David H. Phillips and Volker M. Arlt (September 2019). Cellular responses of the environmental carcinogen benzo[a]pyrene in human gastric and pancreatic tissue organoid cultures. Young Scientists Workshop, German Society for Environmental Mutation Research (Gesellschaft für Umwelt-Mutationsforschung; GUM) Meeting, Basel, Switzerland.

Poster presentations

Angela L. Caipa Garcia, Jill E. Kucab, Halh Al-Serori, Rebekah S. S. Beck, Volker M. Arlt and David H. Phillips (December 2021). Using organoid cultures from human tissues to study metabolic activation and cellular responses to benzo(*a*)pyrene. UKEMS (United Kingdom Mutagenesis Society) Meeting, London, UK.

Angela L. Caipa Garcia, Jill E. Kucab, Halh Al-Serori, Rebekah S. S. Beck, Volker M. Arlt and David H. Phillips (September 2021). Using organoid cultures from human tissues to study metabolic activation and cellular responses to benzo(*a*)pyrene. NUKEMS (New Investigators of the United Kingdom Mutagenesis Society) virtual symposium.

*Awarded poster prize.

Angela L. Caipa Garcia, Jill E. Kucab, Halh Al-Serori, David H. Phillips and Volker M. Arlt (September 2019). Cellular responses of the environmental carcinogen benzo[a]pyrene in human gastric and pancreatic tissue organoid cultures. German Society for Environmental Mutation Research (Gesellschaft für Umwelt-Mutationsforschung; GUM) Meeting, Basel, Switzerland.